

**CENTERLINE RUMBLE STRIP EFFECTS
ON PAVEMENT PERFORMANCE**

Final Report

PROJECT SPR 838



Oregon Department of Transportation

CENTERLINE RUMBLE STRIP EFFECTS ON PAVEMENT PERFORMANCE

Final Report

PROJECT SPR 838

by

Joshua Weaver – Graduate Research Assistant
Erdem Coleri – Associate Professor (PI)
Vipul Chitnis – Graduate Research Assistant

School of Civil and Construction Engineering
Oregon State University
101 Kearney Hall
Corvallis, OR 97331
Phone: 541-737-0944

for

Oregon Department of Transportation
Research Section
555 13th Street NE, Suite 1
Salem OR 97301

and

Federal Highway Administration
1200 New Jersey Avenue SE
Washington, DC 20590

June 2023

| | | | | | |
|--|--|---|---|--|-----------|
| 1. Report No. TBD FHWA-OR-RD-23-09 | | 2. Government Accession No. | | 3. Recipient's Catalog No. | |
| 4. Title and Subtitle Centerline Rumble Strip Effects on Pavement Performance | | | | 5. Report Date June 2023 | |
| | | | | 6. Performing Organization Code | |
| 7. Author(s) Joshua Weaver - 0000-0002-8819-633X Erdem Coleri - 0000-0002-1904-878X Vipul Chitnis - 0000-0001-7163-157X | | | | 8. Performing Organization Report No. | |
| 9. Performing Organization Name and Address Oregon Department of Transportation Research Section 555 13 th Street NE, Suite 1 Salem, OR 97301 | | | | 10. Work Unit No. (TRAIS) | |
| | | | | 11. Contract or Grant No. | |
| 12. Sponsoring Agency Name and Address Oregon Dept. of Transportation Research Section 555 13 th Street NE, Suite 1 Salem, OR 97301 | | | | 13. Type of Report and Period Covered Federal Highway Admin. 1200 New Jersey Avenue SE Washington, DC 20590 Final Report | |
| | | | | 14. Sponsoring Agency Code | |
| 15. Supplementary Notes | | | | | |
| 16. Abstract: Despite numerous research studies inspecting the safety benefits of CLRS on pavements, there has been limited exploration into the impact on pavement durability as a result of the installation of CLRS. The major purpose of this study was to corroborate what specific factors are controlling the cracking failures due to the installation of CLRS and find solutions to mitigate CLRS-related failures on the roadway. The first component of the study was Finite Element Analysis (FEA) modeling. FEA was conducted to simulate moving tire loads over a full-scale asphalt pavement section containing CLRS. The optimal CLRS configuration included sinusoidal rumble strips installed adjacent to the longitudinal joint with a shorter wavelength. The FEA results verified the findings of the laboratory testing while allowing for the examination of additional factors not tested in the laboratory component of this study. In the second phase of this study, a test strip was constructed at the Knife River facility in Corvallis, Oregon where CLRS were milled into the asphalt pavement. The primary findings showed that sinusoidal CLRS had optimal performance, shallower and smaller rumble strips had a less structural impact, and chip seal surface treatment is an effective method to prevent moisture infiltration, which is expected to be a major factor controlling CLRS performance. The next portion of the study was X-ray Computed Tomography (CT) imaging to determine the presence of microcracks in the asphalt pavement due to rumble strip milling. Results demonstrated the presence of microcracks at all milled rumble strip locations. This finding pointed out the importance of applying a surface treatment on the CLRS right after installation to reduce moisture-related cracking failures. Potential failure mechanisms and construction recommendations were developed based on the results of laboratory testing, X-ray CT imaging, and FEA. | | | | | |
| 17. Key Words rumble strips; asphalt; finite element; milling; grinder; sinusoidal; cracking; fog seal; chip seal; surface treatment; freeze and thaw; X-Ray CT imaging. | | | 18. Distribution Statement Copies available from NTIS, and online at http://www.oregon.gov/ODOT/TD/TP_RES/ | | |
| 19. Security Classification (of this report) – Unclassified | | 20. Security Classification (of this page) – Unclassified | | 21. No. of Pages 170 | 22. Price |

SI* (MODERN METRIC) CONVERSION FACTORS

| APPROXIMATE CONVERSIONS TO SI UNITS | | | | | APPROXIMATE CONVERSIONS FROM SI UNITS | | | | |
|--|-------------------|-------------|---------------------|-----------------|---------------------------------------|---------------------|---------------------|----------------------|-----------------|
| Symbol | When You Know | Multiply By | To Find | Symbol | Symbol | When You Know | Multiply By | To Find | Symbol |
| <u>LENGTH</u> | | | | | <u>LENGTH</u> | | | | |
| in | inches | 25.4 | millimeters | mm | mm | millimeters | 0.039 | inches | in |
| ft | feet | 0.305 | meters | m | m | meters | 3.28 | feet | ft |
| yd | yards | 0.914 | meters | m | m | meters | 1.09 | yards | yd |
| mi | miles | 1.61 | kilometers | km | km | kilometers | 0.621 | miles | mi |
| <u>AREA</u> | | | | | <u>AREA</u> | | | | |
| in ² | square inches | 645.2 | millimeters squared | mm ² | mm ² | millimeters squared | 0.0016 | square inches | in ² |
| ft ² | square feet | 0.093 | meters squared | m ² | m ² | meters squared | 10.764 | square feet | ft ² |
| yd ² | square yards | 0.836 | meters squared | m ² | m ² | meters squared | 1.196 | square yards | yd ² |
| ac | acres | 0.405 | hectares | ha | ha | hectares | 2.47 | acres | ac |
| mi ² | square miles | 2.59 | kilometers squared | km ² | km ² | kilometers squared | 0.386 | square miles | mi ² |
| <u>VOLUME</u> | | | | | <u>VOLUME</u> | | | | |
| fl oz | fluid ounces | 29.57 | milliliters | ml | ml | milliliters | 0.034 | fluid ounces | fl oz |
| gal | gallons | 3.785 | liters | L | L | liters | 0.264 | gallons | gal |
| ft ³ | cubic feet | 0.028 | meters cubed | m ³ | m ³ | meters cubed | 35.315 | cubic feet | ft ³ |
| yd ³ | cubic yards | 0.765 | meters cubed | m ³ | m ³ | meters cubed | 1.308 | cubic yards | yd ³ |
| NOTE: Volumes greater than 1000 L shall be shown in m ³ . | | | | | | | | | |
| <u>MASS</u> | | | | | <u>MASS</u> | | | | |
| oz | ounces | 28.35 | grams | g | g | grams | 0.035 | ounces | oz |
| lb | pounds | 0.454 | kilograms | kg | kg | kilograms | 2.205 | pounds | lb |
| T | sr tons (2000 lb) | 0.907 | megagrams | Mg | Mg | megagrams | 1.102 | short tons (2000 lb) | T |
| <u>TEMPERATURE (exact)</u> | | | | | <u>TEMPERATURE (exact)</u> | | | | |
| °F | Fahrenheit | (F-32)/1.8 | Celsius | °C | °C | Celsius | $\frac{1.8C+32}{2}$ | Fahrenheit | °F |

*SI is the symbol for the International System of Measurement

ACKNOWLEDGEMENTS

The authors would like to thank the Oregon Department of Transportation (ODOT) for providing funding for this research. The authors thank the members of the ODOT Project Technical Advisory Committee and ODOT Research for their advice and assistance in the preparation of this report. In particular, Jon M. Lazarus, Cristhian Galvez, Dean M. Chess, Paul D. Woodworth, Cole F. Mullis, Joel R. McCarroll, Christina A. McDaniel-Wilson, and Frank Belleque who participated on the TAC. The authors would also like to thank Richard Villarreal, Jon Weinberg, and Zachary Allen Newton for their help with the literature review. The authors also show immense gratitude to Knife River Corporation for providing the space at the Corvallis plant for the test strip construction. The authors would also like to thank Keven Heitschmidt of Albina Asphalt for providing the asphalt emulsion for chip sealing. Also, a special thank you to all undergraduate research assistants of the OSU-Asphalt Materials and Pavements (AMaP) research group for their help with sample preparation and testing, as well as James Batti for his help in the laboratory.

In memory of Anthony D Boesen, who supported this research effort and will be missed.

DISCLAIMER

This document is disseminated under the sponsorship of the Oregon Department of Transportation and the United States Department of Transportation in the interest of information exchange. The State of Oregon and the United States Government assume no liability of its contents or use thereof.

The contents of this report reflect the view of the authors who are solely responsible for the facts and accuracy of the material presented. The contents do not necessarily reflect the official views of the Oregon Department of Transportation or the United States Department of Transportation.

The State of Oregon and the United States Government do not endorse products of manufacturers. Trademarks or manufacturers' names appear herein only because they are considered essential to the object of this document.

This report does not constitute a standard, specification, or regulation.

TABLE OF CONTENTS

| | | |
|-------|---|----|
| 1.0 | INTRODUCTION | 1 |
| 1.1 | ORGANIZATION OF THIS RESEARCH REPORT | 2 |
| 1.2 | KEY OBJECTIVES OF THIS STUDY | 2 |
| 2.0 | LITERATURE REVIEW | 3 |
| 2.1 | BENEFITS OF RUMBLE STRIP APPLICATIONS..... | 3 |
| 2.2 | CLRS APPLICATION STRATEGIES | 4 |
| 2.2.1 | Design Dimensions, Geometry, and Installation Criteria | 5 |
| 2.2.2 | Impact of Installation Methods on Benefits from Rumble Strips | 11 |
| 2.3 | FACTORS CONTROLLING THE LONG-TERM PERFORMANCE OF CLRS | 14 |
| 2.3.1 | Climate..... | 14 |
| 2.3.2 | Asphalt Mixture Type – Emulsified Asphalt versus Conventional Asphalt..... | 17 |
| 2.3.3 | The Thickness of the Surface Layer | 18 |
| 2.3.4 | Roadway Roughness and Related Excessive Dynamic Loads | 19 |
| 2.3.5 | Location of the CLRS relative to the Longitudinal Joint..... | 20 |
| 2.3.6 | Age of Asphalt Surfacing..... | 22 |
| 2.3.7 | Surface Treatments | 22 |
| 2.4 | USE OF FINITE ELEMENT ANALYSIS FOR RUMBLE STRIP PERFORMANCE EVALUATION..... | 24 |
| 3.0 | FINITE ELEMENT MODELING FOR CENTERLINE RUMBLE STRIPS..... | 29 |
| 3.1 | INTRODUCTION | 29 |
| 3.2 | MODEL METHODOLOGY | 29 |
| 3.2.1 | Sensitivity Analysis – Finding the Optimum Mesh Size and Loading Time Increment; Determining Critical Load Case | 33 |
| 3.2.2 | Modeling Factorial..... | 39 |
| 3.3 | MODELING RESULTS AND DISCUSSION..... | 45 |
| 3.3.1 | Results for the Control Models (No CLRS) | 48 |
| 3.3.2 | Results for the Models with CLRS | 50 |
| 4.0 | CENTERLINE RUMBLE STRIPS LABORATORY TESTING | 59 |
| 4.1 | INTRODUCTION | 59 |
| 4.2 | MATERIALS AND METHODS..... | 61 |
| 4.2.1 | Experimental Design..... | 61 |
| 4.3 | LABORATORY TEST METHODS | 71 |
| 4.3.1 | Indirect Tensile (IDT) Strength Test..... | 71 |

| | | |
|--------|--|-----|
| 4.3.2 | Resilient Modulus (RM) Test | 71 |
| 4.3.3 | Air Voids Measurement..... | 71 |
| 4.3.4 | Field Infiltration Test Method..... | 72 |
| 4.3.5 | Rainfall Simulation and Moisture Infiltration Tests | 73 |
| 4.3.6 | Three-point Flexural Fatigue Test | 76 |
| 4.3.7 | Hamburg Wheel Tracking Test (HWTT) | 80 |
| 4.3.8 | Chip Seal Application..... | 84 |
| 4.3.9 | Freeze-Thaw Cycling..... | 87 |
| 4.3.10 | Pavement Roughness | 90 |
| 4.3.11 | X-Ray Computed Tomography (CT) Imaging | 91 |
| 4.4 | LABORATORY RESULTS AND DISCUSSION..... | 93 |
| 4.4.1 | Indirect Tensile (IDT) Strength, Resilient Modulus (RM), and Air Void Tests..... | 93 |
| 4.4.2 | Field Infiltration Tests..... | 97 |
| 4.4.3 | Laboratory Rainfall Simulation and Moisture Infiltration Tests | 97 |
| 4.4.4 | Three-Point Flexural Fatigue Test | 106 |
| 4.4.5 | Hamburg Wheel Tracking Test (HWTT) | 117 |
| 4.4.6 | Pavement Roughness | 126 |
| 4.4.7 | X-ray CT Imaging..... | 128 |
| 5.0 | SUMMARY, CONCLUSIONS, AND RECOMMENDATIONS..... | 133 |
| 5.1 | DISCUSSION | 133 |
| 5.2 | CONSTRUCTION RECOMMENDATIONS | 135 |
| 5.3 | FUTURE WORK..... | 135 |
| 6.0 | REFERENCES | 137 |
| | APPENDIX A: SUPPLEMENTARY MATERIAL OF CHAPTER 4 | A-1 |

LIST OF FIGURES

| | |
|---|----|
| Figure 2.1: Example of a centerline rumble strip on asphalt pavement (Smadi & Hawkins, 2016) | 3 |
| Figure 2.2: Illustration of rumble strip dimensions (Himes et al., 2017)..... | 5 |
| Figure 2.3: ODOT DET 4556 Rural Highway CLRS dimensions and geometry | 7 |
| Figure 2.4: Rolled or formed rumble strips (Richards & Saito, 2007)(Guin et al. 2014)..... | 11 |
| Figure 2.5: Examples of milled rumble strips from the Oregon State University test section | 12 |
| Figure 2.6: Raised rumble strips and pavement markers (Cottingham, 2020) (Raised Pavement Markers, 2020)..... | 13 |

| | |
|---|----|
| Figure 2.7: Sinusoidal rumble strip design from MNDOT optimization study (Terhaar et al. 2016) | 13 |
| Figure 2.8: Transverse and longitudinal cracking at milled rumble strips (Coffey and Park, 2016) | 15 |
| Figure 2.9: Fatigue cracking at milled rumble strips (Coffey and Park, 2016) | 15 |
| Figure 2.10: The relationship between TTR and curve radius (a) TTR with respect to curve radius for left bend (b) TTR with respect to curve radius for right bend (c) illustration for TTR (Xu et al. 2018) | 19 |
| Figure 2.11: Required turning radius per vehicle type (Institute of Transportation Engineers, 2016) | 20 |
| Figure 2.12: MDOT CLRS design for non-freeway roads (MDOT, 2010)..... | 21 |
| Figure 2.13: Rumble strip designs for FEA of exterior noise generation (Kalathas et al. 2019) . | 24 |
| Figure 2.14: Three modified CLRS designs tested by the FEA model developed by (Kim & Rilett, 2017) | 26 |
| Figure 2.15: Finite element mesh cross-sectional profile of the composite pavement structure (Kim & Rilett, 2017)..... | 27 |
| Figure 2.16: Position of two tire loading scenarios used in the Nebraska study (Kim & Rilett, 2017) | 27 |
| Figure 2.17: Zoomed-in views of CLRS edges/corners: (a) 2 nd loading, (b) 1 st loading (Kim & Rilett, 2017) | 28 |
| Figure 3.1: FEA model structure | 32 |
| Figure 3.2: Loading configuration for the Class 9 truck; lengths are feet and inches, and circled axle weights are given in pounds (“Self-Issue Permit Program Manual,” 2021) | 33 |
| Figure 3.3: Mesh sensitivity analysis – Time step increments | 34 |
| Figure 3.4: Mesh sensitivity analysis – Mesh density | 34 |
| Figure 3.5: Meshed model structure in Abaqus – Traffic flows in the X direction | 35 |
| Figure 3.6: Meshed model structure in Abaqus – Closer view with rumble strips and applied wheel loads..... | 35 |
| Figure 3.7: Critical load cases - Tire orientations..... | 38 |
| Figure 3.8: Critical load case – Maximum principal stresses | 38 |
| Figure 3.9: FEA rumble strip locations with respect to longitudinal construction joints | 41 |
| Figure 3.10: Conventional rectangular CLRS, 40.64 cm x 17.78 cm (16 in x 7 in), dimensions in inches (“ODOT Standard Details Traffic 4000 Series,” n.d.)..... | 42 |
| Figure 3.11: Modified rectangular CLRS, 20.32 cm x 17.78 cm (8 in x 7 in), dimensions in inches (“ODOT Standard Details Traffic 4000 Series,” n.d.)..... | 43 |
| Figure 3.12: Sinusoidal CLRS, dimensions in inches (Hurwitz et al, 2019)..... | 44 |
| Figure 3.13: Sinusoidal CLRS cross-section views from the developed FEA models..... | 45 |
| Figure 3.14: FEA dynamic loading effect..... | 46 |
| Figure 3.15: Nodes along the wheel path utilized for stress and strain output extraction | 48 |
| Figure 3.16: Control case (no CLRS) at 25°C with dual tires passing over the longitudinal joint - High and low speeds for stiff and soft asphalt models, 1 mph = 1.61 kph..... | 48 |
| Figure 3.17: Control case at 25°C with soft asphalt layer - Impact of axle type on maximum principal elastic microstrain response, 1 mph = 1.61 kph..... | 49 |
| Figure 3.18: Control case at 25°C with dual tires passing adjacent to the longitudinal joint - High and low speeds for stiff and soft asphalt models, 1 mph = 1.61 kph..... | 50 |

| | |
|---|-----|
| Figure 3.19: Rectangular CLRS over the longitudinal joint, 1 inch (“) = 2.54 cm and 1 mph = 1.61 kph..... | 51 |
| Figure 3.20: Distribution of maximum principal elastic microstrain | 53 |
| Figure 3.21: Sinusoidal CLRS over the longitudinal joint, 1 inch (“) = 2.54 cm and 1 mph = 1.61 kph..... | 54 |
| Figure 3.22: Rectangular CLRS adjacent to longitudinal joint, 1 inch (“) = 2.54 cm and 1 mph = 1.61 kph – M: Modified; C: Conventional..... | 55 |
| Figure 4.1: Test strip construction and sample extraction | 64 |
| Figure 4.2: CLRS installation plan at the test strip (“ corresponds to inches and ‘ corresponds to feet) | 65 |
| Figure 4.3: Coring and permeability testing plan (“ corresponds to inches and ‘ corresponds to feet) | 66 |
| Figure 4.4: Field infiltration test | 73 |
| Figure 4.5: Moisture infiltration sample preparation | 74 |
| Figure 4.6: Rainfall simulator test setup | 76 |
| Figure 4.7: Three-point flexural fatigue sample varieties..... | 77 |
| Figure 4.8: Cutting samples using water-cooled diamond blade..... | 78 |
| Figure 4.9: Three-point bending test jig, sample placement, and sample preparation | 79 |
| Figure 4.10: Tested three-point flexural fatigue sample..... | 80 |
| Figure 4.11: Hamburg Wheel Tracking Test samples | 81 |
| Figure 4.12: Hamburg Wheel Tracking sample preparation | 82 |
| Figure 4.13: HWTT equipment and tested block sample | 84 |
| Figure 4.14: Chip seal application system components..... | 85 |
| Figure 4.15: Chip seal application procedure | 87 |
| Figure 4.16: Freeze-thaw procedure | 89 |
| Figure 4.17: SurPRO 3000..... | 90 |
| Figure 4.18: SurPRO elevation profiles for conventional (orange), modified (blue), and sinusoidal (green) CLRS..... | 91 |
| Figure 4.19: Core locations extracted from conventional CLRS..... | 92 |
| Figure 4.20: Cores for X-ray CT imaging | 92 |
| Figure 4.21: IDT, RM, and air void test results | 93 |
| Figure 4.22: South end of construction - Contour maps of IDT strength, RM, and Corelok air void content..... | 94 |
| Figure 4.23: North end of construction - Contour maps of IDT strength, RM, and Corelok air void content..... | 95 |
| Figure 4.24: Air void contents, SSD versus Corelok..... | 96 |
| Figure 4.25: Moisture infiltration results - Control samples (R: replicate) | 98 |
| Figure 4.26: Moisture infiltration results - Rectangular CLRS, middle of the lane (R: replicate)..... | 99 |
| Figure 4.27: Moisture infiltration results - Rectangular CLRS, edge of the lane (R: replicate)..... | 100 |
| Figure 4.28: Moisture infiltration results - Rectangular CLRS, over longitudinal joint (R: replicate) | 102 |
| Figure 4.29: Moisture infiltration results - Sinusoidal CLRS, middle of lane (R: replicate) | 104 |
| Figure 4.30: Moisture infiltration results - Sinusoidal CLRS, over the longitudinal joint (R: replicate) | 105 |
| Figure 4.31: Typical flexural fatigue test deflection curve..... | 107 |
| Figure 4.32: Flexural fatigue test deflection curve and performance parameters..... | 107 |

| | |
|--|-----|
| Figure 4.33: Flexural fatigue parameter versus sample thickness | 108 |
| Figure 4.34: Test section spatial variability of air voids..... | 110 |
| Figure 4.35: Flexural fatigue test – Travel lane versus the edge of construction (error bars are 1 standard deviation)..... | 111 |
| Figure 4.36: Flexural Fatigue Test – Longitudinal joint versus travel lane (error bars are 1 standard deviation)..... | 112 |
| Figure 4.37: Flexural Fatigue Test – Freeze-thaw conditioning versus no treatment versus freeze-thaw with chip seal treatment (error bars are 1 standard deviation)..... | 113 |
| Figure 4.38: Flexural Fatigue Test – Rectangular CLRS versus sinusoidal CLRS (error bars are 1 standard deviation)..... | 114 |
| Figure 4.39: Flexural Fatigue Test – Shallow versus deep CLRS (error bars are 1 standard deviation) | 115 |
| Figure 4.40: Flexural Fatigue Test – Modified versus conventional rectangular CLRS (error bars are 1 standard deviation)..... | 116 |
| Figure 4.41: Flexural Fatigue Test – Chip seal surface treatment versus no treatment (error bars are 1 standard deviation)..... | 117 |
| Figure 4.42: Hamburg Wheel Tracking Test (HWTT) typical rutting curve | 118 |
| Figure 4.43: HWTT - Control versus rectangular CLRS versus sinusoidal CLRS (error bars are 1 standard deviation)..... | 119 |
| Figure 4.44: HWTT - Composite rutting curves for control, rectangular CLRS, and sinusoidal CLRS..... | 120 |
| Figure 4.45: HWTT - Cracking patterns after freeze-thaw conditioning | 121 |
| Figure 4.46: HWTT - Cracking patterns after freeze-thaw conditioning and chip seal surface treatment | 122 |
| Figure 4.47: Tested HWTT cross-section views, with chip seal surface treatment..... | 123 |
| Figure 4.48: HWTT – Chip seal treatment with correction factor versus no treatment (error bars are 1 standard deviation)..... | 124 |
| Figure 4.49: HWTT - Shallow versus deep rectangular CLRS (error bars are 1 standard deviation) | 125 |
| Figure 4.50: SurPRO IRI results..... | 127 |
| Figure 4.51: X-ray CT imaging cross-section views | 131 |
| Figure A.1: Hamburg Wheel Tracking (HWTT) composite rutting curves | A-7 |
| Figure A.2: Tested HWTT samples demonstrating different treatment strategies | A-8 |

LIST OF TABLES

| | |
|--|----|
| Table 2.1: The Impact of CLRS on Accident Rates (Russell and Rys, 2005)..... | 4 |
| Table 2.2: National Average Dimension (in Inches) for Shoulder Rumble Strips (SRS) and Centerline Rumble Strips (CLRS) (Himes et al. 2017) | 6 |
| Table 2.3: Michigan DOT Two-Year Study of CLRS Rate of Crack Propagation Data (Datta et al. 2012) | 17 |
| Table 2.4: Recommended Minimum Pavement Thickness for Rumble Strip Installation (FHWA, 2015a) | 18 |
| Table 3.1: Finite Element Model Input Parameters for Soft and Stiff Asphalt Layers (Estaji et al., 2019)..... | 31 |

| | |
|--|-----|
| Table 3.2: Numerical Modeling Factorial – Rectangular CLRS Models | 39 |
| Table 3.3: Numerical Modeling Factorial – Sinusoidal CLRS Models..... | 39 |
| Table 3.4: Numerical Modeling Factorial – Control Models (No rumble strips on the pavement) | 40 |
| Table 4.1: Test Section Rumble Strip Features | 62 |
| Table 4.2: Laboratory Experimental Plan - Phase 1, Modified 20.32 cm x 17.78 cm (8 in x 7 in) CLRS, in the Lane..... | 67 |
| Table 4.3: Laboratory Experimental Plan - Phase 2, Modified 20.32 cm x 17.78 cm (8 in x 7 in) CLRS, Over the Longitudinal Joint | 68 |
| Table 4.4: Laboratory Experimental Plan – Phase 3, Modified 20.32 cm x 17.78 cm (8 in x 7 in) CLRS, Adjacent to the Longitudinal Joint..... | 68 |
| Table 4.5: Laboratory Experimental Plan - Phase 4, Conventional 40.64 cm x 17.78 cm (16 in x 7 in) CLRS, in the Lane | 68 |
| Table 4.6: Laboratory Experimental Plan - Phase 5, Sinusoidal 50.8 cm (20 in) wide CLRS, in the Lane..... | 69 |
| Table 4.7: Laboratory Experimental Plan - Phase 6, Sinusoidal 50.8 cm (20 in) wide CLRS, Over the Longitudinal Joint | 69 |
| Table 4.8: Laboratory Experimental Plan - Phase 7, Control Samples, in the Lane | 69 |
| Table 4.9: Core and Field Permeability Experimental Plan | 70 |
| Table 4.10: Field and Laboratory Air Void Contents | 96 |
| Table 4.11: Moisture Infiltration Summary Results | 106 |
| Table 4.12: Average measured CLRS depths | 109 |

1.0 INTRODUCTION

Centerline rumble strips (CLRS) are devices proven to increase safety on the roadway by alerting drivers of a potential departure into opposing lanes of traffic through audio cues and haptic vibrations on the steering wheel. These alerts are created through the milled components in the roadway and tires that create noise and vibration. Rumble strips are also used on the shoulder to prevent lane departures; however, the focus of this study will be on center line rumbles. CLRS are installed to distinguish between opposite sides of the road and therefore have been widely used to produce significant safety benefits at a very low cost. CLRS are generally installed on roads that do not have a divider (median, K-Barrier, concrete barrier, cable barrier, rail, etc.). In recent years, however, the Oregon Department of Transportation (ODOT) has been observing failures of the asphalt pavement surface that may be due to the installation of CLRS on rural and low-density mountainous roadways. Timothy Earnest and Justin Moderie (personal communication, October 19, 2018) developed a technical memorandum to provide scoping guidance and considerations for regions to reduce CLRS-related distresses on Oregon roadways. However, determining the major mechanisms behind the CLRS-related failures on roadways and recommending strategies to mitigate those failures were not within the scope of the memorandum.

Despite numerous research studies inspecting the safety benefits of CLRS on pavements, there has been limited exploration into the impact on pavement durability as a result of the installation of CLRS. Existing studies that have investigated asphalt pavement durability relating to CLRS installation have generally concluded that CLRS has a limited effect on pavement performance. Only Alaska and Oregon have reported major failures related to the installation of CLRS (Datta et al., 2012). Although CLRS installation could be reducing pavement performance and life, many states and countries continue to actively implement CLRS on roads to improve safety. Most of the literature presented in this report regarding pavement performance is anecdotal and needs actual testing to corroborate what specific factors are controlling the cracking failures due to the construction of CLRS.

The installation practices of CLRS vary between state agencies and are based on numerous components such as agency standards, existing pavement surface types, climate, traffic, etc. Also, there are multiple types of CLRS, and they can be introduced to the roadway through a number of methods. The most common types of CLRS are “milled CLRS”, which are installed at any point during a pavement’s life cycle by cutting consistent-sized grooves into the pavement using a rotary rumble strip grinder. Another type of CLRS is “rolled CLRS”, which is installed concurrently with the placement of a new asphalt surface by pressing grooves into the fresh hot-mix asphalt mat using a wheel-like device. Rolled CLRS typically have a V-shape or sinusoidal waveform. Raised rumble strips are another type that are installed on new or existing pavements with epoxy and are either rounded or rectangular with widths ranging from 2-12 inches (FHWA, 2015a). Detailed testing and evaluation of milled and rolled installation methods is necessary to better understand and quantify the impact of CLRS types on pavement performance. Milled CLRS was the focus of this research project since it is the most commonly used CLRS type in Oregon.

Although several states have identified pavement performance concerns associated with CLRS installation, there has been a limited number of scientific research studies evaluating and quantifying the impacts of CLRS on pavement performance. Since CLRS have proven to be cost-effective safety measures in reducing lane departure crashes, pavement failures due to the installation of CLRS, particularly in rural mountainous areas or snow zones, should be reduced. However, these early cracking failures of CLRS in Oregon point out a need to develop innovative methods and strategies to improve installation methods and maintenance strategies for pavements with CLRS (Earnest and Moderie, 2018). This research project intends to evaluate, quantify, and mitigate the potential negative impacts of CLRS on the condition and serviceability of the pavement while preserving (or enhancing) the existing safety benefits of CLRS.

1.1 ORGANIZATION OF THIS RESEARCH REPORT

This research report is structured as follows:

- Chapter 2.0 provides a comprehensive literature review summarizing the safety benefits and applications of rumble strips, CLRS application strategies, factors controlling the long-term performance of CLRS, and the use of finite element analysis (FEA) for rumble strip performance evaluation.
- Chapter 3.0 summarizes the process followed in this study for dynamic 3D viscoelastic FEA model development and the major findings from the model outputs.
- Chapter 4.0 presents the followed research methodology and results and conclusions from the field test strip construction and laboratory testing.
- Chapter 5.0 summarizes all major conclusions, provides suggestions for implementation, and recommends future work.

1.2 KEY OBJECTIVES OF THIS STUDY

The primary objectives of this study are to:

- Quantify the impacts of CLRS installation on the performance and maintenance of asphalt surfaced pavements, particularly in mountainous areas and/or snow zones;
- Identify the best construction practices for CLRS installation to minimize negative impacts on pavement performance; and
- Identify, evaluate, and compare the effectiveness of chip sealing (or other surface treatments) to mitigate any pavement performance issues post-installation of CLRS while considering performance, cost, and safety.

2.0 LITERATURE REVIEW

2.1 BENEFITS OF RUMBLE STRIP APPLICATIONS

Centerline rumble strips (CLRS), as shown in Figure 2.1 (Smadi & Hawkins, 2016), seek to prevent head-on collisions from vehicles crossing over the centerline into opposing traffic. CLRS act as a speed mitigation measure and alert drivers of impending lane departures by producing sound and vibration inside and outside the vehicle (Kalathas et al., 2019). This alert raises situational awareness and encourages drivers to make minor course corrections back into their proper travel lane and to avoid on-coming traffic in the opposite direction. CLRS are typically applied to rural two-lane roads and yet, can also be applied to multilane undivided facilities (FHWA, 2015). Louisiana crash data between the years 2007 and 2016 showed that 29.3% of all state highway crashes were due to roadway departure and might have been partially avoided by using CLRS or similar devices (LTRC, 2020). Data from urban and rural two-lane highways have also shown significant safety improvements from the installation of CLRS (Torbic et. al., 2009) (Donnell et al., 2014). CLRS on rural two-lane highways have also been shown to reduce head-on and opposite-direction fatal and injury crashes by 45 % (FHWA, 2016). A 64 % reduction on urban two-lane roads was also observed (FHWA, 2016) (Smadi & Hawkins, 2016).



Figure 2.1: Example of a centerline rumble strip on asphalt pavement (Smadi & Hawkins, 2016)

According to Russell and Rys (2005), the installation of CLRS on rural two-lane roads and four-lane highways created about an 80% reduction in cross-over crashes in Oregon (See Table 2.1). The reduction in accident rates for other states is significantly lower than in Oregon. However, it should be noted that the data collected for Oregon in the study was limited when compared to the data from the other seven states. According to the before-after crash analysis recently conducted by ODOT (see ODOT, 2022), the installation of CLRS reduced head-on fatalities by 54 %. Safety benefits for the relative cost have led the Oregon DOT to be proactive with CLRS installation (ODOT, 2022).

Table 2.1: The Impact of CLRS on Accident Rates (Russell and Rys, 2005)

| | | | Before Period | | | | After Period | | | |
|-------------------|-------|-------|---------------|---------|-------------|--------|--------------|---------|-------------|--------|
| | | | Mile | Average | Crash Count | | Mile | Average | Crash Count | |
| State | Miles | Sites | Years | AADT | Total | Injury | Years | AADT | Total | Injury |
| California | 47.8 | 29 | 206.5 | 2,235 | 679 | 257 | 112.5 | 10,430 | 351 | 144 |
| Colorado | 16.9 | 10 | 118.4 | 5,000 | 551 | 262 | 84.6 | 6,154 | 415 | 187 |
| Delaware | 2.9 | 1 | 8.4 | 16,500 | 34 | 16 | 21.3 | 21,685 | 82 | 38 |
| Maryland | 30.4 | 11 | 91.4 | 11,680 | 156 | 55 | 42.5 | 12,991 | 55 | 14 |
| Minnesota | 66.2 | 24 | 508.6 | 9,305 | 751 | 158 | 158.6 | 10,315 | 275 | 41 |
| Oregon | 3.1 | 2 | 22.8 | 11,400 | 31 | 20 | 4.6 | 11,150 | 6 | 3 |
| Washington | 43.5 | 21 | 166.5 | 7,200 | 308 | 116 | 173.3 | 7,963 | 297 | 109 |
| Total | 210.8 | 98 | 1,122.6 | 8,820 | 2,510 | 882 | 597.3 | 9,858 | 1,481 | 536 |

Note: AADT=average annual daily traffic. (Source: Persaud et al. 2003)

Pavement markings are often placed over CLRS (see Figure 2.7) and are sometimes also referred to as centerline rumble stripes (FHWA, 2011). CLRS can help drivers identify the centerline pavement marking better during nighttime or on wet pavement (FHWA, 2015). The retroreflective capacity of pavement markings can be seriously reduced in a rain event. When placed on a CLRS, the vertical component of the rumble stripe is still visible under adverse conditions (FHWA, 2011). CLRS vibration also acts as a navigational aid during fog, snow, or blinding rain to assist drivers from crossing the centerline during these conditions (FHWA, 2011). Most, if not all, benefits of rumble strip applications are related to safety.

Rumble strips can be milled (carved into the existing pavement surface), raised, or rolled (applied to fresh asphalt) onto a pavement surface, giving flexibility to the type of rumble strips used on pavements. However, the majority of CLRS installed on two-lane roads are milled since milled rumble strips are better at alerting the driver due to more noise and vibrations created in the vehicle (Hawkins et al., 2016). According to the current literature summarized above, there is no added benefit to pavement performance as a result of using milled rumble strips (which is the most commonly used CLRS type in Oregon). There is, however, a great concern of accelerated pavement deterioration from the installation of milled rumble strips. The hypothesis presented is that the milling process is creating micro-cracks in the pavement structure that may propagate to macro cracks over time with freeze/thaw cycles and traffic loading. Despite this concern, at the time of writing this literature review, there is no scientific research available in the literature quantifying the effects of milled rumble strips on pavement performance.

2.2 CLRS APPLICATION STRATEGIES

CLRS are known to improve the safety of the roadway and reduce head-on collisions. Most agencies have implemented CLRS based on crash history data or a more systematic approach (based on a risk assessment process) (Himes et al., 2017). According to the literature, application strategies of CLRS also differ widely from agency to agency because of no national standardization. In this section, possible CLRS application strategies are discussed based on the findings from the literature.

2.2.1 Design Dimensions, Geometry, and Installation Criteria

Rumble strip and stripe (stripe is the name of a rumble strip when an edge line or center line pavement marking is applied on the rumble strip) have four main dimensions (Himes et al., 2017) (also shown in Figure 2.2).

- **Offset (A):** Distance from the pavement marking (delineating the edge of the traveled way) to the inside edge of the rumble strip.
- **Length (B):** Sometimes referred to as the transverse width, is measured lateral to the travel direction.
- **Width (C):** Measured parallel to the travel lane.
- **Depth (D):** Measured from the top of the pavement surface to the bottom of the rumble strip groove in the vertical direction. This distance is the maximum depth. If part of the rumble strip goes above the pavement surface (such as sinusoidal rumble strips), effective depth is the distance between the lowest and higher points (minimum peak to maximum peak) on the rumble strips.
- **Spacing (E):** Distance between rumble strip patterns can be measured either from the center of one rumble strip to the center of an adjacent rumble strip, or it could be measured from the beginning of one rumble strip to the beginning of an adjacent rumble strip.

Center Line Rumble Strips

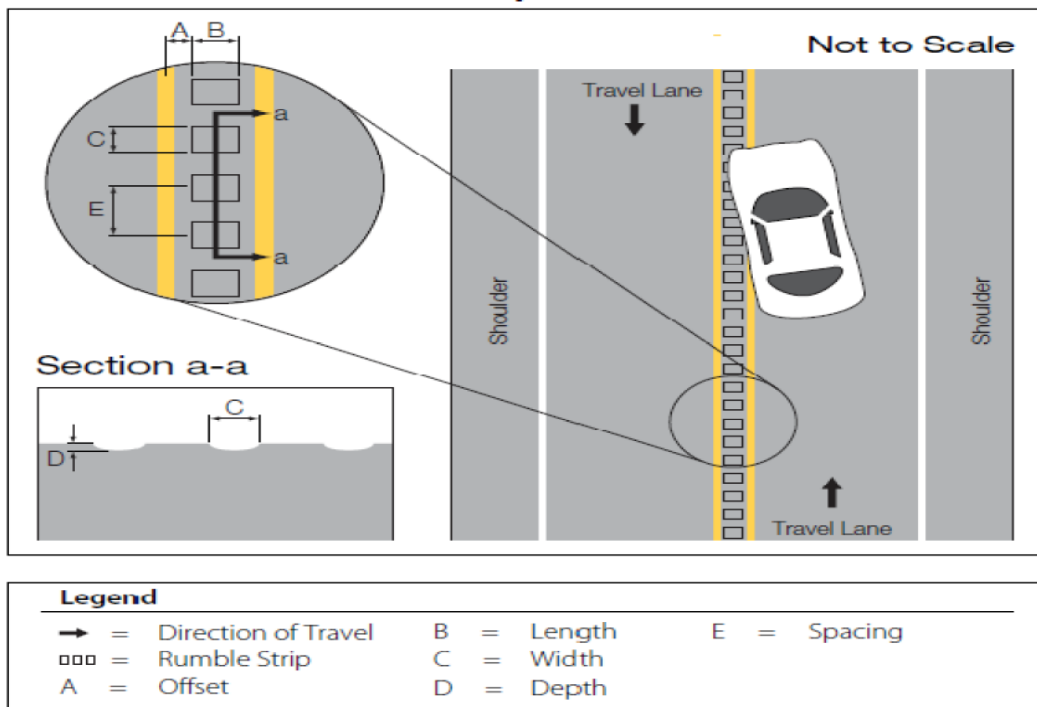


Figure 2.2: Illustration of rumble strip dimensions (Himes et al., 2017)

Since there is no national standard of rumble strip dimensions, standard dimensions can vary from state to state. Himes et al. (2017) documented all standard dimensions of shoulder and centerline rumble strips from each state and presented average dimensions of width, length, depth, and spacing, as shown in Table 2.2.

Table 2.2: National Average Dimension (in Inches) for Shoulder Rumble Strips (SRS) and Centerline Rumble Strips (CLRS) (Himes et al. 2017)

| TYPE | WIDTH (C) | LENGTH (B) | DEPTH (D) | SPACING (E) |
|-------------------------|------------------|-------------------|------------------|--------------------|
| Traditional SRS | 7 | 16 | 0.5 to 0.625 | 12 |
| Traditional CLRS | 7 | 12 or 16 | 0.5 | 12 |

Most agencies follow different methods to prepare existing rumble strips prior to overlay (to avoid any reflection cracking on the new pavement layer) and to re-install the rumble strips after completing the pavement overlay based on field experience with no research to support these methods (Donnell et al. 2014). CLRS installation for new construction, reconstruction, or resurfacing are usually done following a systematic approach based on pavement condition, posted speed limit, and lane/pavement width, while the contractor follows methods to ensure that pavement performance and quality are not reduced by milling to prevent resurfacing in the near future (Himes et al. 2017). According to several agencies, application of CLRS may also happen on an existing pavement section if: i) the pavement meets the “good condition” requirements, ii) the pavement is thick enough to avoid any permanent damage during the installation of the rumble strip; and iii) no pavement maintenance is planned within the next 2-3 years (Himes et al. 2017). ODOT Pavement Service Unit also has a list of recommendations within their guidelines for CLRS installations (Timothy Earnest and Justin Moderie (personal communication, October 19, 2018)). These recommendations are given in the next section (Section 2.2.1.1). CLRS installation decisions are generally based on an agreement between the Traffic, Roadway, and Pavements divisions at ODOT. Consultation with the Districts is also required before making the CLRS installation decisions.

Current systematic installation selection criteria, according to the literature, focus mostly on the condition of the pavement across all states. The existing pavement condition is primarily considered for CLRS construction by agencies because of the potential for increasing pavement deterioration (Himes et al. 2017). Most DOTs require the pavement to be in good condition, the analysis of which relies mainly on the DOTs’ maintenance and district offices’ expertise. While CLRS implementation policies and strategies related to pavement conditions have been consistently developed by state agencies, the argument on the placement location of CLRS related to longitudinal joints varies (Himes et al. 2017). It is well-known that the longitudinal joints are weak spots with lower densities on an asphalt-surfaced pavement and can seriously impact pavement longevity. Milling a CLRS across a longitudinal joint could accelerate pavement deterioration and allow water to infiltrate the pavement foundation (subgrade), causing accelerated structural damage. Although most state DOTs try to avoid CLRS installation on the longitudinal joints, limited road width might require the installation of CLRS on a construction joint (Himes et al. 2017).

2.2.1.1 Oregon Department of Transportation (ODOT)

Centerline rumble strips are commonly used throughout the state of Oregon as a safety countermeasure. According to the 2019 ODOT Pavement Design Guide, CLRS installed on dense-graded pavement has a low risk of expected failure for pavements with good to very good pavement condition (pavement condition rating of 76 out of 100, or better). CLRS can be installed on fair or lower condition pavements in Oregon (pavement condition rating for fair condition ranging from 50 to 75), but should be consulted with ODOT Pavement Service Unit, as there is the potential for higher risk of failure (ODOT, 2019b). Dimensions and geometry of the most common CLRS for rural highways in Oregon (ODOT DET 4556 details) are shown in Figure 2.3 (ODOT, 2019a). If there is not enough room in the middle of the lane, the length of the rumble strip can be decreased to 8 inches (ODOT DET 4557).

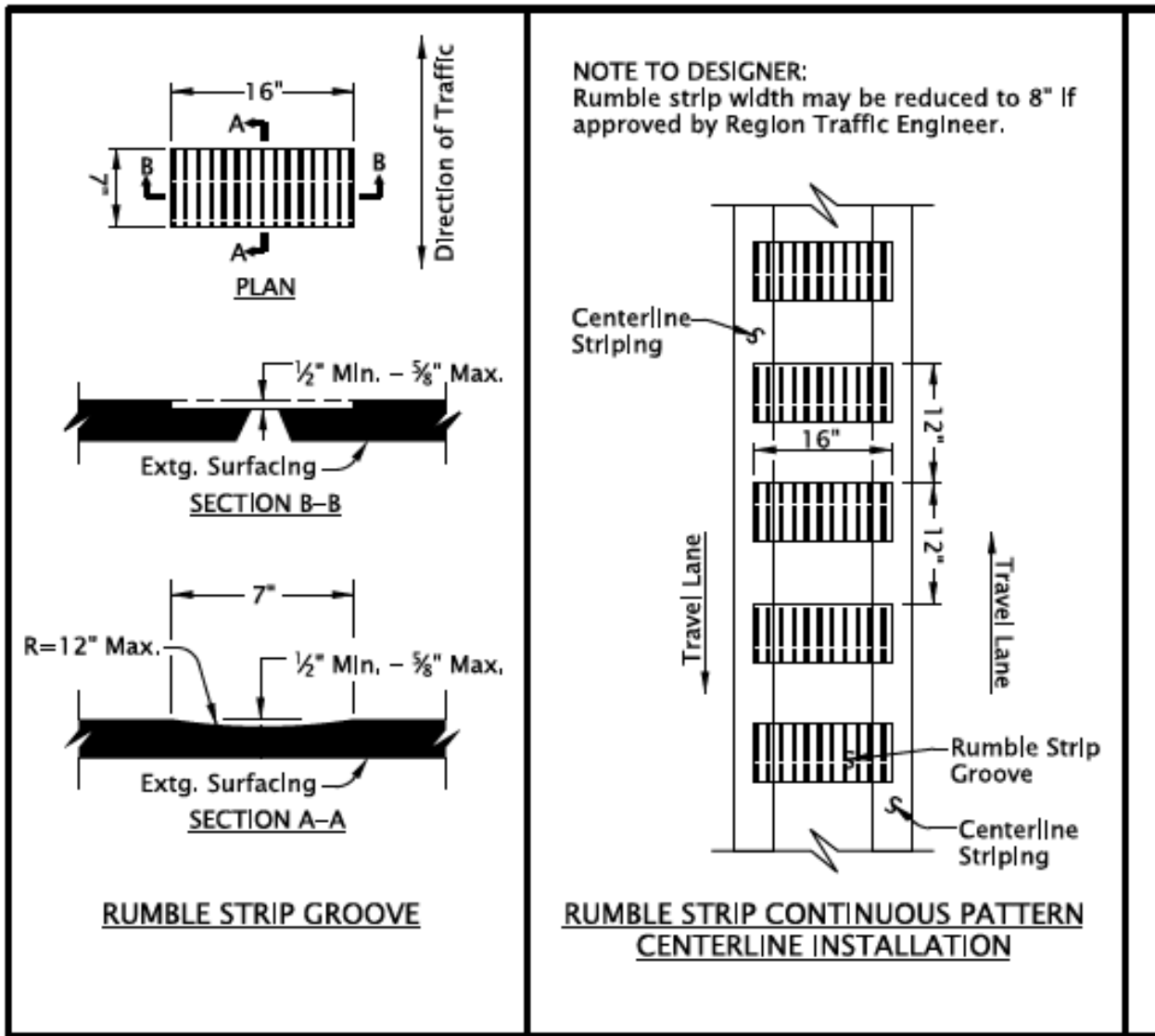


Figure 2.3: ODOT DET 4556 Rural Highway CLRS dimensions and geometry

ODOT's current dimensions (width, spacing, length, and depth) are all within the national averages (as shown in Table 2.2). ODOT Pavement Service Unit has the following recommendations within their guidelines for CLRS installations (Timothy Earnest and Justin Moderie (personal communication, October 19, 2018)).

Dense-Graded Pavements

- CLRS installed in a dense-graded pavement which is rated in good to very good condition (76 out of 100, or better) has a low risk of expected failures.
- Dense-graded pavements in a fair or lower condition (0 to 75 out of 100) have a higher risk of failure, and the ODOT Pavement Services Unit should be contacted early in the design phase to evaluate the potential impacts on these pavements. [Note that fair pavements may have a deteriorated longitudinal joint, which could require some additional work.]
- At elevations above 2500' in the Cascade Mountains, CLRS should only be placed on the dense pavement, which is 5 years old or less and in good or better (76 – 100) condition. If CLRS is installed in the pavement that does not meet these criteria, then a chip seal should be applied over the rumble strips for a minimum width of 2'.
- If CLRS are placed in a dense pavement that has been chip sealed, then a chip seal should be applied over the rumble strips for a minimum width of 2'.
- If CLRS are being installed over a deteriorated longitudinal joint, it is recommended to fog seal the CLRS and the joint.
- CLRS are not recommended in thin lifts of dense-graded pavement (less than or equal to 1.5" thick).
- All dense-graded pavements older than 2 years should be fog sealed.
- It should be noted that there is an issue with pavement marking materials adhering to fog seals. Paint has to be applied multiple times, and it typically takes 2 years before urethane will adhere.

Open-Graded Pavements

- There is a moderate risk when installing CLRS on an unsealed, open-graded pavement. The CLRS may not last due to raveling.
- CLRS should not be installed on sealed open-graded pavements. There is a high risk for pavement deterioration and failure.

Emulsified Asphalt Concrete (EAC) Pavements

- Regardless of condition, it is not recommended to install CLRS in an EAC pavement due to a high risk of early failure. The cost and safety impacts of pavement failure likely outweigh the safety benefit gained on these typically low-volume highways.
- Portland Cement Concrete (PCC)
- CLRS can be installed into good or better PCC pavements provided that the centerline joint is cleaned and resealed, and only if the CLRS are intended to be permanent.

ODOT's pavement services recommended not to install CLRS on thin lift dense-graded pavements (pavements ≤ 1.5 inches thick) (ODOT, 2019b). No explanation or research was provided to explain why CLRS is not recommended for dense-graded thin lift pavements in Oregon. However, intuitively, the concern is that a milled CLRS on a new thin lift pavement would cause significant damage and undermine the lifespan of the lift and underlying road condition. Sufficient layer thickness to be able to install the CLRS without damaging the new lift and the bond between the new and the existing pavement layers is probably the major reasoning with regard to this recommendation. They also recommended fog sealing for CLRS that was installed on dense-graded pavements older than 2 years (ODOT, 2019b). ODOT's current installation criteria for CLRS depend mainly on the condition of the pavement, just like most other agencies. Existing recommendations on CLRS for ODOT are based on field experience and the current, limited literature.

Sinusoidal CLRSs are not commonly used in Oregon. However, a research study conducted by Kalathas et al. (2019) suggested that sinusoidal CLRS can create a significant reduction in noise levels impacting the residential areas near the roadway. According to Staats et al. (2020), although the sinusoidal CLRS significantly reduces noise levels for the surrounding residential areas, they still create the required vibrations and noise in the vehicles to alert the drivers.

2.2.1.2 Other States

Installation criteria and policy developed by other states differ from ODOT depending on surface treatment, lift thickness and age of pavement. Donnell et al. (2014) conducted a transportation agency survey of all 50 agencies to understand the current installation criteria and policy for CLRS. The major findings of this survey are summarized as follows:

- Rumble strip installation policy for thin overlays exist for Kansas, Maine, New Hampshire, New York, South Dakota, and Washington State. They have the most detailed recommendations regarding the application.
- New Hampshire allows milled CLRS to be installed on asphalt pavement layers at least 1.25 inches thick with a CLRS groove depth of 0.5 inches. If a pavement overlay is going to be constructed over an existing rumble strip, the existing

rumble strip should be milled and inlayed before the thin pavement overlay is constructed.

- For thin asphalt pavement overlays (preferred 1-inch), state of New York mills out 2-inch deep and 2 feet wide over the centerline joint if the centerline is deemed inadequate for implementation of milled CLRS. The new CLRS is installed after the milled area is cleaned, tacked, and hot-mix asphalt is inlayed. This process can also be followed with 0.75-inch-thick chip seals, micro-surfacing, and asphalt overlays.
- South Dakota allows for the application of one asphalt surface treatment over the existing rumble strip pattern. If additional asphalt surface treatments are later required, then the rumble strip is fog sealed and re-installed/re-milled.
- Washington State mills existing rumble strips for chip seal overlays and requires at least 3-inch thickness to re-install milled rumble strips pattern on chip seal overlays. For hot-mix asphalt overlays, the existing rumble strip does not have to be milled out if the overlay thickness is 1.75-inches or greater. Also, lane configurations cannot require traffic to cross over the pre-existed rumble strip, as the underlying rumble strip will reflect to the surface layer.
- Pennsylvania has developed separate design-decision matrices for rumble strips. These matrices consider the type of rumble strip (center, edge, shoulder), type of overlay (hot-mix asphalt, micro-surfacing, chip seal, etc.), dimension, inlay materials, depth of rumble strip groove based on surface thickness, and whether existing rumble strips should be milled. These matrices were developed based on a literature review of best practices developed by evaluating the rumble strip installation decision-making processes followed by various state and other transportation agency stakeholders and state transportation agency surveys.

Other state agencies' rumble strip installation requirements in terms of dimension, geometry, and pavement condition are similar to ODOT's current designs. Although agencies agree on installing CLRS on pavements in good condition, the term "good condition" varies from agency to agency. The following summarizes the "good condition pavement" definition for some of the state agencies (Himes et al. 2017).

- Maine DOT: a pavement less than 5 years old with no signs of distress and a minimum surface thickness of 1.25 inches or a total depth of at least 3 inches.
- ConnDOT: a pavement less than 4 years old.
- LaDOT: a pavement installed within the last 10 years.
- NYSDOT: a pavement with no more than one longitudinal crack.
- Oregon DOT: A pavement condition rating ranging from 80 to 95 is called GOOD, while the VERY GOOD condition is from 96 to 100.

The list above exemplifies the definition variance of “good condition pavement” across agencies, of which there is no scientifically supported standard. State agencies do agree, however, that CLRS should only be installed on pavements in good condition.

2.2.2 Impact of Installation Methods on Benefits from Rumble Strips

The most common types of CLRS are milled into the pavement surface with a specialized diamond bit to form grooves in the pavement. Other installation methods of CLRS are rolled, raised, or some other experimental patterns. These other installation methods are usually seen in non-snowy climates and allow for flexibility with installation (FHWA, 2015a) (Hurwitz et al. 2019). This section will discuss CLRS installation methods and how they impact rumble strip benefits.

2.2.2.1 Rolled Rumble Strips

Rolled rumble strips, sometimes referred to as formed rumble strips, are introduced into the pavement surface with a steel pipe attached to a roller compactor drum while the asphalt is still hot and malleable (FHWA, 2011)(Guin et al. 2014). This makes rounded grooves for the rumble strip and is shown in Figure 2.4. This type of rumble strip creates less noise and is less expensive when compared to other rumble strip types (Corkle et al. 2001)(Guin et al. 2014). Although rolled rumble strips cost less, they can only be installed on new construction or reconstruction projects of a pavement surface before the pavement surface hardens (Corkle et al. 2001)(Guin et al. 2014).



Figure 2.4: Rolled or formed rumble strips (Richards & Saito, 2007)(Guin et al. 2014)

2.2.2.2 Milled Rumble Strips

Milled rumble strips are the most common type of CLRS installed throughout the United States (Figure 2.5). CLRS milling operations can be performed anytime for any scale project (FHWA, 2011). Maintenance for milled rumble strips is minimal. They have also shown negligible effects from snow plowing, according to a study conducted by FHWA (2015a). However, in Oregon, it was observed that some plow blades may drop into the

rumble strip grooves and damage either the plow blade or the rumble strips. As previously stated, milled rumble strips have been known to help direct drivers in heavy rain and snow events. Complications caused by normal crowned (standard centerline cross sloped) pavements present issues for attaining the required depth for milled rumble strips. To avoid these issues, a vertical alignment guide should be equipped to the milling machine to position rumbles with the horizontal level, and not milled at an angle due to the crown of the road. This may result in one side of the rumble deeper than the other, however, agencies need to specify the maximum and minimum depth, how they will be measured, and acceptable tolerances. Due to this installation method, agencies should expect that rumble strip depth could change transversely across the roadway (FHWA, 2011). A major key to the successful installation of milled rumble strips is to have a state agency inspector and contractor present during the milling operation (FHWA, 2015a).



Figure 2.5: Examples of milled rumble strips from the Oregon State University test section

2.2.2.3 Raised Rumble Strips

Raised rumble strips can be installed onto new or existing pavements with epoxy and are either rounded or rectangular ranging from 2-12 inches wide (FHWA, 2015a). Examples of different types of raised rumble strips are shown in Figure 2.6. Raised rumble strips are used mainly in warmer climates with no snowfall since snow plowing can damage the rumble strip and make them less effective (FHWA, 2015a). In Oregon, raised rumble strips are not commonly used. However, raised pavement markings are common and generally installed on a milled groove to avoid any snowplow damage. As climate plays an important role in the performance of raised rumble strips, so does deciding on the proper product to use. Raised rumble strips comprised of raised pavement markers that can improve visibility on the roadway but may be less effective in warning the driver through noise and vibration (FHWA, 2011). Lastly, another critical factor in the performance of raised rumble strips is the proper adhesion of the pavement markings to the surface (FHWA, 2015b). If the raised rumble strip does not properly adhere to the pavement surface, all the safety benefits become insignificant.



Figure 2.6: Raised rumble strips and pavement markers (Cottingham, 2020) (Raised Pavement Markers, 2020)

2.2.2.4 Experimental Designs

State agencies have modified and experimented with multiple rumble strip designs, mainly to reduce noise levels in urban areas (FHWA, 2015). According to the literature, no experimental rumble strip designs have looked at reducing rumble strip related pavement deterioration. Regarding noise level reduction, sinusoidal rumble strips have gained momentum (Figure 2.7). Sinusoidal rumble strips are continuously milled into the pavement following a sinusoidal wave pattern and do not have spacing in between strips compared to traditional milled rumble strips (Hurwitz et al. 2019). This technology is designed to decrease the amount of exterior noise generated when struck by a tire while providing tactics (internal noise and vibration) to alert the driver, much like milled rumble strips (Himes et al. 2017) (Hurwitz et al. 2019). There is debate regarding the efficacy of sinusoidal rumble strips providing sufficient internal noise to alert distracted or drowsy drivers (Kalathas et al., 2019; FHWA, 2015b). WSDOT is currently testing several experimental rumble strip designs to reduce noise levels by increasing spacing between strips and decreasing the groove depth of the rumble strip (Olsen, et al., 2012) (FHWA, 2015b).



Figure 2.7: Sinusoidal rumble strip design from MNDOT optimization study (Terhaar et al. 2016)

2.3 FACTORS CONTROLLING THE LONG-TERM PERFORMANCE OF CLRS

The literature has no significant quantitative data on what controls the long-term performance of pavements with CLRS (Datta et al. 2012) (Smadi & Hawkins, 2016). The majority of the research studies identifying the impacts of installing rumble strips on pavement deterioration are subjective visual field assessments (Himes et al. 2017). Studies conducted in Colorado and Texas found that rumble strips have minimal to no significant effect on pavement deterioration or pavement life (Datta et al. 2012). A 2015 survey explored issues related to rumble strip installation and revealed that 17 DOTs rated pavement deterioration as an important issue, while 18 DOTs rated it as not important (Smadi & Hawkins, 2016). Although there is limited information available on how CLRS affects the pavement deterioration mechanism, the following sections present the potential factors controlling the long-term performance of CLRS.

2.3.1 Climate

It is known that climate has a direct impact on asphalt pavement performance and properties. Temperature, humidity, freeze and thaw cycles, and precipitation all have an influence on pavement deterioration and pavement life, with varying degrees of impact. Precipitation or rainwater on the pavement surface can have serious negative effects on pavement deterioration and long-term performance. Also, the temperature is known in the literature as one of the main factors in controlling the long-term performance of asphalt-surfaced pavements. In this literature review, freeze and thaw cycles, low temperature cracking resistance, and moisture susceptibility are the three major factors that are expected to affect the performance of rumble strips on roadways in Oregon.

2.3.1.1 Low-Temperature Cracking Resistance

Cold weather, with temperatures significantly below freezing, is responsible for low-temperature cracking, which leads to accelerated deterioration of asphalt pavements. Rapid changes in surface temperature, with a surface and bottom temperature difference of more than 9.5°C (15°F), can result in the development of cracks due to differential thermal expansion and contraction in the pavement layer (Voigt, 2002) (Ahmad & Khawaja, 2018). These cracks usually propagate in the shortest direction, which for asphalt pavements is the transverse direction of the roadway, because the stress in that direction is greater than the tensile strength of the pavement material. Milled CLRS are vulnerable to this type of low-temperature cracking because of potential micro-cracks formed during the application of the rumble strip. It is hypothesized that in cold weather, the micro-cracks introduced to the rumble strip will connect and propagate through the CLRS, accelerating pavement deterioration. Although Oregon usually has relatively mild weather in highly populated regions, not a lot of cold weather days throughout the year, significant temperature fluctuations can still be experienced on a given day. Significant temperature fluctuations in a given day have been shown to aid in the development of low-temperature cracking (Scherozman, 1991) (Ksaibati & Erickson, 1998). Since milled CLRS are the most common application method in Oregon, daily temperature cycling in colder regions should be of great concern for CLRS performance on asphalt pavements.

Figure 2.8 displays typical longitudinal and transverse cracking in asphalt pavement at the rumble strips.

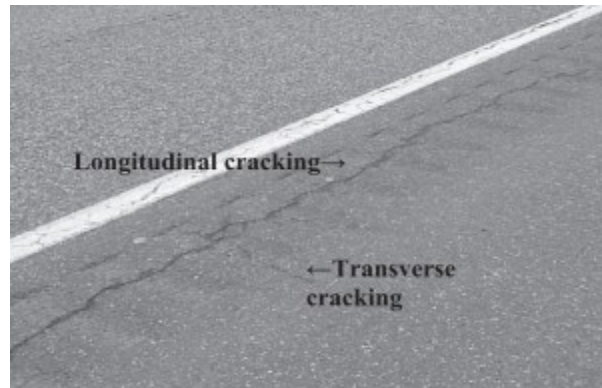


Figure 2.8: Transverse and longitudinal cracking at milled rumble strips (Coffey and Park, 2016)

2.3.1.2 Hydro Static Damage from Rainwater

Water is known to have negative effects on asphalt pavements and cause deterioration. The milling process to create rumble strips on the pavement's surface may result in micro-cracks that may allow water to infiltrate through the surface lift into subsequent pavement lifts (Datta et al. 2012). This would accelerate stripping within the pavement at the CLRS. Water entering between the top and the underlying lift can also damage the bond between the two lifts and result in delamination. This increases tensile strains at the bottom of the asphalt layer, which can cause premature bottom-up fatigue cracking and ultimately lead to early pavement failure (Coleri et al. 2020). Typical fatigue cracking at milled rumble strip locations is shown in Figure 2.9.



Figure 2.9: Fatigue cracking at milled rumble strips (Coffey and Park, 2016)

ODOT conducted research at four paving sites in 2009 to identify the mechanisms of moisture infiltration in the pavements and the resulting pavement damage. One method of water infiltration identified was through surface infiltration into the pavement structure

“through or between lifts (layers) of dense-graded material” (Scholz and Rajendran, 2009). The primary pavement damage observed at the sites was the rutting of the pavement structure caused by the combination of moisture infiltration and traffic loading. Milling CLRS could be a factor initiating increased moisture infiltration of the layers and subsequently cracking of the pavement (in addition to observed rutting). Also, ODOT stated that cold milling (milling conducted after construction at ambient temperatures) at the sites could have disrupted the bond between the asphalt binder and the newly exposed aggregates. These were identified as critical locations of moisture infiltration between layers, and milling CLRS has the potential to induce similar effects (Scholz and Rajendran, 2009).

Other theories about milled rumble strips’ increasing surface area of exposed pavement have raised concern with regard to accelerated pavement deterioration due to water accumulation and freeze and thaw damage (Watson et al. 2008)(Guin et al. 2014). However, vibration from wheels passing by the rumble strips may remove water, ice, and debris from the grooves, disproving the previous hypothesis (Carlson & Miles, 2003)(Guin et al. 2014). This mechanism to remove water out of the milled rumble strip grooves relies on the significant traffic flow of trucks (FHWA, 1999) (FHWA, 2011)(Guin et al. 2014). Standing water in rumble strips has been noted by state agencies to have no effect on accelerated pavement deterioration (Bahar & Parkhill, 2005)(Guin et al. 2014), although no quantitative data was available.

2.3.1.3 Freeze-Thaw Cycle

Water that infiltrates or collects in CLRS can experience freeze-thaw cycles in cold weather that expand water within the micro-cracks along the rumble strip or in the asphalt layer, potentially leading to increased cracking damage (FHWA, 1999)(Guin et al. 2014). Oregon DOT responded to a survey in 1999 and indicated that water would gather in the rumble after a rain event and, upon encountering cold weather, would freeze, creating a trench of ice (FHWA, 1999)(Guin et al. 2014). The Missouri DOT, on the other hand, has mentioned that most locations remain in good condition after several freeze-thaw cycles (Himes et al. 2017). The majority of the literature on the freeze-thaw cycle effects of CLRS is anecdotal, with little to no scientific data to support these theories. Although freeze and thaw cycles were proven to directly affect the cracking resistance of concrete, the impact on asphalt-based materials is expected to be less due to the more elastic and ductile nature of asphalt concrete.

In 2012, there was a short-term observation study conducted by Michigan DOT trying to capture this phenomenon. Regions with different climatic conditions were selected to determine how the difference in the number of freeze-thaw cycles could affect the performance of rumble strip installed pavements on non-freeway roads (Datta et al., 2012). Climate information for both Michigan and Oregon are available under these links: [Michigan climate](#) (WorldData, n.d.-a) versus [Oregon climate](#) (WorldData, n.d.). In the study, the rate of crack propagation between road segments with and without CLRS were compared (Datta et al., 2012). Table 2.3 summarizes the rate of crack propagation for each region from the two-year study (Datta et al., 2012). The study ultimately determined that there was not a statistically significant difference in crack propagation

between the control sections (without CLRS) and sections with installed CLRS and concluded that CLRS did not adversely impact pavement performance in the short-term (Datta et al., 2012). However, with this being the only scientific data looking at CLRS performance and performance data available for only two years, more research is needed to confirm the findings from this study.

Table 2.3: Michigan DOT Two-Year Study of CLRS Rate of Crack Propagation Data (Datta et al. 2012)

| Region | Increase in cracks per 0.1 mile during a two-year period | | | | t-test statistic | p-value | significant difference? |
|------------|--|--------------------|------------------|--------------------|------------------|---------|-------------------------|
| | Rumble strip Sections | | Control sections | | | | |
| | Mean | Standard Deviation | Mean | Standard Deviation | | | |
| I | 3.04 | 4.32 | 3.26 | 5.77 | -0.82 | 0.41 | No |
| II | 3.30 | 5.07 | 3.51 | 5.40 | -0.78 | 0.44 | No |
| III | 4.57 | 5.14 | 4.70 | 4.92 | -0.44 | 0.66 | No |

2.3.2 Asphalt Mixture Type – Emulsified Asphalt versus Conventional Asphalt

Emulsified Asphalt Concrete (EAC), also known as “Cold Mix”, has been commonly used for maintenance and rehabilitation on rural roads in Oregon. Emulsified asphalt emulsion contains asphalt, water, and an emulsifying agent (surfactant/soap), which reduces the viscosity of the binder below that of conventional asphalt binder at ambient temperatures. This low viscosity at ambient temperatures allows emulsified asphalt to be mixed with graded aggregates without any heating, which consequently lowers energy consumption and emissions [when compared with conventional hot mix asphalt (HMA)] (Huang & Di Benedetto, 2015). Energy savings of 95% can be achieved when using EAC compared to conventional asphalt (Chappat, 2003) (Chehovits & Galehouse, 2010)(Goyer et al. 2012)(Fang et al. 2016). Another benefit of EAC is the ability to retain its flexibility at high temperatures (also known as “self-healing capability”). EAC is also an excellent choice to control reflective cracking, as Emulsified Asphalt can withstand 25% more tensile strain than conventional HMA (ODOT, 2019b). ODOT typically uses EAC in Eastern Oregon, where the climatic conditions take advantage of these benefits. However, it is important to understand the factors controlling the benefits of EAC, as they become drawbacks in some climatic conditions.

A major drawback of EAC is the need to have it cured completely before opening the road to traffic. The water in the EAC needs to completely evaporate from the emulsion to promote adhesion between the binder and aggregate. This process can take several weeks to achieve full strength (Nageim et al. 2012)(Fang et al. 2016). Thus, ODOT recommends the use of EAC only in Eastern Oregon (hot and dry climate compared to the rest of Oregon) to be able to reach reasonable curing times during construction (ODOT, 2019b). According to the Oregon Pavement Design Guide, EAC can only be placed on low-traffic roads with less than 2,500 average daily traffic due to the long curing time of the material. Another important yet often overlooked factor controlling the performance of EAC is proper material storage. (Davis, 2013). Due to the complex nature of asphalt emulsions, improper storage of these materials can have severe

negative impacts on their performance. From a temperature standpoint, in order to ensure that the water and the emulsifying agent stay bonded, a minimum temperature of 50°F is required or the emulsion becomes susceptible to possible freezing at low temperatures. These factors are therefore of paramount importance when considering the long-term performance of EAC.

According to a comparison study conducted in India on EAC and HMA, EAC had about 25% higher air voids than the HMA after construction (Ghale & Pataskar, 2017). Higher air-void content of EAC can result in increased moisture damage due to higher permeability and reduced strength, ultimately reducing long-term structural durability (Al-Busaltan et al. 2012) (Needham, 1996) (Thanaya, 2003) (Cheng, 2013) (Khalid & Monney, 2009)(Fang et al. 2016). These drawbacks raised serious concerns regarding the installation of rumble strips on EAC. In fact, ODOT’s Pavement Design Guide recommends against installing rumble strips on existing EAC (ODOT, 2019b).

2.3.3 The Thickness of the Surface Layer

As discussed in the previous sections, milled rumble strip installation is the most common method followed to install rumble strips on pavements. Because the rumble strip milling process reduces surface layer thickness, a minimum layer thickness needs to be specified for all pavement types and treatments (FHWA, 2016). Overlay thickness needs to exceed the depth of the rumble strip to avoid exposure of underlying pavement layers (FHWA, 2016). Damaging the underlying pavement layers during the rumble strip installation can compromise the integrity of the surface overlay, creating a fast-track path for moisture to infiltrate and accelerate stripping in the pavement structure (FHWA, 2016). Water accumulating between the overlay and the underlying layer can also result in delamination. Delamination of the two layers increases tensile strains at the bottom of the asphalt layer, which can cause premature bottom-up fatigue cracking and ultimately lead to early pavement failure (Coleri et al. 2020). FHWA stated that most state agencies require a minimum pavement thickness for rumble strip installation (FHWA, 2016). Table 2.4 outlines the minimum recommended pavement thickness for rumble strip installation of five state agencies.

Table 2.4: Recommended Minimum Pavement Thickness for Rumble Strip Installation (FHWA, 2015a)

| State | Recommended Minimum Pavement Thickness |
|---------------------|--|
| Missouri | 1.75” |
| New York | 2.5” |
| Pennsylvania | Less than 1 year old – 1.5” Older-greater than 2.5” |
| Texas | 2.5” |
| Washington | 3” |
| Oregon ¹ | 1.5” |

¹ Idaho and California do not have any recommended standard minimum thickness, per the FHWA report.

2.3.4 Roadway Roughness and Related Excessive Dynamic Loads

As previously mentioned, the installation of rumble strips on good condition pavement is important to avoid any rumble strip-related pavement cracking on roads. Smadi and Hawkins (2016) concluded that heavy traffic and excessive dynamic loads on rumble strips do not cause any cracking failures on roads with fair, good, and very good conditions (pavement condition rating ranging from 50 to 100). Coffee and Park (2016) confirmed that the impact of traffic volume on rumble strip performance is minimal. However, only observational studies have been performed to characterize pavement deterioration resulting from rumble strips. There are also no studies available in the literature evaluating the impact of rumble strip roughness on cracking performance.

In Oregon, mountainous road failures potentially related to CLRS placement are of growing concern. Vehicles traveling on mountain roads, especially large semi-trucks, are more likely to unintentionally drive over rumble strips due to the curvy nature of the roadway. Therefore, the CLRS on these mountain roadway sections could be experiencing much higher numbers of heavy dynamic truckloads than CLRS on less curvy roadway sections or lower elevations. The common use of studded tires and chains by vehicles traveling on mountain roads might be another reason for CLRS-related cracking. Although literature regarding the trajectory of semi-trucks on curvy mountain roadway sections is limited, there have been research studies conducted regarding the trajectory of personal vehicles. These studies have confirmed that drivers are more likely to unintentionally cross into opposing lanes of traffic on curved roads, thus impacting CLRS. Xu et al. (2018) concluded that *“occupation of the oncoming lane at bends is a common driving behavior on two-lane mountain roads, especially at small-radius curves”*. Figure 2.10 from Xu et al. (2018) shows trajectory transection rates (TTRs), a ratio of pavement width occupied by the driver to the total width of the pavement at a given bend, versus curve radius.

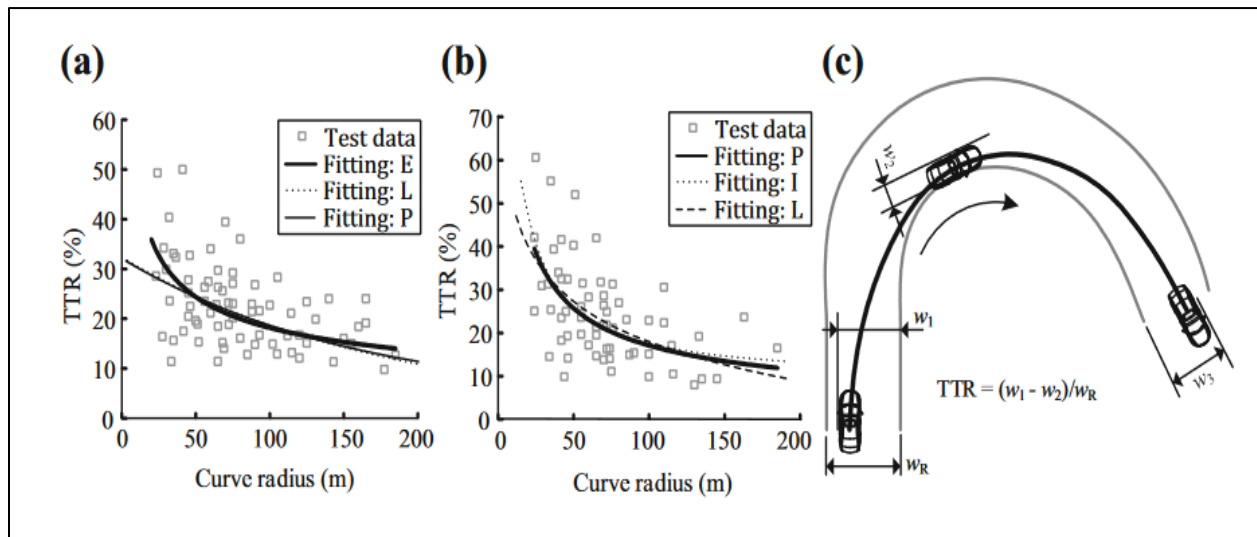


Figure 2.10: The relationship between TTR and curve radius (a) TTR with respect to curve radius for left bend (b) TTR with respect to curve radius for right bend (c) illustration for TTR (Xu et al. 2018)

In summary, the data from Figure 2.10 for personal vehicles concludes that drivers would cover more pavement width on bends with smaller curve radii (sharper curves). Due to the larger length of semi-trucks and, consequently, wider turning radius compared to personal vehicles (as shown in Figure 2.11 below from the Traffic Engineering Handbook), the previously mentioned results would likely be amplified when observing semi-trucks on curvy roads. Given this information, it could be hypothesized that CLRS on curvy mountainous roadway sections are more frequently impacted by high dynamic loads generated by semi-trucks crossing into opposing lanes due to sharp curves within mountain roadways. This hypothesis requires scientific research to prove its validity.

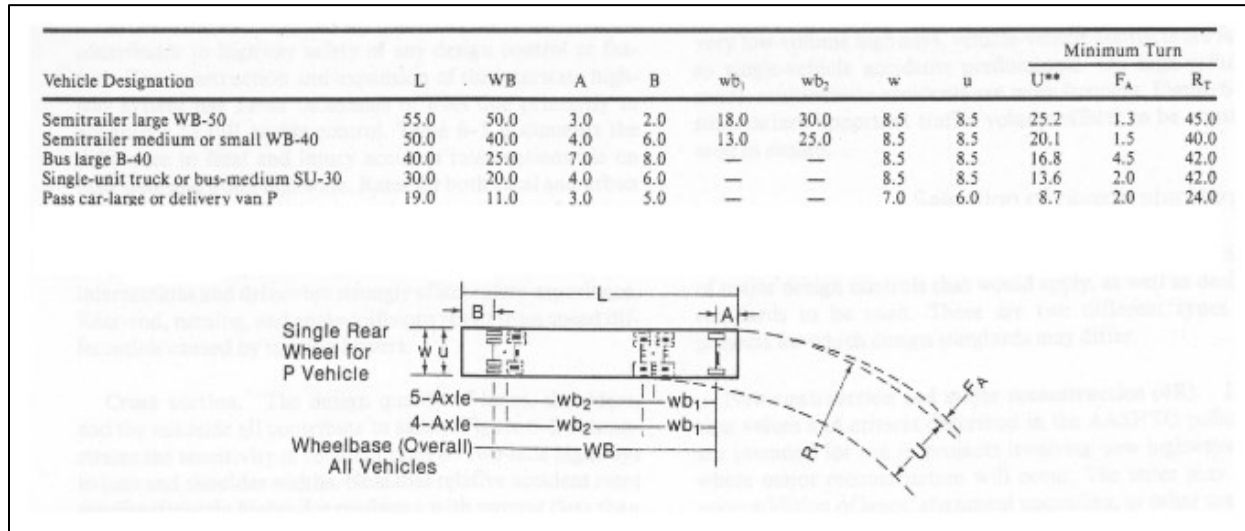


Figure 2.11: Required turning radius per vehicle type (Institute of Transportation Engineers, 2016)

With heavy dynamic truck loads being a potential threat to the long-term performance of CLRS, especially on mountainous roadways compared to less curvy roadways, the impact of high vibrations (vertical movement of the truck's axle) caused by the loading of the rumble strip with high surface roughness may cause accelerated deterioration of the pavement surface. Although there is no literature regarding pavement deterioration due to heavy dynamic loads on rumble strips, there have been numerous studies that correlate roadway roughness to pavement damage. Cebon (1986) determined that some portions of a roadway experience loads up to 50% higher than the gross vehicle weight due to the speed of the vehicle and roughness of the roadway. Given the correlation between roadway roughness and high dynamic loading, it seems rational to investigate the damage implications of heavy trucks on rough CLRS surfaces, especially in mountainous roadway sections (Amjadi et al., 2014).

2.3.5 Location of the CLRS relative to the Longitudinal Joint

When hot-mix asphalt (HMA) is placed next to the previously constructed lane (cold mat) during construction, a longitudinal joint occurs between the newly constructed lane and the old one. Due to the particles in the HMA bouncing back from the stiff-cold mat under heavy compactor loads during compaction, proper compaction around the joint generally cannot be achieved, and the

density of the longitudinal joint is generally lower than the constructed lane. For this reason, longitudinal joints are accepted to be weaker spots on the pavements that are more vulnerable to cracking and permanent deformation. Because of the inherent weakness, it is generally recommended to leave an offset between the CLRS and the joint. However, CLRS sometimes needs to be constructed on longitudinal joints when the lane is not wide enough to allow the installation of the CLRS with an offset. (FHWA, 2015a). However, according to surveys and interviews of many state agencies, longitudinal joint location is not a critical factor for the installation of milled CLRS unless the joint is already in poor condition (FHWA, 2015a). Alternative milling strategies to limit the impact on the joint when installing CLRS also exist (Torbic et al., 2009). For instance, Nebraska DOT mills two rumble strips on each side of the joint with a gap between them, while Michigan DOT uses a CLRS pattern that skips every third rumble strip (See Figure 2.12) (FHWA, 2015a). Other states have tried offsetting CLRS on one side or the other of the joint to reduce the impact on the longitudinal joint (FHWA, 2015a).

An anecdotal field study conducted for the Kentucky Transportation Cabinet noted that pavement deterioration from CLRS along centerline joints was observed for two locations in their study (Smadi & Hawkins, 2016). However, the pavement was already in poor condition before installation, and a retrofit CLRS application was used during the study (Smadi & Hawkins, 2016). No significant issues arose from other locations of the study, with good condition pavement with the retrofit application (Smadi & Hawkins, 2016). Illinois, Iowa, Nebraska, Nevada, and Washington have all experienced issues related to CLRS on longitudinal joints, but all hypotheses for failure are related to previously mentioned factors: poor pavement condition or flawed construction practices (WSDOT, 2022)(Guin et al. 2014). As there is no strong scientific pavement performance data to corroborate these hypotheses, it is difficult to conclude that CLRS installation near longitudinal joints has an impact on pavement deterioration.

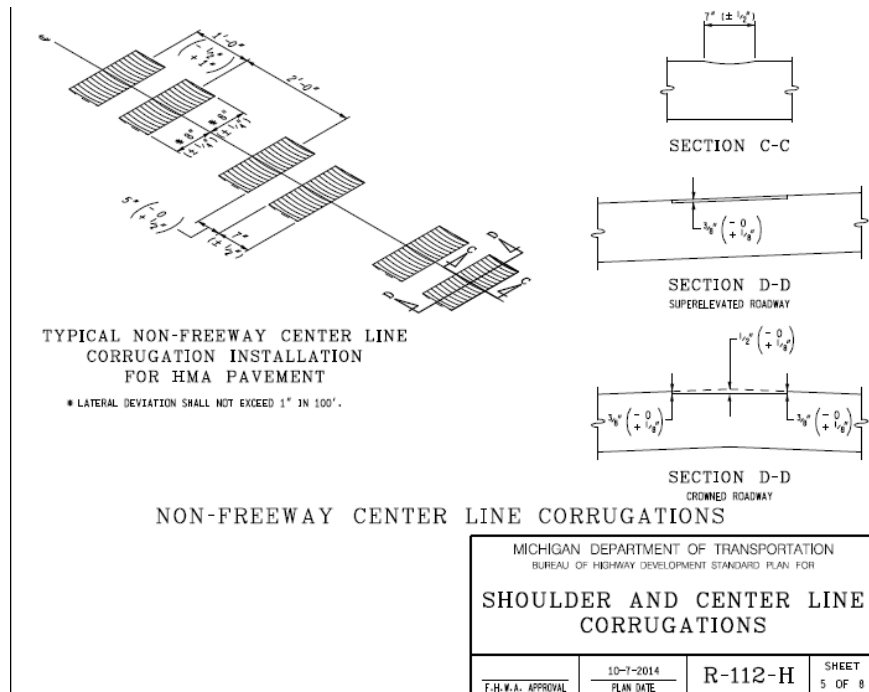


Figure 2.12: MDOT CLRS design for non-freeway roads (MDOT, 2010)

2.3.6 Age of Asphalt Surfacing

As the asphalt binder ages, it loses maltenes due to oxidation and volatilization, reducing the ductility of the asphalt concrete material, which leads to cracking on the pavement surface. The literature predominantly cites pavement condition, rather than pavement age, as an important factor when installing rumble strips on existing pavements (FHWA, 2015a). As mentioned in an earlier section, the term pavement condition lacks standardization across state agencies, though asphalt age strongly contributes to any denotation of pavement condition. Milling rumble strips into older (aged) asphalt-surfaced pavements could be creating more microcracks in the asphalt layer, compared to rumble strip installation on fresh (new) asphalt surfaces. It should be noted that asphalt binder type and the recycled asphalt content (RAP) also play an important role in the aging process. Asphalt mixtures with higher RAP contents and softer binders lose their ductility at a much slower rate than mixtures with lower RAP and stiffer binders. However, since the initial ductility of the mixtures with low RAP contents and softer binders will be significantly higher, they should be less likely to crack due to the installation of rumble strips. However, it should be noted that the density of the asphalt layer (air-void content) also plays an important role in ductility and cracking resistance (Coleri et al., 2017). A 1% increase in density can create a 33.8% to 66.3% improvement in the long-term fatigue cracking and rutting performance of asphalt mixtures (Tran et al., 2016), respectively.

According to FHWA, some agencies do not re-install rumble strips immediately after resurfacing and sometimes wait for area-wide installation (Donnell et al. 2014). This delay could lead to accelerated deterioration due to microcracking from rumble strip installation on older pavements. However, there is little to no scientific proof that the age of the pavement is leading to pavement cracking failure from CLRS and has more to do with the overall condition of the pavement. Michigan DOT had few issues when installing milled rumble strips on older asphalt pavements in fair or better condition (FHWA, 2016). This is all still very anecdotal, with very limited scientific data quantifying how the long-term performance of CLRS depends on asphalt age.

2.3.7 Surface Treatments

Rumble strips have been installed with many different types of surface treatments (fog seal, chip seal, micro-surfacing, thin hot-mix overlays, etc.) over the years, with each strategy having its own benefits and drawbacks. This section will try to uncover the pros and cons of different surface treatments related to the performance of CLRS.

2.3.7.1 Fog Seals

Fog Seals are light applications of a slow-setting emulsion, typically used to increase the flexibility of a previously aged asphalt surface. According to FHWA (2011), milled-in rumble strips with deterioration concerns can be covered with asphalt fog seals to reduce oxidation and moisture infiltration into succeeding pavement lifts (FHWA, 2011) (FHWA, 2016). The application of fog seals after the installation of milled rumble strips could prevent or decelerate the propagation of damage created by the introduction of “micro-cracks” from the highly aggressive nature of the milling process. This once commonly used strategy, however, has been discontinued by many States due to a lack of scientific validation of increased pavement life from applying fog seals over rumble strips

(FHWA, 2016). It is worth noting that thermoplastic materials sometimes used for pavement markings have been shown to be incompatible with fog seals (FHWA, 2016). For the reasons above, the use of fog seals on CLRS needs further scientific investigation to determine whether there is a significant benefit to applying this type of surface treatment strategy on CLRS.

2.3.7.2 Chip Seals

Chip sealing is the most commonly used surface treatment of all the different strategies for rumble strips. Chip sealing a roadway involves the application of a special protective wearing surface on an existing roadway, made typically from asphalt emulsion and graded crushed aggregates. Existing rumble strips that have been chip sealed exhibit a reduction in depth and cross-sectional area, but generally still retain the overall basic shape and functionality of the rumble strip design while the applied chip seal layer serves its function of reducing water infiltration into the pavement (FHWA, 2016)(Himes et al., 2017). According to ODOT Pavement Design Guide, chip seals are used over rumble strips to prevent accelerated deterioration from moisture, which can emerge in some pavement types that respond negatively to the aggressive action of milling rumble strips (ODOT, 2019).

Despite the common implementation of chip seals as a surface treatment for rumble strips, there is a lack of literature related to the effectiveness and durability of this treatment. The Nebraska Transportation Center conducted a study to determine the effectiveness of different milled rumble strip depths with applied chip seal surfaces. The study also evaluated the effectiveness of chip-sealed rumble strips in terms of alerting vehicle drivers. It was concluded that there is no significant difference in the efficacy of the rumble strip to alert drivers, provided the rumble strip was reduced no more than 1/8-inch depth after the application of the chip seal (Tufuor et al. 2017).

2.3.7.3 Micro-Surfacing and Ultra-Thin Asphalt Overlays

Micro-surfacing is a process similar to a slurry seal, typically the application of an asphaltic mixture consisting of asphalt emulsion, water, finely crushed aggregates, polymers, and chemical additives. The major difference between micro-surfacing and a slurry seal (or chip seal) is the curing mechanism. Micro-surfacing hardens quicker than a chip seal due to the presence of chemical additives in the mixture. Micro-surfacing and ultra-thin hot-mix asphalt overlays can fill in ruts and rumble strips on existing pavements (FHWA, 2016). Micro-surfacing is both cost-effective and efficient for reopening roadways to traffic after 2-3 hours of application. Micro-surfacing can also be applied in adverse weather conditions and requires minute energy levels to apply. According to FHWA, milled-in rumble strips can be installed into pavements previously treated with micro-surfacing or ultra-thin hot-mix asphalt overlay, without significant delamination occurring (FHWA, 2016). Whereas for chip seals, milled-in rumble strips should be installed before application of the surface treatment.

There are no research studies in the literature quantifying the performance benefits of using micro-surfacing or ultra-thin overlay surface treatments on pavements with CLRS.

According to research conducted by TXDOT, micro-surfacing can be installed with a minimum thickness of approximately 1.5 times the nominal maximum aggregate size of the asphalt mixture (West et al. 1996). In NCHRP Synthesis 411, the micro-surfacing thickness can be two to three times the size of the largest aggregate (Transportation Research Board, 2010). The most common thickness for a micro-surfacing treatment is typically about $\frac{3}{8}$ inch. Since ODOT's current rumble strip design depth requirement is ranging from $\frac{1}{2}$ to $\frac{5}{8}$ inch, multiple micro-surfacing lifts would have to be placed to avoid infiltration and deterioration of the pavement after the installation of rumble strips. Further evaluation and scientific data are needed to identify whether micro-surfacing and ultra-thin overlays provide beneficial impacts on the performance of CLRS.

2.4 USE OF FINITE ELEMENT ANALYSIS FOR RUMBLE STRIP PERFORMANCE EVALUATION

Finite Element Analysis (FEA) is a numerical modeling process constructed by covering a virtual material with a mesh with finite points (called nodes) in a computer simulation. Properties of the material are generally modeled by conducting laboratory or field experiments and entered into the software by following a complex equation system. By modeling the behavior of the material, the changes in the properties (e.g., changes in deformation, temperature, moisture, noise, etc.) of all nodes under different external factors (e.g., vehicular loading) are calculated and reported. Once the model has been developed, FEA allows multiple scenarios to be tested/simulated in a short time period and with minimal effort and cost. Input parameters of the FEA model can be correlated with laboratory or field performance data to strengthen the model's field performance prediction accuracy and precision. In a previous ODOT research project, Kalathas et al. (2019) conducted FEA to quantify the noise generated by three different design profiles for rumble strips and compared those outputs to the noise generated by the current rumble strip designs followed in Oregon. The three rumble strip design profiles evaluated by FEA are given in Figure 2.13.

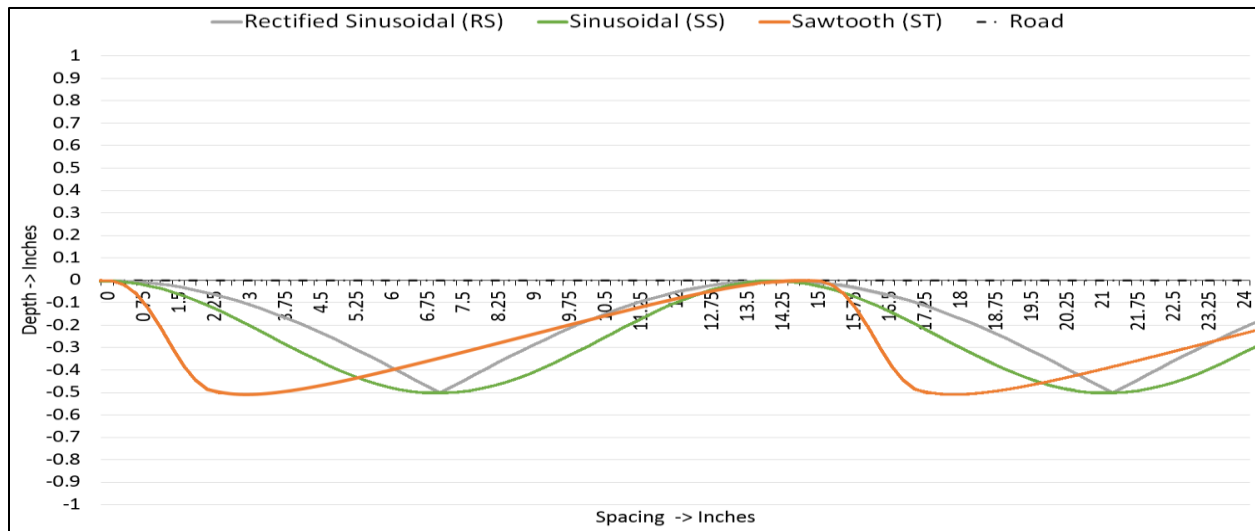
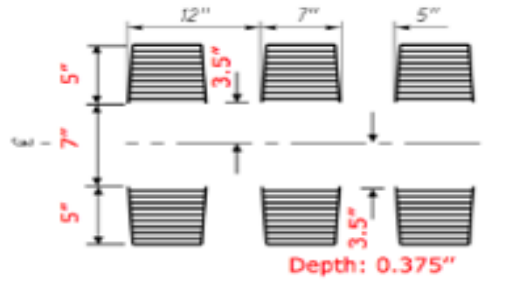


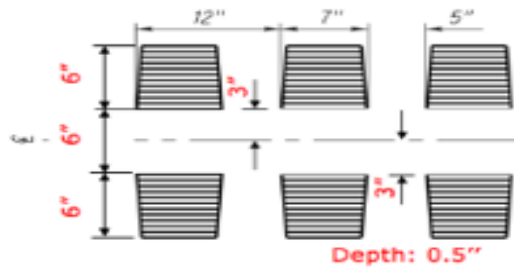
Figure 2.13: Rumble strip designs for FEA of exterior noise generation (Kalathas et al. 2019)

By modeling the three design profile categories (Rectified Sinusoidal, Sinusoidal, and Sawtooth) via FEA, Kalathas et al. (2019) developed and tested 20 different model cases by rolling a standard road tire on the rumble strip designs. Simulated noise values were extracted from the models to determine which rumble strip designs had lower exterior noise values while still being able to alert the driver. Although this FEA model focused on the safety and noise aspect of rumble strip performance, it also demonstrates that rumble strips could be modeled using FEA for other analyses (Kalathas et al., 2019).

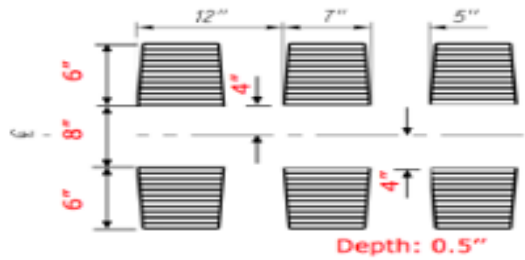
Kim et al. (2017) conducted 2D FEA to determine the impact of CLRS on stress and strain levels experienced by pavements by comparing model outputs with and without CLRS for composite pavements (asphalt overlay on top of concrete) and concrete pavements. Along with the two different pavement structures, the study also investigated the impacts of three modified rumble strip designs shown in Figure 2.14, tire footprints with varying widths and pressure distributions, and two tire loading scenarios of the CLRS on pavement's response (Kim et al., 2017). Although the developed models were 2D and did not consider the impact of the 3rd dimension on the pavement response, they can be considered as one of the first comprehensive FEA models investigating the impact of rumble strips on pavement performance.



Design #1
 (a) Modified Design 1



Design #2
 (b) Modified Design 2



Design #3
 (c) Modified Design 3

Figure 2.14: Three modified CLRS designs tested by the FEA model developed by (Kim & Rilett, 2017)

In Figure 2.14, the viewer is looking in plan view transversely along the roadway. This means traffic is moving from left to right (or vice versa). The modified designs utilize rumble strips on either side of the longitudinal joint, and 3 sets of rumbles are shown to demonstrate dimensions. The finite element models in the study were developed to focus on the high-stress gradient zone in the center of the pavement at the surface layer where the CLRSs are placed, as shown in Figure 2.15 below.

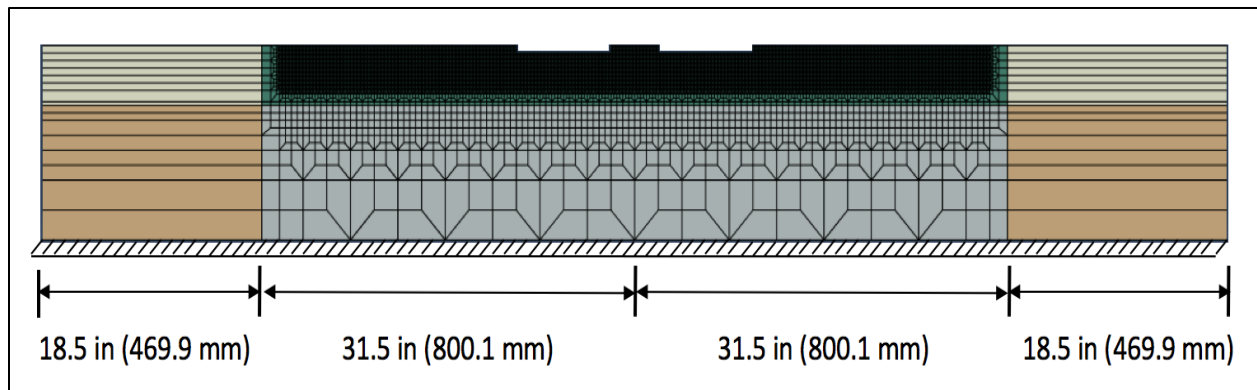


Figure 2.15: Finite element mesh cross-sectional profile of the composite pavement structure (Kim & Rilett, 2017)

As seen in Figure 2.15, the lower pavement layers' mesh is coarser than the upper/surface layers' mesh. With the model focusing on attempting to understand damage potential and pavement responses around CLRS, model accuracy around the upper layers is more important than the bottom layers of the structure (Kim et al., 2017). Also, two different tire loading scenarios were employed in the FEA, one scenario placing the tire in the middle of the CLRS and the other placing the center rib of the tire on the right edge of the CLRS (Kim et al., 2017). The tire pattern and loading scenarios used for the FEA are shown in Figure 2.16.

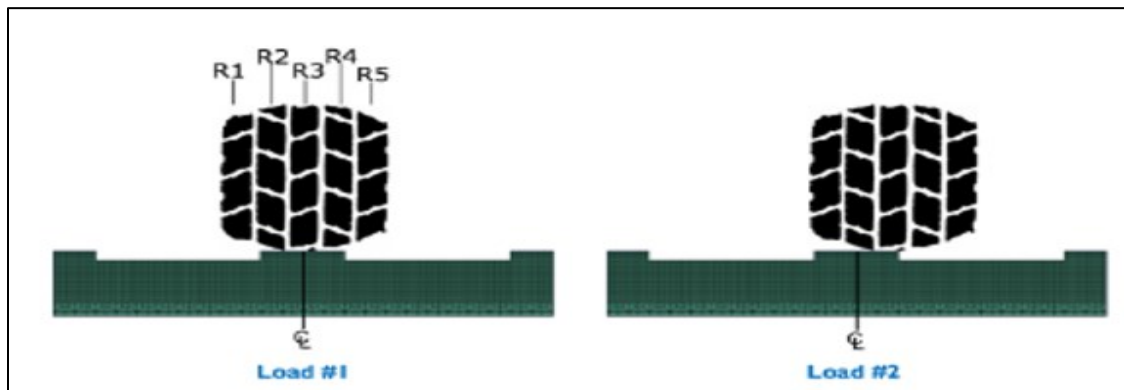


Figure 2.16: Position of two tire loading scenarios used in the Nebraska study (Kim & Rilett, 2017)

The two tire loading scenarios in Figure 2.16 were simulated on the three modified CLRS designs, the current CLRS design (length - 8", width - 4", and depth - 0.5"), and without a CLRS (control case) (See Figure 2.14 for all three evaluated CLRS designs). In both loading scenarios, the case without a CLRS had the lowest stress values (Kim & Rilett, 2017), as expected. The current CLRS design had a higher stress distribution than the modified CLRS designs, with the highest stress levels being observed usually in the corners of the CLRS (Kim & Rilett, 2017). Zoomed in images of the stress profiles at the corner/edge of the CLRS modeled in the study for both tire loading scenarios are shown in Figure 2.17.

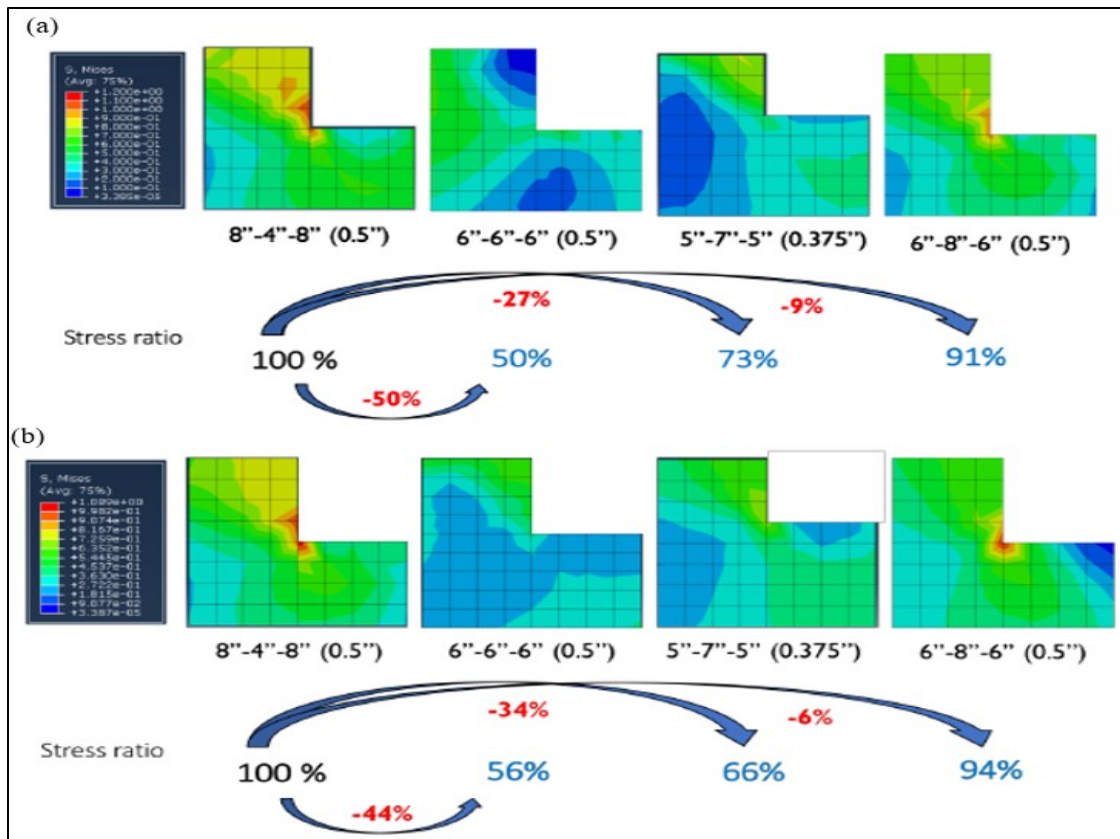


Figure 2.17: Zoomed-in views of CLRS edges/corners: (a) 2nd loading, (b) 1st loading (Kim & Rilett, 2017)

Kim et al. (2017) gives the stress ratio percentages in Figure 2.17 for each modified CLRS design, with the reference case being the current CLRS design for a composite pavement. In both tire loading scenarios, the second modified design from Figure 2.14 (6''-6''-6'' with 0.5'' depth) experienced the lowest amount of stress compared to the reference case. The previously mentioned modified CLRS design experienced about half the stress for both tire loading scenarios when compared to the reference CLRS design. Also shown in Figure 2.17, each modified CLRS design had a lower stress ratio percentage compared to the reference CLRS design for both center and edge tire loading. However, these modified CLRS designs have not been tested and validated by laboratory and field testing to determine whether these new designs could reduce pavement damage (Kim et al., 2017). Functionality in terms of safety was also not tested or evaluated in the study.

3.0 FINITE ELEMENT MODELING FOR CENTERLINE RUMBLE STRIPS

3.1 INTRODUCTION

In this study, 3D dynamic viscoelastic FEA modeling was used to simulate loaded truck tires rolling on the pavement surface with CLRS to determine the stress, strain, and displacement response of the pavement structure under different conditions. This model is the first 3D FEA model in the literature for rumble strips for structural response evaluation. Model details, experimental factorial, and results are given in the following sections.

3.2 MODEL METHODOLOGY

A 3D dynamic implicit FEA model was developed to determine the stress, strain, and displacement response of different CLRS strategies to truck loading on asphalt pavements. AbaqusTM software was used for the development of the FEA models. The FEA mesh consisted of Lagrange elements with modified second-order interpolation functions. Tetrahedral elements were used to accommodate the compact geometry at rumble strip corner points. The selected elements employ full numerical integration using the method of virtual work.

In the finite element model, an asphalt layer was placed on top of an aggregate base with an “infinite” (5 meters [16.4 ft] thick) subgrade beneath. Layer properties and finite element model input parameters are given in Table 3.1. In order to characterize the viscoelastic behavior of the stiff and soft asphalt layers, the generalized Maxwell model was used in this study to simulate the time dependency of asphalt materials used in the surface layer. The model consists of two basic units, a linear elastic spring in series with multiple Maxwell elements (Coleri and Harvey, 2013).

Mathematically, the behavior of this model follows the Prony series and is described as:

$$E(t) = E_e + \sum_{i=1}^n E_i e^{-\left(\frac{t}{\tau_i}\right)} \quad (3-1)$$

where:

E_e is the equilibrium modulus of the elastic spring, E_i and τ_i are the relaxation modulus and relaxation time of the i^{th} member among n Maxwell elements.

The viscoelastic behavior of two stiff and soft asphalt materials was characterized using the falling weight deflectometer (FWD) test (a non-destructive field test to determine material properties through back-calculation) results from two pavement sections (one with stiff and one

with soft asphalt layers on the surface). Using the relaxation modulus outputs, the constants of the Prony series were back-calculated and then imported into the finite element models as the inputs to model the asphalt behavior (Coleri and Harvey, 2013) (Estaji et al., 2019) (Harvey et al., 2016).

The temperature dependency of the asphalt mix was defined by using the Williams-Landel-Ferry (WLF) equation, given as follows (Ferry, 1980).

$$\log(a_T) = \frac{-C_1(T - T_{ref})}{C_2 + (T - T_{ref})} \quad (3-2)$$

where:

a_T = the time-temperature shift factor,

C_1 and C_2 = regression coefficients,

T_{ref} = the reference temperature, and

T = test temperature.

To optimize the regression coefficients C_1 and C_2 , the shear modulus data were first fitted to a sigmoid function, in the form of:

$$\log(G(\xi)) = \delta + \frac{\alpha}{1 + \exp(\beta + \gamma \log(\xi))} \quad (3-3)$$

where:

α , β , γ and δ = regression coefficients, and

ζ =reduced time.

Shift factors were calculated by fitting the measured or back-calculated modulus to the sigmoidal function (Eqn. 3-3). Finally, the dynamic modulus master curve for each section was obtained by processing the test results for the stiff and soft asphalt materials. Back-calculated input parameters for the finite element model development are given in Table 3.1.

Table 3.1: Finite Element Model Input Parameters for Soft and Stiff Asphalt Layers (Estaji et al., 2019)

| Material | Long term elastic modulus [MPa] | Poisson's ratio | Density [Tonne/mm ³] | Viscoelastic model inputs | | WLF model coefficients | | |
|---------------|---------------------------------|-----------------|----------------------------------|---------------------------|----------|------------------------|-------|--------|
| | | | | g_i | τ_i | T_{ref} | C_1 | C_2 |
| Soft Asphalt | 2,447 | 0.35 | 2.3E-09 | 0.28 | 6.4E-05 | 19 | 11.03 | 123.81 |
| | | | | 0.31 | 0.01 | | | |
| | | | | 0.17 | 2.6E-07 | | | |
| | | | | 0.14 | 1.33 | | | |
| | | | | 0.08 | 152.31 | | | |
| Stiff Asphalt | 20,414 | 0.35 | 2.3E-09 | 0.21 | 4.6E-05 | 19 | 16.17 | 283.73 |
| | | | | 0.23 | 0.003 | | | |
| | | | | 0.15 | 3.9E-07 | | | |
| | | | | 0.25 | 0.18 | | | |
| | | | | 0.15 | 71.2 | | | |

In the developed viscoelastic FEA model, linear behavior was considered (small strain domain). No nonlinearity (fatigue, permanent deformations, and cracks) was taken into account to reduce the model details to achieve reasonable model run times. Simulating cracking and permanent deformation in an FEA model is not common and is expected to increase the model run-time significantly. The boundary conditions along the edges of the model allowed for movement in only the vertical direction. The boundary condition at the base of the model fixed the displacements/rotations for all directions (encastre). Complete bonding was assumed between the different pavement layers. An unconstrained longitudinal joint was included in the models to simulate an unbonded joint. Due to considerable stress concentration in the asphalt layers, half-lane width models were developed to reduce the computational running time. The total FEA model length was 4.9 meters (16 feet), and the width was 3.8 meters (12.5 feet). The FE model developed in this study was not calibrated with field-measured pavement responses, but the comparisons between evaluated cases and their impact on the strain with respect to each other should be close to reality.

The tire was represented by an extremely stiff block with semi-circular ends. The utilized shape was selected for simplicity, to avoid the tire “falling” into rumble strips, and to smoothen the tire edges to reduce contact errors in the FEA model. In order to simulate moving loads in the viscoelastic FEA model, a velocity boundary condition was applied to the loading body to simulate the constant-speed passage of axles over the pavement section (dynamic loading). The loading body permitted movements only along the vertical y-axis and the x-axis for the specified velocity boundary condition (no rotations). The projected contact pressure from a tire was applied to the simulated tire shape. The distribution of contact pressure on the tire was assumed to be constant and uniform. The square loading area was approximated as the ratio of tire load to pressure. Additionally, the mesh was refined under the wheel path to improve the accuracy and

precision of the model outputs. Figure 3.1 shows a typical model structure with 16 centerline rumble strips and a dual tire tandem axle loading configuration.

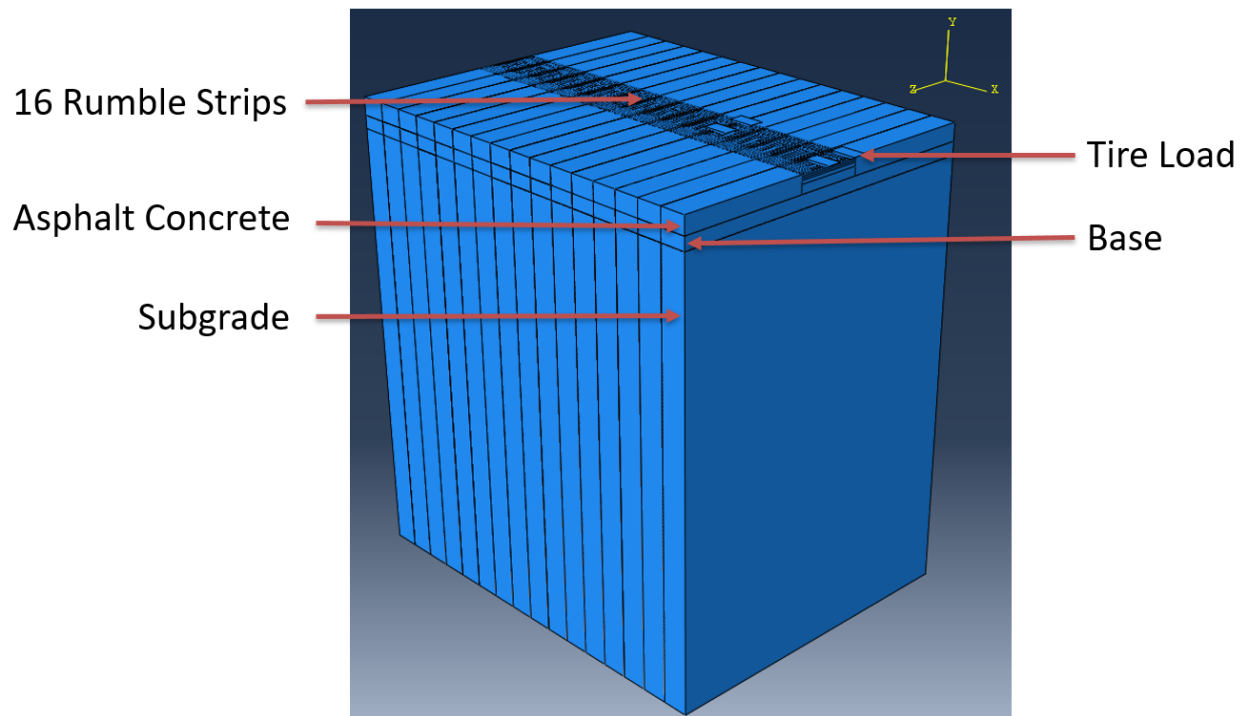


Figure 3.1: FEA model structure

Moving tire loads in the FEA model were selected based on the axle configuration of a typical Class 9 truck with one steering single and two dual tandem axles (8 tires on one axle). Truck tire pressure was assumed to be 725kPa (105psi). The spacing between dual tires was assumed to be 360 mm (14.2 in), and the spacing between tandem axles was assumed to be 1,372 mm (54 in). Figure 3.2 shows the loading configuration of the Class 9 truck used in the factorial for model development.

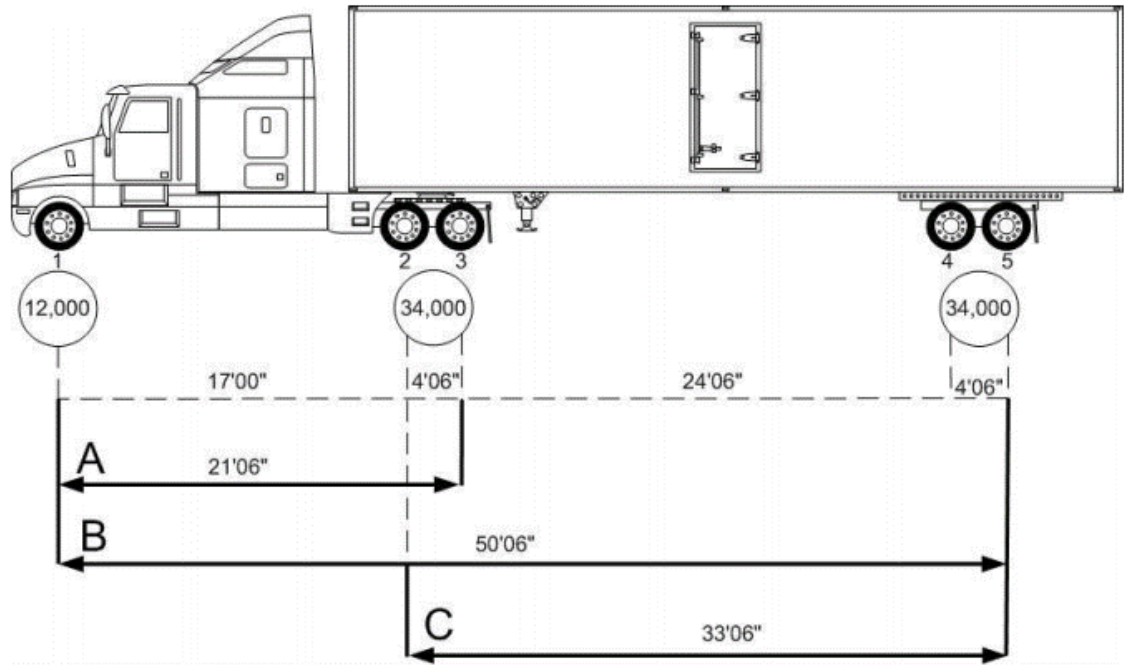


Figure 3.2: Loading configuration for the Class 9 truck; lengths are feet and inches, and circled axle weights are given in pounds (“Self-Issue Permit Program Manual,” 2021)

3.2.1 Sensitivity Analysis – Finding the Optimum Mesh Size and Loading Time Increment; Determining Critical Load Case

A mesh sensitivity analysis was performed to determine the optimum mesh density and number of step increments. A coarse mesh is one with a limited number of large-sized elements, while a fine mesh consists of numerous small elements. The number of step increments describes the rate at which a tire load moves across the FEA model. A large number of increments corresponds to a tire load moving very small distances at a time, while fewer increments mean a tire load travels longer distances at a time. The goal of the mesh sensitivity analysis was to find the balance between a fine mesh with many increments (longest model runtime, highest level of detail) versus a coarse mesh with minimal increments (shortest model runtime, lowest level of detail).

Trial meshes were examined using coarse, medium, and fine meshes with 2,000, 6,700, and 8,700 elements, respectively. Trial time increments of 50, 100, 150, 300, and 450 were also assessed to determine the optimum time increment that will provide the most accurate model outputs with a reasonable model runtime.

Figure 3.3 shows the vertical displacement profiles using various loading time increments for a base corner point of a mid-section rumble strip with a standard (coarse) mesh. The base corner point corresponds to the node located along the asphalt surface at the corner of the deepest point of the rumble strip. Figure 3.4 demonstrates the vertical displacement profiles for varying mesh densities for a base corner point of a mid-section rumble strip with 150 increments.

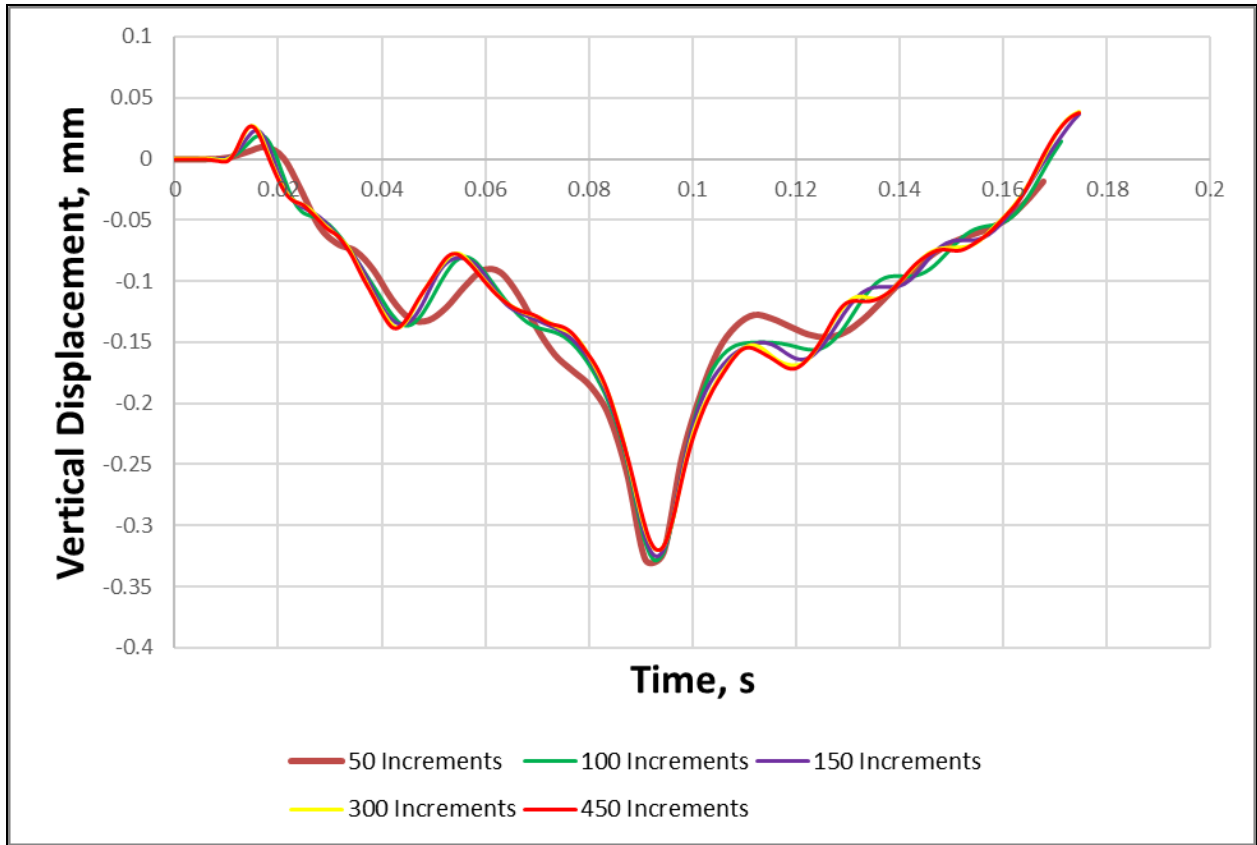


Figure 3.3: Mesh sensitivity analysis – Time step increments

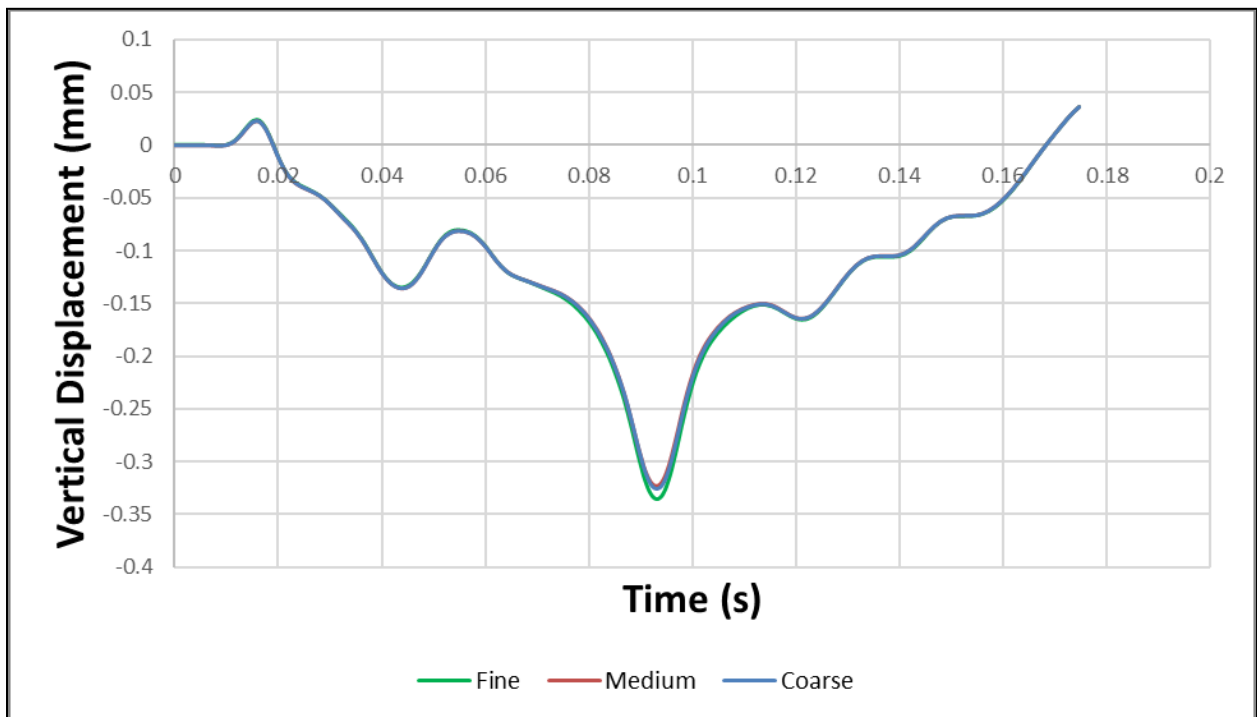


Figure 3.4: Mesh sensitivity analysis – Mesh density

Optimal mesh density and time step increments correspond to the point at which convergence occurs. This is the scenario in which smaller time increments and a finer mesh structure will not provide significantly different outputs. The sensitivity analysis resulted in the coarse mesh with 150 increments chosen as optimal. Over the course of model development, the selected number of time step increments was increased to 200, and minor mesh density modifications were made. Figure 3.5 and Figure 3.6 display the typical meshed model structure.

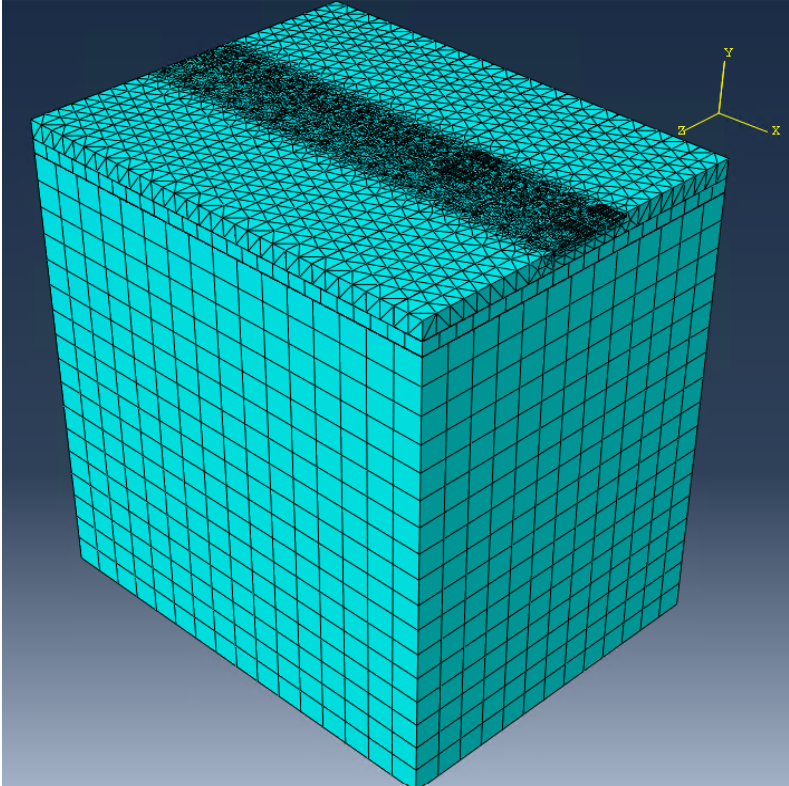


Figure 3.5: Meshed model structure in Abaqus – Traffic flows in the X direction

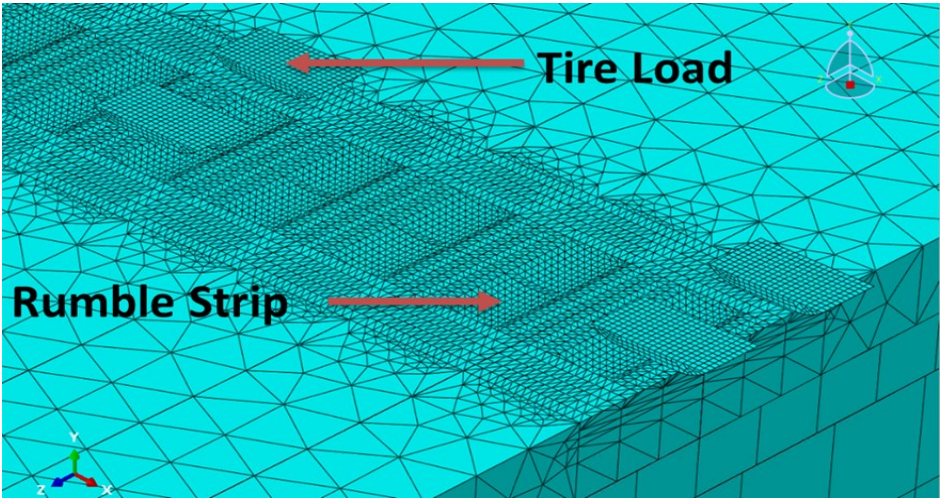
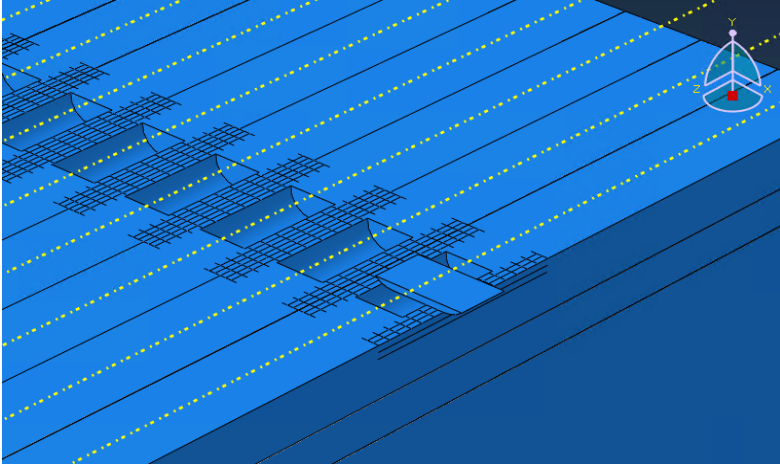
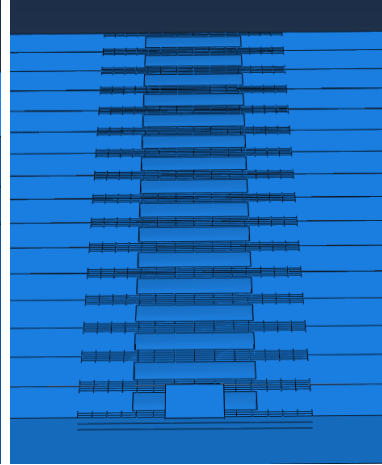


Figure 3.6: Meshed model structure in Abaqus – Closer view with rumble strips and applied wheel loads

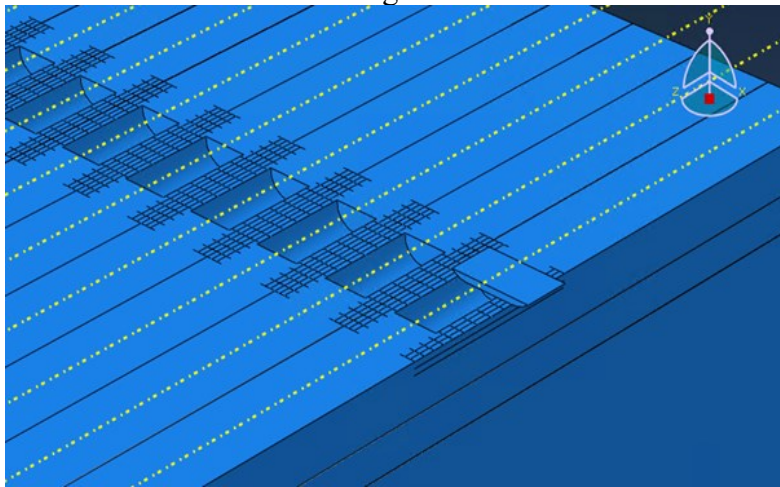
Five tire orientations of a typical Class 9 loaded truck were examined to create the maximum impact on the rumble strip structure. The five orientations were Middle Single, Edge Single, Middle Dual, Edge Dual, and Adjacent Dual, as demonstrated in Figure 3.7. Middle Single and Edge Single cases correspond to the front axle tire running directly over the rumble strip or along the edge of the rumble strip. Middle Dual, Edge Dual, and Adjacent Dual cases correspond to the rear dual tandem axles running with both tires centered over the rumble strip, one tire directly over the rumble strip, or one tire along the edge of the rumble strip, respectively. Only the tire orientation and axle loading were varied among the strategies analyzed. The maximum principal stress was utilized to determine the critical loading scenario. This value was extracted at the critical node along the asphalt surface at the mid-section rumble strip in each model. The critical node was the node with peak stress among all time step increments. These results are given in Figure 3.8.



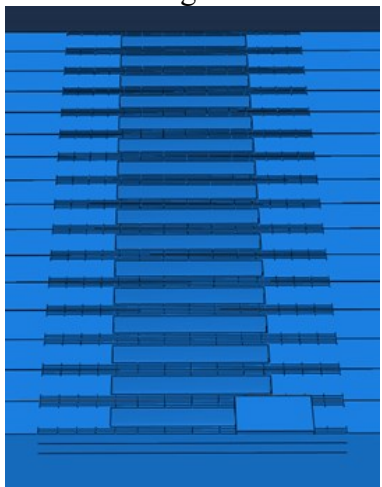
Middle Single – View 1



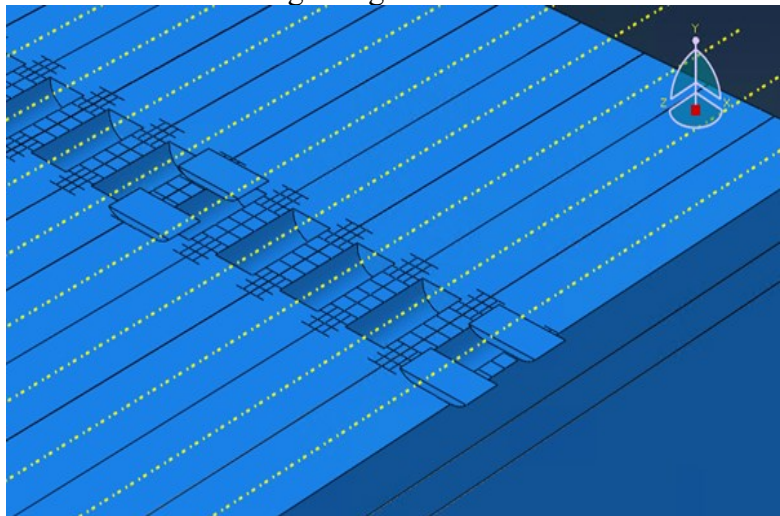
Middle Single – View 2



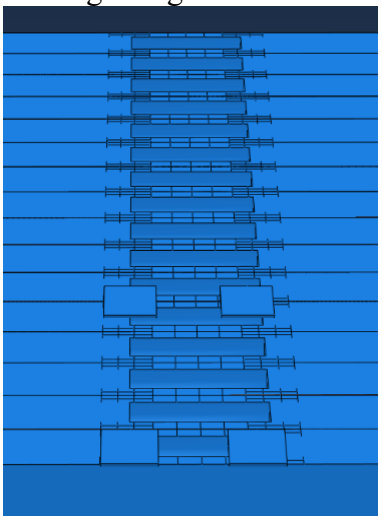
Edge Single – View 1



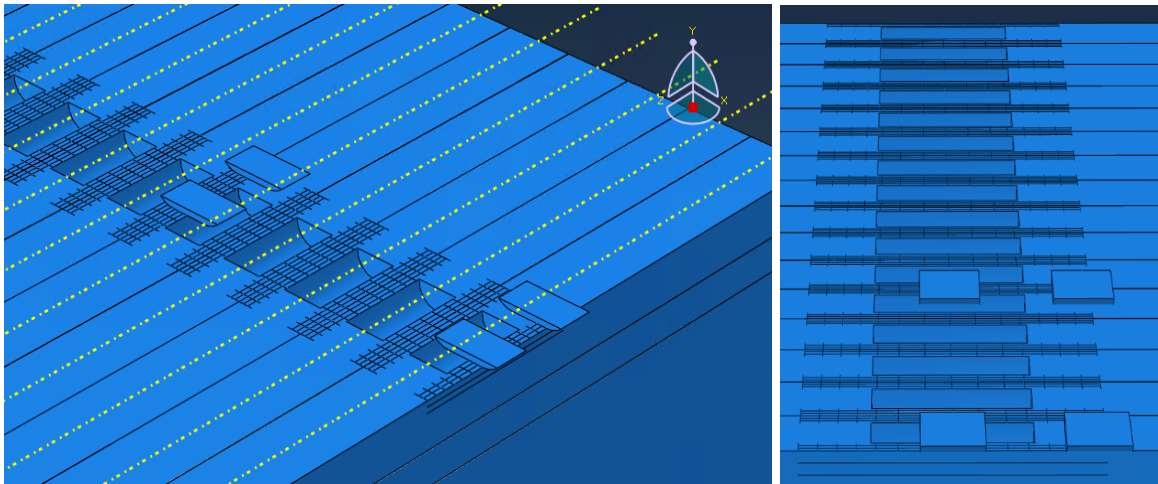
Edge Single – View 2



Middle Dual – View 1

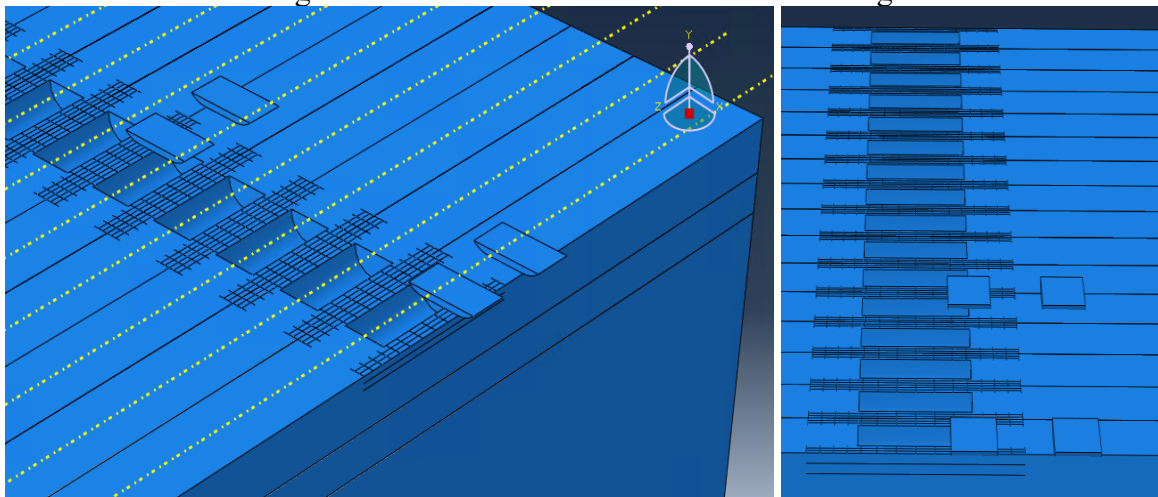


Middle Dual – View 2



Edge Dual – View 1

Edge Dual – View 2



Adjacent Dual – View 1

Adjacent Dual – View 2

Figure 3.7: Critical load cases - Tire orientations

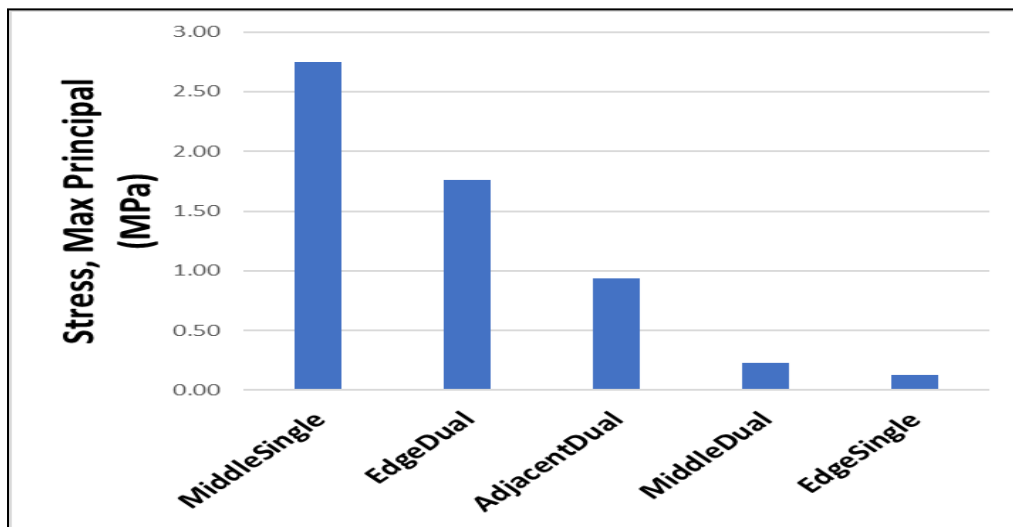


Figure 3.8: Critical load case – Maximum principal stresses

Based on the results of the analysis, the two critical tire orientations for FEA modeling were selected as Middle Single and Edge Dual cases.

3.2.2 Modeling Factorial

Several factors were considered in the numerical modeling factorial to assess the structural response under different conditions, which included speed, temperature, asphalt layer stiffness, rumble strip depth, rumble strip type and geometry (rectangular versus sinusoidal, conventional versus modified), tire orientation, sinusoidal wavelength, and longitudinal joint location with respect to CLRS. Table 3.2 through Table 3.4 show the FEA numerical factorial that was followed in this study. A total of 72 FEA models were developed with typical runtimes of approximately four hours for each model, utilizing a computer with 12 logical processors and 32 GB of memory.

Table 3.2: Numerical Modeling Factorial – Rectangular CLRS Models

| Factor | Subcategories |
|-------------------------------|---|
| Speed | 48.28 kph, 96.56 kph (30 mph, 60 mph) |
| Temperature | 25°C (77°F) |
| Asphalt type | Stiff, Soft |
| Depth | Deep (15.88 mm [5/8 in]), Shallow (12.7 mm [1/2 in]), Very Shallow (6.35 mm [1/4 in]) |
| CLRS Geometry | Conventional (40.64 cm x 17.78 cm [16 in x 7 in]), Modified (20.32 cm x 17.78 cm [8 in x 7 in]) |
| Tire Orientation | Rear dual tandem axle |
| Tire and CLRS Location | Over joint Adjacent to joint |

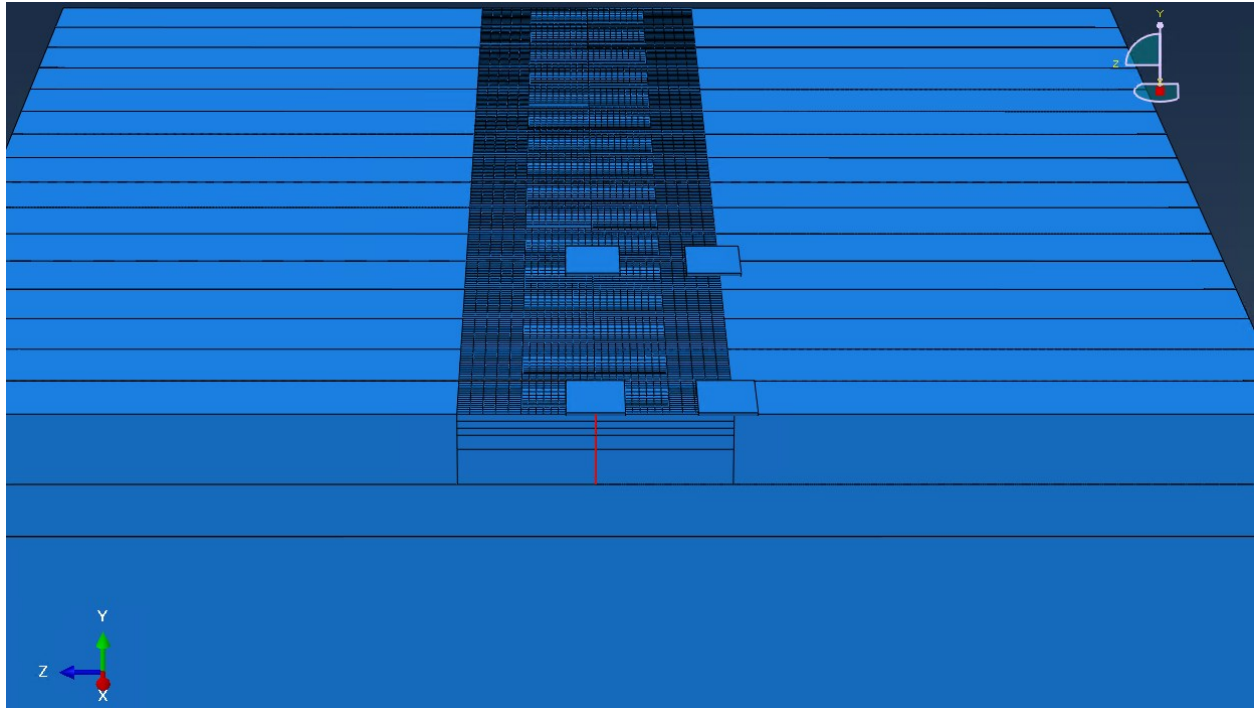
Table 3.3: Numerical Modeling Factorial – Sinusoidal CLRS Models

| Factor | Subcategories |
|-------------------------------|---------------------------------------|
| Speed | 48.28 kph, 96.56 kph (30 mph, 60 mph) |
| Temperature | 25°C (77°F) |
| Asphalt type | Stiff, Soft |
| Depth | 12.7 mm (1/2 in) |
| Wavelength | 355.6 mm (14 in), 609.6 mm (24 in) |
| Tire Orientation | Rear dual tandem axle |
| Tire and CLRS Location | Over joint |

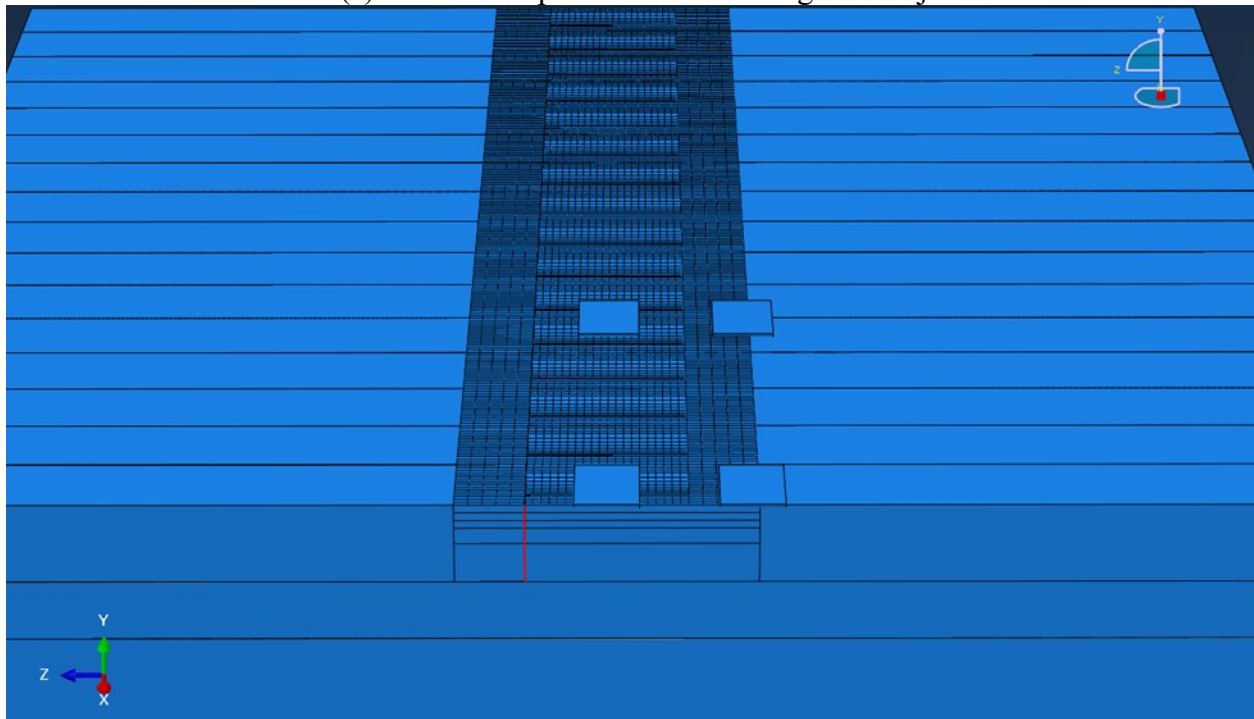
Table 3.4: Numerical Modeling Factorial – Control Models (No rumble strips on the pavement)

| Factor | Subcategories |
|-------------------------|--|
| Speed | 48.28 kph, 96.56 kph (30 mph, 60 mph) |
| Temperature | 25°C (77°F) |
| Asphalt type | Stiff, Soft |
| Tire Orientation | Rear dual tandem axle Front single axle |
| Tire Location | Over joint Adjacent to joint |

Stiff and soft asphalt layer inputs are given in Table 3.1. The tire orientation described in Table 3.2 through Table 3.4 is the critical dual tire orientation shown in Figure 3.8 and is labeled Edge Dual in Figure 3.7. The single tire orientation was excluded from the analysis in Table 3.2 and Table 3.3, as discussed in Section 3.3.1 below. The red lines in Figure 3.9 show the locations of the longitudinal construction joint with respect to the rumble strips.



(a) Rumble strips and tires over longitudinal joint



(b) Rumble strips and tires adjacent to longitudinal joint

Figure 3.9: FEA rumble strip locations with respect to longitudinal construction joints

Conventional ODOT rectangular rumble strips (40.64 cm x 17.78 cm [16 in x 7 in]) and modified rectangular rumble strips (20.32 cm x 17.78 cm [8 in x 7 in]) referenced for FEA modeling are shown in Figure 3.10 and Figure 3.11, respectively.

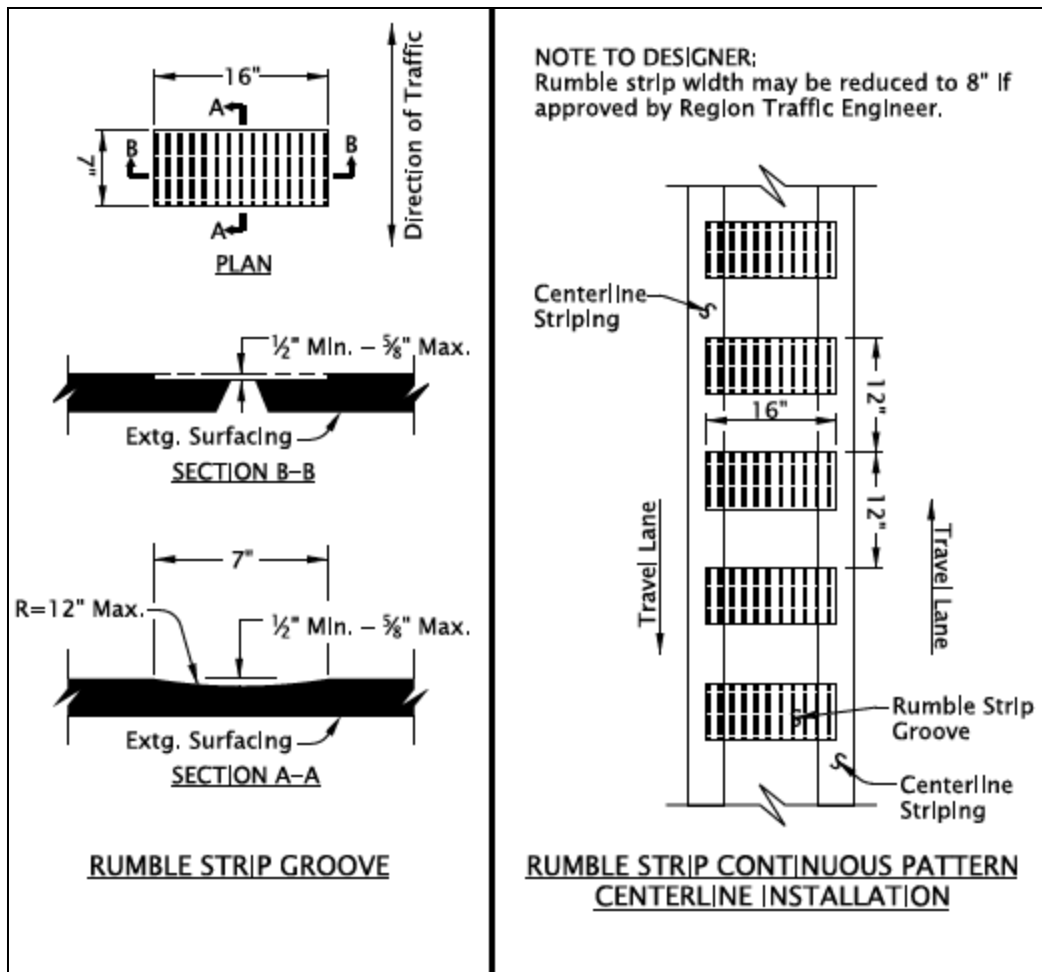


Figure 3.10: Conventional rectangular CLRS, 40.64 cm x 17.78 cm (16 in x 7 in), dimensions in inches (“ODOT Standard Details | Traffic 4000 Series,” n.d.)

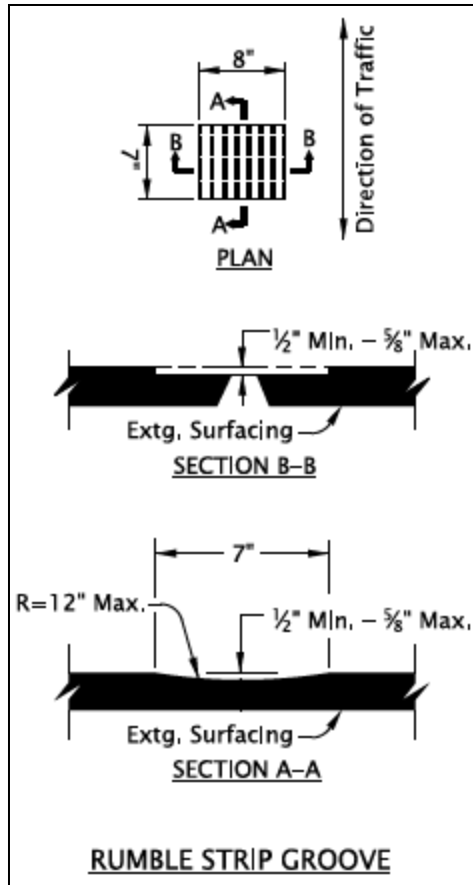


Figure 3.11: Modified rectangular CLRS, 20.32 cm x 17.78 cm (8 in x 7 in), dimensions in inches (“ODOT Standard Details | Traffic 4000 Series,” n.d.)

Typical sinusoidal rumble strips referenced for modeling purposes, as well as cross-section views of the sinusoidal CLRS, are shown in Figure 3.12 and Figure 3.13. Wavelength refers to the spacing from rumble strip peak-to-peak in the sine wave function, where 40.64 cm (16 in) is typical, as shown in Figure 3.12. The FEA models simulated 35.56 cm (14 in) and 60.96 cm (24 in) sinusoidal wavelengths to determine the impact of higher and lower wavelengths.

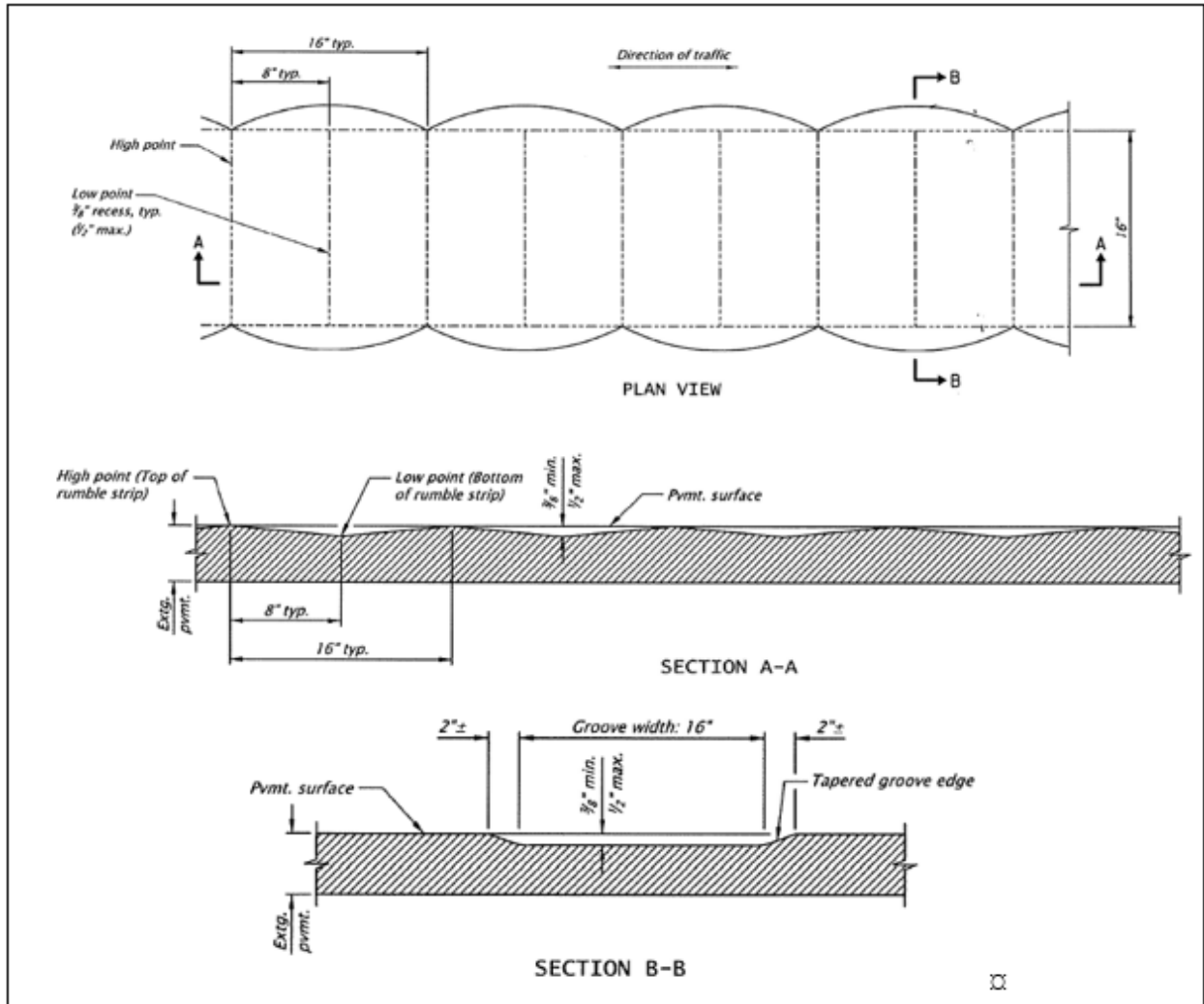
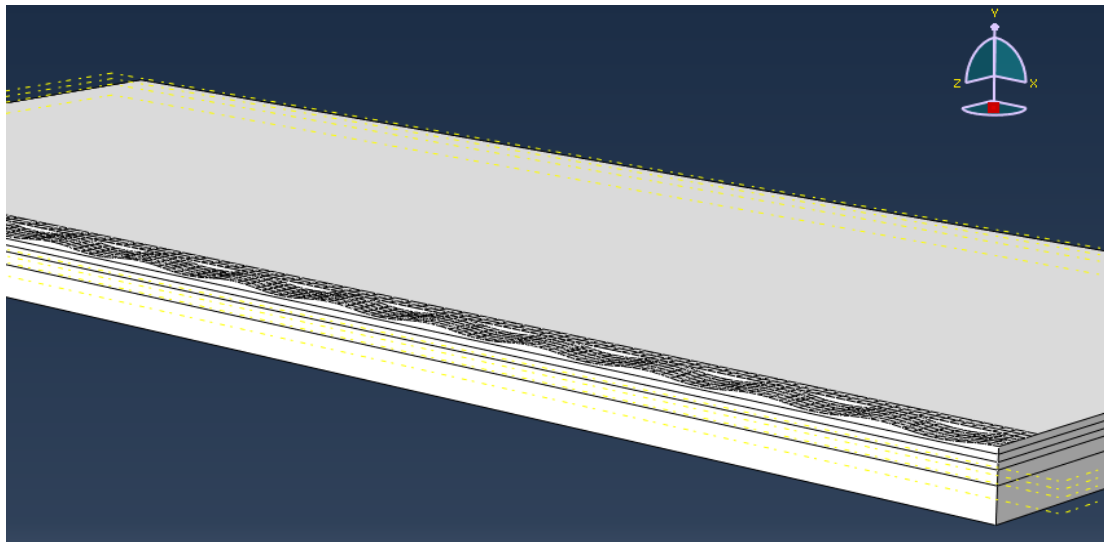
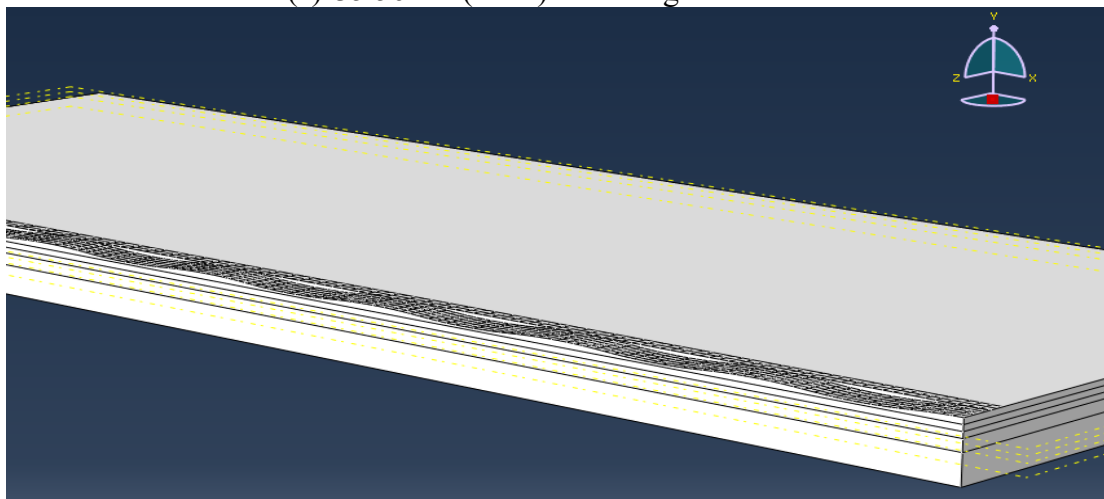


Figure 3.12: Sinusoidal CLRS, dimensions in inches (Hurwitz et al, 2019)



(a) 35.56 cm (14 in) wavelength cross-section



(b) 60.96 cm (24 in) wavelength cross-section

Figure 3.13: Sinusoidal CLRS cross-section views from the developed FEA models

3.3 MODELING RESULTS AND DISCUSSION

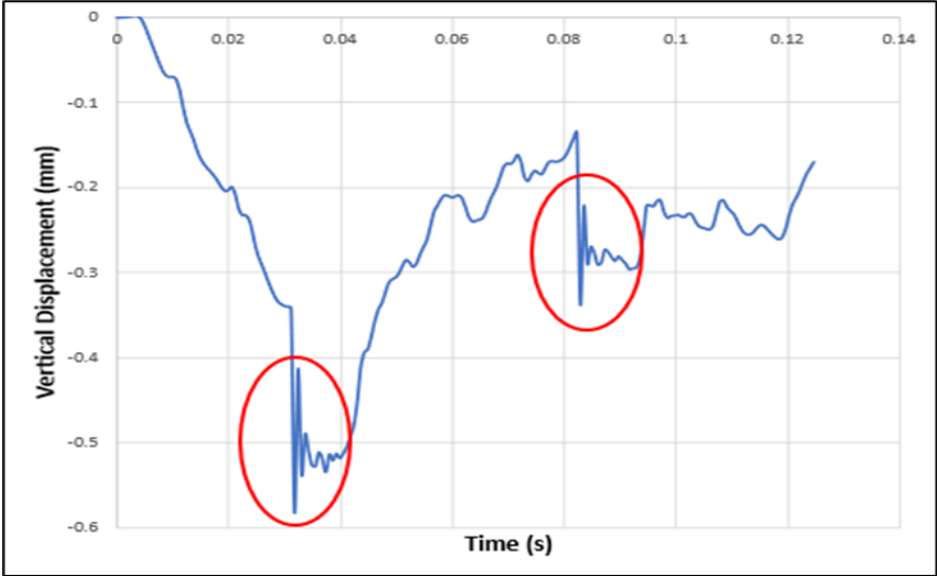
Among the factors included in the modeling factorial of Section 3.2.2, three additional components influenced the modeling results. These additional influencing factors include:

1. The viscoelasticity effect,
2. dynamic loading effect, and
3. vibrational effect.

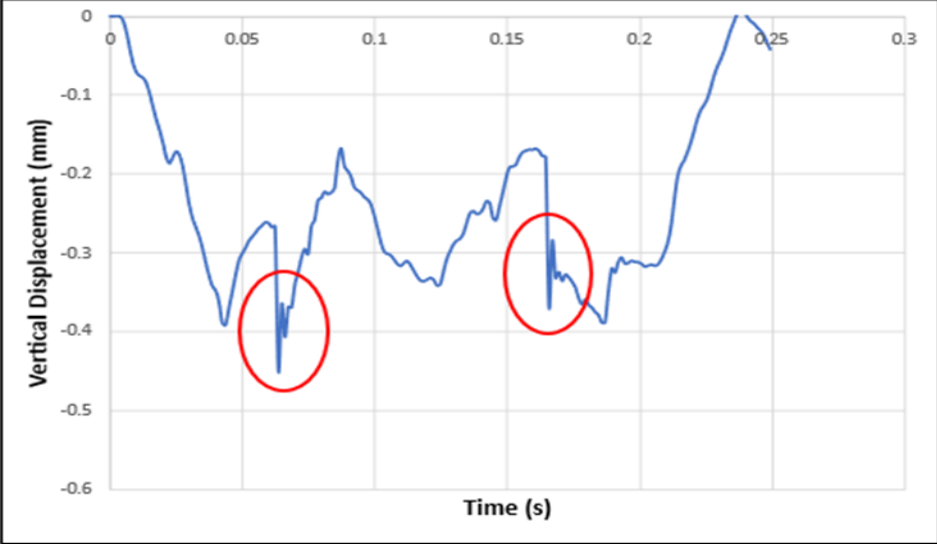
The viscoelastic effect (Section 3.2) is a complex interaction between temperature and loading rate that impacts the viscosity and stiffness of asphalt concrete material. In the finite element modeling, this viscoelastic effect showed itself in high temperature and low tire speed cases,

which corresponded to lower asphalt stiffness and greater displacements. Conversely, low temperature and high tire speed cases corresponded with higher asphalt stiffness and less displacement.

The dynamic loading effect is the increased impact loads applied to the pavement structure due to high-speed interaction between the vehicle suspension systems and rumble strips. This dynamic loading is relatively minimal on a smooth roadway but increases drastically as a vehicle's tire enters a rumble strip groove. In the finite element modeling, this suspension effect was captured by the front edge of the tire load plate impacting the front edge of a rumble strip, rebounding from the impact, then returning to the pavement surface. The dynamic loading effect was greater at higher speeds (increased noise in the displacement outputs), as shown in Figure 3.14 for 48.28 kph (30 mph) and 96.56 kph (60 mph) cases.



(a) High speed, 96.56 kph (60 mph)



(b) Low speed, 48.28 kph (30 mph)

Figure 3.14: FEA dynamic loading effect

Figure 3.14 demonstrates the vertical displacement profile for a critical node on the front edge of the mid-section rumble strip. The portions of the displacement curve circled in red correspond to the impact of the tire load plate upon the front edge of the rumble strip. The larger displacement spikes observed for the high-speed model compared to the low-speed model show the dynamic loading effect.

The vibrational effect is related to the movement of the tire load plate along the asphalt surface. In finite element modeling, the dynamic implicit model type was used. The model does not function such that each time increment is solved as an individual matrix of equations, unrelated to the results of the previous increment. Instead, matrices are directly influenced by the results of the previous increments. This phenomenon allowed the tire load plate to be continuously pushed along the surface of the asphalt concrete. The combination of this motion, the modeled viscoelasticity of the asphalt concrete layer, and the speed of the tire load created a vibrational response throughout the models.

The viscoelasticity effect, dynamic loading effect, and vibrational effect were present in all models of the testing factorial. One effect was typically dominant in each model and as described previously, the controlling effect depended primarily upon asphalt stiffness, speed, and temperature. The impacts of the viscoelastic, dynamic, and vibration effects give insight into the variations observed in the modeling results and are discussed in the remainder of this section.

Maximum principal stress and elastic strain outputs were extracted from models in the factorial. Stress and strain outputs were taken for all nodes within the width and depth of the asphalt layer. Results for a distance equivalent to three rectangular CLRS on either end of the model were excluded to avoid any edge effects in the model outputs. From the output data, the average maximum principal stress and elastic strain of the peak 10 nodes (critical nodes) were extracted. Results for the peak 10 nodes were used to capture the critical stress and strain in the models. These critical values mark the onset of cracking in the asphalt layer and are assumed to indicate the pavement's structural performance. It should be noted that the rough nature of the CLRS surfaces controlled the critical strain outputs by creating higher dynamic impact loads on the rumble strips. For this reason, peak strains due to these dynamic loads are significantly higher than the typical strain levels used for pavement design (about 30-40% higher according to Cebon (1986)), which are extracted from linear elastic theory and FEA models without any dynamic components. It is assumed in this study that those high critical dynamic impact loads as a result of the extremely rough nature of the rumble strips created early age cracking and failures along the rumble strips on roadways. Figure 3.15 displays the typical nodes in the asphalt layer utilized for output extraction.

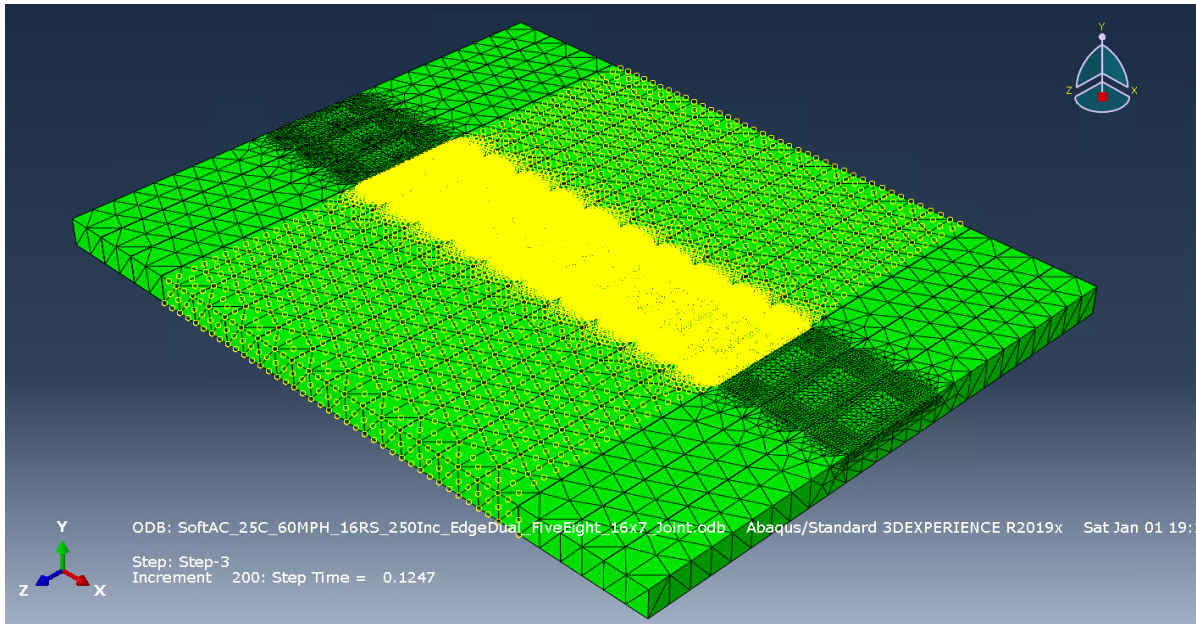


Figure 3.15: Nodes along the wheel path utilized for stress and strain output extraction

3.3.1 Results for the Control Models (No CLRS)

Maximum principal elastic microstrain outputs for control models (models with no CLRS) over the longitudinal joint are shown in Figure 3.16.

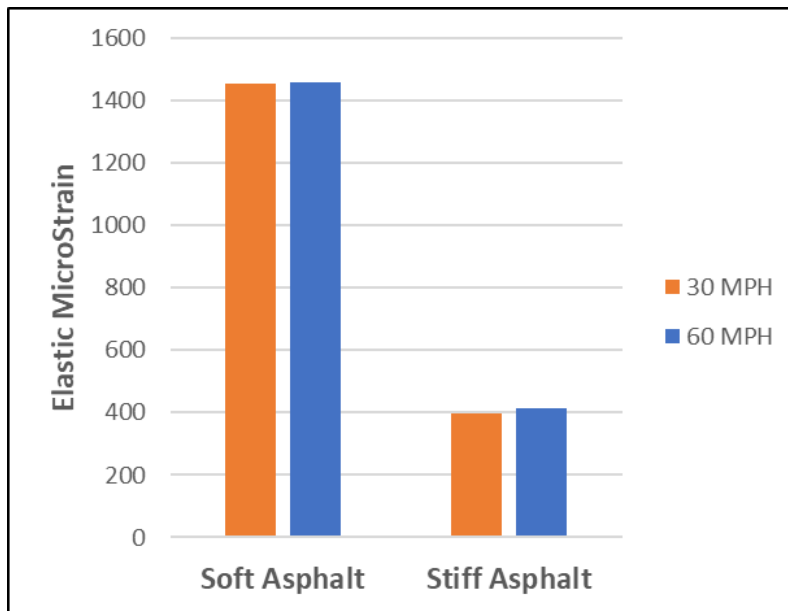


Figure 3.16: Control case (no CLRS) at 25°C with dual tires passing over the longitudinal joint - High and low speeds for stiff and soft asphalt models, 1 mph = 1.61 kph

It can be observed from Figure 3.16 that greater speed is creating slightly higher strain outputs for both comparisons. Although the viscoelastic response of the asphalt material should result in

higher strain values for the slow 48.3 kph (30.0 mph) cases, the dynamic load effect is dominating the viscoelastic response and resulting in higher strain values for the cases with higher speed levels (96.6 kph [60mph]) due to the higher dynamic loads experienced by the pavement at greater speeds. Among the stiff asphalt layer models, average peak microstrains for the high-speed cases are 5% higher than the strain levels for the slower speed level (mostly due to the dynamic loading effect). It can also be observed that soft asphalt results in 259% more strain than stiff asphalt for the cases with tires passing on the longitudinal joint.

Figure 3.17 shows the impact of axle type on the overall strain response.

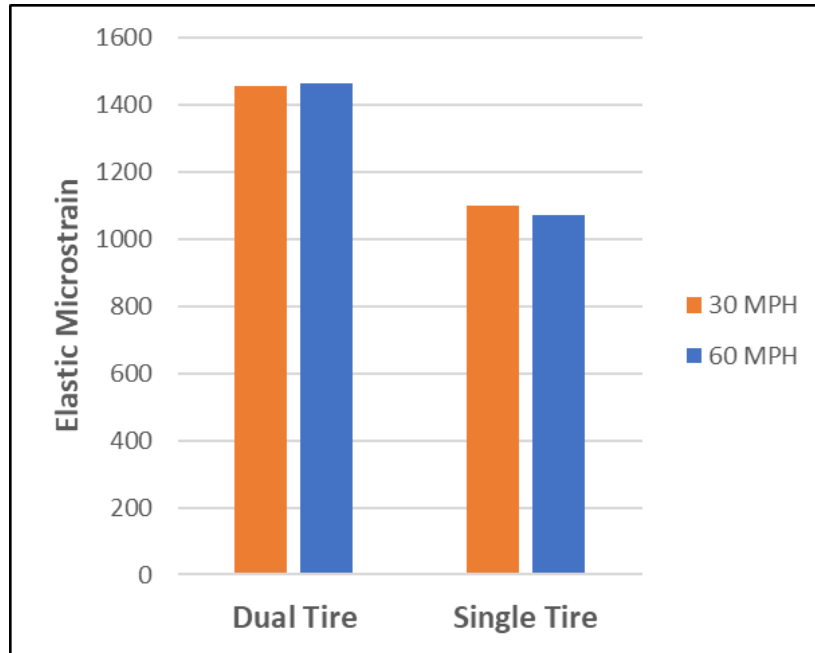


Figure 3.17: Control case at 25°C with soft asphalt layer - Impact of axle type on maximum principal elastic microstrain response, 1 mph = 1.61 kph

It can be observed in Figure 3.17 that the dual tire scenario results in greater maximum principal elastic microstrain outputs in the asphalt layer. The total load applied by the four tires in the dual tire with tandem axle scenario was 75.6 kN (17,000 lbs), and the total load applied by the single tire in the front axle scenario was 26.7 kN (6,000 lbs). The higher total load, load interaction due to spacing between tires, and the smaller tire footprint in the dual tire scenario led to higher critical microstrains.

Maximum principal elastic microstrain outputs for control models adjacent to the longitudinal joint are shown in Figure 3.18.

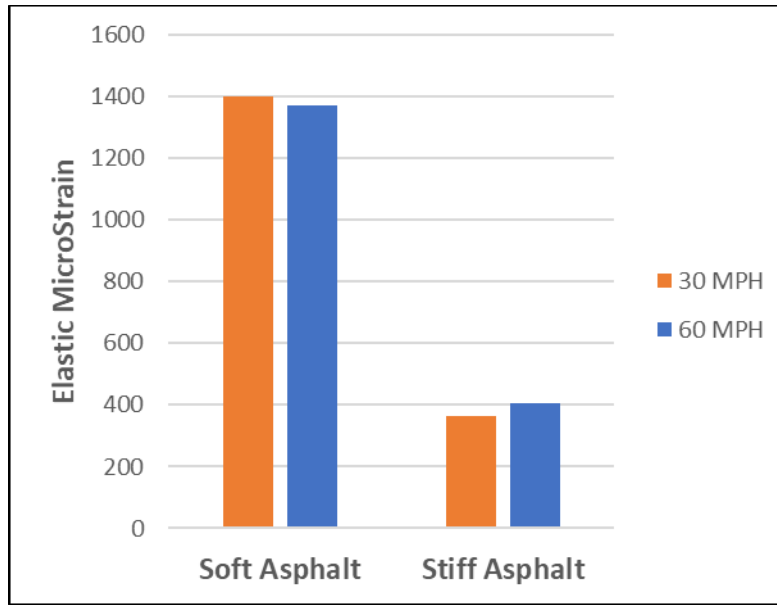
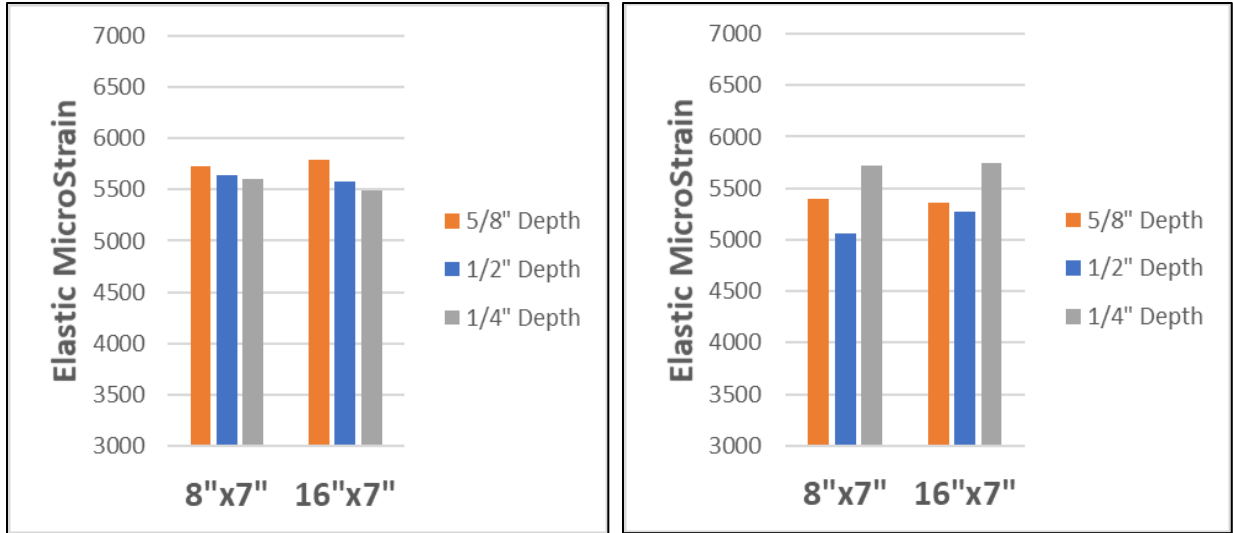


Figure 3.18: Control case at 25°C with dual tires passing adjacent to the longitudinal joint - High and low speeds for stiff and soft asphalt models, 1 mph = 1.61 kph

It can be observed from Figure 3.18 that the soft asphalt models have 262% higher average elastic strain values than the stiff asphalt models. By comparing the strain outputs for the control models loaded with the dual axle over the longitudinal joint to the models loaded with the axle adjacent to the joint, it can be observed that the models loaded over the longitudinal joint have 5% higher elastic strain on average due to the proximity of the axle with respect to the joint. It was also determined that the control models with no CLRS had significantly lower (214%) critical microstrains than the models with rectangular and sinusoidal CLRS, which are presented in the next section.

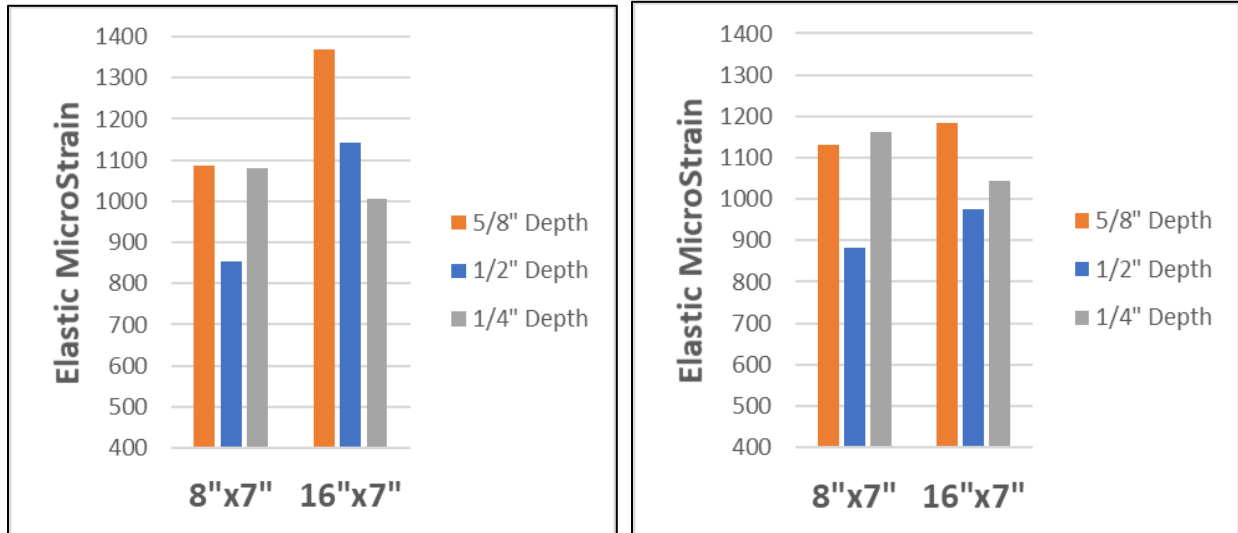
3.3.2 Results for the Models with CLRS

Figure 3.19 through Figure 3.22 display the maximum principal elastic strain outputs for models with CLRS in the numerical modeling factorial. Figures for maximum principal stress were not included since the principal elastic strain parameter is expected to represent the cracking susceptibility of the asphalt layer, while stress is expected to be highly controlled by the applied truck loads and less affected by the asphalt layer properties. Elastic strain is a function of both load and displacement and serves as an effective measure of pavement structural performance and cracking resistance. Axles with dual tires are used for all models in this section since they were determined to provide higher (more critical) strain levels according to the simulations with the control models (see Figure 3.17). Figure 3.19 displays the maximum principal elastic microstrain outputs for rectangular CLRS over the longitudinal joint.



(a) Soft Asphalt - 25°C - 60MPH - Dual Tires

(b) Soft Asphalt - 25°C - 30MPH - Dual Tires



(c) Stiff Asphalt - 25°C - 60MPH - Dual Tires

(d) Stiff Asphalt - 25°C - 30MPH - Dual Tires

Figure 3.19: Rectangular CLRS over the longitudinal joint, 1 inch (") = 2.54 cm and 1 mph = 1.61 kph

It can be observed from Figure 3.19 that the models with soft asphalt layers have average strain levels 421% higher than the models with stiff asphalt layers. Softer asphalt concrete more easily deforms under loading and, as such, observes greater increases in recoverable strain.

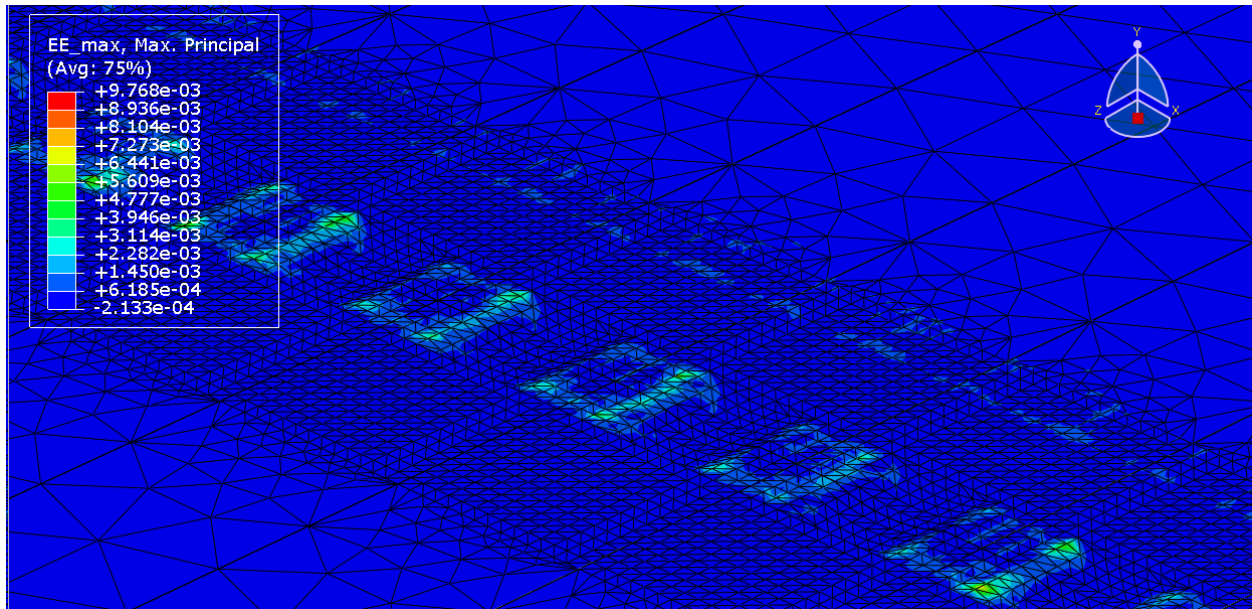
Deeper CLRS provided slightly more strain for high-speed levels, which points out the benefits of reducing CLRS depth on asphalt layer performance. This was an expected result since thicker CLRS depths reduce the pavement's thickness and provide less resistance to vehicular loads. However, when the speed was reduced from 96.6 kph (60 mph) to 48.3 kph (30 mph), this benefit of CLRS depth diminished. This result is due to the dynamic loads applied in the developed FEA models. Since the asphalt concrete layer was modeled as a viscoelastic layer, it is expected to have significantly higher strain levels at lower speeds. In addition, higher vehicle speeds created higher dynamic loads in many cases, which increased the strain levels in models.

Since these two mechanisms are working inversely at slower speeds, the impact of CLRS depth on strain is reduced because of the reduction in the dynamic loads at lower speed levels.

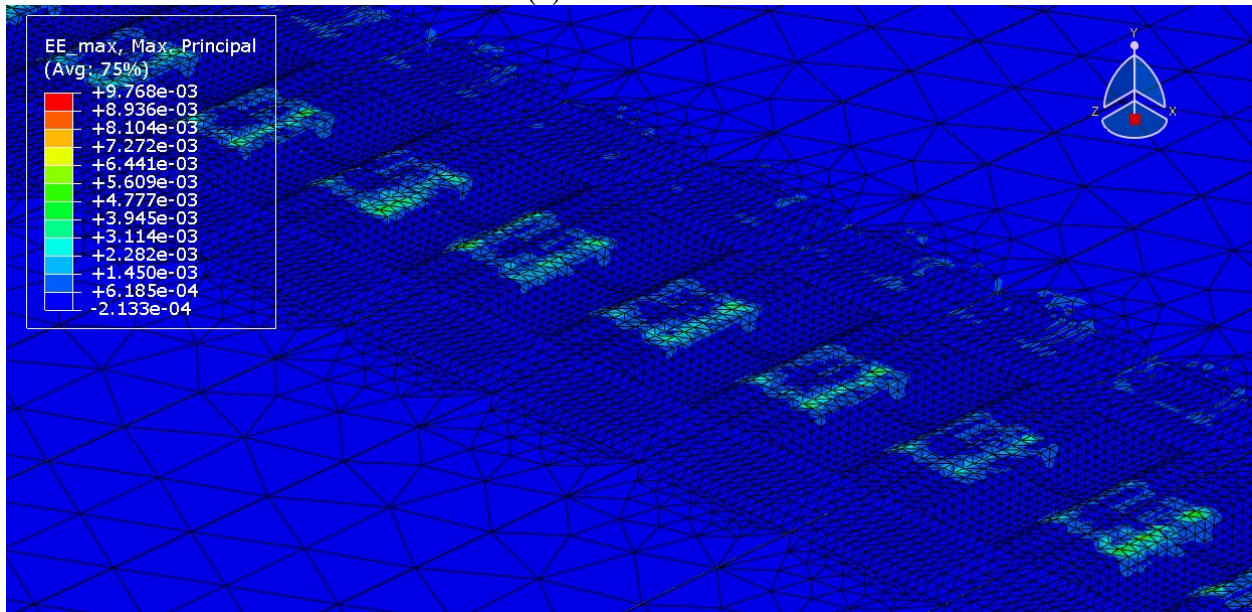
For instance, when the speed is low (48.3 kph [30mph]), the case with 6.35 mm (1/4 in) CLRS depth provides very low vibrations and dynamic loads in the model due to the lower roughness of the CLRS and the slow speed. The reduced dynamic load impact under these conditions allows the viscoelastic effect to dominate and results in a higher strain level for the models with shallow CLRS at slower speeds. For this reason, when the results for soft asphalt models for 96.6 kph (60 mph) and 48.3 kph (30 mph) speed levels were checked, it can be observed that decreasing speed results in lower strain levels for the deep (15.88 mm [5/8 in] and 12.7 mm [1/2 in]) CLRS models due to the reduced dynamic effect. However, there is an increase in strain level with decreasing speed for the model with shallow (6.35 mm [1/4 in] deep) CLRS, due to the dominating viscoelasticity effect at slower speeds (since the dynamic load effect is less significant because of lower roughness on the shallow depth CLRS).

Although, on average, the deepest rumble strips had the highest critical microstrains, it is not possible to conclude from the FEA that reducing CLRS depth can reduce critical strain levels and reduce CLRS cracking when it is installed on the construction joint. However, this conclusion changes when the results for the CLRS installed adjacent to the construction joint were analyzed later in this section (shallow CLRS provides less strain and ultimately better in-situ performance). The minimal difference in critical microstrains between 48.28 kph (30 mph) and 96.56 kph (60 mph) models can also be explained by the counteracting impacts of dynamic loading, and the viscoelasticity effects explained in the previous paragraph. Figure 3.14 shows a visible dynamic effect upon displacement values due to speed, and this trend was slightly visible with 3% higher peak microstrains for the high-speed models.

Overall, models with modified CLRS with smaller milled surface area (20.32 cm x 17.78 cm [8 in x 7 in]) provided 4% lower elastic strain values than those with conventional CLRS (40.64 cm x 17.78 cm [16 in x 7 in]). The comparison between modified and conventional CLRS models showed a small difference because the tire load distribution was equivalent between the model types. The distribution of maximum principal elastic microstrain is visible in Figure 3.20 (critical strains concentrated primarily at tire corner points).



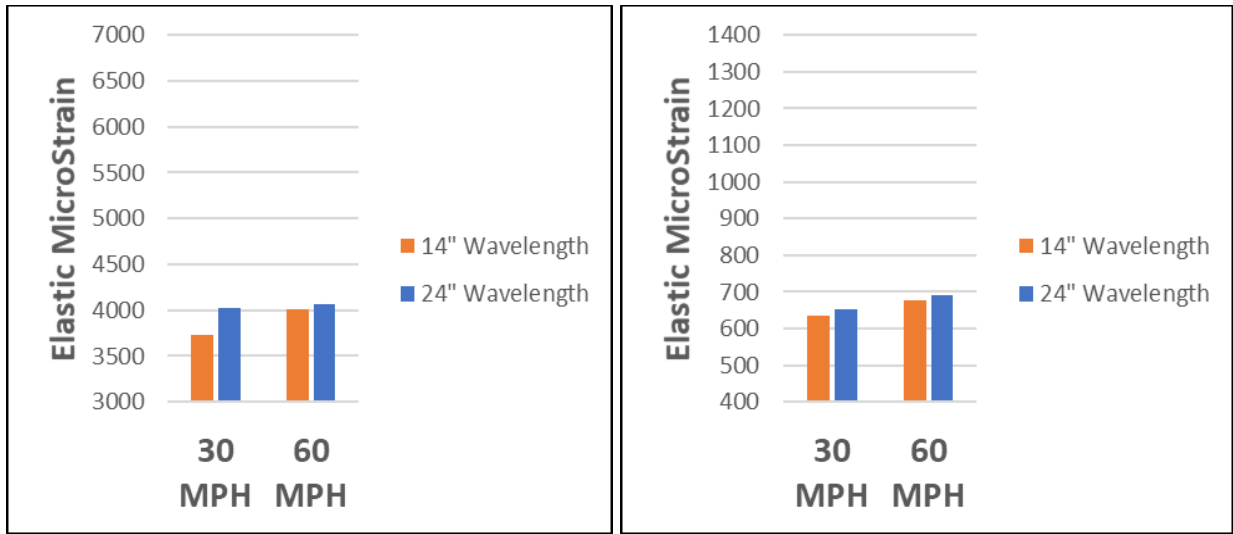
(a) Modified CLRS



(b) Conventional CLRS

Figure 3.20: Distribution of maximum principal elastic microstrain

Maximum principal elastic microstrain outputs for sinusoidal CLRS over the longitudinal joint are shown in Figure 3.21.



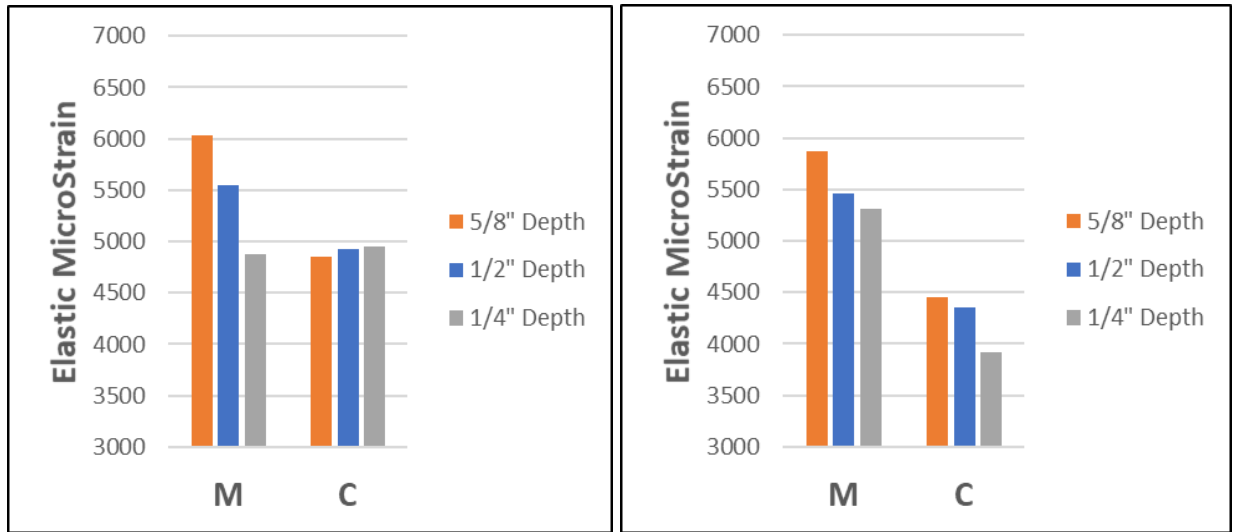
(a) Soft Asphalt - 25°C - Dual Tires

(b) Stiff Asphalt - 25°C - Dual Tires

Figure 3.21: Sinusoidal CLRS over the longitudinal joint, 1 inch (") = 2.54 cm and 1 mph = 1.61 kph

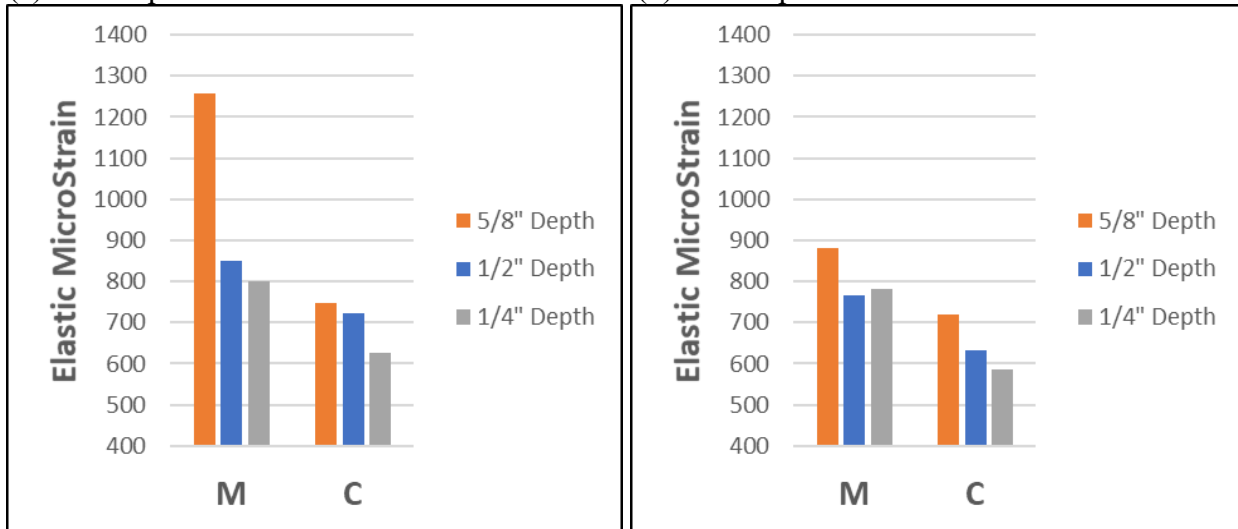
It can be observed from Figure 3.21 that a higher speed level is creating slightly higher peak microstrains (5% higher on average). Greater peak microstrains for higher speed models were an expected trend, and the relationship was stronger when compared to rectangular CLRS models over the longitudinal joint. There was no significant trend between the responses for short and long wavelength models, while shorter wavelength provided slightly less strain distribution along the longitudinal joints (3% lower on average). It is likely that the closer spacing between CLRS peaks in the shorter 355.6 mm (14 in) wavelength models resulted in a hydroplane effect where the tire load moved primarily along the peaks of the rumble strips. In the 609.6 mm (24 in) wavelength models, it was observed that the tire reached lower into the rumble strip groove than in the 355.6 mm (14 in) wavelength models. This factor could be causing increased dynamic loading and higher peak microstrains for longer sinusoidal CLRS wavelengths.

It is important to note that by comparing the strain outputs for the rectangular CLRS models to sinusoidal CLRS models (both with rumble strips directly over the joint), on average 35% lower peak microstrain can be observed for the sinusoidal CLRS models. This important conclusion points out the benefits of using sinusoidal rumble strips on roadways to reduce cracking. The sinusoidal shape of the rumble strips reduces the critical strain locations by avoiding sharp corners and edges. Maximum principal elastic microstrain outputs for rectangular CLRS adjacent to the longitudinal joint are shown in Figure 3.22.



(a) Soft Asphalt - 25°C - 60MPH - Dual Tires

(b) Soft Asphalt - 25°C - 30MPH - Dual Tires



(c) Stiff Asphalt - 25°C - 60MPH - Dual Tires

(d) Stiff Asphalt - 25°C - 30MPH - Dual Tires

Figure 3.22: Rectangular CLRS adjacent to longitudinal joint, 1 inch (") = 2.54 cm and 1 mph = 1.61 kph – M: Modified; C: Conventional

It can be observed from Figure 3.22 that unlike the models with rectangular CLRS over the longitudinal joint, the models with rectangular CLRS adjacent to the longitudinal joint experienced greater changes in trends with modified versus conventional CLRS, deep versus shallow rumble strips, and high versus low speed. The model outputs shown in Figure 3.22 provided 27% greater average peak microstrains for modified CLRS when compared to conventional CLRS. Additionally, the deepest rumble strips had 20% greater microstrains than the shallow rumble strips. Also, higher speed models observed 8% higher microstrains than low-speed models due to the dynamic load effect. Compared to rectangular CLRS adjacent to the longitudinal joint, 27% higher average peak microstrains for models over the joint were observed. This result indicates the benefits of avoiding the construction joints (when possible) when installing CLRS. Due to the weaker nature of the construction joints (not having proper

bonding between the two construction mats), installing CLRS on the joints may result in early cracking failures along the rumble strips.

In the modified rectangular CLRS models with rumble strips adjacent to the joint, the peak microstrains were concentrated primarily at the corner points of the rumble strips away from the joint (same load distribution as Figure 3.20[a]). In the conventional CLRS models, the peak microstrains were more evenly distributed along the front and back edges of the tire with less concentration at the corner points, which led to lower peak microstrains. The improved performance of the conventional CLRS in the models contradicts the laboratory bending beam test results (See Section 4.0). This is likely because of the tire position with respect to the longitudinal joint. Because the joint was completely unbonded in the models, the tire load adjacent to the joint was applied only to the lane with CLRS installed. This led to variations in load transfer in models with CLRS adjacent to the longitudinal joint. For example, modified CLRS showed slightly better performance than conventional rumbles in the models over the joint, as expected. This is because the tire load was directly over the longitudinal joint, and distributed nearly evenly between the travel lanes, as would be the case in physical testing.

The trend of deeper rumble strips experiencing higher peak microstrains is aligned with expectations of less structural resistance since more asphalt is milled from the surface. The other potential reason is the higher impact of dynamic loads on the deeper rumble strips due to the higher roughness of the surface. The trend of higher-speed models seeing higher peak microstrains was expected due to the dynamic loading effect.

The overall average impacts on peak microstrain of the factors tested in the rectangular, sinusoidal, and control models are as follows:

- Sinusoidal CLRS versus rectangular CLRS: Sinusoidal demonstrates superior performance (35% lower peak microstrain).
- Shallow versus deep rumble strip depth: 6.35 mm (1/4 in) depth CLRS (not currently in the ODOT standard) showed improved performance in comparison to 15.88 mm (5/8 in) depth (13% lower peak microstrain).
- Conventional (40.64 cm x 17.78 cm [16 in x 7 in]) versus modified (20.32 cm x 17.78 cm [8 in x 7 in]) rectangular CLRS: Conventional CLRS shows improved performance with 11% lower peak microstrain [contradicts the laboratory bending beam test results (See Section 4.0)].
- 48.28 kph (30 mph) versus 96.56 kph (60 mph) tire speed: Slower tire speed led to decreased critical strains (4% lower peak microstrain).
- Soft asphalt versus stiff asphalt: Stiff asphalt (due to the use of stiffer asphalt binder or aging in the field) results in lower critical microstrains (434% lower peak microstrain).
- Front axle single tire versus rear dual tandem axle: Dual tire load case was critical with 34% higher peak microstrain.

- 355.6 mm (14 in) versus 609.6 mm (24 in) wavelength: Shorter wavelength demonstrates improved performance (3% lower peak microstrain).
- Rumble strips/tires over longitudinal joint versus adjacent to the joint: Installing CLRS adjacent to the joint (3 inches away from the joint) shows better performance (27% lower peak microstrain).

In general, observed trends via maximum principal elastic microstrain outputs are also seen in maximum principal stress outputs. The FEA modeling results provided insight towards improving the cracking and structural performance of CLRS. A major conclusion was that sinusoidal CLRS showed better performance than rectangular CLRS. The sinusoidal shape of the rumble strips reduces the critical strain locations by avoiding sharp corners and edges. This finding agreed with the Hamburg Wheel Tracking and bending beam test results presented in Section 4.0.

Another conclusion was that shallow CLRS depths lead to improved performance, and this was because of two reasons: 1) Less asphalt is milled from the pavement, so there is more structural resistance and less sharp edges, 2) Dynamic loading is reduced due to the shallow rumble strip groove and smoother edges. This was an expected result since thicker CLRS depths reduce the pavement's thickness and provide less resistance to vehicular loads. These results aligned with those of the Hamburg Wheel Tracking and bending beam test results presented in Section 4.0.

The next significant outcome of the FEA modeling was improved performance with CLRS installed adjacent to the longitudinal joint. The construction joints are weak points (improper bonding between the construction mats) in the pavement structure and installing CLRS atop the joint has the potential to weaken it further. Installing CLRS on the joints may result in early cracking failures at the rumble strips.

A potential finding in regard to sinusoidal wavelength was improved performance for shorter wavelength rumbles. It is likely that the closer spacing between CLRS peaks in the short wavelength models resulted in a hydroplane effect where the tire load moved primarily along the peaks of the rumble strips (especially at faster speeds). This factor could be causing increased dynamic loading and higher peak microstrains for longer sinusoidal CLRS wavelengths. It is possible that this conclusion could also be applied to rectangular CLRS, where the shorter spacing between rumbles could result in less critical strains (cracking). However, reducing the spacing has the potential to decrease driver notification due to less dynamic loading. Additional research is needed to measure and determine the potential impact of different CLRS types (including the ones recommended based on the results of this study) on sound, vibrations, and safety.

4.0 CENTERLINE RUMBLE STRIPS LABORATORY TESTING

4.1 INTRODUCTION

The centerline rumble strips (CLRS) literature review identified potential factors influencing the long-term performance of pavements with CLRS. Several of these factors were tested and evaluated in this study to fill the gap in knowledge with respect to cracking failure mechanisms of CLRS. Section 4.0 presents the following research methodology and results and conclusions from the field test strip construction and laboratory testing.

Hydro-static pressure damage from rainwater in asphalt pavements has been identified to have negative impacts on performance and cause deterioration. Milling rumble strips into the pavement surface may cause microcracks allowing water to infiltrate the surface lift as well as subsequent pavement lifts (Datta et al., 2012). The microcracks may also be leading to increased oxidation of the pavement due to increased permeability. Adverse outcomes of water infiltration and high permeability may include stripping, damage to bonding between lifts, and premature bottom-up fatigue cracking. Freeze-thaw cycles might also be affecting the cracking resistance of the rumble strips. Water may be infiltrating the microcracks in the CLRS, which the milling system might introduce, and proceeding to the asphalt layer. In cold climates, this moisture expands as it freezes and leads to increased cracking damage (Guin et al., 2014). The following sections attempt to quantify these potential forms of moisture and freeze-thaw damage in CLRS, as well as the presence of microcracks.

The longitudinal construction joint within HMA construction generally cannot be properly compacted, and thus density is lower than in the travel lane. These joints are accepted to be weaker spots that are more vulnerable to cracking and permanent deformation. As such, CLRS are suspected of causing increased damage when milled on or near the longitudinal joint (FHWA, 2015a). Although one of the objectives of this study was to determine the impact of longitudinal joints on CLRS cracking resistance, longitudinal joint evaluations were excluded from the results due to the unavailability of the asphalt plant for constructing two pavement lanes on separate days (two productions with the same asphalt mixture). For this reason, according to the nuclear density gauge and laboratory density measurements, the density of the asphalt concrete along the longitudinal joints is almost the same as the density of the asphalt concrete in the travel lane of the test section. This was expected since the two lanes along the test strip were constructed within the same hour without waiting for the first lane to cool or age. The following sections include investigations of control samples, samples in the travel lane, samples along the edge of construction, and samples along the longitudinal joint and adjacent to the joint. As mentioned, no assessments were made regarding the impact on pavement performance of CLRS installed along the longitudinal joint. However, using the test results from the asphalt specimens removed from the edge of the test strip (which had significantly lower density than the specimens removed from the middle of the test section), the impact of asphalt layer density on cracking resistance was quantified in this study. These results are expected to reflect the impact

of installing CLRS on longitudinal construction joints. In addition, the impact of installing CLRS on longitudinal joints was also evaluated in Section 3.0 via FEA.

Surface seals (fog seal and chip seal) are expected to positively impact pavement performance following CLRS installation. Applying fog seals and chip seals can reduce oxidation and moisture infiltration and may mitigate damage stemming from CLRS microcracks (FHWA, 2011) (FHWA, 2015a). The impact of chip sealing on CLRS permeability and cracking resistance was explored in this study.

CLRS size, depth, and type are suspected to impact pavement durability differently. Rather than the rectangular style rumble strips, the sinusoidal geometry has unknown impacts on pavement performance. Conventional 40.64 cm x 17.78 cm (16 in x 7 in) and modified 20.32 cm x 17.78 cm (8 in x 7 in) CLRS geometries that are currently used by the Oregon Department of Transportation (ODOT) may provide different structural performances. The depth of the rumble strip may also impact the pavement's durability. These factors are also examined in this part of the research study.

Vehicle dynamic impact loads have been correlated to roadway roughness (Cebon, 1993). These dynamic loads may be further increased due to CLRS installation. The following sections seek to quantify pavement roughness with varying rumble strip scenarios according to ODOT TM 772 (2011) to determine the impact of CLRS installation on roughness and dynamic loads. Extremely high roughness of the CLRS might be resulting in dynamic truckloads that are significantly higher than the static load of the vehicle. This excessive dynamic load might result in single event cracking with just a one-time passage of a heavy truck on the rumble strip.

One of the main goals of this study was to develop testing procedures for CLRS samples to determine the impact of the factors described above. The following methods were used in testing CLRS samples:

1. Rainfall simulation;
2. Freeze-thaw cycling;
3. Moisture infiltration test;
4. Hamburg Wheel Tracking Test;
5. Three-point flexural fatigue test;
6. X-ray CT imaging; and
7. International Roughness Index measurements using a walk-behind profiler.

The FEA modeling helped guide the laboratory testing by demonstrating which factors had the greatest impacts on CLRS structural performance. These factors (sinusoidal versus rectangular, CLRS depth, CLRS distance from longitudinal joint, and CLRS width) were therefore included in the laboratory testing plan.

4.2 MATERIALS AND METHODS

4.2.1 Experimental Design

This section will discuss the various parts of the experimental design to include an on-site test strip constructed at the Corvallis Knife River site and the experimental plan.

4.2.1.1 Test strip construction

To investigate the effects of various factors on pavement durability, Oregon State University (OSU) coordinated with Knife River Corporation in Corvallis to construct a test strip at their local plant. Rumble strips were milled into the asphalt concrete surface, and then samples were extracted (cored and sawn) in order to test at the OSU Asphalt Materials and Pavements (OSU-AMaP) Laboratory. This specimen production method was selected in order to accurately simulate typical field construction conditions, rumble strip installation, and other practices.

The test strip was constructed over an existing gravel base on June 25, 2020. The constructed surface course was 7.62 cm (3 in) thick asphalt concrete. The roadway was constructed following standard ODOT paving procedures, and an ODOT inspector (Brady A. Pauls – ODOT Senior Construction Coordinator, personal communication, June 25, 2020) was present during the construction. Nuclear density gauge measurements were also taken during construction to determine density. Ramps were also constructed for milling machine access at each end of the section. The roadway section was 45.72 m (150 ft) long and 7.32 m (24 ft) wide. Lanes were 3.66 m (12 ft) wide, running along a longitudinal construction joint. There were no seals or surface treatments applied to the surface directly after construction. Photos from the construction and asphalt sampling are given in Figure 4.1.

Approximately one month after construction, 30 random field cores of 15.24 cm (6 in) diameter were extracted to test for density, stiffness, and cracking resistance. The cores were taken from the first 7.93 m (26 ft) at either end of the section (far away from the locations that CLRS were installed), with 10 cores taken directly over the longitudinal joint. Also, at this time, 22 randomly located permeability tests of 15.24 cm (6 in) diameter were conducted within the entire roadway area.

The contractor, Specialized Pavement Marking Inc., milled standard ODOT centerline rumble strips in February 2021. The 8-month time gap between the initial construction and rumble strip installation was due to the unavailability of the contractor. It should be noted that there is no requirement regarding the length of the time interval between construction and RS installation. The only recommendation provided for Oregon is to avoid any RS installation on asphalt-surfaced pavements five years after the construction (Timothy Earnest and Justin Moderie (personal communication, October 19, 2018)). Three equal length sections (9.75 m [32 ft]) of rumble strips were milled with the features described in Table 4.1, where:

- Conventional CLRS: ODOT DET 4556 (see Figure 3.10), 40.64 cm x 17.78 cm (16 in x 7 in)
- Modified CLRS: ODOT DET 4557 (see Figure 3.11), 20.32 cm x 17.78 cm (8 in x 7 in)
- Sinusoidal CLRS: Custom Design (see Figure 3.12), 40.64 cm (16 in) width plus 5.08 cm (2 in) taper, 40.64 cm (16 in) wavelength.

Table 4.1: Test Section Rumble Strip Features

| | | Section 1 | Section 2 | Section 3 |
|--|---------------------------------------|--------------------------|--------------------------|---|
| CLRS Depth | | 1.27 cm (1/2 in) | 1.59 cm (5/8 in) | 1.27 cm (1/2 in) 1.59 cm (5/8 in) ¹ |
| CLRS Type | Over Longitudinal Joint | Modified | Modified | Sinusoidal |
| | Adjacent to Longitudinal Joint | Modified | Modified | Sinusoidal |
| | In Travel Lane | Conventional Modified | Conventional Modified | Sinusoidal |
| Longitudinal CLRS Spacing | | 12.7 cm (5 in) | 12.7 cm (5 in) | Continuous |
| Transverse CLRS Spacing² | | 25.4 cm (10 in) | 25.4 cm (10 in) | 25.4 cm (10 in) |

¹No longitudinal joint

²Increased to 35.56 cm (14 in) near the longitudinal joint

Control asphalt blocks were extracted from the remaining 7.92 m (26 ft) segments at the ends of the test section. The roadway contained a total of approximately 248 conventional CLRS in the lane in sections 1 and 2 combined. Regarding the modified CLRS, there were approximately 496 in the lane, 52 over the longitudinal joint, and 10 adjacent to the longitudinal joint (edge of the CLRS about 3 inches away from the joint) in sections 1 and 2 combined. There were approximately 192 sinusoidal CLRS in the lane and 24 over the longitudinal joint in section 3. It should be noted that (also as described in Section 4.1) due to the unavailability of the plant and the construction team for two different days, both lanes were constructed within the same day, which did not allow for the construction of an actual construction joint with a lower density. However, since the east side of the test strip did not have any restraining support along the shoulder, the density of the 2 feet length along the east edge had 4-5% less density than the rest of the section. For this reason, results from the asphalt specimens extracted from that east edge can be considered to be correlated with an actual construction joint response. Figure 4.1 shows the test section construction as well as the asphalt sampling. See figure 4.2 for a visual representation of the test strip at the Knife River facility (with rumble strip locations) and Figure 4.3 for the coring and permeability test locations.



(a) Section before construction (6/25/2020 – 7am)



(b) Section construction (6/25/2020 – 12pm)



(c) Section after construction



(d) Milling equipment (courtesy Specialized Pavement Marking, Inc.)



(e) Section during CLRS milling (2/26/2021)



(f) Coring for laboratory density measurement and testing



(g) Sampled asphalt cores



(h) Diamond blade walk-behind saw



(i) Typical asphalt slab cuts using the walk-behind saw



(j) Typical asphalt blocks extracted from the test section

Figure 4.1: Test strip construction and sample extraction

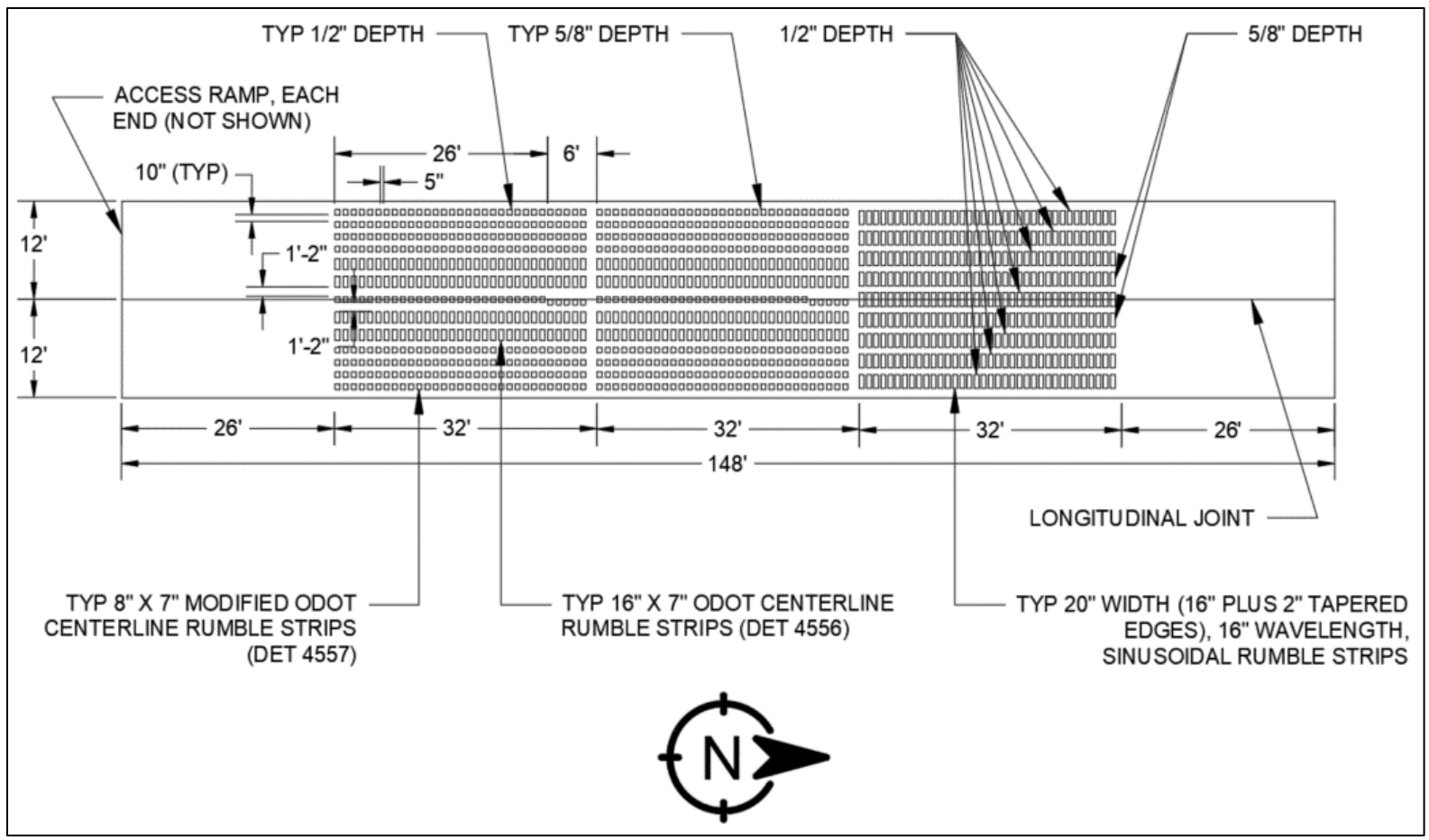


Figure 4.2: CLRS installation plan at the test strip (" corresponds to inches and ' corresponds to feet)

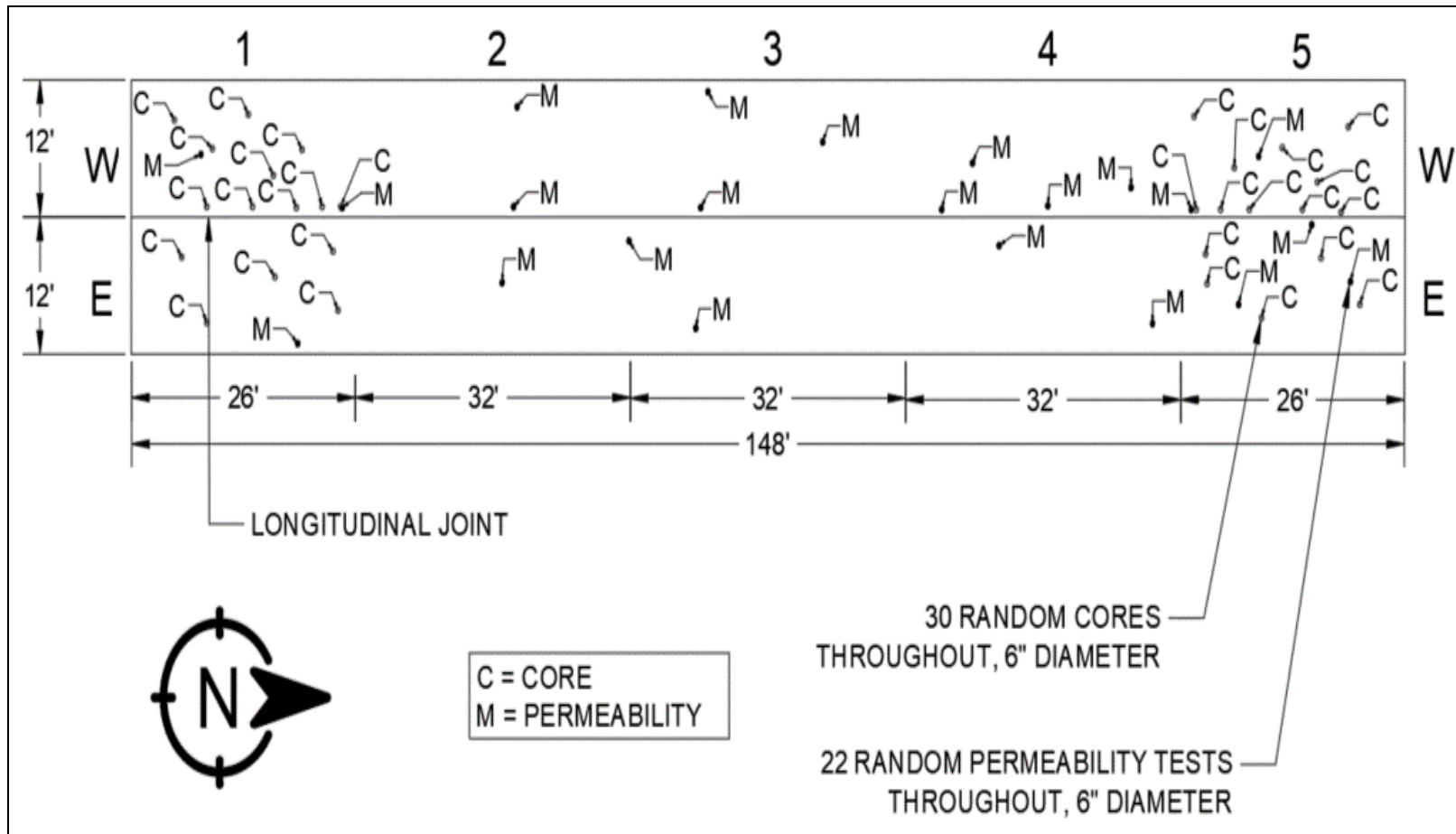


Figure 4.3: Coring and permeability testing plan (“ corresponds to inches and ‘ corresponds to feet)

4.2.1.2 Experimental plan

The following factors were examined for effects on pavement durability due to rumble strip installation:

1. CLRS type (rectangular versus sinusoidal); and
2. CLRS geometry (40.64 cm x 17.78 cm [16 in x 7 in] versus 20.32 cm x 17.78 cm [8 in x 7 in]); and
3. CLRS depth (1.27 cm [1/2 in] versus 1.59 cm (5/8 in)); and
4. Climate (rain [See Section 4.3.5] and freeze-thaw [See Section 4.3.9]); and
5. Surface treatment (chip seal after rumble strip installation) - See Section 4.3.8.

Rumble strips extracted from the test section underwent cyclic three-point flexural fatigue tests, Hamburg Wheel Tracking Tests (HWTT), and moisture infiltration tests. Samples with surface treatment also underwent each testing method. Samples exposed to freeze-thaw cycling were tested in flexural fatigue tests and HWTT only. See Table 4.2 through Table 4.8 for a comprehensive experimental factorial for testing CLRS samples.

Table 4.2: Laboratory Experimental Plan - Phase 1, Modified 20.32 cm x 17.78 cm (8 in x 7 in) CLRS, in the Lane

| Test Type | CLRS Depth | Conditioning | Surface Treatment | Replicates | Minimum Total Tests |
|----------------------------------|------------------|-------------------------------|---------------------------|------------|---------------------|
| Beam Test¹ | 1.27 cm (1/2 in) | Freeze-Thaw No Freeze-Thaw | Chip Seal No Chip Seal | 4 | 16 |
| | 1.59 cm (5/8 in) | No Freeze-Thaw | Chip Seal No Chip Seal | 4 | 8 |
| HWTT | 1.27 cm (1/2 in) | Freeze-Thaw No Freeze-Thaw | Chip Seal No Chip Seal | 3 | 12 |
| | 1.59 cm (5/8 in) | No Freeze-Thaw | No Chip Seal | 3 | 3 |
| Moisture Test² | 1.27 cm (1/2 in) | No Freeze-Thaw | Chip Seal No Chip Seal | 4 | 8 |

¹Eight additional non-chip seal, 1.27 cm (1/2 in) depth samples were extracted from the edge of the lane.

²Six additional samples were extracted from the edge of the lane.

Table 4.3: Laboratory Experimental Plan - Phase 2, Modified 20.32 cm x 17.78 cm (8 in x 7 in) CLRS, Over the Longitudinal Joint

| Test Type | CLRS Depth | Conditioning | Surface Treatment | Replicates | Minimum Total Tests |
|----------------------|------------------|----------------|---------------------------|------------|---------------------|
| Beam Test | 1.27 cm (1/2 in) | No Freeze-Thaw | Chip Seal | 4 | 16 |
| | 1.59 cm (5/8 in) | | No Chip Seal | | |
| HWTT | 1.27 cm (1/2 in) | No Freeze-Thaw | Chip Seal No Chip Seal | 3 | 6 |
| | 1.59 cm (5/8 in) | No Freeze-Thaw | No Chip Seal | 3 | 3 |
| Moisture Test | 1.27 cm (1/2 in) | No Freeze-Thaw | Chip Seal No Chip Seal | 3 | 6 |

Table 4.4: Laboratory Experimental Plan – Phase 3, Modified 20.32 cm x 17.78 cm (8 in x 7 in) CLRS, Adjacent to the Longitudinal Joint

| Test Type | CLRS Depth | Conditioning | Surface Treatment | Replicates | Minimum Total Tests |
|----------------------|--------------------------------------|----------------|-------------------|------------|---------------------|
| Beam Test | 1.27 cm (1/2 in) 1.59 cm (5/8 in) | No Freeze-Thaw | No Chip Seal | 2 | 4 |
| HWTT | 1.27 cm (1/2 in) 1.59 cm (5/8 in) | No Freeze-Thaw | No Chip Seal | 2 | 4 |
| Moisture Test | 1.27 cm (1/2 in) | No Freeze-Thaw | No Chip Seal | 1 | 1 |

Table 4.5: Laboratory Experimental Plan - Phase 4, Conventional 40.64 cm x 17.78 cm (16 in x 7 in) CLRS, in the Lane

| Test Type | CLRS Depth | Conditioning | Surface Treatment | Replicates | Minimum Total Tests |
|------------------|------------------|-------------------------------|---------------------------|------------|---------------------|
| Beam Test | 1.27 cm (1/2 in) | Freeze-Thaw No Freeze-Thaw | Chip Seal No Chip Seal | 4 | 16 |
| | 1.59 cm (5/8 in) | No Freeze-Thaw | Chip Seal No Chip Seal | 4 | 8 |

Table 4.6: Laboratory Experimental Plan - Phase 5, Sinusoidal 50.8 cm (20 in) wide CLRS, in the Lane

| Test Type | CLRS Depth | Conditioning | Surface Treatment | Replicates | Minimum Total Tests |
|----------------------|------------------|-------------------------------|---------------------------|------------|---------------------|
| Beam Test | 1.27 cm (1/2 in) | Freeze-Thaw No Freeze-Thaw | Chip Seal No Chip Seal | 4 | 16 |
| | 1.59 cm (5/8 in) | No Freeze-Thaw | Chip Seal No Chip Seal | 4 | 8 |
| HWTT | 1.27 cm (1/2 in) | No Freeze-Thaw | Chip Seal No Chip Seal | 3 | 6 |
| | 1.59 cm (5/8 in) | No Freeze-Thaw | No Chip Seal | 3 | 3 |
| Moisture Test | 1.27 cm (1/2 in) | No Freeze-Thaw | Chip Seal No Chip Seal | 4 | 8 |

Table 4.7: Laboratory Experimental Plan - Phase 6, Sinusoidal 50.8 cm (20 in) wide CLRS, Over the Longitudinal Joint

| Test Type | CLRS Depth | Conditioning | Surface Treatment | Replicates | Minimum Total Tests |
|----------------------|------------------|----------------|---------------------------|------------|---------------------|
| Beam Test | 1.27 cm (1/2 in) | No Freeze-Thaw | Chip Seal No Chip Seal | 4 | 8 |
| HWTT | 1.27 cm (1/2 in) | No Freeze-Thaw | Chip Seal No Chip Seal | 3 | 6 |
| Moisture Test | 1.27 cm (1/2 in) | No Freeze-Thaw | Chip Seal No Chip Seal | 2 | 4 |

Table 4.8: Laboratory Experimental Plan - Phase 7, Control Samples, in the Lane

| Test Type | CLRS Depth | Conditioning | Surface Treatment | Replicates | Minimum Total Tests |
|----------------------------------|------------|-------------------------------|---------------------------|------------|---------------------|
| Beam Test | N/A | Freeze-Thaw No Freeze-Thaw | Chip Seal No Chip Seal | 4 | 16 |
| HWTT | N/A | Freeze-Thaw No Freeze-Thaw | Chip Seal No Chip Seal | 3 | 12 |
| Moisture Test¹ | N/A | No Freeze-Thaw | Chip Seal No Chip Seal | 2 | 4 |

¹Five additional control samples without surface treatment were extracted from the edge of the lane

The experimental plan displayed resulted in a total of 61 of the modified 20.32 cm x 17.78 cm (8 in x 7 in) samples extracted in the lane away from the construction joint (Phase 1), 31 samples extracted at the longitudinal joint (Phase 2), and 9 samples extracted adjacent to the longitudinal joint (Phase 3). There were a total of 24 of the conventional 40.64 cm x 17.78 cm (16 in x 7 in) CLRS sampled in the lane (Phase 4). Also, a total of 41 of the sinusoidal CLRS were extracted in the lane (Phase 5) and 18 were extracted over the longitudinal joint (Phase 6). In addition, 37 control samples were extracted away from the construction joint in the lane (Phase 7).

The purpose of comparing the test results from Phase 1 to Phase 2 and the test results from Phase 3 to Phase 1 and Phase 2 was to quantify the impact of CLRS installations on or adjacent to the longitudinal joint. However, as mentioned in Section 4.1, asphalt density at the longitudinal joint was not representative of a typical construction joint. For this reason, comparisons were not made between Phases 1, 2, and 3, but the impacts of the strategies within phases were still examined. The impact of CLRS width on long-term cracking performance was determined by comparing the test results from Phase 4 to Phase 1. In addition, the impact of sinusoidal CLRS on the rumble strip performance was quantified by comparing Phase 5 and Phase 6 to the previous phases. Phase 7 control samples were tested as the baseline for rumble strip samples in Phases 1-6. Test results from all phases were also used to quantify the impact of freeze-thaw damage and surface treatment on the long-term CLRS performance.

In addition to the tests given in the laboratory experimental plan, preliminary experiments were conducted on core specimens from the test strip for density, stiffness, and cracking resistance. The tests included Indirect Tensile (IDT) strength, Resilient Modulus (RM), Corelok method air voids measurement, and saturated surface-dry (SSD) method air voids measurement. Field permeability tests were also conducted at the test strip. Table 4.9 gives the testing plan for the preliminary core and permeability testing. Sample locations are given in figure 4.3.

Table 4.9: Core and Field Permeability Experimental Plan

| Test Type | Location | Replicates | Minimum Total Tests |
|---------------------|--|-------------------|----------------------------|
| IDT | 4 quadrants, in the lane 2 quadrants, over the longitudinal joint | 5 | 30 |
| RM | 4 quadrants, in the lane 2 quadrants, over the longitudinal joint | 5 | 30 |
| Corelok | 4 quadrants, in the lane 2 quadrants, over the longitudinal joint | 5 | 30 |
| SSD | 4 quadrants, in the lane 2 quadrants, over the longitudinal joint | 5 | 30 |
| Permeability | Randomized to quantify spatial variability | 22 | 22 |

4.3 LABORATORY TEST METHODS

This section will detail the testing methods with correlating standards. The section includes the aforementioned IDT test, RM test, Air voids measurement test,

4.3.1 Indirect Tensile (IDT) Strength Test

ASTM D6931-17 (2017a) standard test method was followed for Indirect Tensile (IDT) strength tests. The procedure is useful for determining the cracking potential of asphalt mixes. IDT testing was used in this study to evaluate the cracking performance of field cores extracted from multiple locations at the Knife River test section. The spatial variability of cracking resistance was also determined using the test results. Field cores were approximately 146.5 mm in diameter and were cut to a thickness of 50 mm. The cylindrical cores were tested under a 50 mm/min constant displacement rate by loading along their vertical diametric planes. Tests were performed at 25°C. The peak load at failure was used to calculate the indirect tensile strength of the specimen.

4.3.2 Resilient Modulus (RM) Test

ASTM D7369-11 (2011) standard test method was followed for the Resilient Modulus (RM) tests. The procedure is useful for determining the stiffness of asphalt mixes. The non-destructive RM tests were run prior to IDT tests performed on field cores extracted from the Knife River test section. The cylindrical cores were tested along their vertical diametric planes under a cyclic haversine load of 2,402 N and contact load of 89 N. Samples were loaded for five repetitions with a loading pulse of 250 milliseconds, a rest period of 2750 milliseconds, and a repetition period of 3,000 milliseconds. Tests were performed at 25°C. The instantaneous resilient modulus of the five loading pulses was recorded, and the mean resilient modulus was calculated for every sample.

4.3.3 Air Voids Measurement

4.3.3.1 Saturated surface-dry (SSD) method

Field cores extracted from the Knife River test strip section were tested for air void content following AASHTO T 166 (2022) procedure. The suspension method was utilized. Dry mass, submerged mass, and saturated surface-dry mass were recorded, and bulk specific gravity was calculated. Theoretical maximum specific gravity was used to determine the percent air void content of the specimens. SSD tests were conducted prior to IDT and RM testing.

4.3.3.2 Corelok method

Field cores extracted from the Knife River test strip section were also tested for air void content using the Corelok system. The Corelok method follows the same procedure as AASHTO T 166 (2022), but vacuum seals specimens before submersion. Bulk specific gravity was calculated, and theoretical maximum specific gravity was used to determine

the percent air void content of the samples. Corelok tests were conducted prior to IDT and RM testing.

4.3.4 Field Infiltration Test Method

Field infiltration tests were conducted using a modified version of the ASTM C1701 (2017b) testing procedure. To conduct the test, marks were made inside a 152 mm (6.0 in) hollow cylinder at heights of 10 and 15 mm (0.4 and 0.6 in) to maintain a constant pressure head as the water was added. The cylinder was then adhered in place using a waterproof silicone rubber to prevent water from leaking at the bottom of the cylinder. Prewetting was conducted to fill surface voids and check for leaks by adding 3.6 kg (8.0 lbs.) of water to the cylinder at a rate to maintain a constant head. The prewetting time was recorded, and if under 30 seconds, 18.0 kg (40 lbs.) of water was used. If greater than 30 seconds, 3.6 kg (8.0 lbs.) of water was used. Within 2 minutes of the prewetting stage, the appropriate amount of water was measured and poured into the cylinder until filled between the 10 and 15 mm (0.4 and 0.6 in) mark. The start time was recorded, and water was continually added to the cylinder to maintain a head between the marked lines. The test then stopped, and the time was recorded once all the water poured into the cylinder had infiltrated through the asphalt surface. Tests were stopped if there was no initial infiltration or if water had stopped infiltrating after a span of two hours. An infiltration test using the setup described is shown in Figure 4.4. The infiltration rate for each sample was calculated as follows:

$$I = \frac{KM}{(D^2 * t)} \tag{4-1}$$

where:

- I = infiltration rate (mm/hr),
- M = mass of infiltrated water (kg),
- D = inside diameter of infiltration ring (mm),
- t = time required for measured water to infiltrate (s),
- K = 4,583,666,000 (mm³*s)/(kg*h)



Figure 4.4: Field infiltration test

4.3.5 Rainfall Simulation and Moisture Infiltration Tests

4.3.5.1 Laboratory rainfall simulation and moisture infiltration sample preparation

Rainfall simulation experiments were conducted using a rainfall simulator developed at OSU that simulates a natural rainfall pattern to continually saturate samples over a five-day span. The complete moisture sensor setup is depicted in Figure 4.5. For moisture infiltration tests, two holes were drilled 5.08 cm (2 in) from the surface of the asphalt sample. A moisture sensor was inserted into the holes, and HM-108 Graded Standard Sand was used to fill the remaining voids around the sensor nodes and provide a medium through which any infiltrated water could reach the nodes (Figure 4.5(a) and Figure 4.5(b)). The moisture sensor was then sealed using a silicone gel to prevent water from reaching the sensor from the exterior, as opposed to reaching the sensor by permeating through the asphalt (Figure 4.5(c)). The sensor was wrapped in plastic wrap (Figure 4.5(d)), and a protective cover was placed over the edge of the block to further ensure that no moisture reached the sensor from the sides of the sample or from the insertion point of the sensor nodes (Figure 4.5(e)). Properly sealing the end of the block and exterior of the moisture sensor was critical to ensure that any moisture being detected by the sensor had passed through the asphalt to reach the sensor.



(a) Holes drilled



(b) Sand and sensor inserted



(c) Moisture sensor sealed with silicone gel



(d) Sensor wrapped in plastic



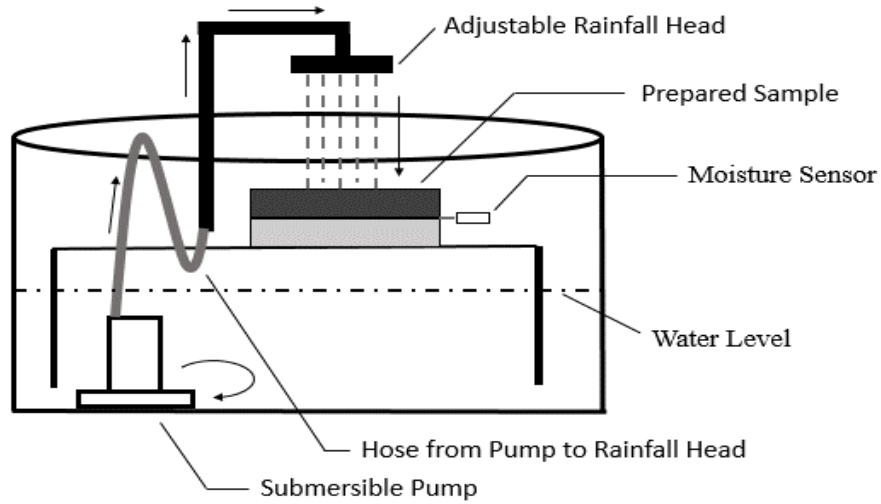
(e) Protective covering placed over the sensor area

Figure 4.5: Moisture infiltration sample preparation

4.3.5.2 Rainfall simulation and moisture infiltration testing procedure

For this test, samples were placed under the rainfall simulator and subjected to a steady simulated rainfall event over a five-day span. A depiction of the rainfall simulator test setup is shown in Figure 4.6(a). A flowrate of 1.9 L/min (0.5 gal/min) was used (Haynes et al., 2020). A customized moisture sensor was embedded 5.08 cm (2 in) below the surface of the asphalt sample. The sensor was used to continually log data for the test and consisted of two main components. The sensor component was comprised of a CS655 Water Content Reflectometer produced by Campbell Scientific, Inc. The CS655 possessed two 30 cm (11.81 in) long nodes and was capable of measuring volumetric water content, bulk electrical conductivity, and temperature. The data logger component was capable of running up to four serial data interface (SDI-12) sensors (such as the CS655) simultaneously. The SDI-12 data logger ran on an open-source Python script and could collect continuous data for months at a time (Liu, 2015).

The moisture sensor used for the tests was calibrated to take moisture readings every 10 seconds and export the readings to a spreadsheet. Moisture readings were directly measured by reading the dielectric permittivity within a sample, then converting the reading to a volumetric water content (m^3/m^3). From the output, the amount of water infiltrated 5.08 cm (2 in) below the surface of the asphalt sample was tracked over time so that the point at which infiltration occurred could be determined (Liu, 2015). If the surface treatment installed on the samples functioned as designed (control, conventional CLRS, modified CLRS, or sinusoidal), no moisture infiltration would be detected by the sensors over the analysis period. Figure 4.6(b) displays a typical moisture infiltration test in operation.



(a) Rainfall simulator diagram



(b) Sample undergoing infiltration test

Figure 4.6: Rainfall simulator test setup

4.3.6 Three-point Flexural Fatigue Test

4.3.6.1 Three-point flexural fatigue sample preparation

Large asphalt blocks were sawn from the Knife River test strip for three-point flexural fatigue testing. The block samples were cut to 34.29 cm (13.5 in) long by 24.13 cm (9.5 in) wide by using a high-precision saw at the OSU-AMaP laboratory. Flexural fatigue sample varieties included in the experimental factorial of Section 4.2 are shown in Figure 4.7.



(a) Control sample (no CLRS), view 1



(b) Control sample (no CLRS), view 2



(c) 20.32 cm x 17.78 cm (8 in x 7 in)
CLRS sample, view 1



(d) 20.32 cm x 17.78 cm (8 in x 7 in) CLRS
sample, view 2



(e) 40.64 cm x 17.78 cm (16 in x 7 in)
CLRS sample, view 1



(f) 40.64 cm x 17.78 cm (16 in x 7 in) CLRS
sample, view 2



(g) Sinusoidal CLRS sample, view 1



(h) Sinusoidal CLRS sample, view 2

Figure 4.7: Three-point flexural fatigue sample varieties

The bottom edge of every sample was cut to achieve a thickness of 6.99 cm (2.75 in) using a water-cooled high-precision diamond blade saw (Figure 4.8). Samples were allowed to dry for a minimum of seven days under ambient laboratory conditions (approximately 25°C [77°F]). Sample length, width, and thickness after cutting were recorded with tolerances of ± 1.27 cm ($\pm 1/2$ in), ± 1.27 cm ($\pm 1/2$ in), and ± 0.64 cm ($\pm 1/4$

in), respectively. The tolerance for skewness in sample thickness due to uneven cuts was ± 0.64 cm ($\pm 1/4$ in).



Figure 4.8: Cutting samples using water-cooled diamond blade

After drying, samples were conditioned for a minimum of 24 hours in a sealed chamber with an air temperature of 25°C (77°F). A specialized testing jig was developed at OSU by CEOAS Machine and Technical Development Facility staff for testing the block samples (Figure 4.9(a)). The jig consisted of two rollers positioned underneath the sample on either side to allow freedom of movement during the bending of the sample. A custom load plate was centered on top of the sample to evenly distribute applied loads along its width. A lubricated rubber membrane was placed at the three contact points to reduce stress concentrations at the load plate and allow for horizontal movement of the sample as deflection occurred. Samples were inverted for testing in order to simulate CLRS surface cracking conditions. Samples that were unable to rest flat atop the rollers due to rumble strip curvature or chip seal aggregates were leveled using Devcon 10240 Plastic Steel 5 Minute Putty (Figure 4.9(c) & (d)).



(a) Three-point bending frame developed at OSU



(b) Three-point bending sample positioned in the Universal Testing Machine (UTM)



(c) Devcon used to flatten ends due to rumble strip curvature



(d) Devcon used to flatten ends due to chip seal aggregates

Figure 4.9: Three-point bending test jig, sample placement, and sample preparation

4.3.6.2 Three-point flexural fatigue testing procedure

The three-point flexural fatigue test was utilized to determine the cracking and deformation resistance of the samples. To conduct the test, samples were placed and centered on the loading frame in the Universal Testing Machine (UTM) at OSU. The actuator of the UTM was then lowered down, and a repeated cyclic haversine shaped load with a peak force of 0.7 kN (157.4 lbs.) and a loading frequency of 10 Hz (10 loading cycles per second) was applied at the center of the asphalt slab. This frequency would approximately correspond to the loading frequency of a vehicle tire at a single point on an asphalt pavement if that vehicle were traveling at approximately 97 kph (60 mph). Tests were displacement controlled, ending at a total of 24 mm (0.94 in) vertical displacement (see Figure 4.10 for a typical tested sample). Displacement of the actuator within the UTM was tracked throughout the duration of the test via a displacement transducer. Following the test, an output parameter was extracted from the displacement curve (see Section 4.4.4).



Figure 4.10: Tested three-point flexural fatigue sample

The three-point flexural fatigue test allows for understanding the effects of cracking and deformation resistance based on: CLRS type (conventional versus sinusoidal), CLRS depth (1.27 cm [1/2 in] versus 1.59 cm [5/8 in]), CLRS geometry (40.64 cm x 17.78 cm [16 in x 7 in] versus 20.32 cm x 17.78 cm [8 in x 7 in]), CLRS position relative to the longitudinal joint, climate (rain and freeze-thaw), and surface treatment (chip seal).

4.3.7 Hamburg Wheel Tracking Test (HWTT)

4.3.7.1 Hamburg Wheel Tracking Test (HWTT) sample preparation

Asphalt block samples utilized in laboratory Hamburg Wheel Tracking Tests (HWTT) were extracted from the test strip construction and prepared in the same manner as the three-point flexural fatigue testing block samples. HWTT sample types included in the experimental factorial of Section 4.2 are shown in Figure 4.11.

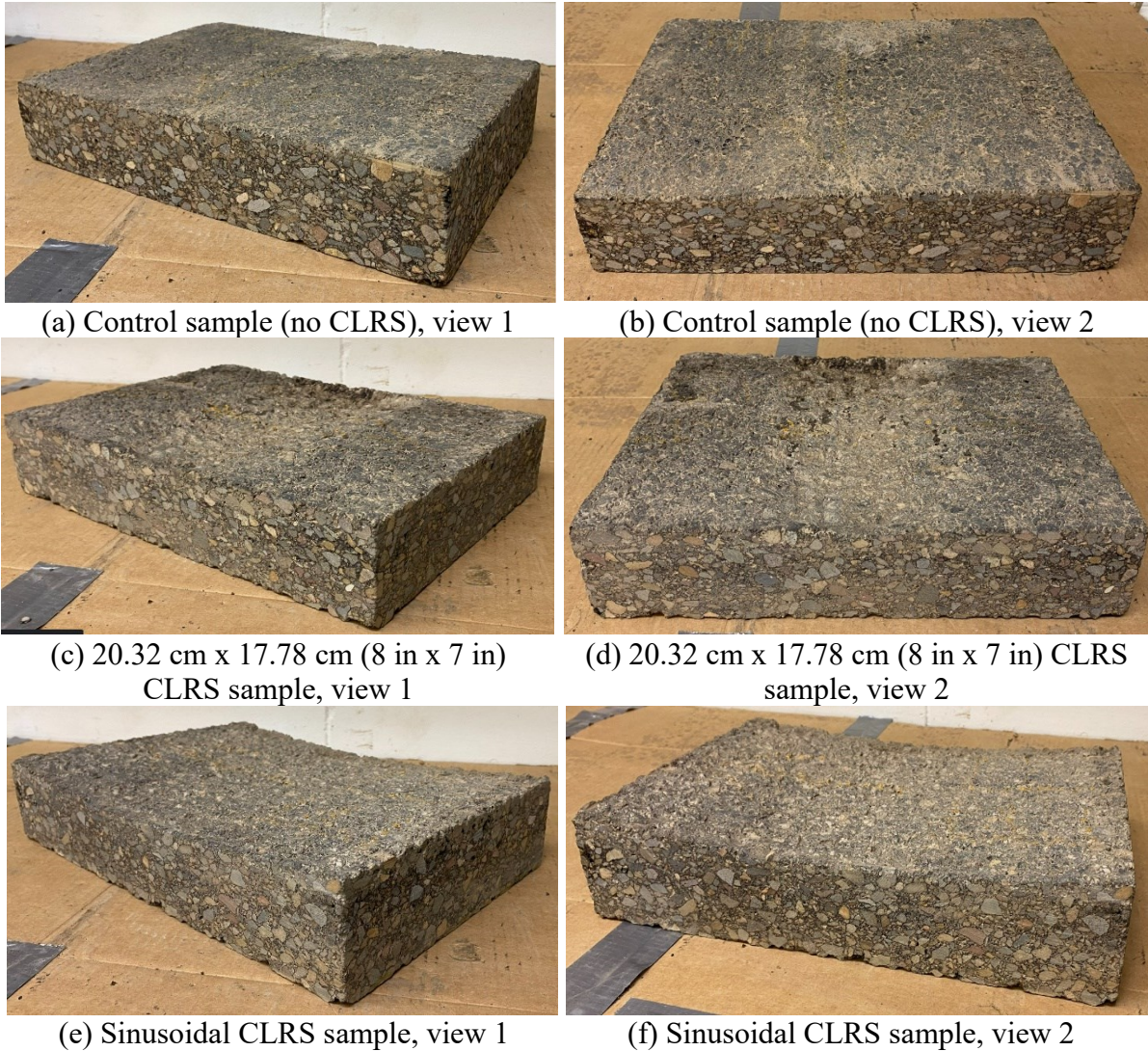


Figure 4.11: Hamburg Wheel Tracking Test samples

After cutting and drying, the asphalt blocks were placed in the HWTT testing mold with the following dimensions: 40.01 cm (15.75 in) long, 30.48 cm (12 in) wide, and 10.48 cm (4.125 in) deep. The testing mold was first filled with approximately 3.49 cm (1.38 in) of HM-108 Graded Standard Sand in order for the asphalt block to be level with the top edge of the mold (Figure 4.12(a) and Figure 4.12(b)). A 3.5 mil plastic sheet was inserted between the sand and the asphalt sample. After centering the sample in the mold, a 2.54 cm (1 in) thick layer of plaster was poured into the gaps between the mold and the block to ensure proper operation (no lateral movement under the wheel loads) and simulate partial asphalt confinement (Figure 4.12(c) through Figure 4.12(e)). The plaster's working time was 6-10 minutes (sets in 20-30 minutes), after which the sample was placed in the HWTT system for conditioning. Preconditioning time consisted of 3 hours with a chamber temperature specified for 50°C (122°F) under dry conditions. After conditioning, the test system automatically started the tests. It took approximately 14 hours to conduct one experiment, and two samples were tested at a time. The complete

sample preparation process is displayed in Figure 4.12. A total of 75 HWTT samples were prepared and tested by following this process..



(a) HWTT mold with sand base layer



(b) Asphalt sample level with the surface of HWTT mold



(c) Asphalt sample centered in HWTT mold



(d) Pouring plaster between mold and asphalt block



(e) 2.54 cm (1 in) plaster depth

Figure 4.12: Hamburg Wheel Tracking sample preparation

4.3.7.2 Hamburg Wheel Tracking testing procedure

The Hamburg Wheel Tracking Test (HWTT) device was developed to measure an asphalt concrete sample's rutting and moisture damage (stripping) susceptibility. In this study, tests were conducted under dry conditions to avoid introducing factors related to moisture into the test results. The primary purpose of the sand layer was to simulate a softer layer (weak subgrade) beneath the asphalt. Typically, HWTT samples are placed directly upon the steel mold. The goal of the sand base and partially unconfined edges were to simulate cracking of the CLRS as observed in the field. The 2.54 cm (1 in) plaster thickness was selected after testing various plaster thicknesses ranging from no confinement to full confinement. The 2.54 cm (1 in) partial confinement was chosen to allow for a full testing cycle without experiencing too little or excessive rutting and deformation. Tests were conducted by first conditioning the sample to 50°C (122°F) and then rolling a steel wheel across the surface of the sample to simulate vehicle loading. 30,000-wheel passes were applied to determine the resistance of a sample. A wheel speed of 35 passes per minute was used to avoid dynamic loading effects and bouncing of the wheel due to rumble strip curvature. Figure 4.13 shows the HWTT system used for running experiments in this study and a typical tested CLRS sample.



(a) Test system used for conducting experiments – closed



(b) Tested CLRS block sample with cracking



(c) Test system used for conducting experiments – open



(d) Tested CLRS block sample with cracking

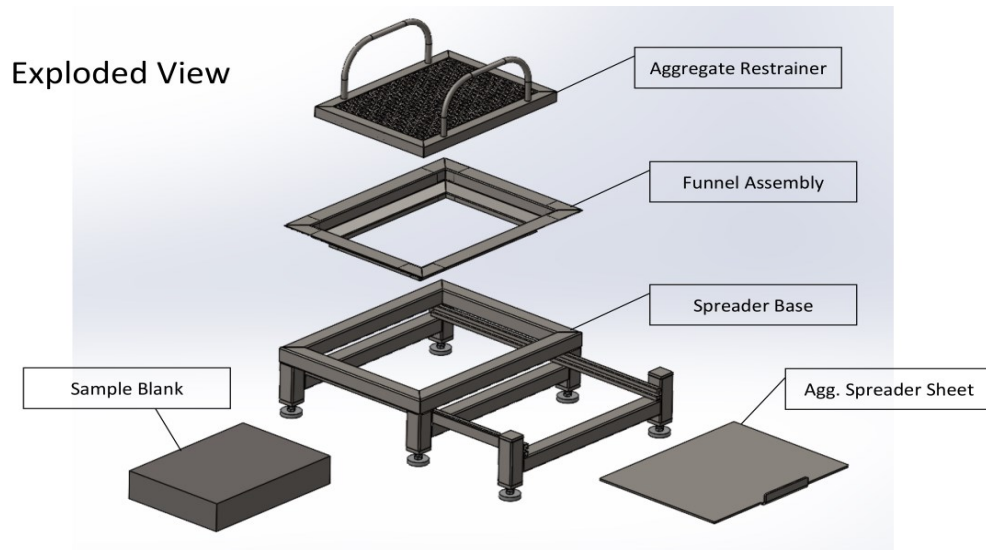
Figure 4.13: HWTT equipment and tested block sample

The HWTT allows for understanding the effects on durability of CLRS type (conventional versus sinusoidal), CLRS depth (1.27 cm [1/2 in] versus 1.59 cm [5/8 in]), CLRS geometry (40.64 cm x 17.78 cm [16 in x 7 in] versus 20.32 cm x 17.78 cm [8 in x 7 in]), CLRS position relative to the longitudinal joint, climate (rain and freeze-thaw), and surface treatment (chip seal).

4.3.8 Chip Seal Application

Chip seals are expected to positively impact CLRS performance by reducing oxidation, volatilization, and moisture infiltration and potentially mitigating damage stemming from pavement microcracks (FHWA, 2011) (FHWA, 2015a). Chip seals were applied according to

Section 00710 (Single Application Emulsified Asphalt Chip Seal) of ODOT Standard Specifications for Construction (ODOT, 2021). A fine aggregate chip seal design was utilized to maintain CLRS geometry after aggregate application. The aggregates utilized were sampled from an ODOT Level 4 paving project in the Pacific Northwest using a dense-graded mix with a nominal maximum aggregate size of 12.7 mm (1/2 in). The emulsified asphalt used was BL-HRT emulsion (from Albina Asphalt). Intermediate application rates of 1.47 L/m² (0.325 gal/yd²) and 0.0059 m³/m² (0.0065 yd³/yd²) were used for the emulsified asphalt and aggregate quantities, respectively. The laboratory chip seal application equipment utilized was developed based on a 2013 FHWA report for chip sealing guidance (Howard et al., 2013), and the efforts of the OSU CEOAS Machine and Technical Development Facility staff. The components included the spreader base, spreader sheet, funnel assembly, and aggregate restrainer (Figure 4.14).



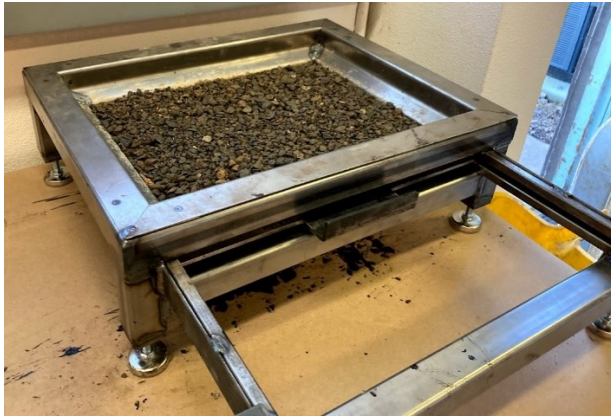
(a) The laboratory chip seal application equipment components – Modeled (Courtesy of OSU CEOAS Machine & Technical Development Facility)



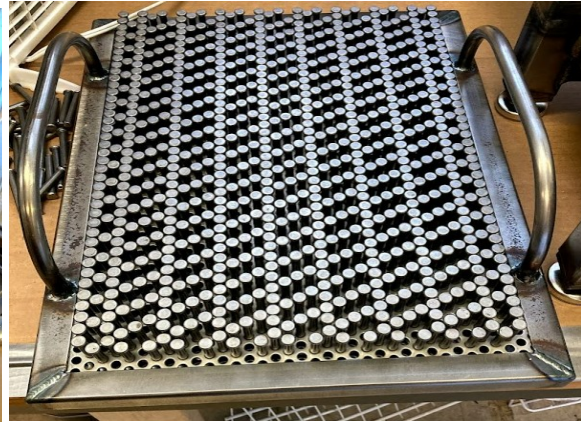
(b) The laboratory chip seal application equipment components - Fabricated

Figure 4.14: Chip seal application system components

Chip seals were applied to CLRS block samples by first mixing and moisturizing the batched aggregates (1.68 kg dry weight per sample) until damp surface conditions were achieved. Next, the aggregate spreader sheet was inserted into the spreader base, and the moisturized aggregates were spread evenly over the sheet (Figure 4.15(a)). Then the aggregate restrainer was placed overtop the moistened aggregates. The purpose of the aggregate restrainer was to maintain the position and orientation of the aggregates while the spreader sheet was being removed. The restrainer kept aggregates in place using a specialized layout of bolts which were inserted into a perforated metal plate (Figure 4.15(b)) (Howard et al., 2013). Aggregates would rest in the gaps between the bolts and maintain their position and orientation while the spreader sheet was being removed. After preparing the aggregates, the next step was to apply the emulsion to the asphalt blocks. The edges of the samples were taped to prevent emulsion runoff. 100 ml of the emulsion was poured over the surface of the sample and spread evenly using a miniature paint roller (Figure 4.15(c)). At this point, the sample was placed beneath the spreader sheet which was then pulled from the spreader base in under one second (Figure 4.15(d)). Removing the sheet allowed the aggregates to free-fall onto the surface of the sample. The final task was to compact the aggregates. This was performed using a handheld rubber wheel that was rolled four sets of passes both longitudinally and transversely over the block (Figure 4.15(e)). After at least 48 hours of curing time, excess aggregates were brushed off from the surface of the sample. The full chip seal application process is shown in Figure 4.15.



(a) Aggregates spread evenly atop spreader sheet



(b) Aggregate restrainer with specialized bolt layout



(c) Spreading emulsion



(d) Removing spreader sheet



(e) Compacting aggregates



(f) Finished CLRS chip seal block sample

Figure 4.15: Chip seal application procedure

4.3.9 Freeze-Thaw Cycling

The freeze-thaw cycling procedure involved placing sealed test section block samples under the rainfall simulator to saturate the samples, then subjecting them to repeated extreme temperature

cycles. To prepare samples for freeze-thaw cycling, the samples were completely sealed from the sides and bottom. Doing so ensured that moisture that had infiltrated through the asphalt would be retained within the sample to freeze and re-freeze as opposed to simply draining out of the sample after several cycles. To seal the bottom of samples, a thick plastic covering was taped in place, covering the bottom and extending 25.4 mm (1.0 in) up the sides of each sample. Silicone gel was then spread along the sides and bottom of the sample to completely seal it and prevent water from escaping the sides or bottom. Samples were placed under the rainfall simulator for 48 hours, long enough to ensure complete saturation of the asphalt sample if permeable (Haynes et al., 2019). Once 48 hours had passed, samples were placed into a freezer set to -20°C (-4°F) for 14 hours. The frozen samples were removed from the freezer to thaw for 10 hours at ambient laboratory temperature (approximately 22°C [72°F]). This freezing and thawing process was repeated for 15 days to simulate 15 freeze-thaw cycles. Sealed samples were taped along the edges, and water was poured onto the asphalt surface prior to each freeze cycle to simulate field conditions. The freeze-thaw cycling procedure is shown in Figure 4.16.



(a) Sample sealed on all sides



(b) Sample sealed on the bottom surface



(c) Sealed samples undergoing rainfall simulation



(d) Freeze-thaw cycling

Figure 4.16: Freeze-thaw procedure

4.3.10 Pavement Roughness

Pavement roughness (correlated with the vehicle's accumulated suspension movement) is an indicator of ride quality, the impacts due to the vehicle dynamic loading effect, and resulting excess fuel consumption and vehicle operating costs. SurPRO 3000 equipment (a walk-behind profiler) was utilized at the Knife River finite road test section to determine the International Roughness Index (IRI) of different pavement areas with different CLRS types (ODOT TM 772, 2011). The SurPRO is a walk-behind profiler system with a maximum pace of approximately 4 kph (2.5 mph), and uses patented inertial technology to record surface profile, which is later converted to pavement roughness. SurPRO runs were done in control sections with no rumble strips; sections with conventional 40.64 cm x 17.78 cm (16 in x 7 in), modified 20.32 cm x 17.78 cm (8 in x 7 in), and sinusoidal 50.8 cm (20 in) wide CLRS; shallow and deep CLRS sections; and sections over the longitudinal joint and away from the joint. SurPRO runs were performed both along the centerline of the rumble strips as well as the right edge of the rumble strips. The SurPRO 3000 equipment is shown in Figure 4.17.



Figure 4.17: SurPRO 3000

The collected SurPRO data was processed using the ProVAL software. Figure 4.18 displays typical SurPRO roadway profile data collected along the centerline of conventional, modified, and sinusoidal CLRS. The y-axis corresponds to roadway elevation (inches), and the x-axis corresponds to distance (feet).

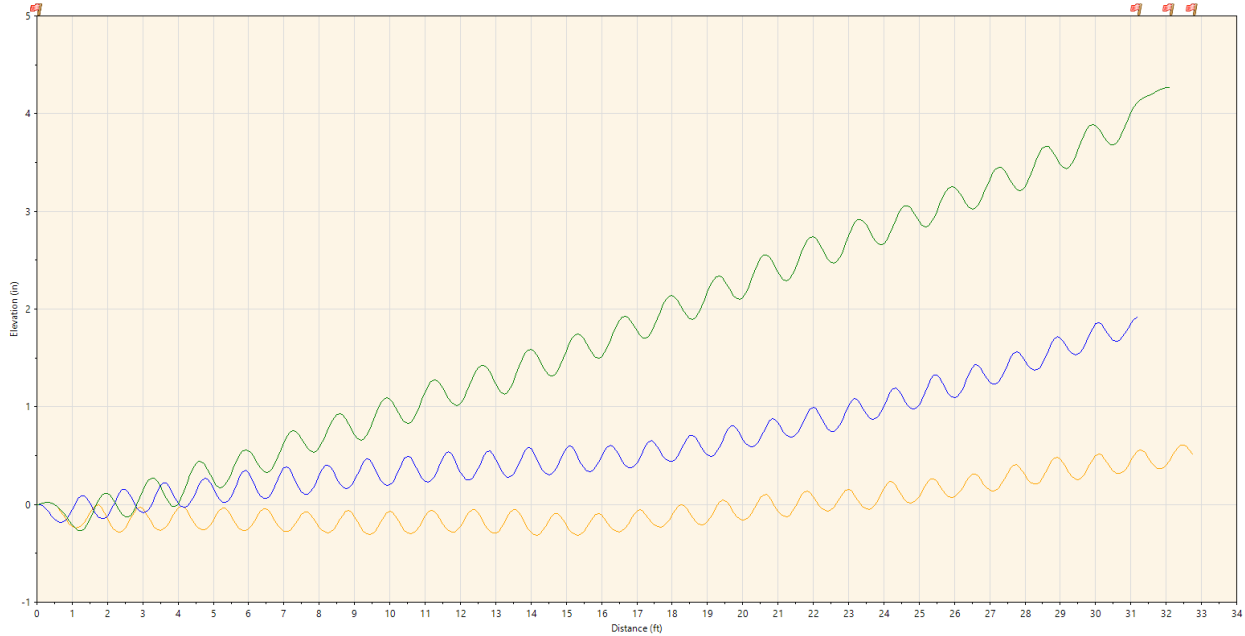


Figure 4.18: SurPRO elevation profiles for conventional (orange), modified (blue), and sinusoidal (green) CLRS

The consistent peaks and valleys of the SurPRO data shown in Figure 4.18 demonstrate the outcome of the wheel rolling through the rumble strip grooves in the sections analyzed.

4.3.11 X-Ray Computed Tomography (CT) Imaging

This portion of the study aimed to determine the presence of microcracks due to rumble strip milling in asphalt layer at the Knife River test section. X-ray Computed Tomography (CT) scanning was performed on four cores extracted from a rectangular, conventional (40.64 x 17.78 cm [16 x 7 in]), 15.88 mm (5/8 in) deep rumble strip in the middle of the travel lane. Cores were scanned at the Oregon State University MicroCT Facility.

The four cores were extracted from the following locations on the rumble strip: Center, corner, long (40.64 cm [16 in]) edge, and short (17.78 cm [7 in]) edge. The cylindrical cores were 4.5 cm (1.8 in) in diameter. Figure 4.19 shows the locations of the cores that were extracted on a 40.64 cm x 17.78 cm (16 in x 7 in) rumble strip.

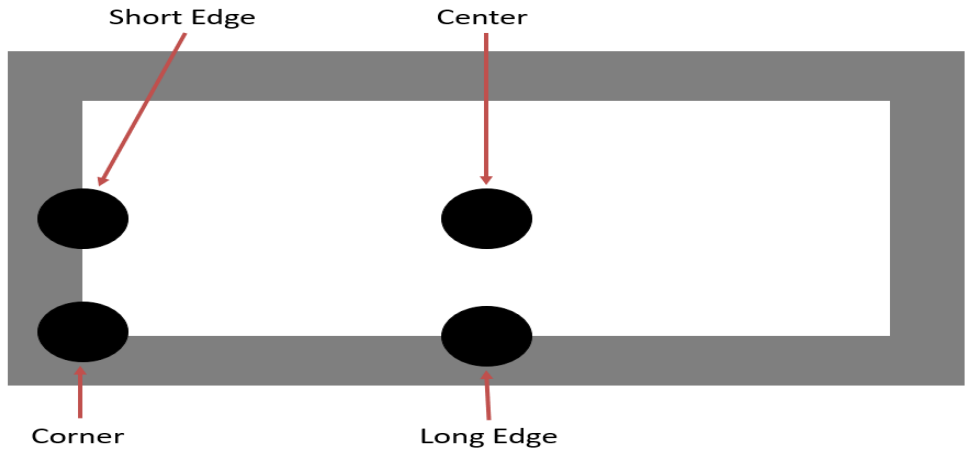


Figure 4.19: Core locations extracted from conventional CLRS

Figure 4.20 shows the extracted cores that were scanned.



Figure 4.20: Cores for X-ray CT imaging

4.4 LABORATORY RESULTS AND DISCUSSION

4.4.1 Indirect Tensile (IDT) Strength, Resilient Modulus (RM), and Air Void Tests

Field cores extracted from the Knife River test strip section were tested for Indirect Tensile (IDT) Strength, Resilient Modulus (RM), and air void content (both saturated surface-dry [SSD] and Corelok methods). Cores were extracted from either end of the construction, in the west and east lanes, and along the joint as well. Cores were also extracted near the edges of the construction. A total of 30 cores were extracted and tested. The averaged values per section are shown in Figure 4.21.

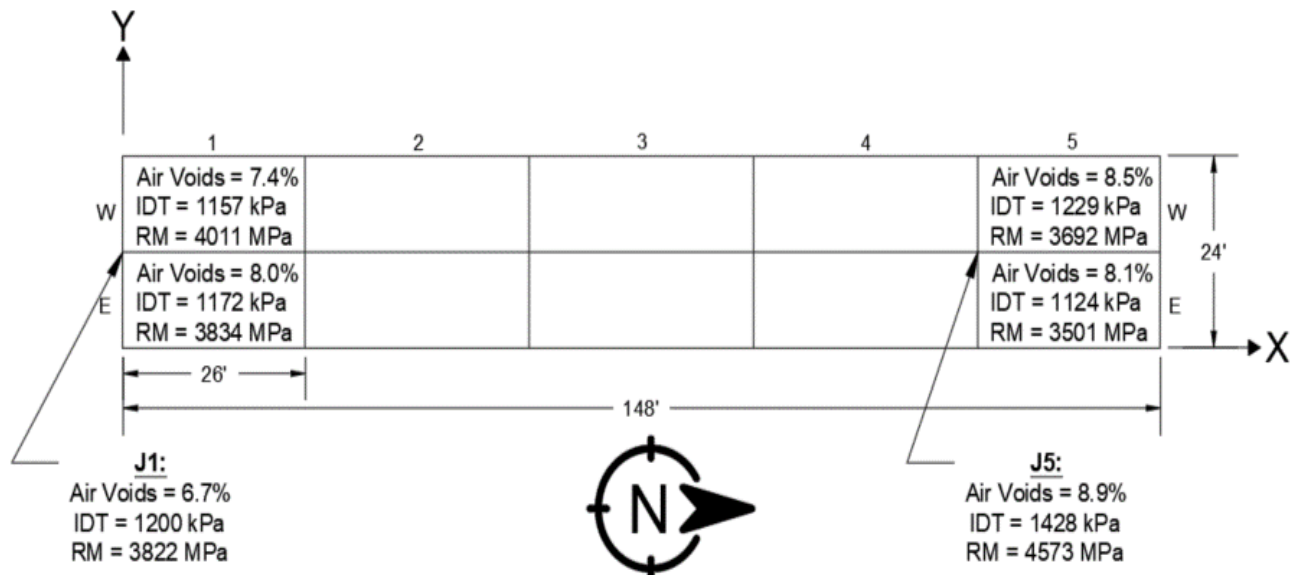


Figure 4.21: IDT, RM, and air void test results

The results show minimal variation in stiffness, cracking resistance, and air void content for samples in the lane versus along the joint, and for samples in the north, south, east, and west quadrants. Cores extracted near the edges of construction had higher air void content which may have influenced the average air void contents displayed in Figure 4.21. There is an observed difference in the performance parameters at the joint along the north end of construction, but this is likely due to inherent variations in sampling and limited sample size. As discussed in section 4.1, asphalt density at the longitudinal joint was not representative of a typical construction joint. The similarity in test results between the longitudinal joint and the travel lane is visible in Figure 4.21. In addition to those, 8 cores were also removed from section 3 in Figure 4.21 with about 1-foot intervals from the east end of the test strip. It was observed that the locations within 2 feet distance from the east end have about 4-5% less density than the rest of the test strip. After the 2 feet distance, measured densities were similar. This low density only along the east end is a result of having a non-restrained edge during compaction. Asphalt specimens from the 2 feet segment were used to determine the impact of having CLRS on the construction joints with low densities.

Contour maps were also developed to further understand IDT strength, RM, and air voids' spatial distribution in the test strip sections. Results are displayed in Figure 4.22 and Figure 4.23, where the X and Y dimensions (shown in Figure 4.21) correspond to the longitudinal and transverse directions, respectively. The horizontal red line in the figures represents the approximate location of the longitudinal joint.

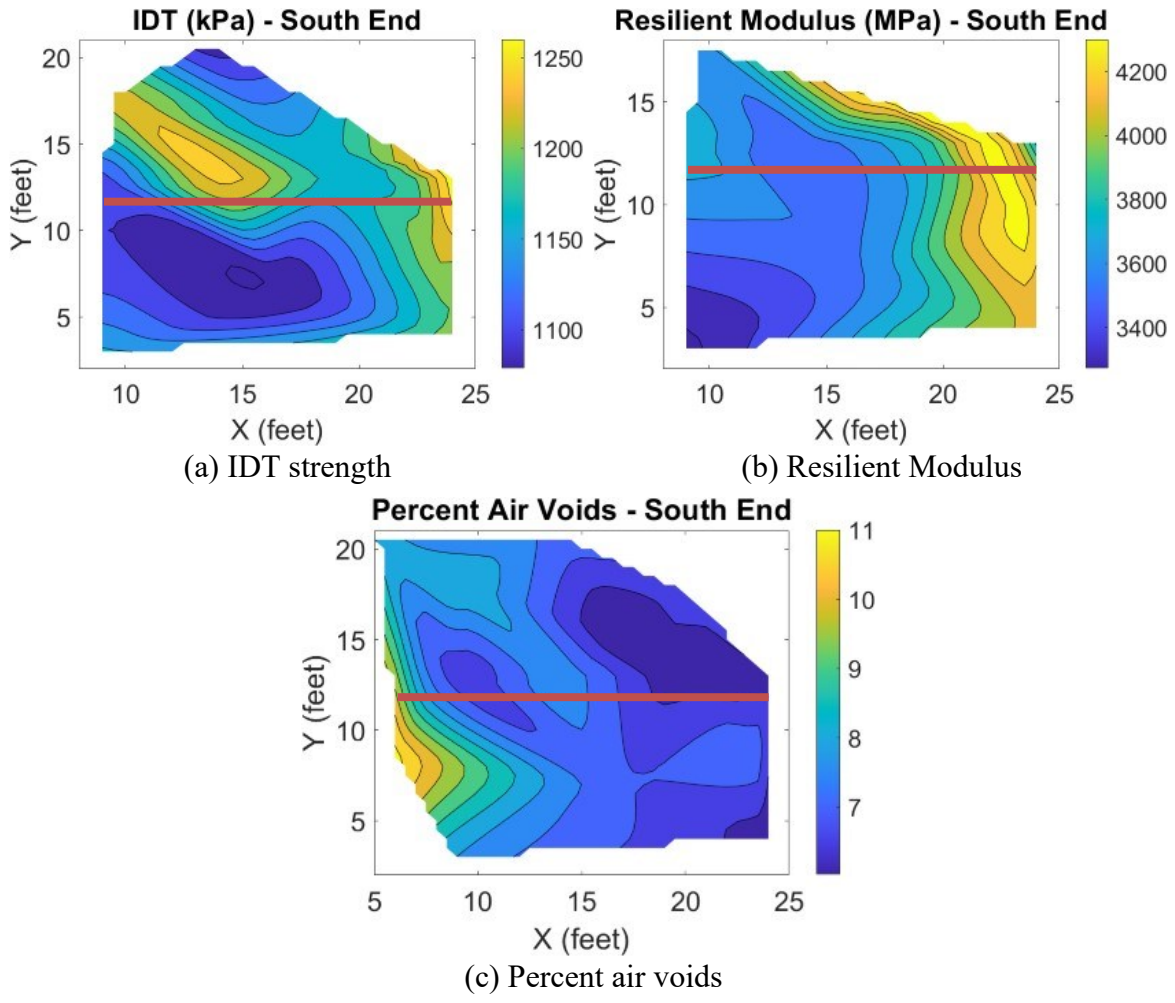


Figure 4.22: South end of construction - Contour maps of IDT strength, RM, and Corelok air void content

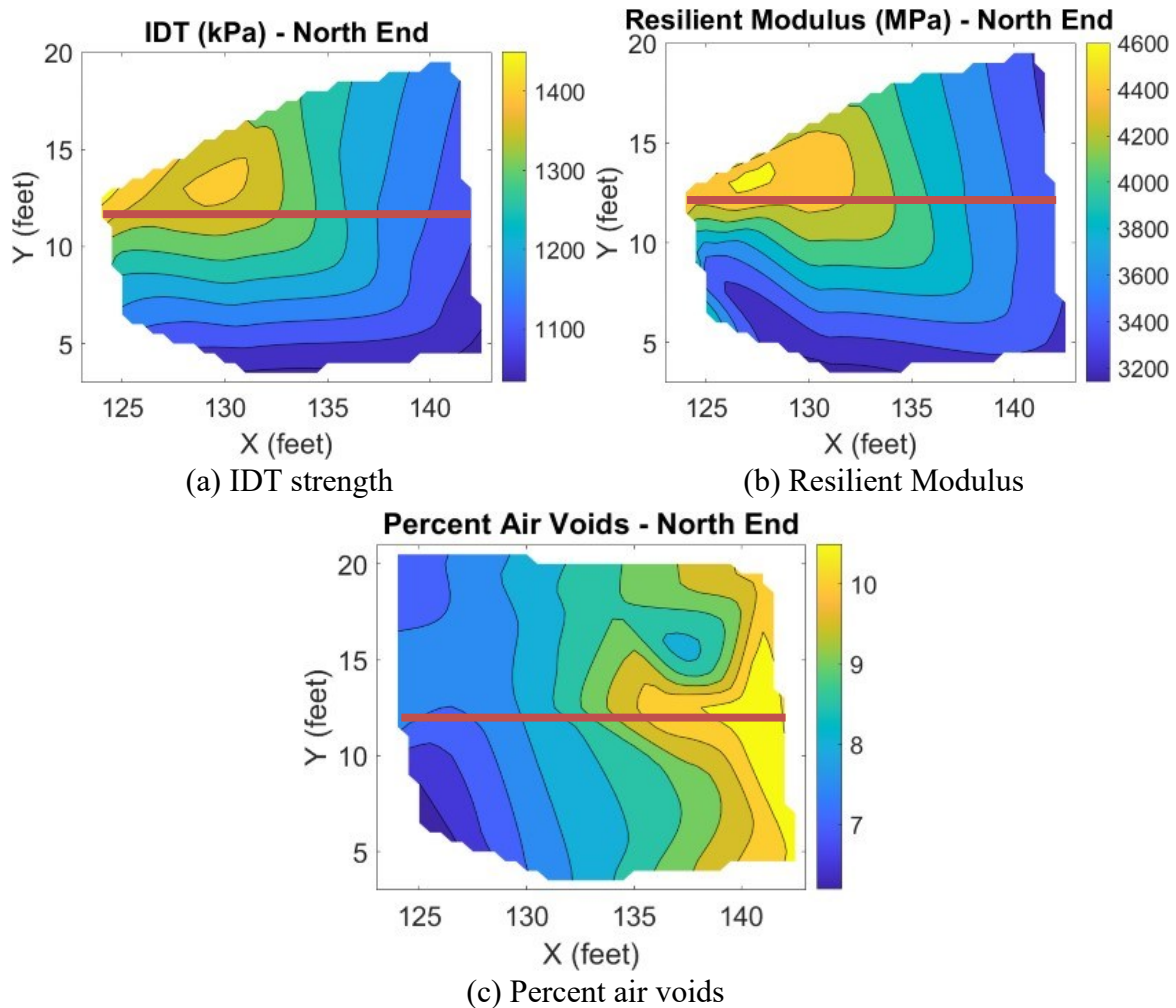


Figure 4.23: North end of construction - Contour maps of IDT strength, RM, and Corelok air void content

Figure 4.22 and Figure 4.23 both display consistent trends of decreased IDT strength and RM near the edges of construction, as well as increased air void content near the edges. This is expected because the increased air voids lead to lowered asphalt cracking resistance and measured stiffness. Again, there were no observable differences in performance parameters for samples located along the longitudinal joint.

Air voids were greatest at the north and south ends of construction, but this longitudinal effect was minimized moving in the x-direction towards the sections with CLRS. CLRS samples were located outside this range and are not expected to have been impacted by the longitudinal air void effect. Air voids were also greatest near the transverse edges of construction, particularly the unconfined edge. This edge effect was steadily reduced moving in the transverse direction (y-direction) away from the edges (after 2 feet distance, density was constant and high). CLRS samples located near the transverse edges of construction are expected to be impacted by this air void effect, but these impacts on test results were accounted for in the following sections.

A comparison of air void contents was made using the SSD and Corelok methods, with results shown in Figure 4.24. Although the measured air void contents are highly correlated, the Corelok method provides a higher air void content.

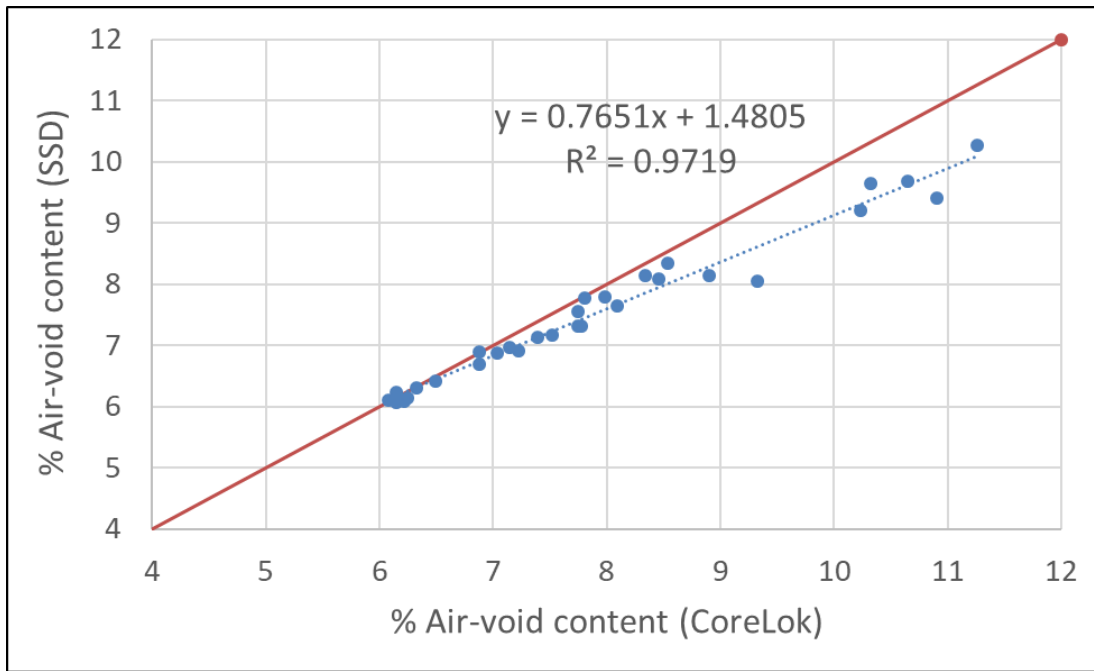


Figure 4.24: Air void contents, SSD versus Corelok

As expected, the air void contents measured using the SSD and Corelok methods were closely associated with an R^2 value of 0.97. It is evident that at higher air void contents, the two methods begin to diverge. This result is expected because some water in the pores was being lost in the SSD method (for samples with high air void contents) when the sample was removed from the water bath for weighing. This result is also in agreement with other studies in the literature (Sholar et al., 2005).

The results can also be compared to those taken during construction via nuclear density gauge (NDG), as shown in Table 4.10.

Table 4.10: Field and Laboratory Air Void Contents

| | Nuclear Density Gauge | Corelok | SSD |
|---------------------------|------------------------------|----------------|------------|
| West Panel | 7.7% | 8.0% | 7.6% |
| East Panel | 7.1% | 8.0% | 7.6% |
| Longitudinal Joint | 7.6% | 7.8% | 7.4% |

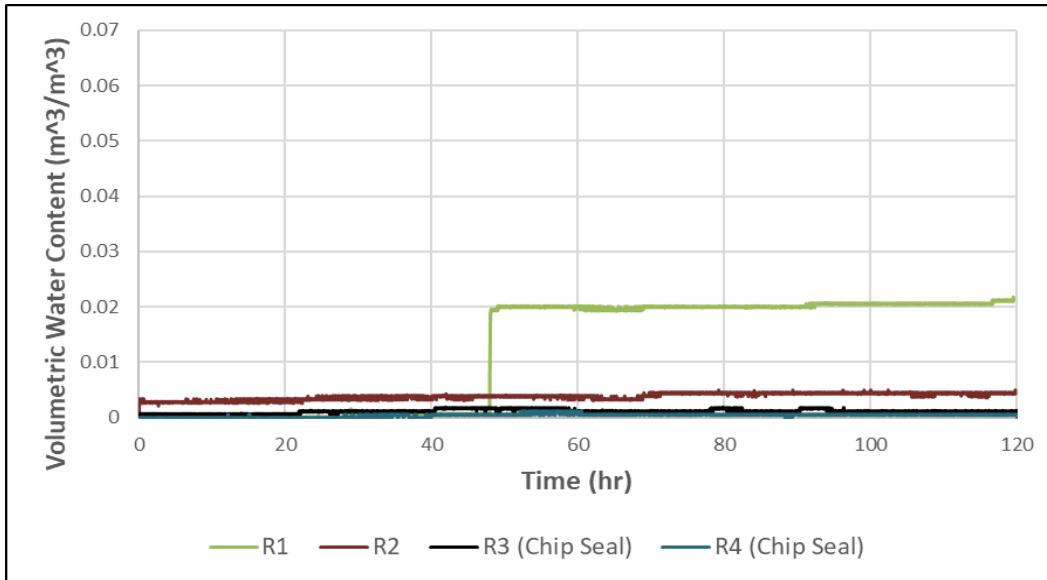
Table 4.10 shows that Corelok air void measurements were greater than those of both the NDG and the SSD methods. The air void contents for the field NDG and laboratory SSD methods were, on average, comparable to one another.

4.4.2 Field Infiltration Tests

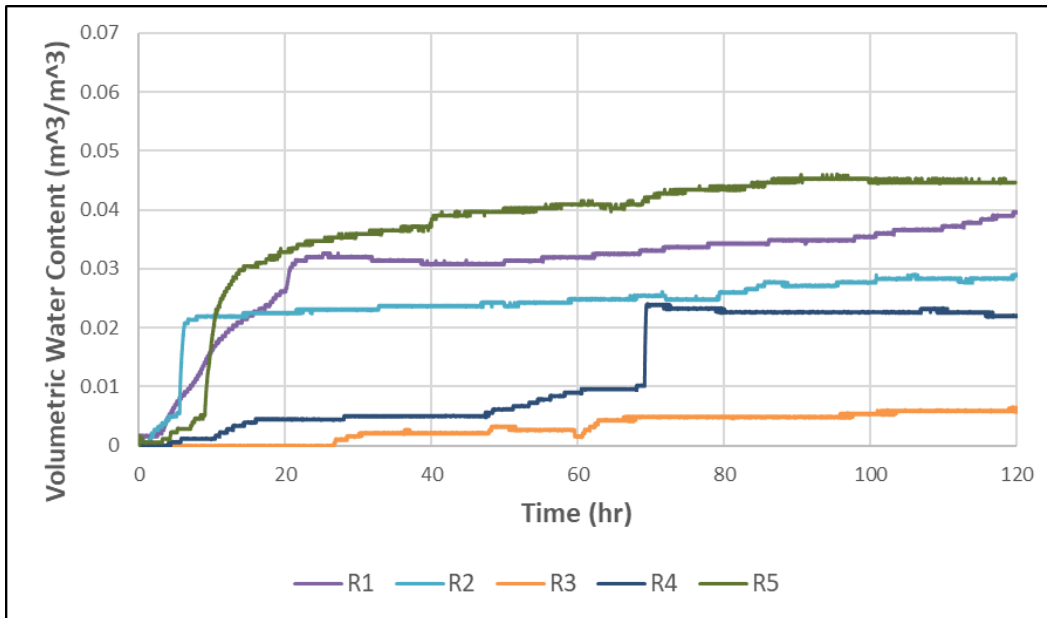
Field infiltration tests at the Knife River test strip resulted in little to no water infiltration for most of the locations. A total of 22 field infiltration tests were conducted. It was expected that the dense gradation of the asphalt mixture with an acceptable level of compaction (also approved by the ODOT inspector) provided impermeability. Moisture infiltration was observed near the edges of the section (where the air void content was about 4-5% higher than the rest of the test section). See Figure 4.22(c). There were 14 samples with no moisture infiltration and 8 samples experiencing infiltration with an average rate of 100.4 mm/hr.

4.4.3 Laboratory Rainfall Simulation and Moisture Infiltration Tests

Results of the laboratory rainfall simulation and moisture infiltration testing are shown in Figure 4.25 to Figure 4.30. The figures demonstrate the total volumetric water content infiltrated through the sample over a five-day span. Figure 4.25(a) corresponds to control samples (no CLRS) extracted from within the center of the travel lane, and Figure 4.25(b) corresponds to control samples extracted near the edge of the travel lane (approximately 0.3 m [1 ft] from the edge of construction).



(a) Middle of lane

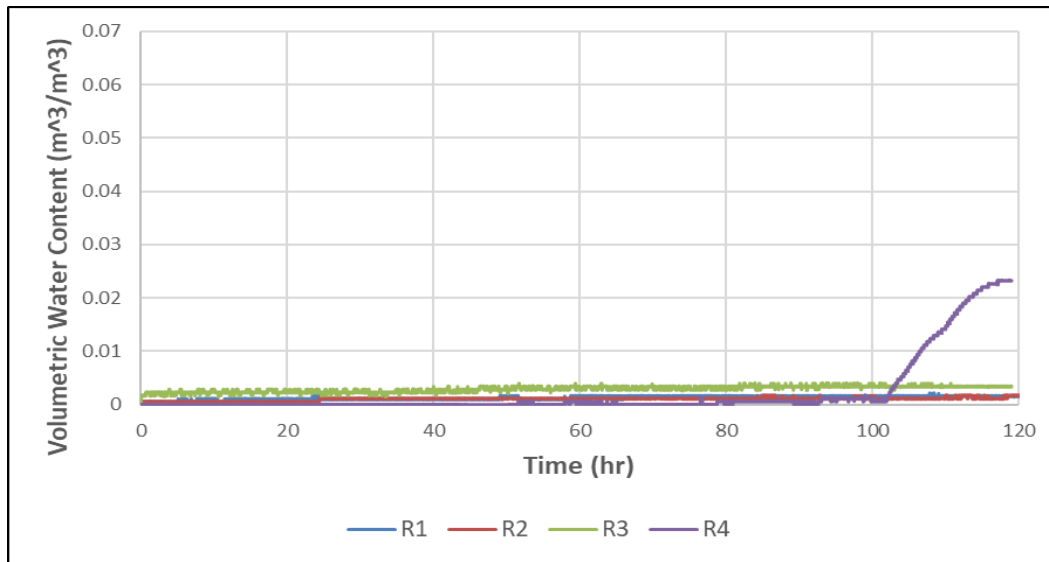


(b) Edge of lane

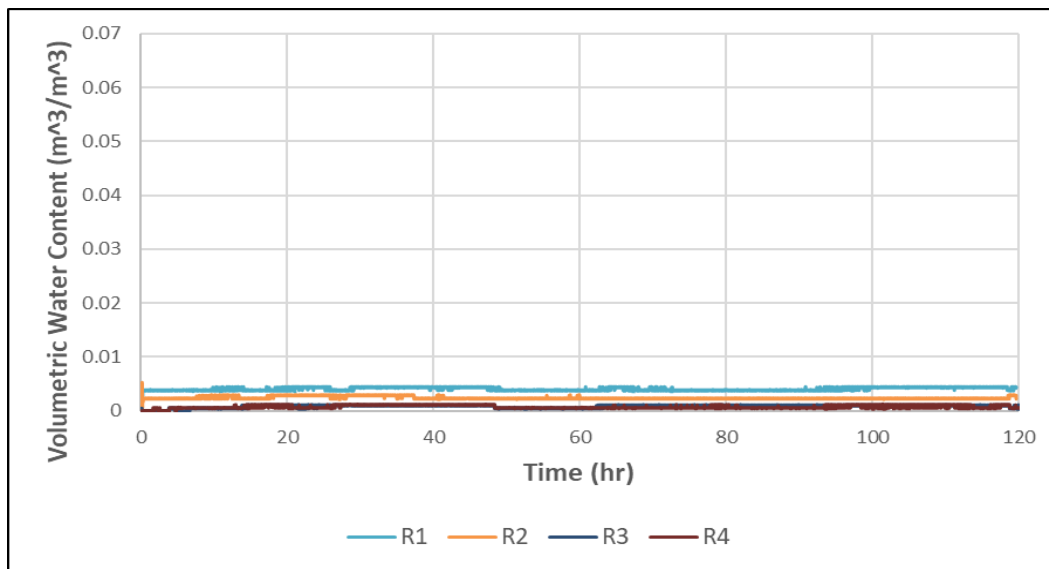
Figure 4.25: Moisture infiltration results - Control samples (R: replicate)

As shown in Figure 4.25, one sample within the lane experienced moisture infiltration and was a replicate test without chip seal treatment. At the edge of the lane, 80% of samples saw significant moisture infiltration, but none were treated with chip seal. It was expected that samples near the edges of construction would have moisture infiltration occur. The edges of paving construction are typically areas of low density and thus high air voids (about 4-5% higher than the rest of the mat). This is typically due to having an unconfined edge, which reduces compaction and density.

Figure 4.26 shows the moisture infiltration results for rectangular CLRS samples extracted from the middle of the travel lane. Figure 4.26(a) corresponds to samples without surface treatment, and Figure 4.26(b) corresponds to samples with chip seal treatment.



(a) No sealant



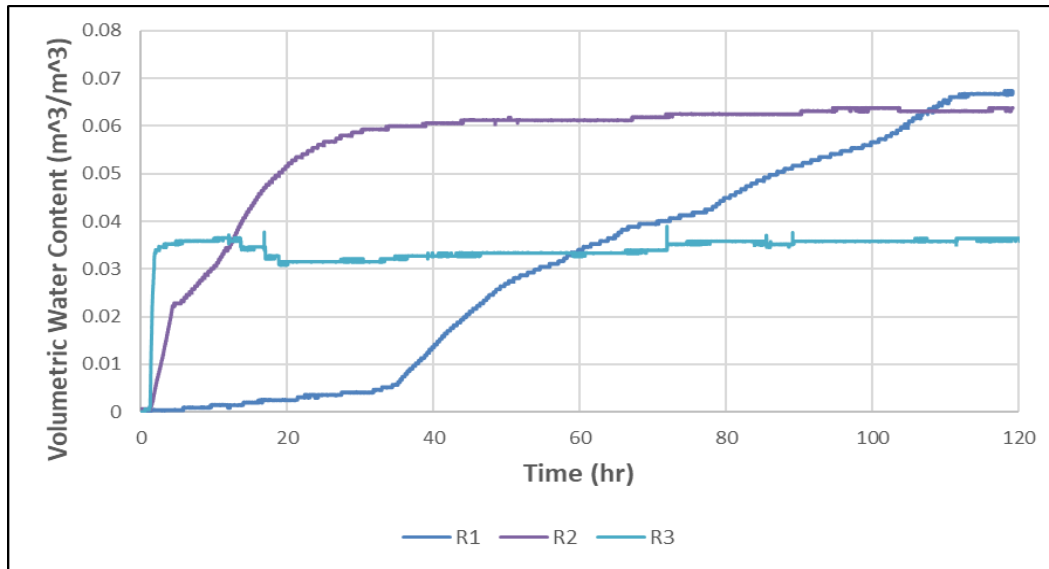
(b) Chip seal

Figure 4.26: Moisture infiltration results - Rectangular CLRS, middle of the lane (R: replicate)

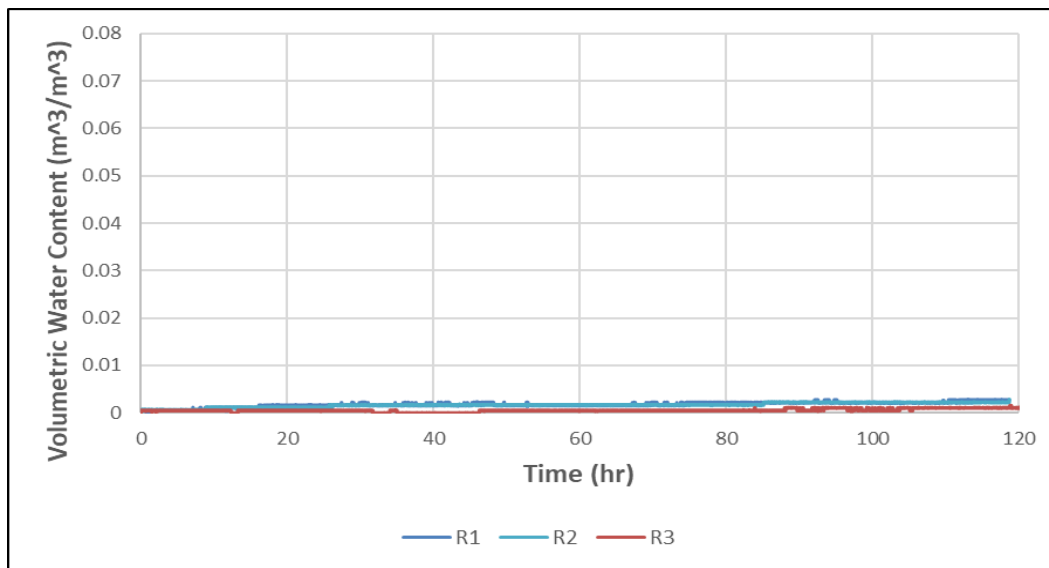
As shown in Figure 4.26(a), Replicate 4 with rectangular CLRS and no chip seal had water infiltration occur at approximately 102 hours while no other sample had moisture infiltration. The middle of the lane and the longitudinal joint were well compacted during the test section's construction, which led to few interconnected air voids. These results were supported by the field permeability testing discussed in Section 4.4.2. Therefore, little moisture infiltration was seen for the rectangular CLRS samples with and without chip seal due to the unconnected air voids.

Additionally, it was expected that the application of a chip seal would seal the surface of the samples and restrict the infiltration of water. Comparing Figure 4.26 results to control samples in the lane, there were cases of delayed infiltration of non-sealed samples in both scenarios, and there was no infiltration among chip sealed samples.

Figure 4.27 displays the moisture infiltration results for rectangular CLRS samples extracted near the edge of the travel lane (approximately 0.3 m [1 ft] from the edge of construction). Figure 4.27(a) corresponds to rectangular CLRS samples extracted from the edge of the travel lane with no surface treatment, and Figure 4.27(b) corresponds to rectangular CLRS samples extracted from the edge of the travel lane with chip seal treatment.



(a) No sealant

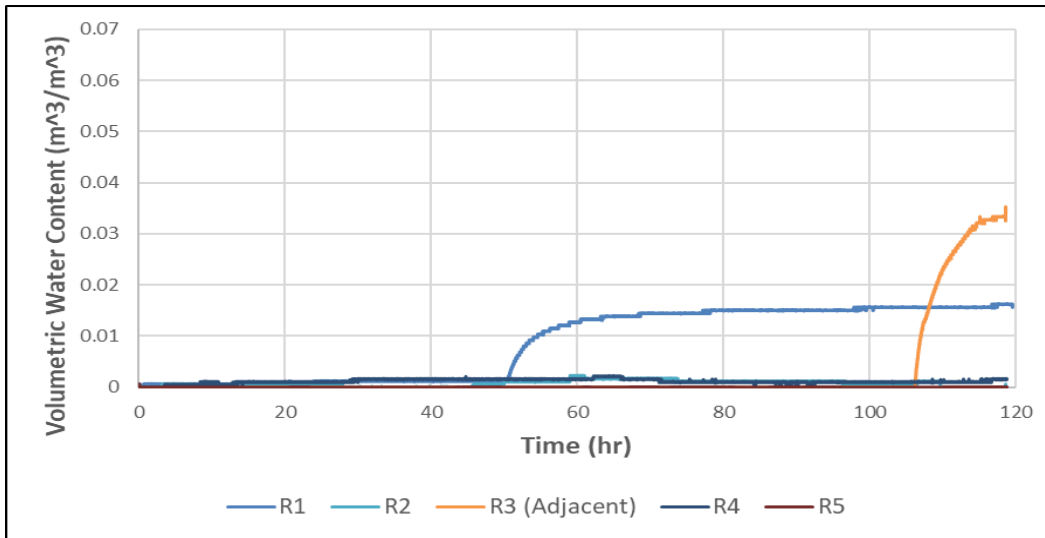


(b) Chip seal

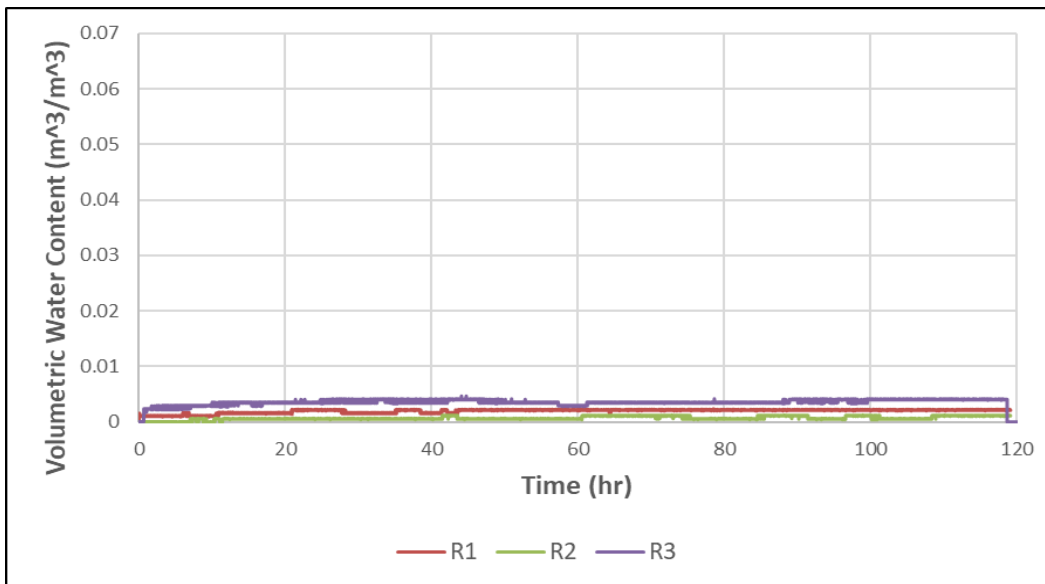
Figure 4.27: Moisture infiltration results - Rectangular CLRS, edge of the lane (R: replicate)

Figure 4.27 shows that all samples without surface treatment experienced moisture infiltration. Replicate 2 and Replicate 3 asphalt blocks were immediately infiltrated, while Replicate 1 began rapid infiltration at approximately 34 hours. None of the samples with chip seal treatment experienced moisture infiltration. As discussed previously and shown in Figure 4.27, samples near the edges of construction were expected to experience moisture infiltration due to poor compaction along the edges (due to being unconfined with no support). Since longitudinal construction joints are also areas with significantly lower density than the rest of the mat, this type of high moisture infiltration is also expected along the longitudinal joints. The results also demonstrated the effectiveness of chip sealing in eliminating moisture infiltration. For this reason, for CLRS constructed on the longitudinal joints, the application of a surface treatment should be required to reduce the impact of moisture infiltration on CLRS cracking and overall pavement performance. Comparing Figure 4.27 results to control samples at the edge of the lane without surface treatment, both showed infiltration of all samples with similar times to reach infiltration.

Figure 4.28 displays the moisture infiltration results for rectangular CLRS samples extracted over the longitudinal joint. Figure 4.28(a) corresponds to rectangular CLRS samples extracted over the longitudinal joint with no surface treatment, and Figure 4.28(b) corresponds to rectangular CLRS samples extracted over the longitudinal joint with chip seal treatment.



(a) No sealant



(b) Chip seal

Figure 4.28: Moisture infiltration results - Rectangular CLRS, over longitudinal joint (R: replicate)

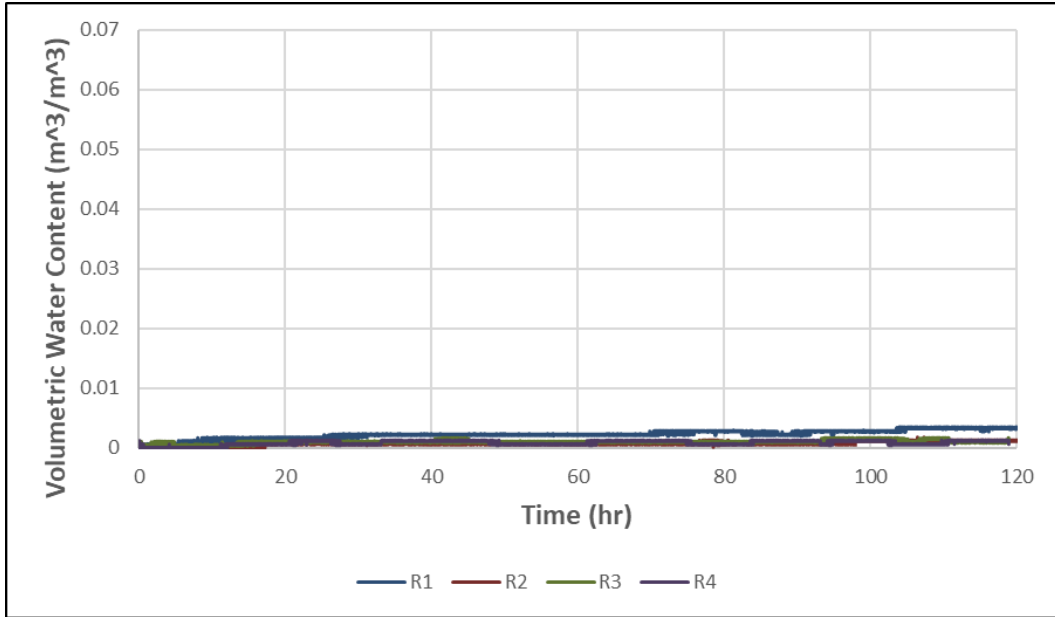
Figure 4.28 shows that 40% of samples without surface treatment experienced moisture infiltration. Infiltration began at approximately 50 hours and 107 hours for Replicate 1 and Replicate 3, respectively. Replicate 3 was a CLRS sample extracted adjacent to the longitudinal joint. None of the samples with chip seal treatment experienced moisture infiltration, as expected.

Results for rectangular CLRS over the longitudinal joint were similar to those of rectangular CLRS in the travel lane. This is because both mats in the test section were paved within hours of one another, which allowed the longitudinal joint to be properly compacted within that time. Typical field construction involves multiple days between the construction of lanes. During that

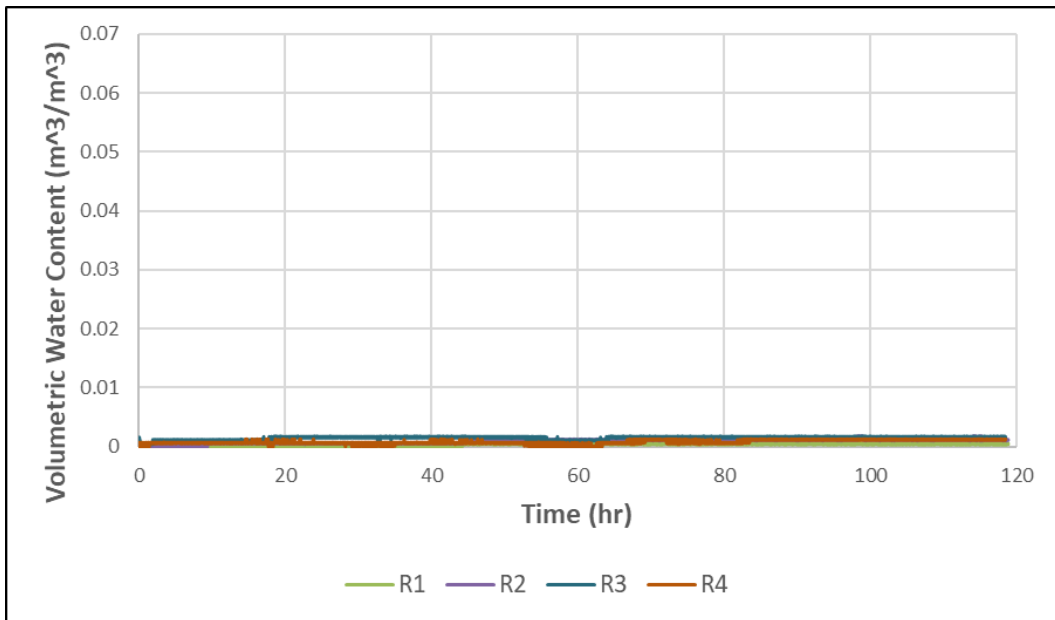
time, the paved asphalt cools and does not bond properly to the subsequent adjacent lane that is paved. This leads to lower densities between lanes and the creation of longitudinal joints. In the test section, samples along the longitudinal joint and within the travel lane were considered equivalent to one another in terms of density and amount of compaction. These results also point out the effectiveness of potential echelon paving (two pavers paving next to each other at the same time, which requires a traffic closure for both lanes) in the field to avoid weak/low density joints with low fatigue cracking resistance.

Samples along the edges of the test section were more indicative of conditions at a longitudinal joint in the field. It is likely that the test section longitudinal joint would have the same or similar permeability as the edge of construction if field conditions were exactly matched. It is also important to note that asphalt temperatures were high (best case scenario) during paving at the test section due to its close proximity to the asphalt supplier. This might have led to better compaction, lower density, and less permeability.

Figure 4.29 displays the moisture infiltration results for sinusoidal CLRS samples extracted in the center of the travel lane. The samples in Figure 4.29(a) are without surface treatment, and Figure 4.29(b) corresponds to samples with chip seal treatment.



(a) No sealant



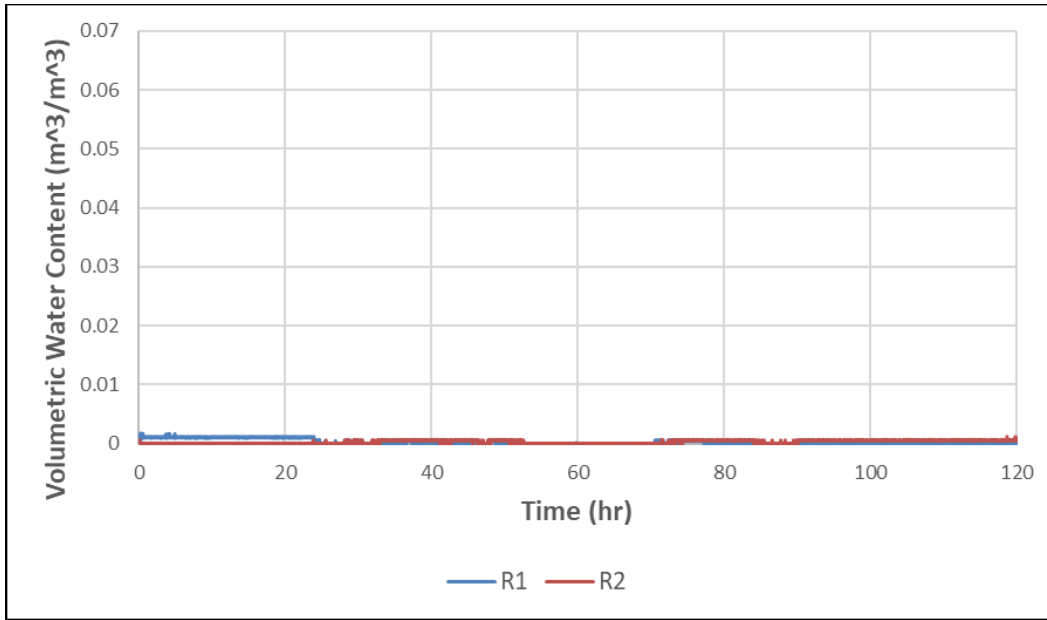
(b) Chip seal

Figure 4.29: Moisture infiltration results - Sinusoidal CLRS, middle of lane (R: replicate)

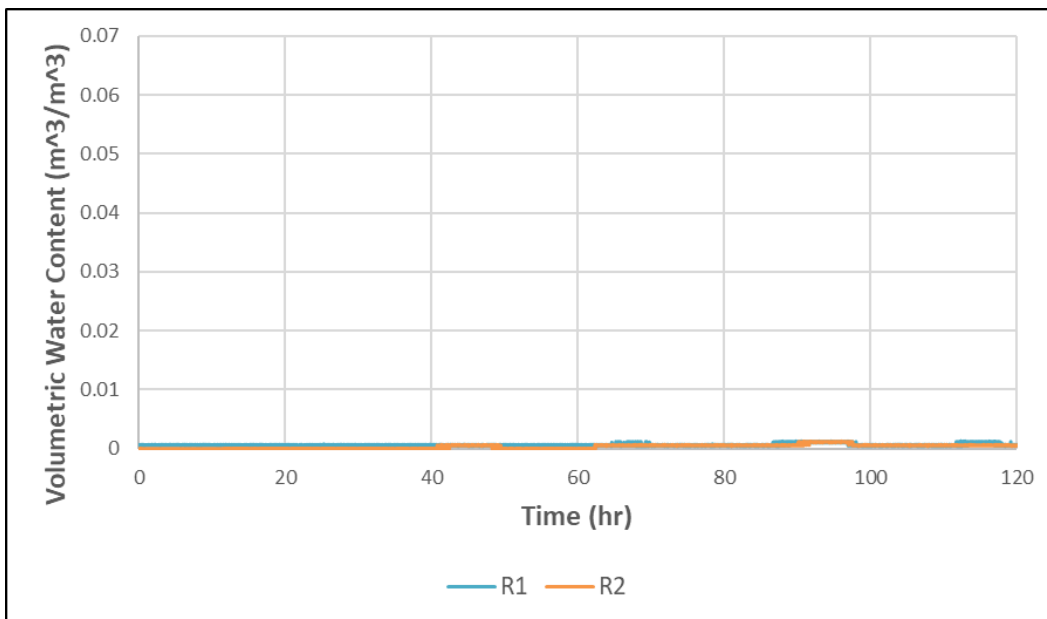
In Figure 4.29, none of the samples showed evidence of moisture infiltration. Compared to rectangular CLRS samples extracted from the travel lane, the sinusoidal CLRS showed a major advantage in that a non-sealed rectangular CLRS sample showed delayed moisture infiltration. This result is expected to be due to the less destructive nature of sinusoidal CLRS installation, in which the sharp edges and corners of the rectangular CLRS were removed to create the sinusoidal shape. Having the sharp edges and corners in the rectangular CLRS might be causing thermal cracking over time due to day and night temperature changes. The absence of those edges and corners in the sinusoidal CLRS might have avoided the accumulation of thermal stresses and

avoided the formation of microcracks. This may have been the mechanism resulting in lower permeability for the sinusoidal CLRS samples.

Figure 4.30 displays the moisture infiltration results for sinusoidal CLRS samples extracted over the longitudinal joint. The samples in Figure 4.(a) are without surface treatment and Figure 4.30(b) corresponds to samples with chip seal treatment.



(a) No sealant



(b) Chip seal

Figure 4.30: Moisture infiltration results - Sinusoidal CLRS, over the longitudinal joint (R: replicate)

Again, none of the samples showed evidence of moisture infiltration. Compared to rectangular CLRS from the longitudinal joint, the sinusoidal CLRS showed a major advantage in that two non-sealed rectangular CLRS samples showed delayed moisture infiltration. The summarized results of the moisture infiltration tests are shown in Table 4.11.

Table 4.11: Moisture Infiltration Summary Results

| | | <i>Percent Samples Infiltrated</i> | | |
|--------------|-------------------|------------------------------------|--------------------|-------------------|
| | | Control | Rectangular | Sinusoidal |
| <i>Lane</i> | No Sealant | 1/2 | 1/4 | 0/4 |
| | Chip Seal | 0/2 | 0/4 | 0/4 |
| <i>Edge</i> | No Sealant | 4/5 | 3/3 | -- |
| | Chip Seal | -- | 0/3 | -- |
| <i>Joint</i> | No Sealant | -- | 2/5 | 0/2 |
| | Chip Seal | -- | 0/3 | 0/2 |

Table 4.11 shows that there was 64% infiltration at the edges of the paved section, 17% infiltration at the longitudinal joint and 10% infiltration in the travel lane. It is notable that sinusoidal CLRS without chip seal treatment had 0% total infiltration while rectangular CLRS had 19% total infiltration. Samples with chip seal surface treatment had no moisture infiltration, demonstrating its effectiveness in preventing moisture infiltration. The results demonstrated that the longitudinal construction joint at the test facility had similar performance to samples in the travel lane. Overall, the CLRS configuration with optimal performance in terms of moisture infiltration resistance was sinusoidal CLRS with surface treatment.

4.4.4 Three-Point Flexural Fatigue Test

A typical deflection curve for a slab sample extracted from the Knife River test strip is shown in Figure 4.31. The displayed test ran for approximately 70,000 seconds (700,000 loading cycles). Each sample consisted of three phases in the deflection curve: Primary, secondary, and tertiary. In Figure 4.31, the primary phase (initial loading) corresponds to approximately 0-10,000 seconds, the secondary phase (linear deflection) corresponds to approximately 10,000-50,000 seconds, and the tertiary phase (failure) corresponds to approximately 50,000-70,000 seconds. The three phases are marked with vertical lines and labeled as I, II, and III in Figure 4.31. Cracking failure is expected to start at the end of the secondary phase (repetition 50,000 in this example).

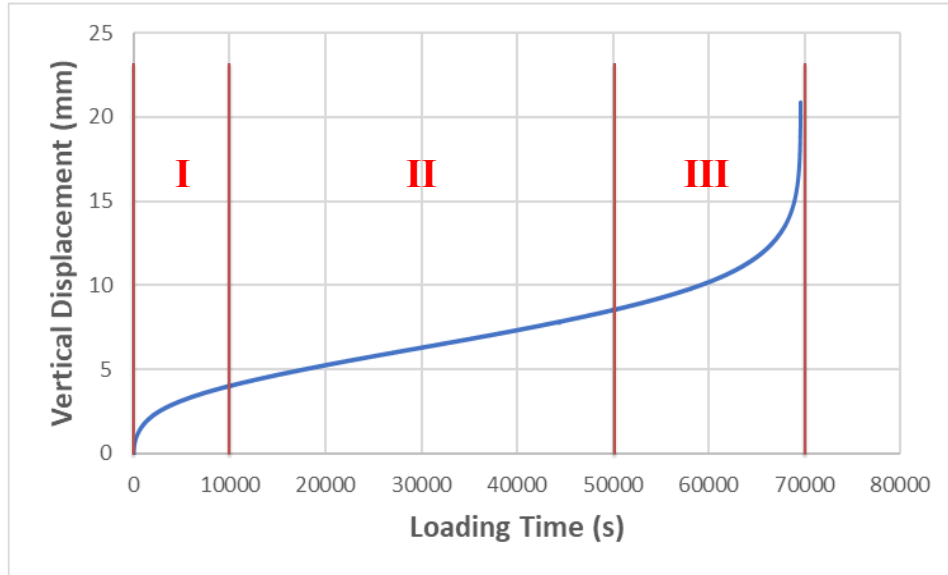


Figure 4.31: Typical flexural fatigue test deflection curve

A flexural fatigue performance parameter was developed to capture the difference in fatigue cracking resistance among testing strategies. The purpose of the parameter was to capture both the vertical deformation experienced at a specific number of loading cycles, as well as the rate at which the sample was deflecting. Vertical deformation was recorded at 200,000 cycles (20,000 seconds). 200,000 cycles were selected because it was at the linear portion of the deflection curve for the majority of tested samples (see Figure 4.32). The vertical displacement value was extrapolated to 200,000 cycles in cases when the sample had failed before the specified number of cycles or when 200,000 cycles was within the tertiary phase of the displacement curve. The slope of the secondary phase of deformation was also extracted for each test and represented the rate of deflection for the sample.

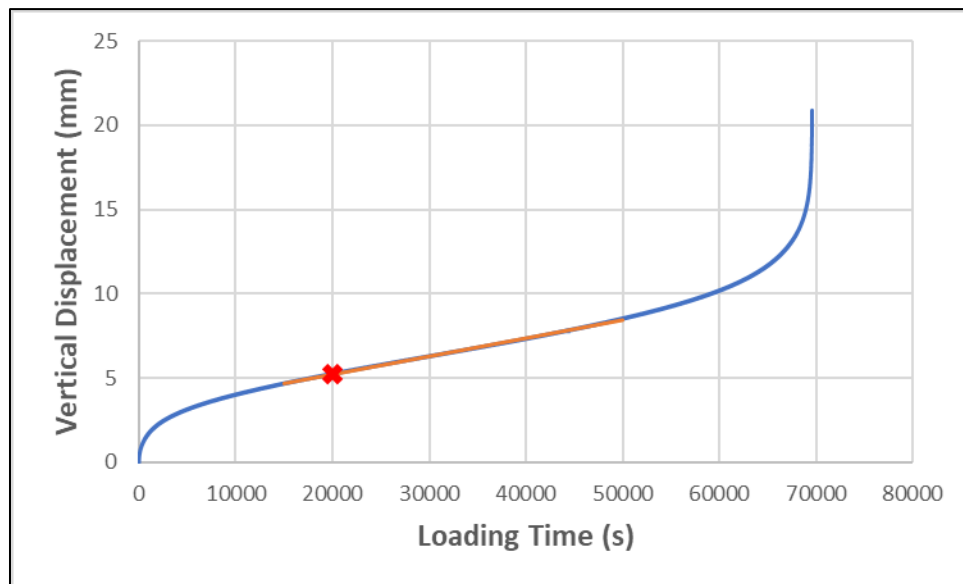


Figure 4.32: Flexural fatigue test deflection curve and performance parameters

The 200,000 cycle (20,000 seconds) displacement value is marked by the red cross in Figure 4.32. The orange portion of the displacement curve in Figure 4.32 is the fitted line of the secondary phase. The slope of the line was determined and utilized as the rate of sample deflection. A large displacement value at 200,000 cycles and a steep slope of the fitted line both corresponded to poor performance (shorter time to failure). The final output parameter used for the flexural fatigue testing was the product of the 200,000-cycle displacement and the slope of the fitted line (called $D_{200k} * m_{stage2}$). Therefore, a low output parameter corresponded to optimal performance, while a high output parameter corresponded to poor performance.

Small variations in field sample thickness, width, and length were present as described in Section 4.3.6. Correction factors were investigated for sample dimensions among all sets of replicates. Sample thickness appeared to influence output results (poor performance with less thickness, better performance for thicker samples). However, there was no thickness trend in some scenarios, or the opposite trend was observed in some cases. Figure 4.33 shows the overall relationship between sample thickness and the bending test output parameter.

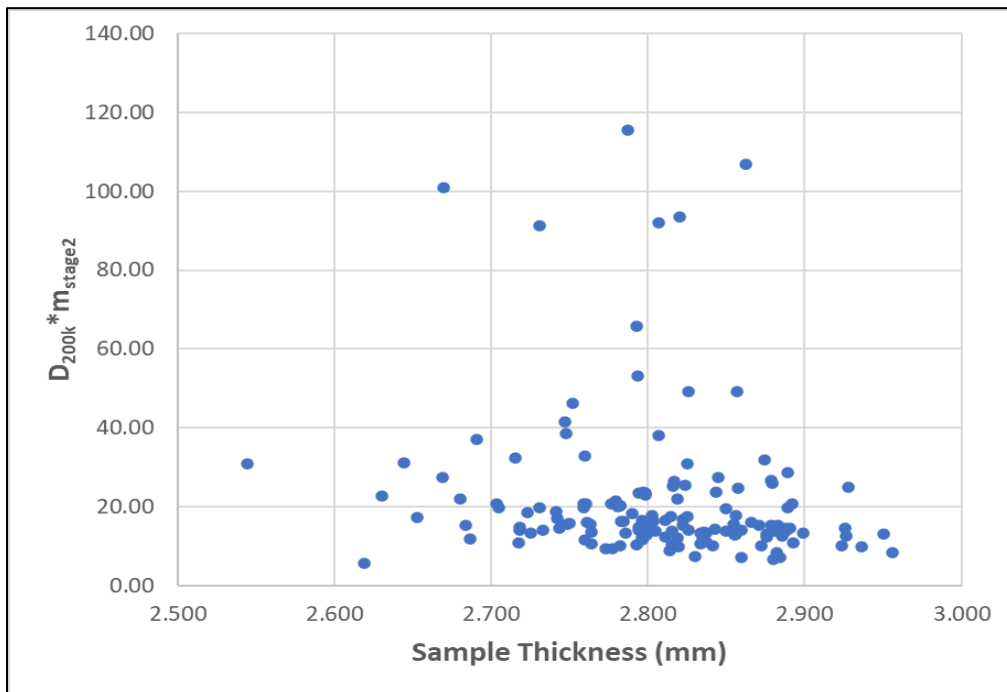


Figure 4.33: Flexural fatigue parameter versus sample thickness

Figure 4.33 demonstrates no trend of improved performance with increased sample thickness. No trends were observed regarding sample width or length. Therefore, no sample thickness, width, or length correction factors were applied to the flexural fatigue test results.

Both deep and shallow milling depths were utilized at the test section for rectangular modified, rectangular conventional, and sinusoidal CLRS. The average recorded milling depths of extracted samples for the three CLRS varieties had variations as expected in field construction. Table 4.12 displays the average CLRS depth among the section types.

Table 4.12: Average measured CLRS depths

| | CLRS Depth (mm) |
|---|------------------------|
| Rectangular - Shallow Modified | 14.8 |
| Rectangular - Shallow Conventional | 13.8 |
| Rectangular - Deep Modified | 17.1 |
| Rectangular - Deep Conventional | 21.4 |
| Sinusoidal - Shallow | 15.2 |
| Sinusoidal - Deep | 15.5 |

As shown in Table 4.12, the section with the deepest milled CLRS was conventional rectangular CLRS. There was a small difference of 0.3 mm (0.01 in) in measured depth between the deep and shallow sinusoidal CLRS. The modified rectangular CLRS had a 2.3 mm (0.09 in) difference between depths, and the conventional CLRS had a 7.6 mm (0.3 in) difference between depths. Comparing the rectangular and sinusoidal CLRS, the shallow depth sinusoidal was 0.9 mm (0.04 in) greater than the shallow rectangular, and the deep rectangular was 3.8 mm (0.1 in) deeper than the deep sinusoidal.

The average rumble strip depths demonstrate that the expected differences in test results between deep and shallow sinusoidal CLRS should be minimal, and the difference between deep and shallow modified rectangular CLRS should also be minimal. Table 4.12 also shows that the expected difference between deep and shallow conventional rectangular CLRS should be significant. Additionally, shallow depth sinusoidal CLRS should be comparable to shallow depth rectangular CLRS. There may be differences between the deep sinusoidal and deep rectangular CLRS due to changes in average milling depth.

Flexural fatigue test results were influenced by the air void distribution in the test section. The increased air voids and density near the edges of construction greatly reduced the fatigue cracking resistance of the samples tested. A similar response is also expected around the longitudinal joints with low density. This air void distribution is demonstrated in Figure 4.22 and Figure 4.23, as well as by visual inspection of a typical sample in the travel lane compared to a sample near the edge of construction (see Figure 4.34).



(a) Air voids – Travel lane



(b) Air voids – Unconstrained edge of the travel lane

Figure 4.34: Test section spatial variability of air voids

The air voids concentrated near the surface in Figure 4.34(b) are due to the edge confinement effects of the construction. The spatial air void variation throughout the test section was considered when analyzing the flexural fatigue test results. Control samples were extracted in the vicinity of the southeast corner of the test section, where air voids were shown to be greatest in Figure 4.22 and Figure 4.23. The control samples were extracted at an average distance of 6.1 m (20.0 ft) longitudinally and 1.6 m (5.2 ft) transversely from the southeast corner of the construction. As such, control samples demonstrated significantly worse performance than CLRS samples extracted away from the edges of construction. Therefore, control samples were excluded from comparisons with CLRS samples.

The test results clearly showed the impact of air void distribution when comparing CLRS samples from the edge of construction to those in the travel lane (Figure 4.35). CLRS samples at the edge of construction were approximately 18.0 cm (0.6 ft) from the unconfined edge, and samples in the lane were approximately 2.4 m (8.0 ft) from the unconfined edge.

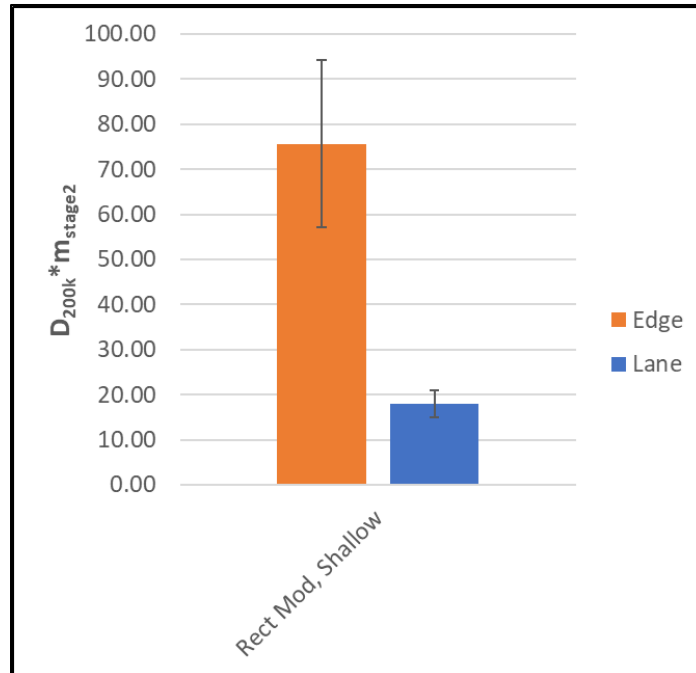


Figure 4.35: Flexural fatigue test – Travel lane versus the edge of construction (error bars are 1 standard deviation)

The flexural fatigue test results in Figure 4.35 demonstrate considerably worse performance for samples extracted near the edge of construction (4-5% less density). This result suggested that asphalt layer density, by far, is the most important factor controlling the cracking resistance of the mix. Installing rumble strips on poorly compacted joints or road shoulders can result in premature cracking failures. Test results for these low-density edge samples were not included in further comparisons.

As discussed in Section 4.1, the presence of a longitudinal joint at the test section was negated due to paving both lanes within a short timeframe (similar to echelon paving) and due to the increased compaction typically employed at the longitudinal joint to reach density requirements. These conclusions were demonstrated in the results of the air void tests on the core samples. The extra compaction and low density at the longitudinal joint were evident in the results of the flexural fatigue testing (see Figure 4.36).

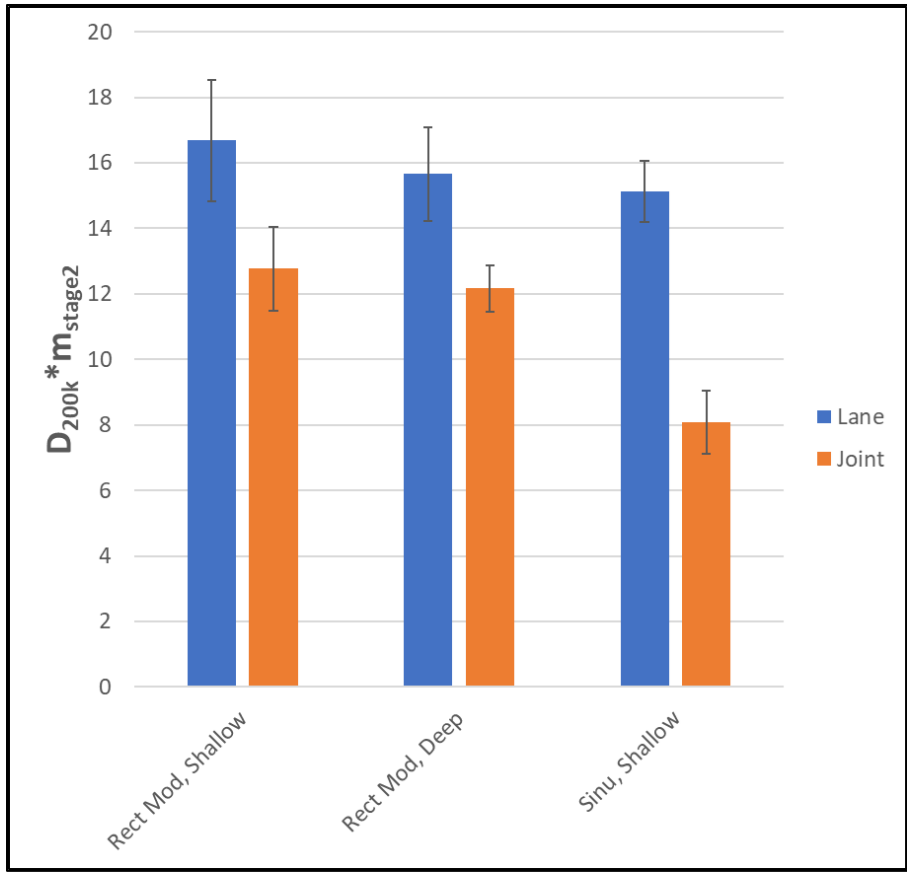


Figure 4.36: Flexural Fatigue Test – Longitudinal joint versus travel lane (error bars are 1 standard deviation)

Figure 4.36 displays all output sets showing superior performance at the longitudinal joint in comparison to samples in the travel lane. Rectangular CLRS samples in the travel lane were 1.1 m (3.5 ft) from the edge of construction, and sinusoidal CLRS samples in the travel lane were 2.2 m (7.4 ft) from the edge. Samples at the longitudinal joint were 3.8 m (12.4 ft) from the edge of construction. Due to the improved performance at the longitudinal joint versus the travel lane, the longitudinal joint will be disregarded as a factor in subsequent results.

Testing strategies involving freeze-thaw conditioning introduced high amounts of variability in the flexural fatigue results. Figure 4.37 demonstrates samples with no treatment compared to samples with freeze-thaw conditioning and samples with both freeze-thaw conditioning and chip seal surface treatment. It was expected that the freeze-thaw cycling would reduce the performance of the CLRS samples due to moisture infiltration into microcracks as well as interconnected air voids, if present. The expectation was that chip seal application would seal the surface of the sample (verified by moisture infiltration results in Section 4.4.3) and negate the impacts of freeze-thaw damage.

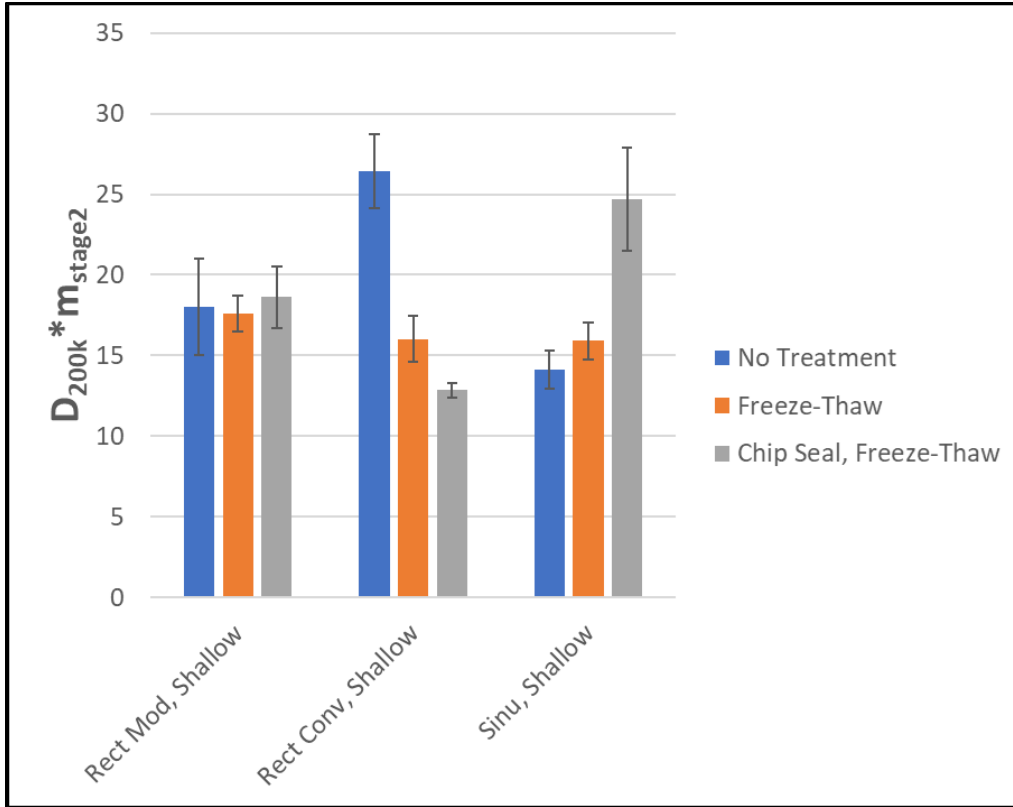


Figure 4.37: Flexural Fatigue Test – Freeze-thaw conditioning versus no treatment versus freeze-thaw with chip seal treatment (error bars are 1 standard deviation)

As displayed in Figure 4.37, there were no consistent trends present after freeze-thaw treatment. Rectangular conventional shallow depth CLRS and sinusoidal shallow depth CLRS showed opposite relationships in comparison to each other. No trends were discerned for rectangular modified shallow depth CLRS. Overall, the variability introduced by the freeze-thaw conditioning did not allow for the analysis of trends regarding this conditioning method for the flexural fatigue tests.

Figure 4.38 demonstrates the comparison between rectangular and sinusoidal CLRS.

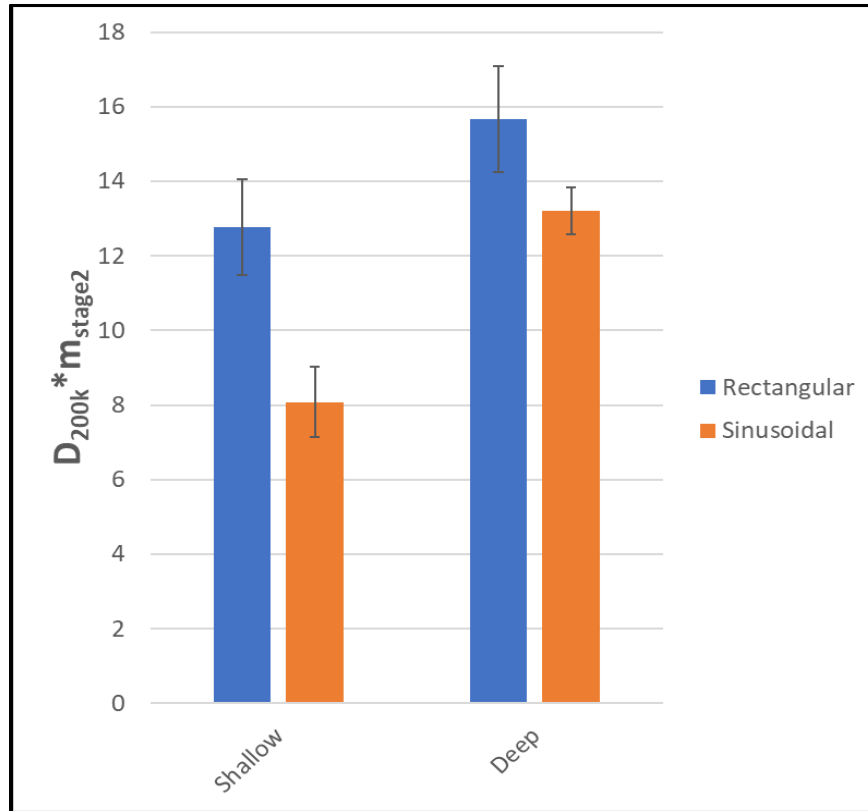


Figure 4.38: Flexural Fatigue Test – Rectangular CLRS versus sinusoidal CLRS (error bars are 1 standard deviation)

As shown in Figure 4.38, an overall trend of 38% improved performance for sinusoidal CLRS was observed. Both the shallow and deep CLRS scenarios demonstrated a statistically significant trend, $t(15) = 2.14$ with $p = 0.02$ (1 tail) and $t(18) = 2.45$ with $p = 0.01$ (1 tail), respectively. This was determined using a two-sample t-test assuming equal variances, with $\alpha = 0.05$ (95% significance). All comparisons made in Figure 4.38 involved rumble strip sections at equal distances from the edge of construction (no spatial effect). The measured rumble strip depths (Table 4.12) for deep and shallow CLRS were similar to one another for the comparisons made in Figure 4.38. The difference in CLRS depths is not expected to have impacted the results discussed in this comparison.

Figure 4.39 compares CLRS milled at a shallow depth to those with deeper CLRS. It was expected that deeper CLRS would result in poor flexural fatigue performance because of less overall sample thickness.

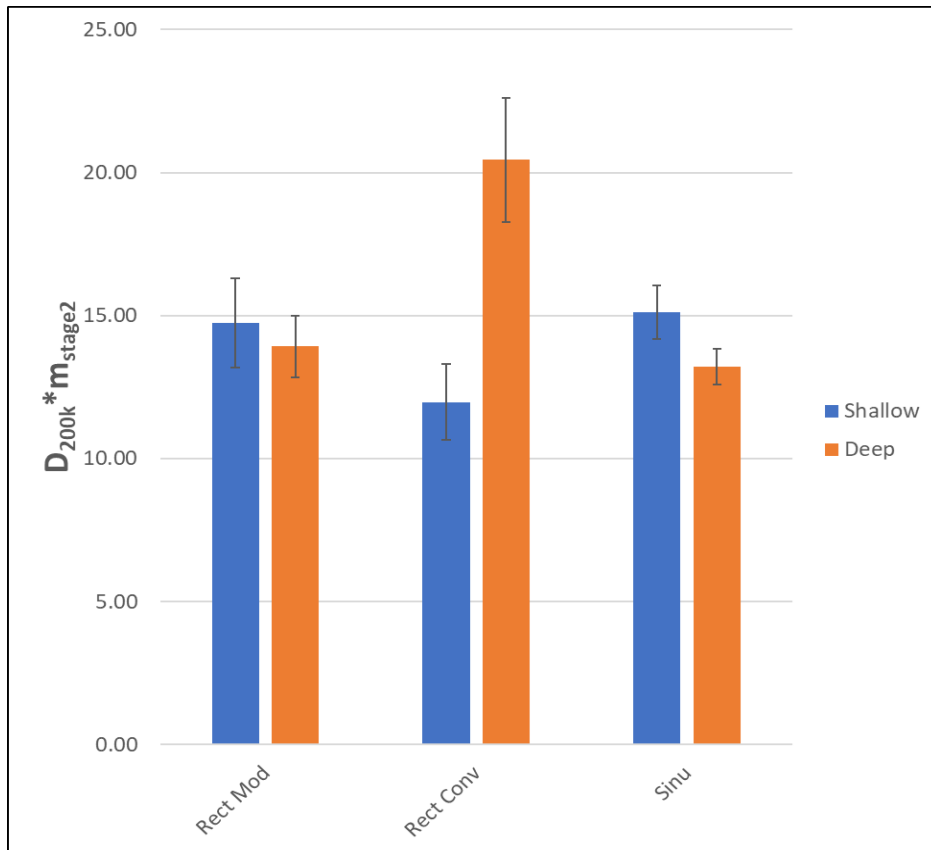


Figure 4.39: Flexural Fatigue Test – Shallow versus deep CLRS (error bars are 1 standard deviation)

The difference in measured rumble strip depth between shallow and deep CLRS for rectangular modified and sinusoidal rumbles was 16% and 2%, respectively. As such, no major differences were expected, and this was visible for rectangular modified rumbles in Figure 4.39. There was a statistically significant difference between sinusoidal CLRS samples, $t(16) = 2.01$ with $p = 0.03$ (1 tail). However, this was likely due to spatial variability effects. Shallow sinusoidal CLRS were extracted 2.2 m (7.4 ft) from the edge of construction, while deep sinusoidal CLRS were removed 3.0 m (10.0 ft) from the edge. This spatial effect resulted in improved overall performance for deep sinusoidal CLRS. The comparisons made in Figure 4.39 for the rectangular CLRS were for samples extracted from the same distance from the edge of construction, meaning that no spatial variability was expected. There was a 55% difference in measured CLRS depth for the conventional rectangular rumbles, and there was a corresponding 71% increase in the output parameter for the deep rumbles. This demonstrated the negative impact of a 7.6 mm (0.3 in) increase in CLRS depth.

Figure 4.40 compares the conventional rectangular CLRS (40.6 cm [16 in] wide) to the modified rectangular CLRS (20.3 cm [8 in] wide). It was expected that the modified CLRS would have improved performance due to less material being milled from the asphalt layer.

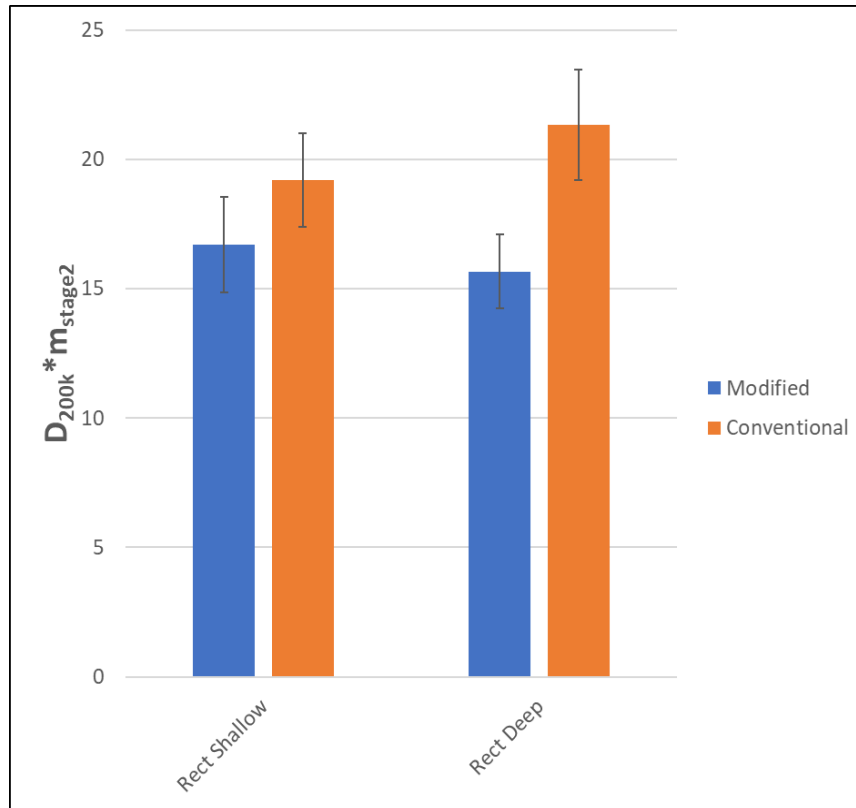


Figure 4.40: Flexural Fatigue Test – Modified versus conventional rectangular CLRS (error bars are 1 standard deviation)

Figure 4.40 shows that in both cases, there was a trend of improved performance for rectangular modified CLRS in comparison to conventional CLRS. There was a statistically significant difference for the rectangular deep CLRS, $t(15) = -3.56$ with $p = 0.001$ [1 tail]. The wider conventional CLRS had an average performance parameter 26% higher than the modified CLRS. Modified CLRS samples in the travel lane were 1.1 m (3.5 ft) away from the edge of construction, and the conventional CLRS were 2.6 m (8.5 ft) from the edge. The potential edge effects would suggest that conventional CLRS performance would surpass that of the modified due to the increased distance from the edge. However, it was seen that the rumble strip size was the controlling factor. Shallow modified CLRS were 1 mm (0.04 in) deeper on average than the shallow conventional CLRS. Deep conventional CLRS were 4.3 mm (0.2 in) deeper on average than the deep modified CLRS. The smaller difference (15%) in output parameters in the shallow rectangular CLRS scenario and the larger difference (36%) in the deep rectangular CLRS scenario are directly related to the variations in rumble strip depth.

Figure 4.41 demonstrates the combined effect among replicates with chip seal surface treatment and those without. It was expected that chip seal application would improve fatigue performance. However, the level of improvement needed to be determined. Since chip seal layers are not applied to improve the load-carrying capacity of the roadways, it is possible that the improvement in cracking resistance due to the chip seal layer can be negligible. When the chip seal emulsion hardens after application, a secondary wearing surface is created on the surface of the samples. Cracking begins on the surface of the asphalt sample in the flexural fatigue tests.

The added thickness, as well as the elasticity of the chip seal emulsion, was expected to lead to extensions in the fatigue cracking resistance of the tested samples.

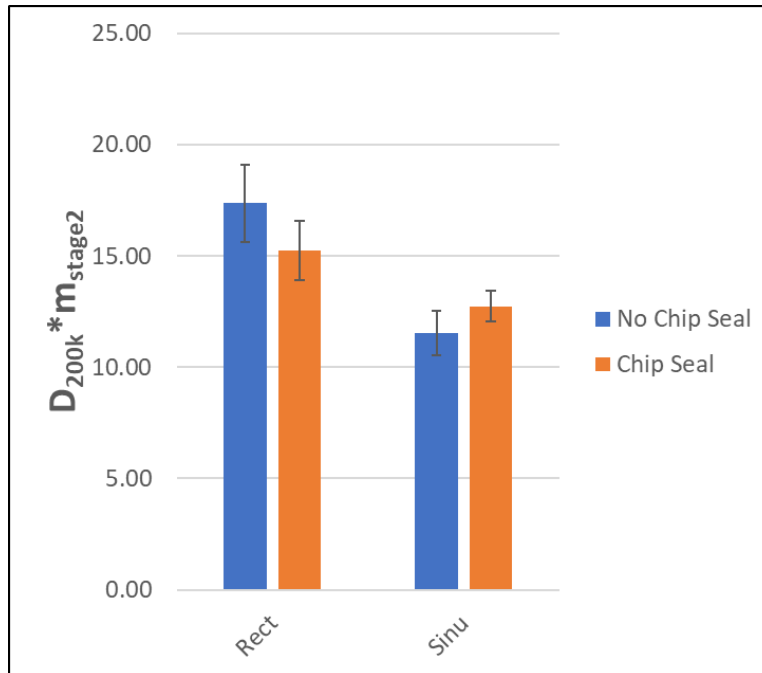


Figure 4.41: Flexural Fatigue Test – Chip seal surface treatment versus no treatment (error bars are 1 standard deviation)

As shown in Figure 4.41, there were no consistent effects on the flexural fatigue performance after chip seal application. This is expected to be a result of the insignificant thickness of the chip seal layer when compared to the asphalt layer thickness. However, it should be noted that chip sealing CLRS can still reduce moisture infiltration and improve durability and long-term pavement performance (which was not simulated in this part of the experimental plan). See prior Section XYZ on this topic.

In summary, the spatial variability of the flexural fatigue test results due to decreased density near the edges of construction and over-compaction of the longitudinal joint was verified. Freeze-thaw conditioning led to large fluctuations in the flexural fatigue test results. This did not allow for determining the effectiveness of sealing the surface using chip seal surface treatment. Sinusoidal CLRS were shown to have improved performance compared to rectangular CLRS (a similar conclusion was also derived from the FEA presented in Chapter 3). Deep and wide rumble strips were both shown to reduce the fatigue cracking resistance of the CLRS. Finally, chip seal surface treatment did not lead to improvements in bending test results.

4.4.5 Hamburg Wheel Tracking Test (HWTT)

A typical rutting curve from the HWTT for a slab sample extracted from the Knife River test strip is shown in Figure 4.42.

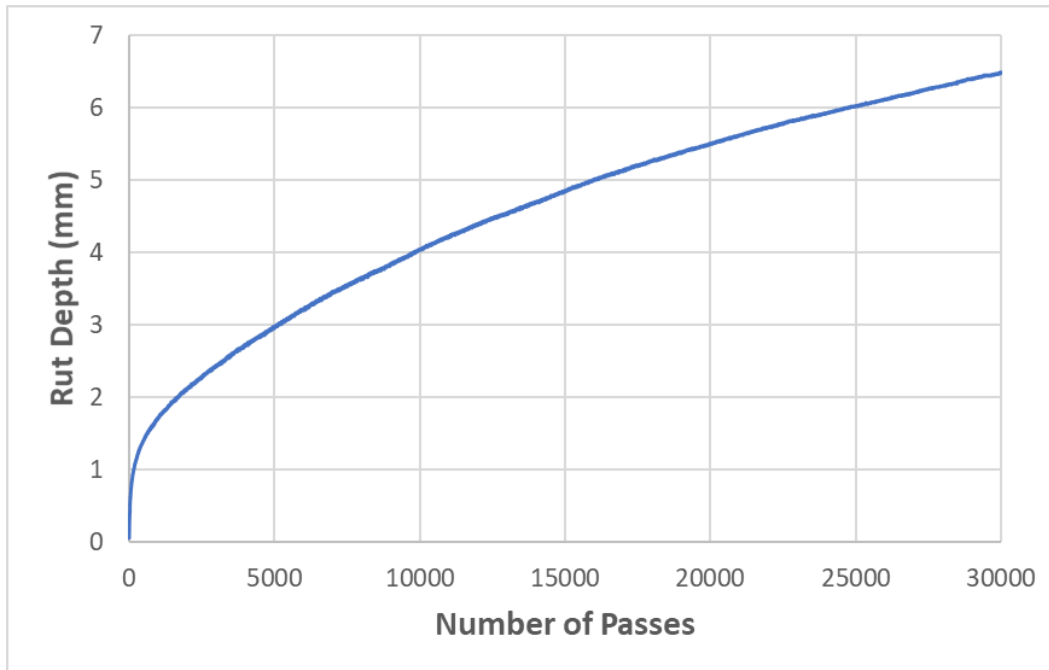


Figure 4.42: Hamburg Wheel Tracking Test (HWTT) typical rutting curve

All HWTT tests ran for 30,000 passes. The performance parameter utilized in the HWTT tests was the accumulated rut depth at 30,000 passes. The purpose of the parameter was to measure rut depth and act as an indicator of cracking and structural performance. Samples were partially unconfined, sitting atop a sand layer (weak base layer). Replicates with poor structural performance would be allowed to crack and deform at a greater rate due to the boundary conditions utilized. This means that samples with a high 30,000 pass rut depth correspond to poor overall performance, while samples with a low 30,000 pass rut depth correspond to improved overall performance.

Trends in HWTT performance due to sample thickness, width, and length were investigated in the same manner as the flexural fatigue testing in Section 4.4.4. No trends were observed. Therefore, no sample thickness, width, or length correction factors were applied to the HWTT test results. Rumble strip milling depths were the same for HWTT samples as they were for flexural fatigue samples (see Table 4.12). The variations in milling depth were expected to impact HWTT test results in the same manner.

As mentioned in Section 4.4.4, the spatial air void variation throughout the test section was considered when analyzing the HWTT test results. Control samples were again extracted in the vicinity of the southeast corner of the test section, where air voids were shown to be greatest in Figure 4.22 and Figure 4.23. The control samples were extracted at an average distance of 4.8 m (15.9 ft) longitudinally and 1.3 m (4.1 ft) transversely from the southeast corner of the construction. Comparable rectangular and sinusoidal CLRS replicates were extracted at similar distances from the edge of construction (1.1 m [3.7 ft] and 1.5 m [4.9 ft], respectively). A comparison between the control, rectangular CLRS, and sinusoidal CLRS is shown in Figure 4.43. Control samples were not extracted at the longitudinal construction joint and are not included in the figure.

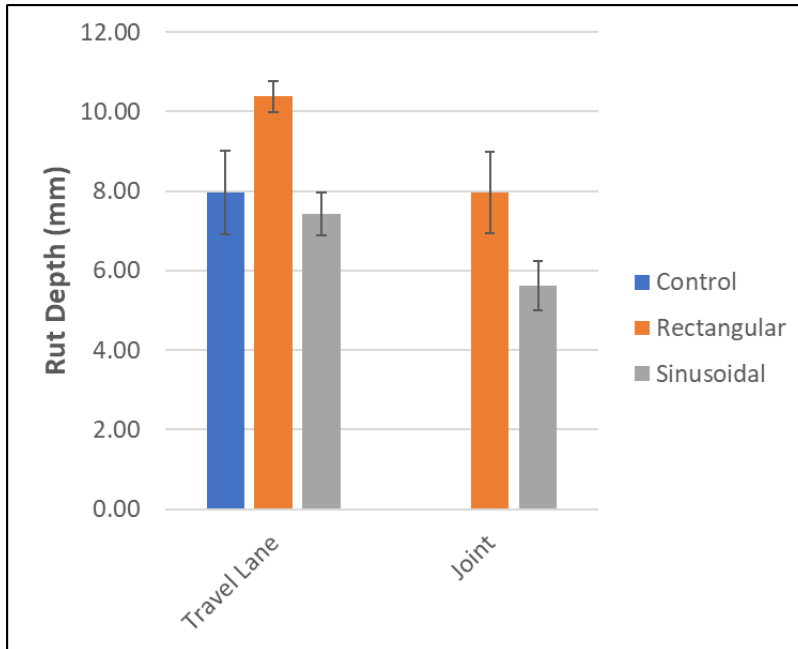


Figure 4.43: HWTT - Control versus rectangular CLRS versus sinusoidal CLRS (error bars are 1 standard deviation)

The travel lane HWTT rutting results in Figure 4.43 demonstrate that sinusoidal CLRS had statistically equivalent, $t(11) = 0.43, p = 0.34$ (1 tail), performance to control replicates with no milled rumble strips. In both mid-lane and centerline scenarios, rectangular CLRS had an overall average rut depth of 41% greater than sinusoidal CLRS. The steel wheel rolling over the rectangular CLRS experienced increased roughness and dynamic loading in comparison to the smooth rolling over sinusoidal CLRS. It is likely that this is the primary reason sinusoidal CLRS had superior performance in the HWTT tests. It is possible that the dynamic loading experienced at highway speeds may lead to different structural impacts for the rectangular and sinusoidal CLRS. Comparisons can also be made in Figure 4.43 among samples extracted along the joint of construction versus those extracted within the travel lane. The same statistically significant, $t(27) = 2.63, p = 0.007$ (1 tail), spatial variability effect as in Section 4.4.4 can be observed. Samples along the joint were further from the unconfined edge and, therefore, had improved performance due to higher densities and increased compaction at the joint. Another reason for higher resistance for the joint samples might be the higher compaction effort applied along the construction joint during construction. This is a typical process followed during construction to improve joint density and performance.

The equivalent performance of sinusoidal CLRS to control samples and the improved performance of sinusoidal CLRS in relation to rectangular CLRS can also be seen in the HWTT rutting curves. Figure 4.44 shows composite rutting curves for the travel lane replicates in Figure 4.43. The composite rutting curve is the combination of the individual rutting curves of replicates, where the average rut depth for each pass is calculated among the replicates for all 30,000 passes.

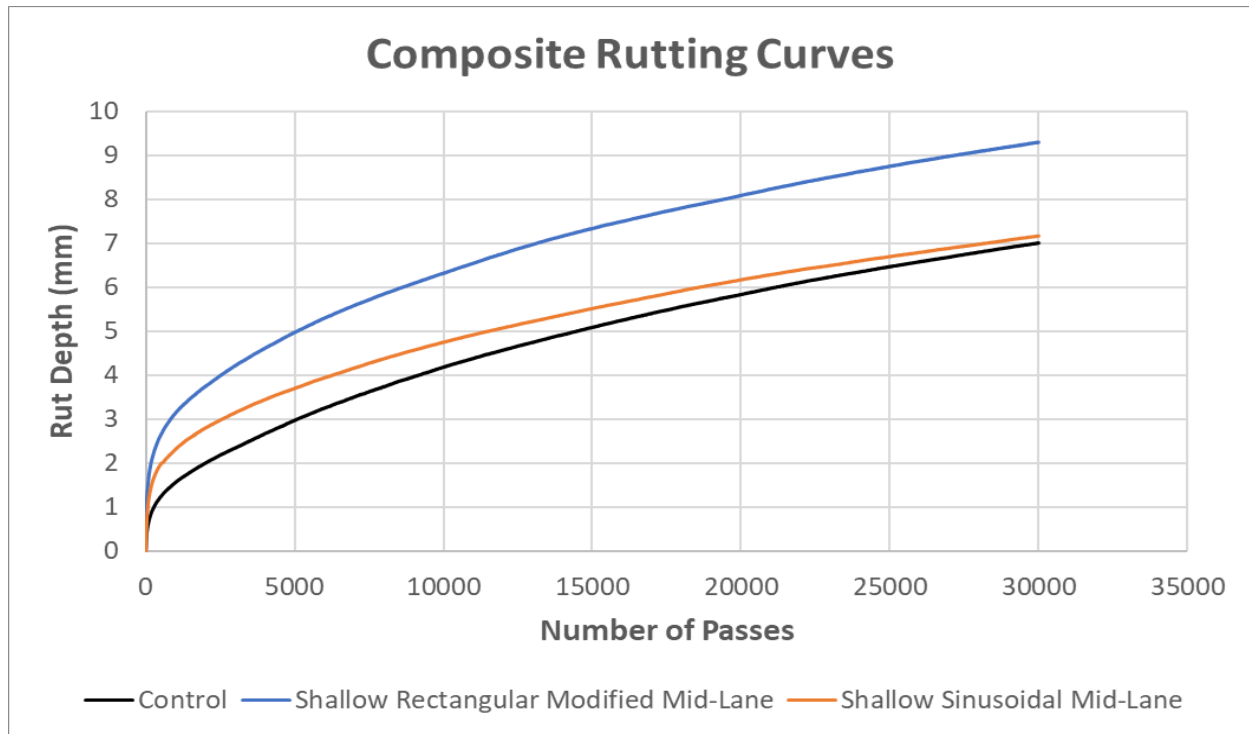


Figure 4.44: HWTT - Composite rutting curves for control, rectangular CLRS, and sinusoidal CLRS

The rectangular CLRS composite rutting curve in Figure 4.44 shows steep initial rutting accumulation, and this is related to the steel wheel entering and exiting the rumble strip as it rolled over the CLRS edges. These edges were critical points for the rectangular rumbles as the steel wheel rolled through. The sinusoidal CLRS, on the other hand, had no sharp critical edge points because it consisted of a smooth, evenly sloped surface throughout. There was, however, greater initial rutting accumulation than the control samples but less than the rectangular CLRS.

Similar to the flexural fatigue testing results, freeze-thaw conditioning introduced significant variability to the HWTT test results (the 30,000-pass rutting output). For this reason, freeze-thaw results were excluded from the quantitative comparisons. However, visual differences in cracking patterns were observed due to freeze-thaw conditioning. The typical difference in failure modes is shown in figure 4.45.

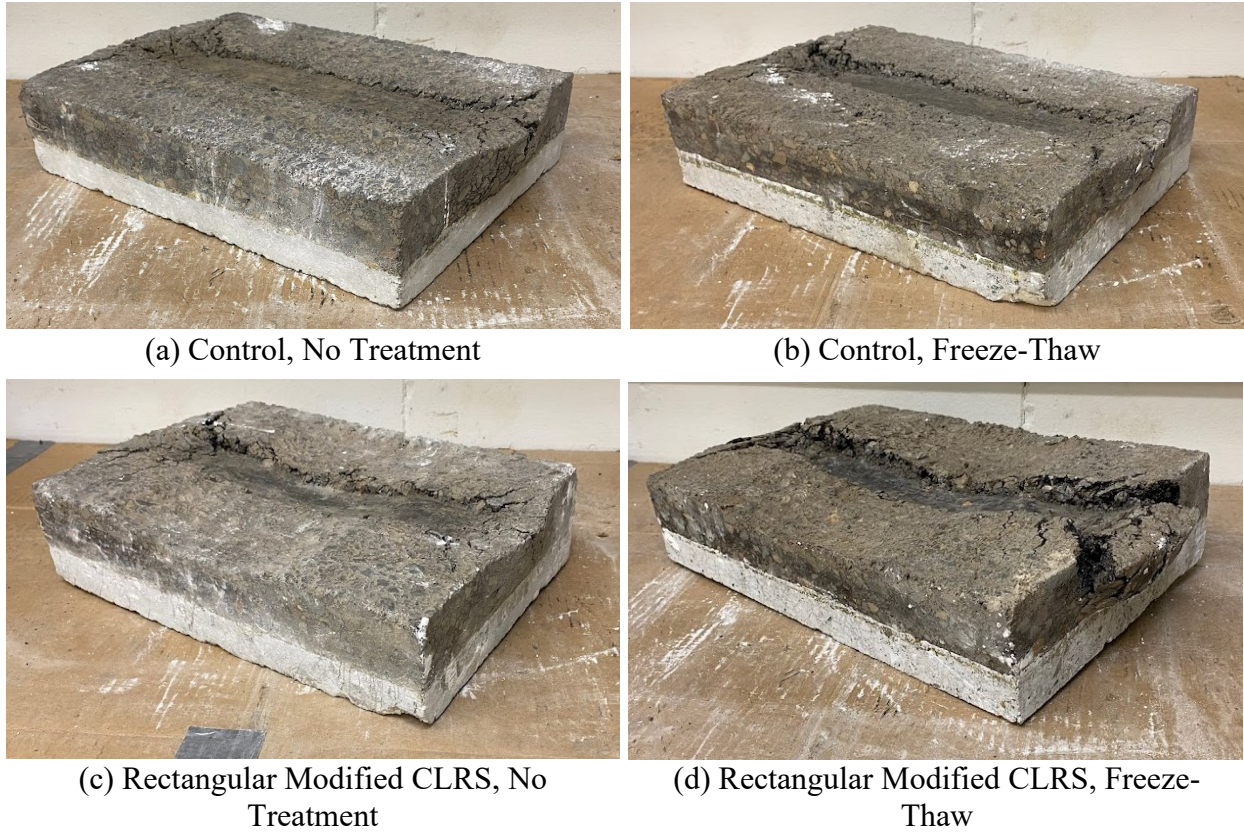


Figure 4.45: HWTT - Cracking patterns after freeze-thaw conditioning

The adverse impacts of freeze-thaw damage on the HWTT samples are demonstrated in Figure 4.45. Typical freeze-thaw impacts increased the shear flow and deformation of the asphalt concrete and increased cracking concentrated at both ends of the sample. Samples without freeze-thaw conditioning observed less of each effect. However, the freeze-thaw effect was not significant for most of the tested specimens. Chip seal application was expected to seal the surface of the asphalt and, therefore, mitigate the negative impacts of the freeze-thaw cycles. Figure 4.46 demonstrates samples with no treatment and samples with both chip seal surface treatment and freeze-thaw conditioning.

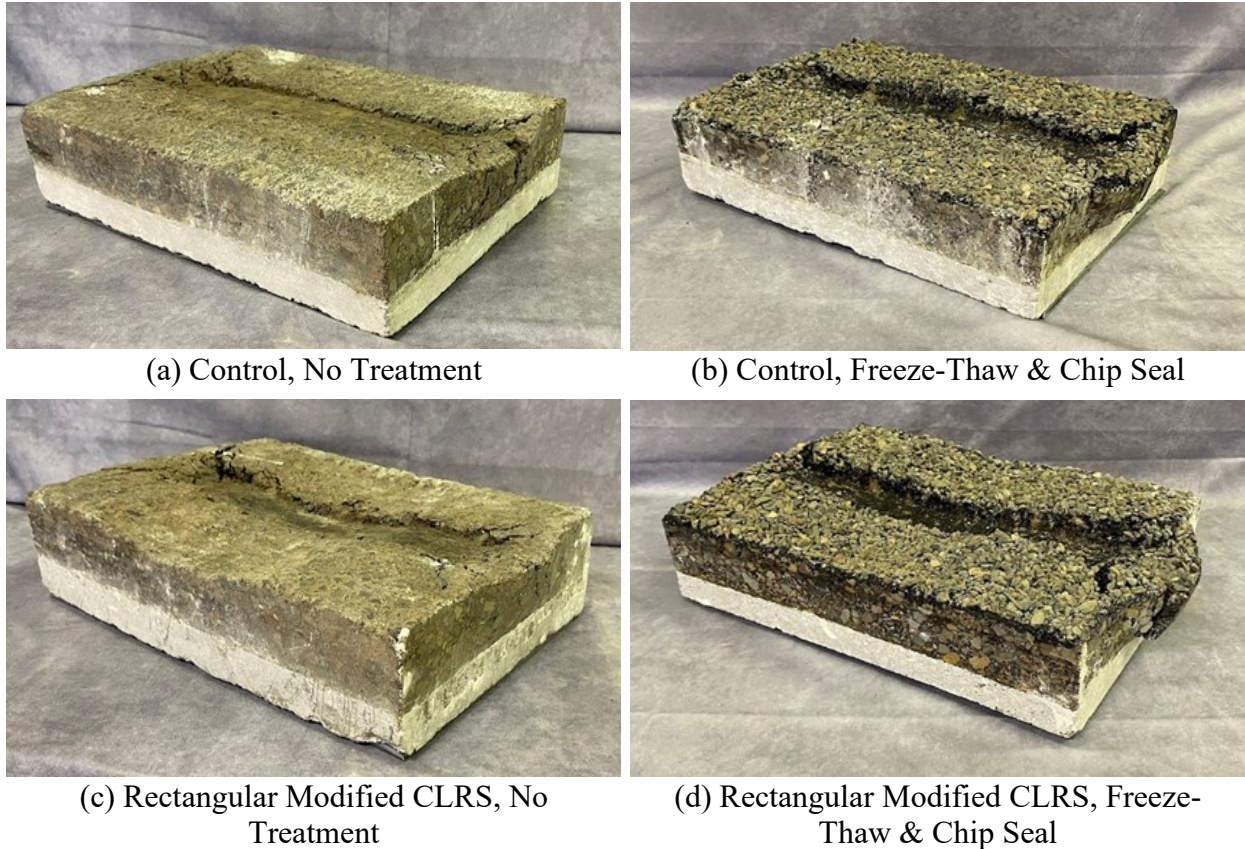


Figure 4.46: HWTT - Cracking patterns after freeze-thaw conditioning and chip seal surface treatment

Figure 4.46 demonstrates that the chip seal surface treatment had minimal effect in mitigating the freeze-thaw damage. Cracking patterns and asphalt shear flow are similar to those of samples with freeze-thaw conditioning and no chip seal (Figure 4.45(b) and Figure 4.45(d)). Additional qualitative comparison photos of tested HWTT samples are shown in Appendix (Figure A.2).

Samples with chip seal surface treatment generally resulted in an increased 30,000 pass rut depth. This is because the LVDT sensor was capturing the crushing of chip seal aggregates, the shear flow movement of the asphalt emulsion layer from the steel wheel path, and the collection of emulsion/aggregates adhering to the steel wheel throughout the test. The flow of the chip seal outside the wheel path can be seen in cross-section views of tested and cut HWTT samples (Figure 4.47).



(a) Control



(b) Rectangular Modified CLRS

Figure 4.47: Tested HWTT cross-section views, with chip seal surface treatment

A correction factor was developed for the high rutting measured for chip seal samples. The average chip seal thickness was measured among multiple samples, and a correction factor of - 5.5 mm (0.2 in) was applied to the 30,000-pass rut depth. It should be noted that chip seal thickness varied by sample type due to the emulsion collecting in the rumble strip grooves. The correction factor was not entirely correct due to differences stemming from chip seal application, and for this reason, comparisons will be made only between samples without surface treatment or between comparable samples with chip seal treatment. Results are shown in Figure 4.48 for corrected chip seal HWTT outputs compared to samples without treatment.

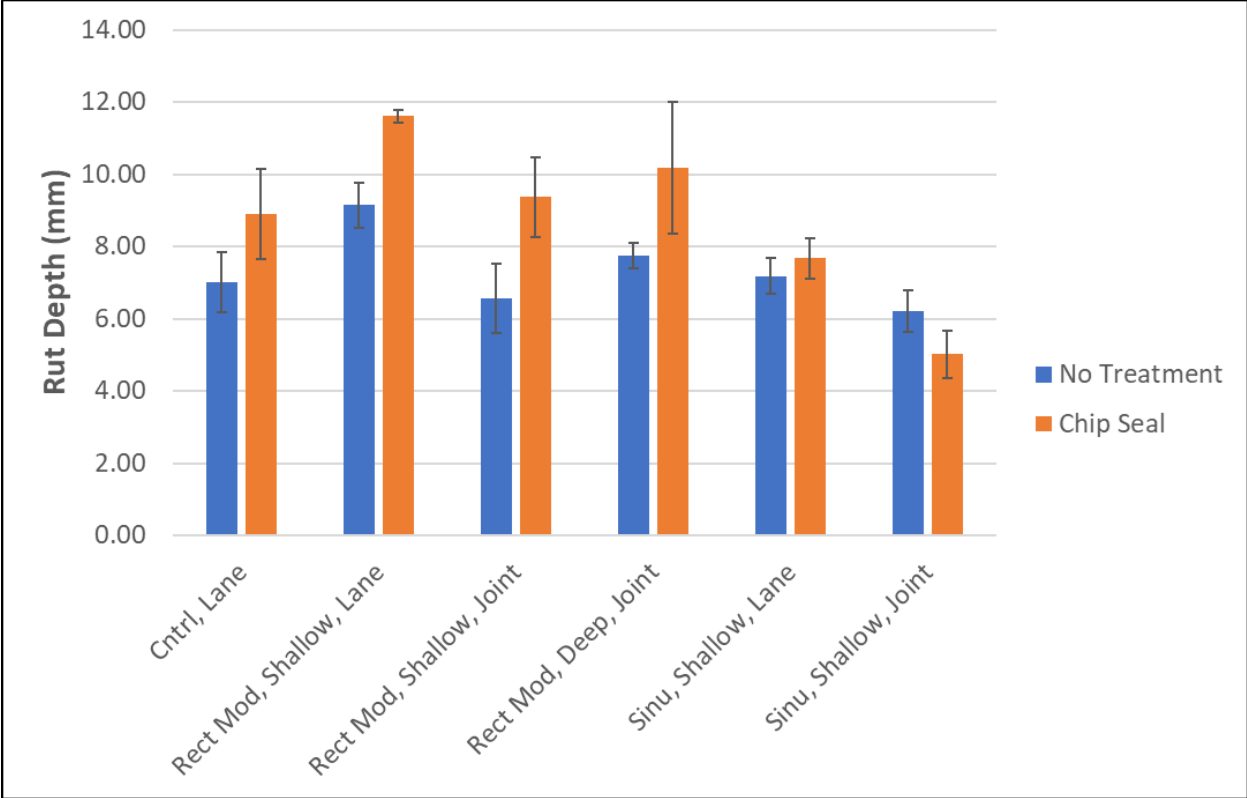


Figure 4.48: HWTT – Chip seal treatment with correction factor versus no treatment (error bars are 1 standard deviation)

As described, chip seal samples with the correction factor incorporated generally had a higher 30,000-pass rut depth in comparison to samples without chip seal. Figure 4.48 demonstrates again the improved performance of sinusoidal CLRS in comparison to rectangular CLRS. This conclusion is in agreement with the flexural fatigue test results and the FEA modeling results. Figure 4.49 compares shallow depth rectangular CLRS to deep rectangular CLRS.

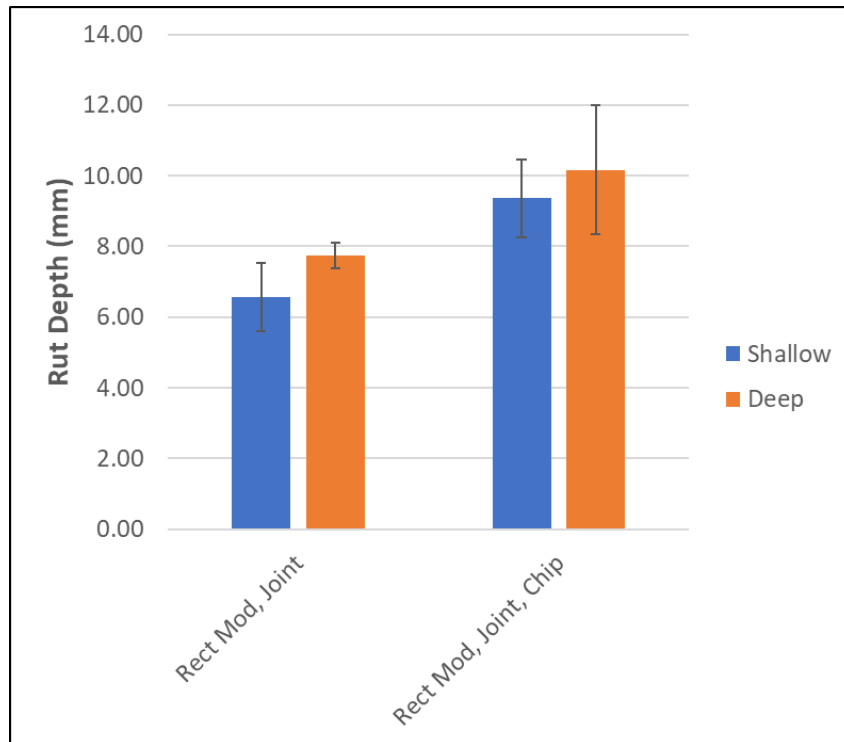


Figure 4.49: HWTT - Shallow versus deep rectangular CLRS (error bars are 1 standard deviation)

Figure 4.49 shows minor trends, $t(13) = -0.50$, $p = 0.31$ (1 tail) of deep CLRS with worse performance than shallow CLRS. Because of spatial effects in the comparison of Figure 4.49, no assessments were made for rectangular or sinusoidal rumbles in the travel lane. The deep CLRS in Figure 4.49 were 16% deeper than the shallow CLRS, and there was a corresponding 13% increase in rut depth for the deep rumbles. This trend aligns with that of the flexural fatigue results, and it is likely that larger differences would again be observed when comparing the deep and shallow conventional CLRS.

No modified versus conventional rectangular CLRS comparison was performed because sample geometries would have been the same for HWTT testing. Composite rutting curves for the remainder of the strategies tested in the experimental plan are included in Figure A.1 in the Appendix.

In summary, the spatial variability of the HWTT test results due to decreased density near the edges of construction and over-compaction at the longitudinal joint was verified. Freeze-thaw conditioning led to fluctuations in the HWTT quantitative test results. However, visual comparison of cracking patterns demonstrated some minor adverse effects due to freeze-thaw damage. The effectiveness of reducing freeze-thaw damage by sealing the surface with a chip seal treatment was also determined via visual comparison. It was concluded that chip seal surface treatment did not mitigate freeze-thaw damage in the HWTT tests. However, chip sealing (or any other surface treatment) is still expected to reduce the moisture-related failures along the CLRS. It was also shown that the corrected rut depth parameter for chip seal samples was not comparable to the parameter for samples without surface treatment. Sinusoidal CLRS were

shown to have improved performance compared to rectangular CLRS. Sinusoidal CLRS were also shown to have equivalent performance to samples without rumble strips. Comparisons were not made between modified and conventional rectangular CLRS due to equivalent geometries in HWTT testing. Finally, deep rumble strips were shown to have poor performance in comparison to shallow rumbles. HWTT conclusions regarding rectangular versus sinusoidal CLRS and deep versus shallow rumbles agreed with the findings of the beam fatigue testing and the FEA.

4.4.6 Pavement Roughness

Results of the SurPRO runs to determine pavement IRI of different CLRS types at the Knife River test section are shown in Figure 4.50. Pavement roughness was calculated as the total vertical suspension movement throughout the analyzed distance using the Proval software.

The SurPRO IRI measurements were inconsistent (high variability) among similar runs in the deep, rectangular CLRS section and the sinusoidal CLRS section due to the extremely rough nature of rumble strips compared to smooth road surfaces. The modified CLRS had 21% higher measured roughness than the conventional CLRS. The longitudinal joint had the lowest IRI, but this was due to shorter section lengths. The full section length was not utilized because a portion of the joint was utilized for CLRS adjacent to the joint and this required that the test be ended early. The findings showed that sinusoidal CLRS had the highest IRI (+17%), followed by deeper rectangular CLRS (+5%), then the shallow rectangular CLRS.

These results indicate that sinusoidal CLRS could be creating increased dynamic loading of the vehicle suspension in comparison to rectangular CLRS. Increased dynamic loading results in more severe tire impact loads and can lead to accelerated pavement damage (fatigue cracking). However, it is important to note that in the test section, the rolling motion of the SurPRO over the sinusoidal CLRS sections was the smoothest despite the fact that these sections had higher measured pavement roughness. This is likely a consequence of the SurPRO data collection system, which is designed for running over relatively flat pavement surfaces. The system was not designed for extremely rough CLRS surfaces.

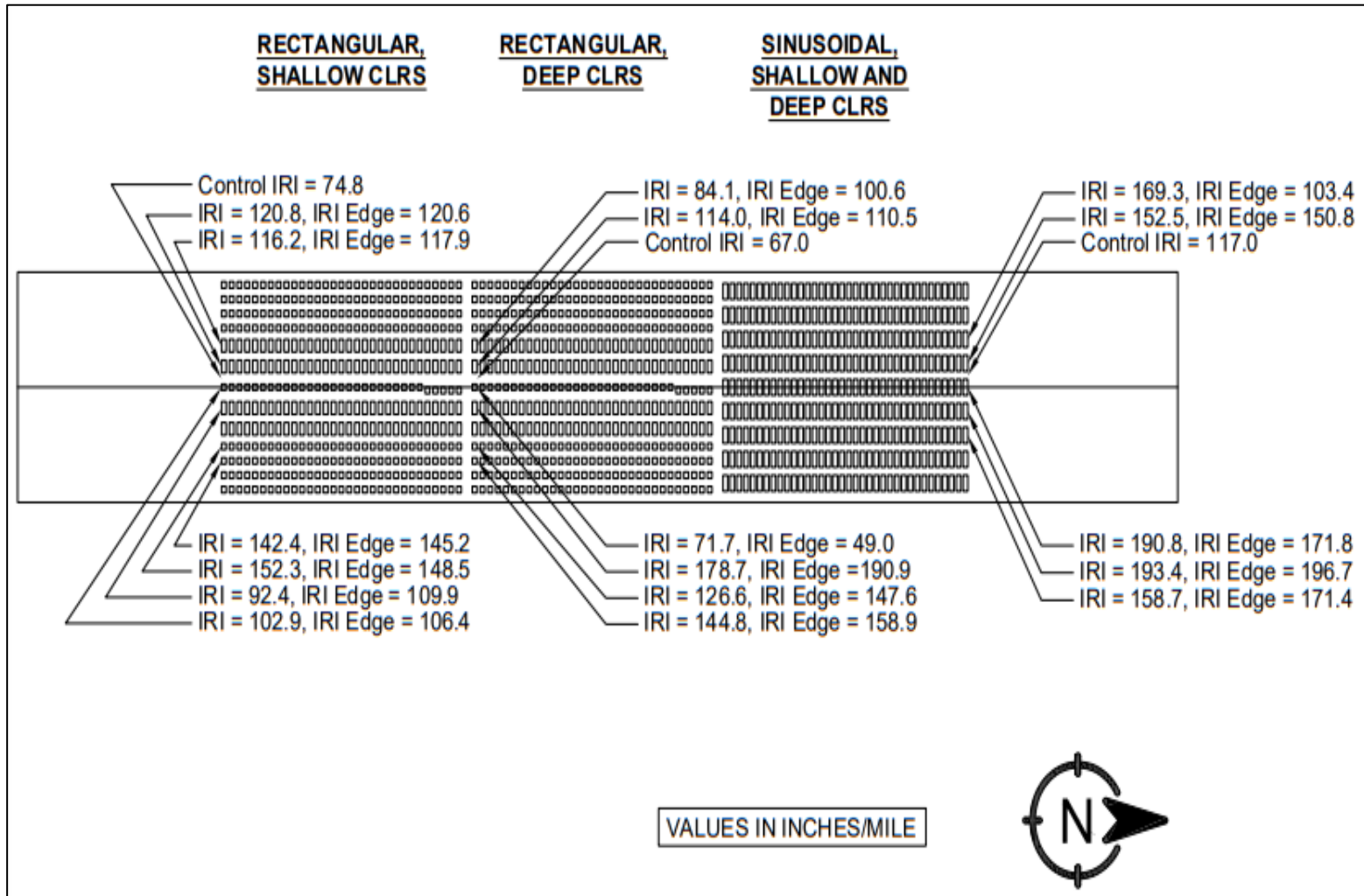


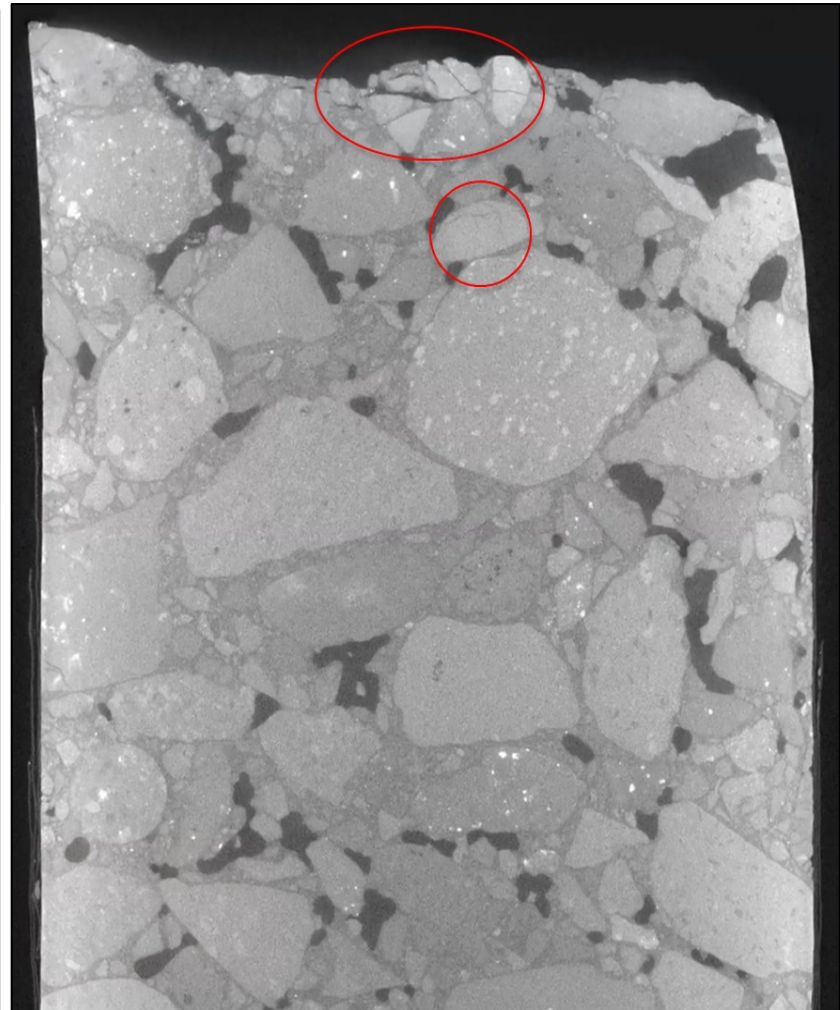
Figure 4.50: SurPRO IRI results

4.4.7 X-ray CT Imaging

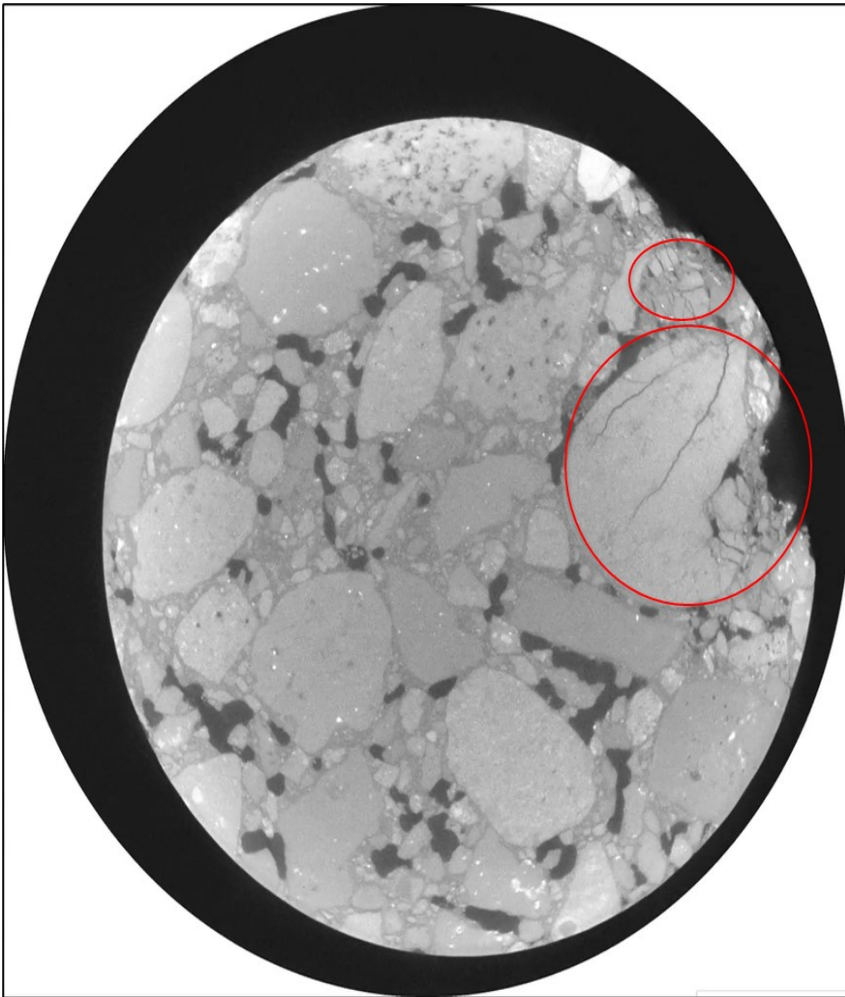
Microcracks were found to be present in the asphalt cores extracted from a milled rumble strip at the Knife River test section. Figure 4.51 displays the presence of microcracks (marked within red zones) in the cross-section images of the core extracted from the center point of the rumble strip, the core extracted from the long edge of the rumble strip, and the core extracted from the short edge of the rumble strip.



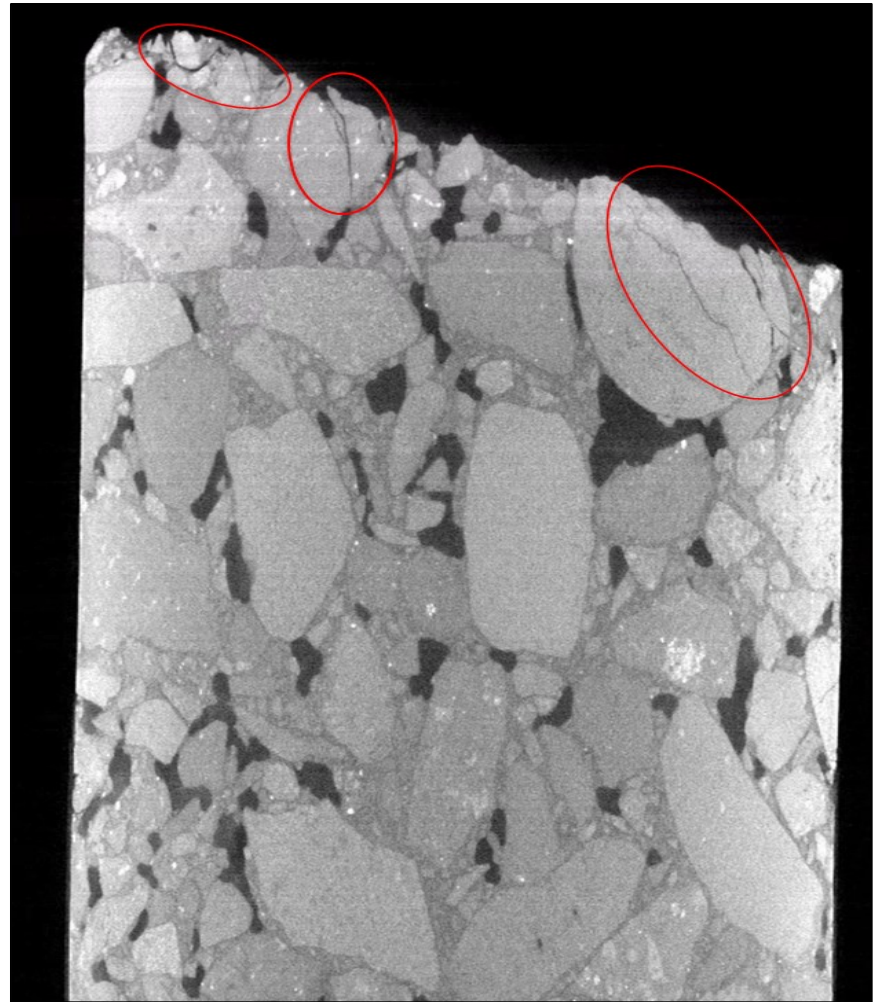
(a) Center Core – Top down view



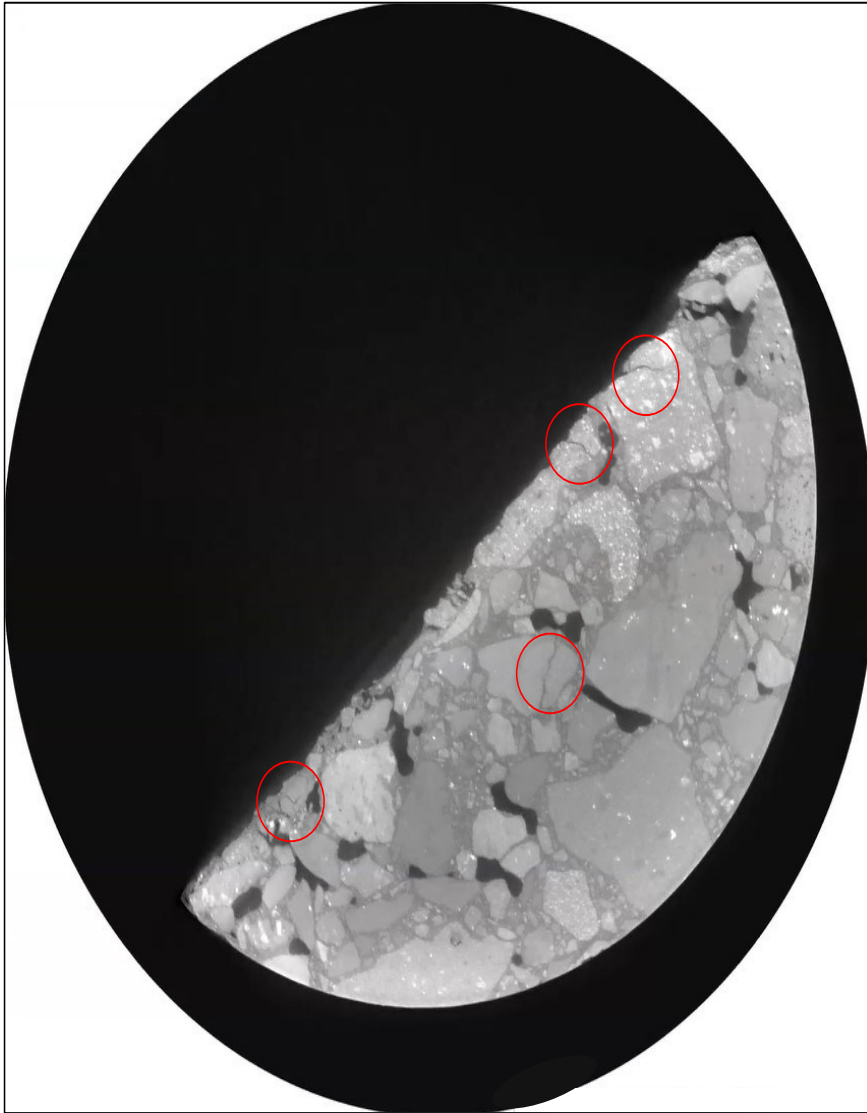
(b) Center Core – Side view



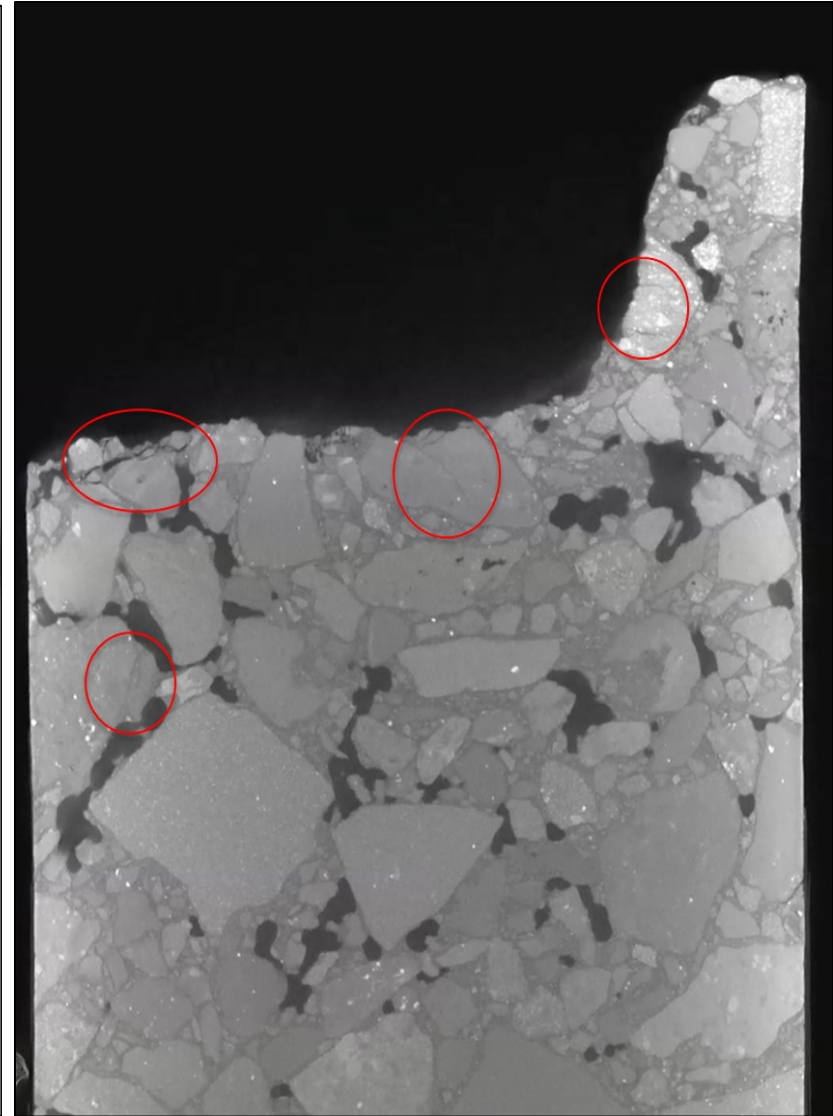
(c) Long Edge – Top down view



(d) Long Edge – Side view



(e) Short Edge – Top down view



(f) Short Edge – Side View

Figure 4.51: X-ray CT imaging cross-section views

The cross-section images shown in Figure 4.51(a), (c), and (e) were taken slightly below the surface of the sample. The cross-section images shown in Figure 4.51(b), (d), and (f) were taken near the midpoint of the core to avoid including cracks on the outside perimeter of the core. Typical hairline microcracks were approximately 50 micrometers in width. The larger cracks present in the cores were typically in the range of 100 micrometers wide. Microcracks extended to a maximum depth of approximately 25.4 mm (1 in) and the majority of microcracks were concentrated within 6.35 mm (0.25 in) of the asphalt surface. Hairline cracks were more common deeper in the core, while larger cracks were more common near the surface. There were significantly fewer microcracks at the maximum 25.4 mm (1 in) depth in comparison to the number of microcracks concentrated at the surface.

All milled surfaces had similar cracking patterns between the four cores analyzed. Cracking was also observed in aggregates along the vertical face of the core extracted from the short edge of the rumble strip (see Figure 4.51[f]). All microcracks were observed in aggregates or at the aggregate-binder interface; there was no cracking observed in the binder. Control samples (without CLRS milling) were also analyzed, and no micro cracks were observed in the control-X-Ray CT images. This result suggests that micro cracks did not form as a result of compaction with roller compactors, but they are solely a result of the milling process. It is possible that milling systems with diamond grinders are creating microcracks on the pavement surface during CLRS installation. These microcracks might be propagating with the application of thermal and vehicular loads and resulting in cracking along the rumble strips. Rainwater filling the microcracks might also be creating hydrostatic pressures when a truckload is applied, resulting in “single-event” cracking (crack formation with one pass of a heavy truck) along the rumble strips. This phenomenon is expected to create more significant damage to the CLRS than the freeze-thaw effect. For this reason, sealing the surface of the CLRS with chip seal or fog seal treatments right after the CLRS installation could be beneficial. A small trailer system with a sweeper (with vacuum) followed by nozzles for asphalt emulsion application can be developed and installed behind the milling systems to fill those microcracks during rumble strip installation before the water gets in them. This type of upfront sealing may improve the longevity of CLRS.

5.0 SUMMARY, CONCLUSIONS, AND RECOMMENDATIONS

5.1 DISCUSSION

This study sought to identify potential factors influencing the long-term performance of pavements with centerline rumble strip (CLRS) installations. The primary goal of the study was to fill the gap in knowledge with respect to the cracking failure mechanisms of CLRS. The study sought to develop testing procedures for CLRS samples as well as analysis methods to determine the impact of potential controlling factors identified in the literature review: Permeability and resulting moisture damage; freeze-thaw; the presence of microcracks; surface layer sealants (chip seal); CLRS size, depth, type, and spacing/wavelength; vehicle dynamic loading; and CLRS location in relation to the longitudinal construction joint. The test methods utilized to analyze the impacts of these factors due to rumble strip installations included: i) Rainfall simulation; ii) Freeze-thaw cycling; iii) Moisture infiltration test; iv) Hamburg Wheel Tracking Test (HWTT); v) Three-point flexural fatigue test; vi) X-ray Computed Tomography (CT) imaging; vii) International Roughness Index (IRI) measurements using a walk-behind profiler; viii) Finite Element Analysis (FEA); ix) Indirect Tensile (IDT) strength; x) Resilient Modulus (RM); and xi) Air voids measurement (Corelok and saturated surface-dry [SSD] methods).

Laboratory testing procedures were developed in order to extract performance parameters for various CLRS strategies. The primary test methods included the HWTT and the three-point flexural fatigue test. A moisture infiltration testing procedure was also developed and utilized. The 3D dynamic viscoelastic FEA rumble strip models (the first 3D FEA model for rumble strips in the literature) were developed to analyze physically tested strategies as well as factors that were not examined in the laboratory.

The most significant conclusion in the study was the superior performance of sinusoidal CLRS in comparison to rectangular CLRS. Sinusoidal rumbles showed 38% improvement in fatigue cracking resistance of the flexural beam fatigue tests, 41% improved cracking and structural performance in the HWTT tests, 0% moisture infiltration in the moisture infiltration testing (both with and without chip seal surface treatment), and 35% lower critical strains (indication of the onset of cracking and pavement structural performance) in the FEA modeling. The HWTT results also showed that sinusoidal CLRS had statistically equivalent performance to control replicates with no milled rumble strips. In addition, the HWTT steel wheel rolled more smoothly over sinusoidal CLRS than rectangular CLRS. This may be an indicator of improved performance in relation to the dynamic loading of the tire-vehicle suspension interaction.

It is important to highlight that two separate past ODOT studies focused on noise-related rumble strip impacts found sinusoidal rumble strips to meet or exceed expectations regarding noise generation and impacts (Hurwitz et al., 2019) (Kalathas et al., 2019). Both studies utilized physical-based analysis methods as well as FEA modeling. The superiority of sinusoidal rumble strips in terms of noise and structural performance was demonstrated by these two studies, as well as from the results of this study.

Another significant finding was that chip seal surface treatment was effective in sealing the surface of CLRS samples and preventing moisture infiltration. Chip sealing had no consistent impact on fatigue cracking resistance in bending beam fatigue tests. Through visual comparison of cracking patterns in HWTT tests, chip seal treatment was not shown to mitigate damage stemming from freeze-thaw cycles. Freeze-thaw cycling resulted in large amounts of variation in HWTT and flexural fatigue test results. As such, qualitative comparisons were made between tested HWTT with and without freeze-thaw treatment. The adverse impacts due to freeze-thaw cycles included increased shear flow and deformation of the asphalt concrete, as well as increased cracking concentrated at both ends of the steel wheel rut path.

According to X-Ray CT imaging results, CLRS core samples were shown to have microcracks present. The milling systems with diamond grinders are creating microcracks on the pavement surface during CLRS installation. These microcracks could be propagating with the application of thermal and vehicular loads and resulting in cracking along the rumble strips. The microcracks were concentrated primarily within the first 6.35 mm (0.25 in) of the asphalt surface and extended to a maximum depth of approximately 25.4 mm (1 in). It is important to note that top-down fatigue cracking is the most common damage type in asphalt surfaced pavements in Oregon. The microcracks potentially being introduced at the surface of the rumble strips during milling could be creating weak spots from which top-down fatigue cracking can propagate. Additionally, rainwater filling the microcracks might also be creating hydrostatic pressures when a truckload is applied, resulting in “single-event” cracking (crack formation with one pass of a heavy truck) along the rumble strips (which is not simulated and investigated in this study). For this reason, sealing the surface of the CLRS with chip seal or fog seal treatments right after the CLRS installation may be beneficial.

Rumble strip milling depth was shown to be a significant factor in CLRS performance, with deeper rumbles strips corresponding to worse performance. The fatigue cracking resistance of CLRS samples was reduced by 71% due to a 7.6 mm (0.3 in) increase in CLRS depth. In HWTT tests, a 13% increase in rutting (an indicator of cracking and structural performance) was observed with a 16% increase in CLRS depth. Deep rectangular CLRS had a slightly higher average IRI than shallow rectangular rumbles. FEA modeling also showed minor improvements for shallow depth CLRS and reduced dynamic loading (shallow rumble strip groove and smoother edges) was identified as a potential factor influencing this result. However, the impact of using shallow CLRS on safety should be investigated in a future study.

Comparing the wider conventional CLRS to the modified CLRS, the modified demonstrates 26% improved performance in fatigue cracking resistance. The FEA model demonstrated that conventional rectangular CLRS had improved cracking and pavement structural performance (11%). However, this result was due to the load transfer effects of placing the tire load adjacent to the longitudinal joint. The FEA also showed that installing CLRS adjacent to the longitudinal joint resulted in improved performance (27%). Additionally, the models demonstrated that shorter sinusoidal wavelengths resulted in lower critical microstrains (3%). It is possible that a hydroplane effect was active, where the close spacing between CLRS peaks allowed the tire load to move primarily along the peaks of the rumble strips creating less dynamic loading (which is more likely to happen at faster speeds). Shorter spacing using rectangular CLRS may also result in less dynamic loading and improved performance.

5.2 CONSTRUCTION RECOMMENDATIONS

The results of the study show that the optimal CLRS configuration corresponds to: Shallow depth sinusoidal CLRS with short wavelength installed adjacent to the longitudinal joint (about 3-4 inches away from the longitudinal joint) with chip seal surface treatment. If rectangular CLRS is utilized, the optimal configuration corresponds to: Shallow depth modified rumbles installed adjacent to the longitudinal joint with chip seal surface treatment applied right after CLRS installation. It should be noted that the improved structural performance following these recommendations may come at the cost of decreased notification for drivers. Smaller and shallower rumble strips with a longer sinusoidal wavelength and chip seal surface treatment will likely lead to less alert for drivers. However, since CLRS are located on the driver's side, they are still expected to alert the drivers. The impact of these changes on driver perception should be checked in a future study.

One option to seal the CLRS surface and prevent water infiltration (including potential hydrostatic pressures resulting in “single-event” cracking) would include a small trailer system with a sweeper (with vacuum) followed by nozzles for asphalt emulsion application. This can be developed and installed behind the milling systems to fill the microcracks during rumble strip installation before the water infiltrates them. This type of upfront sealing is expected to improve the longevity of CLRS.

An alternative to prevent the issue of installing CLRS in the vicinity of the longitudinal joint would be echelon paving. This construction method utilizes two pavers paving simultaneously alongside each other. The paving technique effectively eliminates the longitudinal construction joint. At the Knife River test section, paving of both lanes was completed within a few hours. This led to superior or equivalent air void content and performance parameters of CLRS at the longitudinal joint in comparison to CLRS in the travel lane. This demonstrated the effectiveness of echelon paving in the field to avoid weak/low density joints with low fatigue cracking resistance. The results of the ongoing ODOT research project on developing methods to improve longitudinal joint performance (SPR842) should also be checked before or during the implementation of the results of this study. The impact of several strategies to improve joint density and performance will be investigated in 5 field construction projects by building pilot sections, monitoring long-term performance, and using laboratory testing results. Applying a special proprietary liquid asphalt emulsion technology at the bottom and top of the joint before layer construction (to have it penetrate into the voids at the joints during compaction) might be a promising method that could improve joint performance and density, and ultimately create higher cracking resistance for the CLRS installed on longitudinal construction joints.

In summary, implementation of these CLRS construction methods should lead to reduced asphalt pavement damage stemming from the presence of centerline rumble strips.

5.3 FUTURE WORK

Using the FEA model, the impact of alternative CLRS geometries (other than the ones used in this study) on pavement performance should be investigated. The tire model can be improved to increase the accuracy of the numerical model. The validity of the assumptions followed to simulate the longitudinal joint interactions should be checked by using field and laboratory test

results. The impact of aggregate gradations, asphalt mixture properties, and the accumulation of cracking around the CLRS on crack formation and propagation along the CLRS should also be investigated in a future study.

Regarding construction practices and testing, a sealant application system that can directly apply the asphalt emulsion after CLRS installation should be developed. Alternatively, the application of a surface seal after the CLRS installation before the start of the rainy season should become a common practice in Oregon to avoid any moisture-related failures on CLRS. The impact of CLRS installation on construction joints with variable density levels should also be checked in a future study. The impact of using shallower or smoother (such as the sinusoidal option) CLRS on driver perception should also be tested by using accelerometers (for vibration) and microphones (for noise levels in the vehicle). The impact of using CLRS with longer spacing and chip seal and fog seal surface treatments on the CLRS on driver safety should also be investigated in a future study.

6.0 REFERENCES

- Ahmad, T., & Khawaja, H. A. (2018). Review of Low-Temperature Crack (LTC) developments in asphalt pavements. *The International Journal of Multiphysics*, 12(2). <https://doi.org/10.21152/1750-9548.12.2.169>
- Al-Busaltan, S., Al Nageim, H., Atherton, W., & Sharples, G. (2012). Mechanical properties of an upgrading cold-mix asphalt using waste materials. *Journal of Materials in Civil Engineering*, 24(12), 1484–1491. [https://doi.org/10.1061/\(asce\)mt.1943-5533.0000540](https://doi.org/10.1061/(asce)mt.1943-5533.0000540)
- American Association of State Highway and Transportation Officials (AASHTO). (2022). *Standard method of test for bulk specific Gravity (Gmb) of compacted asphalt mixtures using saturated surface-dry specimens* (Standard No. T 166). Washington, D.C.: AASHTO
- Amjadi, R., Merritt, D., & Sherwood, J. A. (2014). Gaining traction on roadway safety. *Public Roads*, 25(1). Retrieved from <https://trid.trb.org/view/1366493>
- ASTM International. (2011). *Standard test method for determining the resilient modulus of asphalt mixtures by Indirect Tension Test* (Standard No. D7369-11). West Conshohocken, PA: ASTM International. Retrieved from <https://www.document-center.com/>
- ASTM International. (2017a). *Standard test method for Indirect Tensile (IDT) strength of asphalt mixtures* (Standard No. D6931-17). West Conshohocken, PA: ASTM International. Retrieved from <https://www.document-center.com/>
- ASTM International. (2017b). *Standard test method for infiltration rate of in place pervious concrete* (Standard No. C1701). West Conshohocken, PA: ASTM International. Retrieved from <https://www.document-center.com/>
- Bahar, G., & Parkhill, M. (2005). Synthesis of practices for the implementation of centreline rumble strips. In *TAC conference: 2005: Calgary, Alberta*. Ottawa, Ontario: TAC. Retrieved from <http://conf.tac-atc.ca/english/resourcecentre/readingroom/conference/conf2005/docs/s18/bahar.pdf>
- Carlson, P. & Miles, J. (2003). *Effectiveness of rumble strips on Texas highways: First year report* (Report No. FHWA/TX-05/0-4472-1). College Station, Texas: Evaluation of Edgeline and Centerline Rumble Strips. Texas Department of Transportation and Federal Highway Administration. Retrieved from <https://static.tti.tamu.edu/tti.tamu.edu/documents/0-4472-1.pdf>
- Carpark Products. (2020). Raised pavement markers. Retrieved April 16, 2022, from <http://www.carparkproducts.com.au/raised-pavement-markers/>.

- Cebon, D. (1993). Interaction between heavy vehicles and roads. In *SAE International Congress and Exposition: Detroit, Michigan, March 1-5, 1993*. Warrendale, Pa: Society of Automotive Engineers. doi:<https://doi.org/10.4271/930001>
- Cebon, D. (1986). Road damaging effects of dynamic axle loads. In *International Symposium on Heavy Vehicle Weights and Dimensions Transportation Association of Canada (TAC): Kelowna, British Columbia, June 8-13, 1986*. Retrieved from <https://hvtforum.org/wp-content/uploads/2019/11/Road-Damaging-Effects-of-Dynamic-Axle-Loads-Cebon.pdf>
- Chehovits, J., & Galehouse, L. (2010). Energy usage and greenhouse gas emissions of pavement preservation processes for asphalt concrete pavements. In *First International Conference on Pavement Preservation: Newport Beach, California, April 13-15, 2010* (pp. 27-42). Berkeley, CA: Technology Transfer Program, Institute of Transportation Studies, University of California, Berkeley. Retrieved from https://www.pavementpreservation.org/icpp/paper/65_2010.pdf
- Coffey, S., & Park, S. (2016). Observational study on the pavement performance effects of shoulder rumble strip on shoulders. *International Journal of Pavement Research and Technology*, 9(4), 255–263. <https://doi.org/10.1016/j.ijprt.2016.06.005>
- Coleri, E., & Harvey, J. T. (2013). A fully heterogeneous viscoelastic finite element model for full-scale accelerated pavement testing. *Construction and Building Materials*, 43, 14–30. <https://doi.org/10.1016/j.conbuildmat.2013.01.022>
- Coleri, E., Sreedhar, S., Haddadi, S.S., & Wruck, B. (2018). *Adjusting asphalt mixes for increased durability and implementation of a performance tester to evaluate fatigue cracking of asphalt* (Report No. FHWA-OR-18-06). Salem, OR: Oregon Department of Transportation. Retrieved from https://www.oregon.gov/odot/Programs/ResearchDocuments/SPR785_DurabilityCracking.pdf
- Coleri, E., Villarreal, R., Kumar, V., Wruck, B., Sreedhar, S., & Lewis, S. (2020). *Implementation of ODOT tack coat technologies and procedures to improve long-term pavement performance* (Report No. FHWA-OR-RD-20-03). Salem, OR: Oregon Department of Transportation. Retrieved from <https://www.oregon.gov/odot/Programs/ResearchDocuments/SPR818TackCoat.pdf>
- Corkle, J., Martí, M., & Montebello, D. (2001). *Synthesis on the effectiveness of rumble strips* (Report No. MN/RC –2002-07). St. Paul, MN: Minnesota Department of Transportation. Retrieved from <https://www.lrrb.org/pdf/200207.pdf>
- Cottingham, D. (2014). What are raised profile line markings or rumble strips? Retrieved April 16, 2022, from <https://www.driverknowledgetests.com/resources/what-are-raised-profile-line-markings-or-rumble-strips/>
- Datta, T.K., Gates, T.J., & Savolainen, P.T. (2012). *Impact of non-freeway rumble strips – Phase I* (Report No. RC-1575). Lansing, MI: Michigan Department of Transportation. Retrieved from <https://rosap.nhtl.bts.gov/view/dot/24734>

- Davis, J. M. (2012). Seven best practices for storing and handling asphalt emulsions. *Asphalt*, 28(3), 38–41. Retrieved from <https://trid.trb.org/view/1314934>
- Donnell, E.T., Solaimanian, M., Stoffels, S.M., & Kulis, P.N. (2014). *Rumble strips installation on thin pavement overlays* (Report No. FHWA-PA-2014-007-PSU WO 7). Harrisburg, PA: Pennsylvania Transportation Institute. Retrieved from <https://rosap.ntl.bts.gov/view/dot/27859>
- Dorchies, P., Chappat, M., & Bilal, J. (2005). Environmental road of the future: Analysis of energy consumption and greenhouse gas emissions. In *Proceedings of the Fiftieth Annual Conference of the Canadian Technical Asphalt Association (CTAA): Victoria, British Columbia, November 2005; 50th anniversary edition* (pp. 1-26). Laval, Quebec, Canada: Polyscience Publications.
- Estaji, M., Coleri, E., Harvey, J. T., & Butt, A. A. (2019). Predicting excess vehicle fuel use due to pavement structural response using field test results and finite element modelling. *International Journal of Pavement Engineering*, 22(8), 973–983. <https://doi.org/10.1080/10298436.2019.1655563>
- Fang, X., Garcia-Hernandez, A., & Lura, P. (2016). Overview on cold cement bitumen emulsion asphalt. *RILEM Technical Letters*, 1, 116–121. <https://doi.org/10.21809/rilemtechlett.2016.23>
- Federal Highway Administration (FHWA). (2015a). *Rumble strip implementation guide: Addressing pavement issues on two-lane roads* (Report No. FHWA-SA-15-034). Washington, D.C.: Federal Highway Administration. Retrieved from <https://highways.dot.gov/safety/rwd/keep-vehicles-road/rumble-strips/rumble-strip-implementation-guide-addressing-pavement>
- Federal Highway Administration (FHWA). (2015b). *Rumble strip implementation guide: Addressing noise issues on two-lane roads* (Report No. FHWA-SA-15-033). Washington, D.C.: Federal Highway Administration. Retrieved from <https://highways.dot.gov/safety/rwd/keep-vehicles-road/rumble-strips/rumble-strip-implementation-guide-addressing-noise>
- Federal Highway Administration (FHWA). (2011). *Center line rumble strips* (Technical Advisory No. T 5040.40, Revision 1). Federal Highway Administration.
- Ferry, J. D. (1980). *Viscoelastic properties of polymers*. Hoboken, NJ, United States: Wiley.
- Ghale, S. & Pataskar, S. (2017). Comparison of cold mix and hot mix asphalt. *International Journal of Engineering Research in Mechanical and Civil Engineering (IJERMCE)*, 118–121. Retrieved from https://www.technoarete.org/common_abstract/special_pdf/special_14507.pdf
- Goyer, S., Dauvergne, M., Wendling, L., Fabre, J., Roche, C., & Gaudefroy, V. (2012). Environmental evaluation of gravel emulsion. *Proceedings of Life cycle Assessment and*

- Construction International Congress, July 2012, France*, (pp. 170–178). Retrieved from <https://hal.science/hal-00851066/document>
- Guin, A., Hunter, M.P., Rodgers, M.O., & Sin, J. (2014). *Centerline rumble strips safety and maintenance impacts* (Report No. FHWA-GA-14-1212). Forest Park, GA: Georgia Department of Transportation. Retrieved from <https://rosap.ntl.bts.gov/view/dot/35629>
- Harvey, J., Lea, J., Kim, C., Coleri, E., Zaabar, I., Louhghalam, A., Chatti, K., Buscheck, J., & Butt, A. (2016). *Simulation of cumulative annual impact of pavement structural response on vehicle fuel economy for California test sections* (Report No. UCPRC-RR-2015-05). Davis, CA: University of California. Retrieved from <https://escholarship.org/uc/item/3p8312vs>
- Hawkins, N., Smadi, O., Knickerbocker, S., & Carlson, P. (2016). *Rumble stripe: Evaluation of retroreflectivity and installation practices* (Report No. MN/RC 2016-13). St. Paul, MN: Minnesota Department of Transportation. Retrieved from <https://intrans.iastate.edu/app/uploads/2018/03/201613.pdf>
- Haynes, M., Coleri, E., & Sreedhar, S. (2019). Impermeable Asphalt Concrete Layer to Protect and Seal Concrete Bridge Decks. *Transportation Research Record*, 2673(6), 355–367. <https://doi.org/10.1177/0361198119841041>
- Haynes, M., Coleri, E., Sreedhar, S., & Obaid, I.A. (2020). *Bridge deck asphalt concrete pavement armoring* (Report No. FHWA-OR-RD-20-04). Salem, OR: Oregon Department of Transportation. Retrieved from <https://www.oregon.gov/odot/Programs/ResearchDocuments/SPR815Bridgedeckasphalt.pdf>
- Himes, S., McGee, H., Levin, S., & Zhou, Y. (2017). *State of the practice for shoulder and center line rumble strip implementation on non-freeway facilities* (Report No. FHWA-HRT-17-026). Washington, D.C.: Federal Highway Administration. Retrieved from <https://www.fhwa.dot.gov/publications/research/safety/17026/17026.pdf>
- Howard, I.L., Alvarado, A., & Floyd, W.C (2013). *Performance oriented guidance for Mississippi chip seals - Volume II* (Report No. FHWA/MS-DOT-RD-13-211-Volume II). Jackson, MS: Mississippi Department of Transportation. Retrieved from [https://www.cee.msstate.edu/publications/FHWA_MS-DOT-RD-13-211-Volume_II_\(LTP\).pdf](https://www.cee.msstate.edu/publications/FHWA_MS-DOT-RD-13-211-Volume_II_(LTP).pdf)
- Huang, S., & Benedetto, D. H. (2015). *Advances in asphalt materials: Road and Pavement Construction* (1st ed.). Sawston, United Kingdom: Woodhead Publishing.
- Hurwitz, D., Horne, D., & Jashami, H. (2019). *Quantifying the performance of low-noise transverse rumble strips* (Report No. FHWA-OR-RD-20-01). Salem, OR: Department of Transportation. Retrieved from <https://www.oregon.gov/odot/Programs/ResearchDocuments/ODOTSPR829AFinal.pdf>

- Hurwitz, D., Horne, D., Jashami, H., Monsere, C., & Kothuri, S. (2019). *Quantifying the performance of low-noise rumble strips* (Report No. FHWA-OR-RD-19-07). Salem, OR: Department of Transportation. Retrieved from <https://www.oregon.gov/odot/Programs/ResearchDocuments/SPR800FinalReport.pdf>
- Institute of Transportation Engineers (ITE), Wolshon, B., & Pande, A. (2016). *Traffic engineering handbook* (7th ed.). Hoboken, NJ, United States: Wiley.
- Kalathas, P., Parrish, C., & Zhang, Y. (2019). *Rumble strip design evaluation based on exterior noise using finite element analysis* (Report No. OR-RD-19-10). Salem, OR: Oregon Department of Transportation. Retrieved from <https://www.oregon.gov/odot/Programs/ResearchDocuments/RumbleStripsFinal.pdf>
- Khalid, H. A., & Monney, O. K. (2009). Moisture damage potential of cold asphalt. *International Journal of Pavement Engineering*, 10(5), 311–318. <https://doi.org/10.1080/10298430802169838>
- Kim, Y-R., You, T., & Rilett, LR. (2017). *Design and evaluation of modified centerline rumble strips* (Report No. SPR-P1(16) M034). Lincoln, NE: Nebraska Transportation Center. Retrieved from <https://dot.nebraska.gov/media/7904/finalreportm034.pdf>
- Ksaibati, K. & Erickson, R. (1998). *Evaluation of low temperature cracking in asphalt pavement mixes*. Laramie, WY: University of Wyoming. Retrieved from <https://www.ugpti.org/resources/reports/downloads/mpc98-94b.pdf>
- Ling, C. (2013). *Developing evaluation method of moisture susceptibility for cold mix asphalt* (Master Thesis). Madison, WI: University of Wisconsin. Retrieved from https://minds.wisconsin.edu/bitstream/handle/1793/67650/MS_Thesis_Ling_Cheng.pdf?sequence=1&isAllowed=y
- Liu, J. (2015). SDI-12 USB adapter user manual. Retrieved April 17, 2022, from <https://manualzilla.com/doc/5718699/sdi-12-usb-adapter-user-manual>
- Michigan Department of Transportation (MDOT). (2010). MDOT standard plans home. Retrieved April 17, 2022, from <https://mdotjboss.state.mi.us/stdplan/standardPlansHome.htm>
- Nageim, H. A., Al-Busaltan, S., Atherton, W., & Sharples, G. P. (2012). A comparative study for improving the mechanical properties of cold bituminous emulsion mixtures with cement and waste materials. *Construction and Building Materials*, 36, 743–748. <https://doi.org/10.1016/j.conbuildmat.2012.06.032>
- Needham, D. (1996). *Developments in bitumen emulsion mixtures for roads* (Doctoral dissertation, Thesis (Ph. D.), 1996). Nottingham, United Kingdom: University of Nottingham. Retrieved from <https://www.nottingham.ac.uk/research/groups/ntec/documents/theses/needhamphdthesis.pdf>

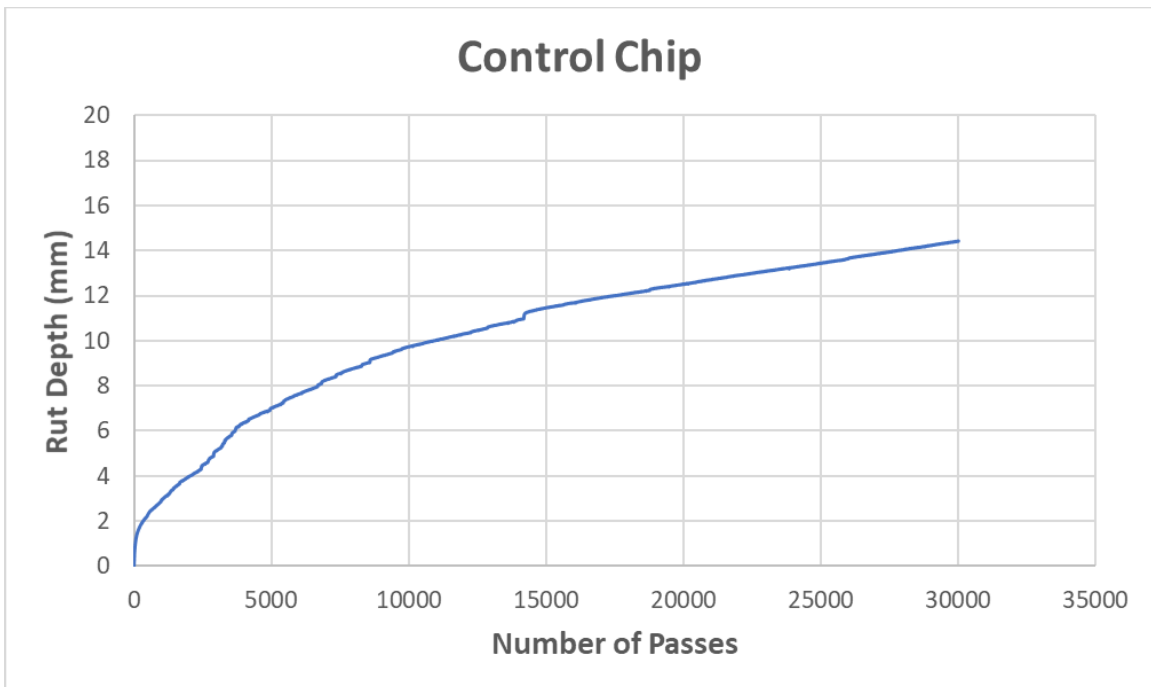
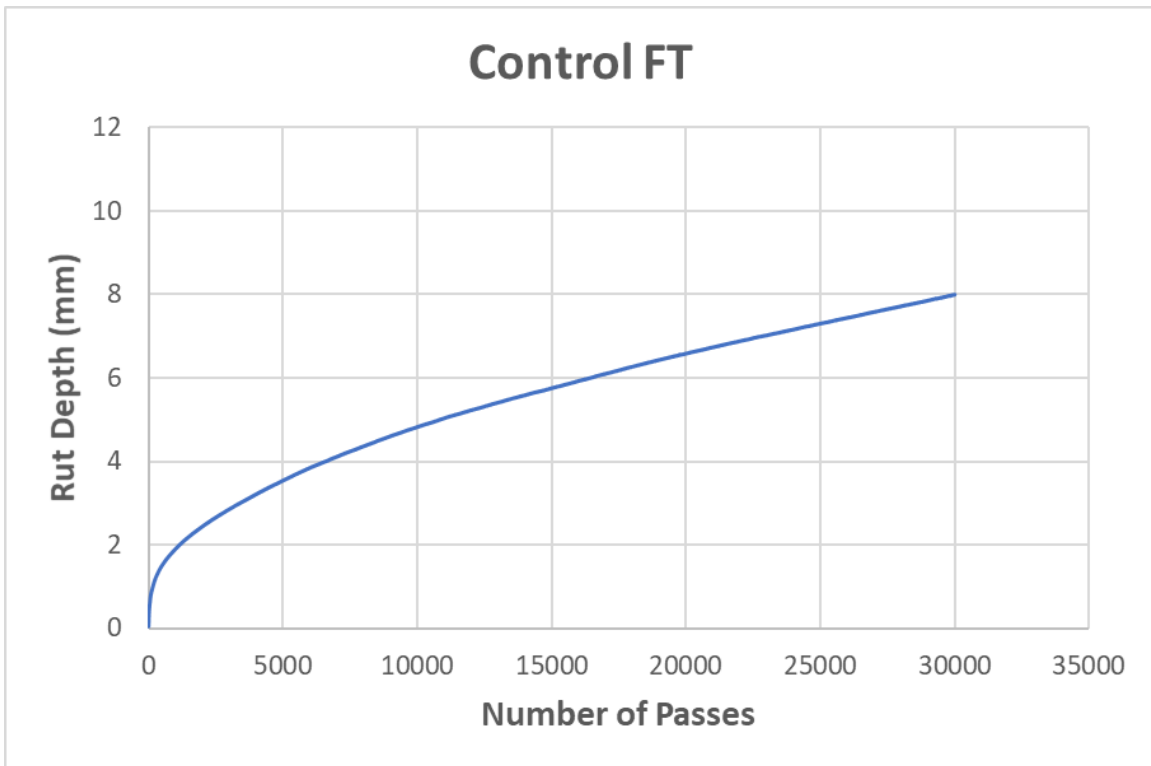
- Oregon Department of Transportation (ODOT). (2011). *Determining the international roughness Index with an inertial laser profiler* (Standard No ODOT TM 772). Salem, OR: Oregon Department of Transportation, Construction Section. Retrieved from https://www.oregon.gov/odot/Construction/Doc_ManualofFieldTestProcedures/2022/01_introduction.pdf
- Oregon Department of Transportation (ODOT). (2019). *ODOT pavement design guide*. Salem, OR: Oregon Department of Transportation. Retrieved from https://www.oregon.gov/odot/Construction/Documents/pavement_design_guide.pdf
- Oregon Department of Transportation (ODOT). (2021). *Oregon standard specifications for construction*. Salem, OR: Oregon Department of Transportation. Retrieved from https://www.oregon.gov/odot/Business/Specs/2021_STANDARD_SPECIFICATIONS.pdf
- Oregon Department of Transportation: Self-issue permit program: Commerce and compliance division: State of Oregon. (2021). Retrieved July 7, 2021, from <https://www.oregon.gov/odot/MCT/Pages/SelfIssuePermit.aspx>
- Oregon Department of Transportation: Standard details | Traffic 4000 series: Engineering: State of Oregon. (n.d.). Retrieved July 22, 2021, from <https://www.oregon.gov/odot/Engineering/Pages/Details-Traffic.aspx>
- Oregon Department of Transportation (ODOT). (2022). *Traffic line manual*. Salem, OR: Engineering & Technical Services Branch Traffic-Roadway Oregon Department of Transportation. Retrieved from https://www.oregon.gov/odot/engineering/documents_trafficstandards/traffic-line-manual.pdf
- Richards, S., & Saito, M. (2007). State-of-the-practice and issues surrounding centerline rumble strips, in: Safety and security engineering II. In *Safe 2007 proceedings, 11-13 April 2007, Washington, D.C., USA* (pp. 365-374). Piscataway, NJ: IEEE. doi:10.2495/SAFE070361
- Russell, E. R., & Rys, M. J. (2005). *Centerline rumble strips*. Washington, D.C.: Transportation Research Board. Retrieved from https://trb.org/publications/nchrp/nchrp_syn_339.pdf
- Scherocman, J. (1991). *International state-of-the-art colloquium on low-temperature asphalt pavement cracking* (Special Report 91-5). Hannover, New Hampshire. Retrieved from <https://erdc-library.erdcdren.mil/jspui/bitstream/11681/11627/1/SR-91-5.pdf>
- Scholz, T.V. & Rajendran, S. (2009). *Investigating premature pavement failure due to moisture* (Report No. FHWA-OR-RD-10-02). Salem, OR: Oregon Department of Transportation. Retrieved from https://www.oregon.gov/odot/Programs/ResearchDocuments/Moisture_Damage.pdf
- Sholar, G. A., Page, G. C., Musselman, J. A., Upshaw, P., & Moseley, H. L. (2005). Investigation of the CoreLok for maximum, aggregate, and bulk specific gravity tests. *Transportation Research Record, 1907*, 135–144. <https://doi.org/10.3141/1907-16>

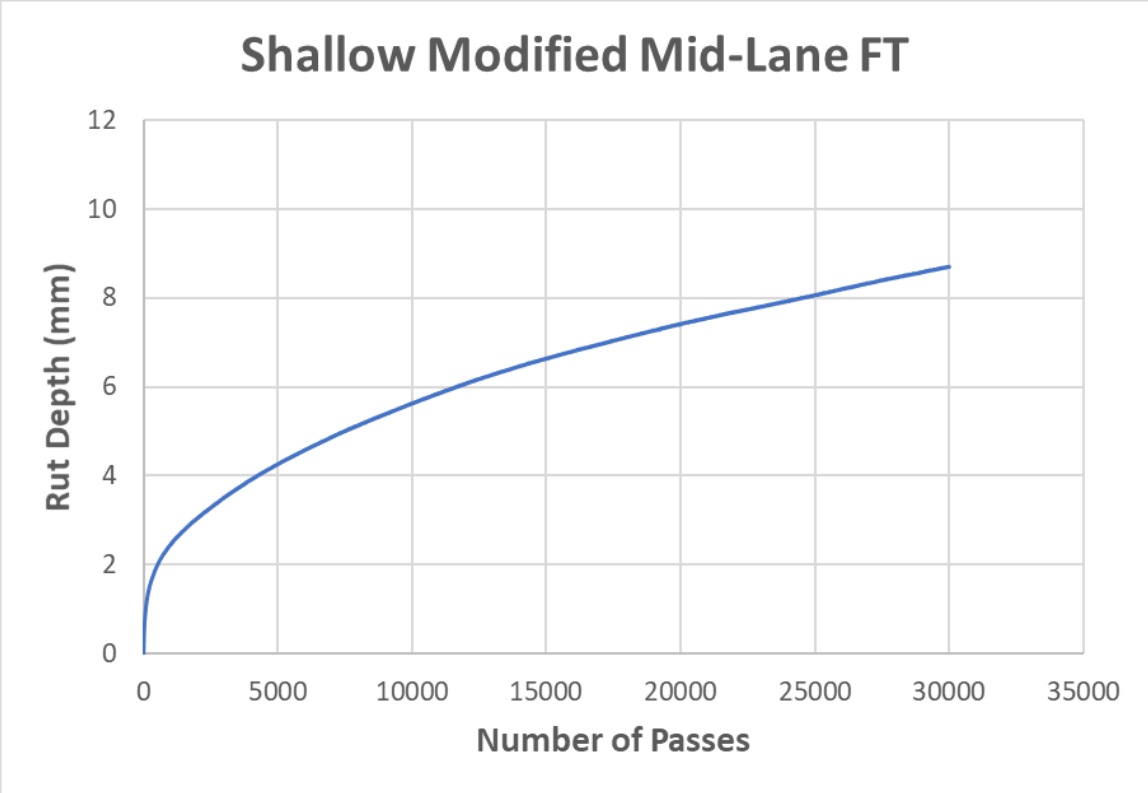
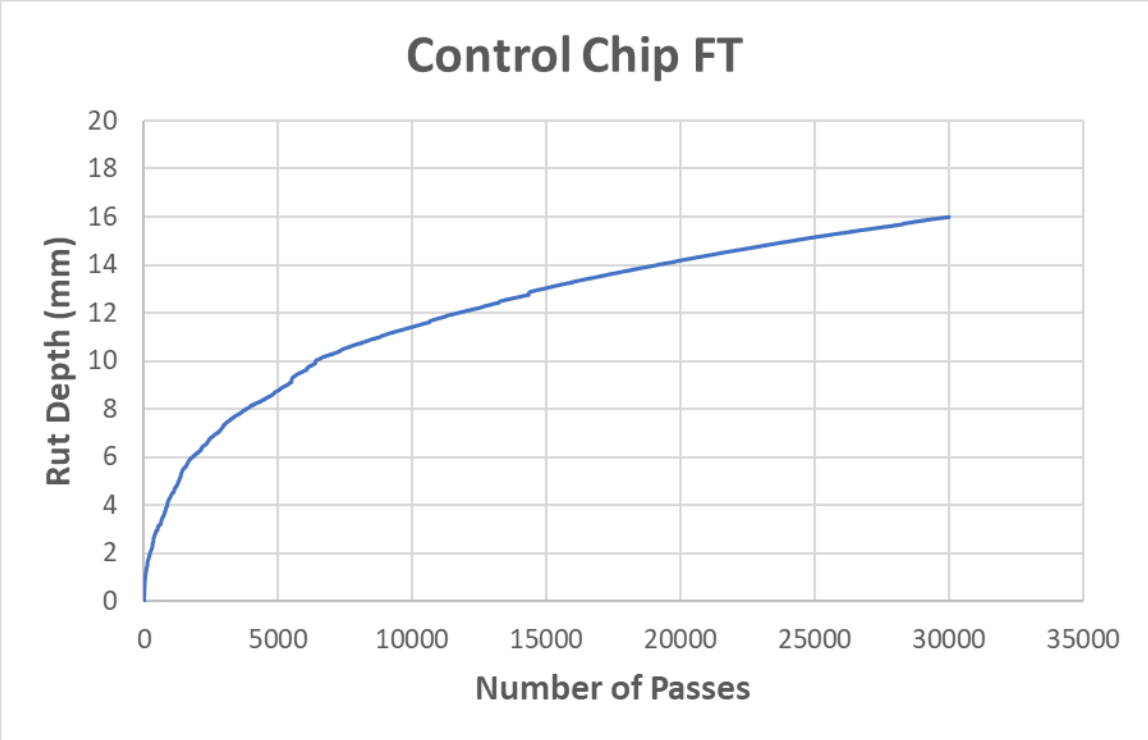
- Smadi, O., Hawkins, N. R., & National Academies of Sciences, Engineering, and Medicine. (2016). *Practice of rumble strips and rumble stripes* (Synthesis Report No. 490). Washington, D.C.: Transportation Research Board. doi:10.17226/23522
- Staats, W., Agent, K., & Howell, B. (2020). *Evaluation of alternative rumble strip designs* (Report No. KTC-20-28/SPR20-595-1F). Frankfort, KY: Kentucky Transportation Center. <https://doi.org/10.13023/ktc.rr.2020.28>
- Sun, X. & Rahman, M.A. (2021). *Impact of center line rumble strips and shoulder rumble strips on all roadway departure crashes in Louisiana two-lane highways* (No. FHWA/LA.17/648). Baton Rouge, LA: Louisiana Department of Transportation and Development. Retrieved from https://ltrc.lsu.edu/pdf/2021/FR_648.pdf
- Terhaar, E., Braslau, D., & Fleming, K. (2016). *Sinusoidal rumble strip design optimization study* (Report No. MN/RC 2016-23). St. Paul, MN: Minnesota Department of Transportation. Retrieved from <https://www.lrrb.org/pdf/201623.pdf>
- Thanaya, I. (2003). *Improving the performance of cold bituminous emulsion mixtures (CBEMs) incorporating waste materials* (Master's thesis, University of Leeds, July 2003). Leeds: University of Leeds. Retrieved from https://etheses.whiterose.ac.uk/386/1/uk_bl_ethos_275778.pdf
- Torbic, D. J., Hutton, J. M., Bokenkroger, C. D., Bauer, K. M., Harwood, D. W., Gilmore, D. K., ... Lyon, C. (2009). *Guidance for the design and application of shoulder and centerline rumble strips*. Washington, D.C.: Transportation Research Board.
- Tran, N., Turner, P., & Shambley, J. (2016). *Enhanced compaction to improve durability and extend pavement service life: A literature review* (NCAT Report 16-02R). Auburn, AL: National Center for Asphalt Technology at Auburn University. Retrieved from <https://eng.auburn.edu/research/centers/ncat/files/technical-reports/rep16-02.pdf>
- Tufuor, E., Rilett, L., & LeFrois, C. (2017). *In-vehicle evaluation of milled rumble strips at pre- and post-chip sealed maintenance periods* (Report No. SPR-P1(15)M037). Lincoln, NE: Nebraska Transportation Center, Nebraska Department of Roads. Retrieved from <https://dot.nebraska.gov/media/7639/finalreportm037.pdf>
- Voigt, G. F. (2002). Early cracking of concrete pavement - Causes and repairs. In *2002 Federal Aviation Administration (FAA) Airport Technology Transfer Conference*. Washington, D.C. Retrieved from <https://citeseerx.ist.psu.edu/viewdoc/download;jsessionid=494582DBA9961DF91D8EE9346BEDDEC3?doi=10.1.1.587.1150&rep=rep1&type=pdf>
- Watson, M., Olsen, R., Pantelis, J., Johnson, E., & Wood, T. (2008). *Long term maintenance effects on HMA pavements caused by rumble strips and available preventive treatment methods* (Report No. MN/RC 2008-50). Maplewood, MN: Minnesota Department of Transportation. Retrieved from <https://www.lrrb.org/media/reports/200850.pdf>

- West, K. & Smith, R. (1996). *Micro-surfacing: Guidelines for use and quality assurance*. College Station, TX: Texas Transportation Institute, Texas Department of Transportation. Retrieved from <https://static.tti.tamu.edu/tti.tamu.edu/documents/1289-3.pdf>
- Washington State Department of Transportation (WSDOT). (2022). *Design manual*. Olympia, WA: Washington State Department of Transportation. Retrieved from <https://www.wsdot.wa.gov/publications/manuals/fulltext/M22-01/design.pdf>
- WorldData. (n.d.). Retrieved from <https://www.worlddata.info/america/usa/climate-oregon.php>
- WorldData. (n.d.-a). Retrieved from <https://www.worlddata.info/america/usa/climate-michigan.php#:~:text=Michigan%20is%20one%20of%20the,deep%20winters%20and%20warm%20summers.&text=The%20number%20of%20hours%20of,the%20sun%20is%20actually%20visible>.
- Xu, J., Luo, X., & Shao, Y. (2018). Vehicle trajectory at curved sections of two-lane mountain roads: a field study under natural driving conditions. *European Transport Research Review*, 10(1). <https://doi.org/10.1007/s12544-018-0284-x>

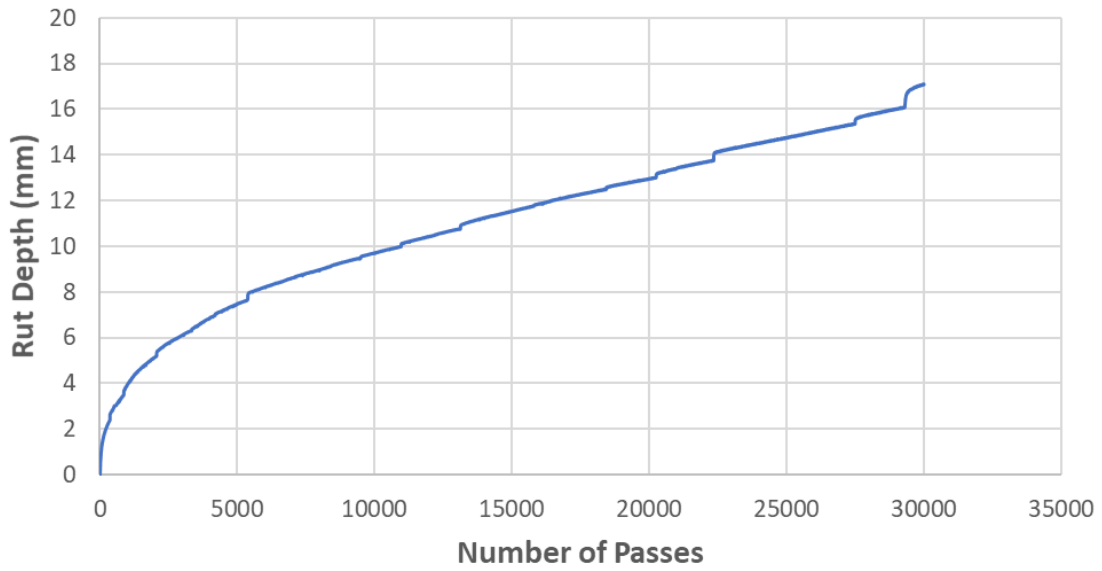
APPENDIX A: SUPPLEMENTARY MATERIAL OF CHAPTER 4

Hamburg Wheel Tracking Test (HWTT) composite rutting curves for all tested strategies are shown in Figure A.1. No correction factors were applied to the composite rutting curves with chip seal surface treatment.

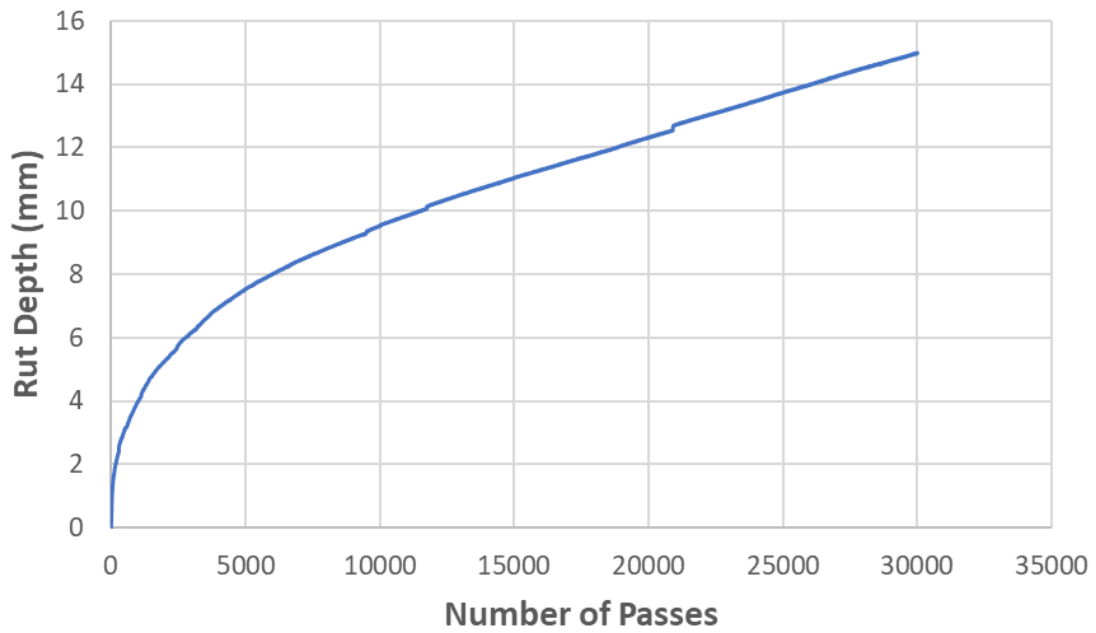




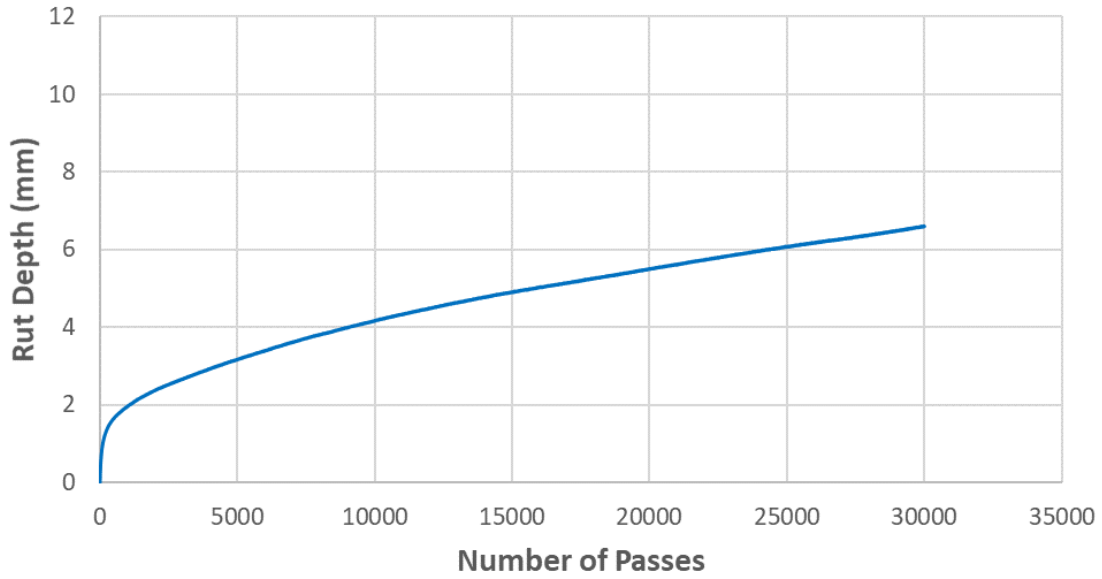
Shallow Modified Mid-Lane Chip



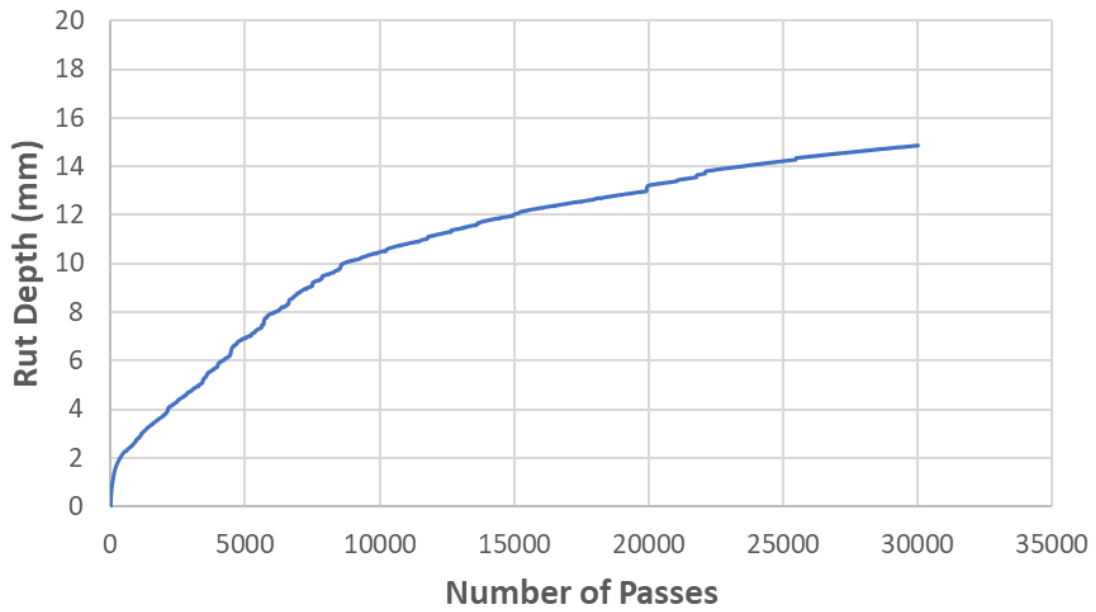
Shallow Modified Mid-Lane Chip FT



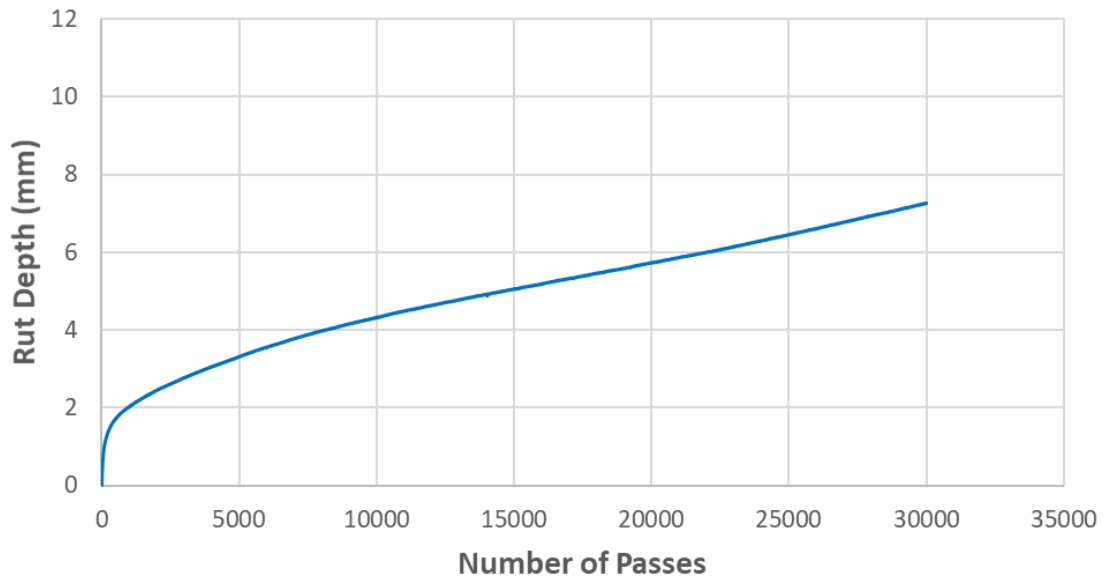
Deep Modified Mid-Lane



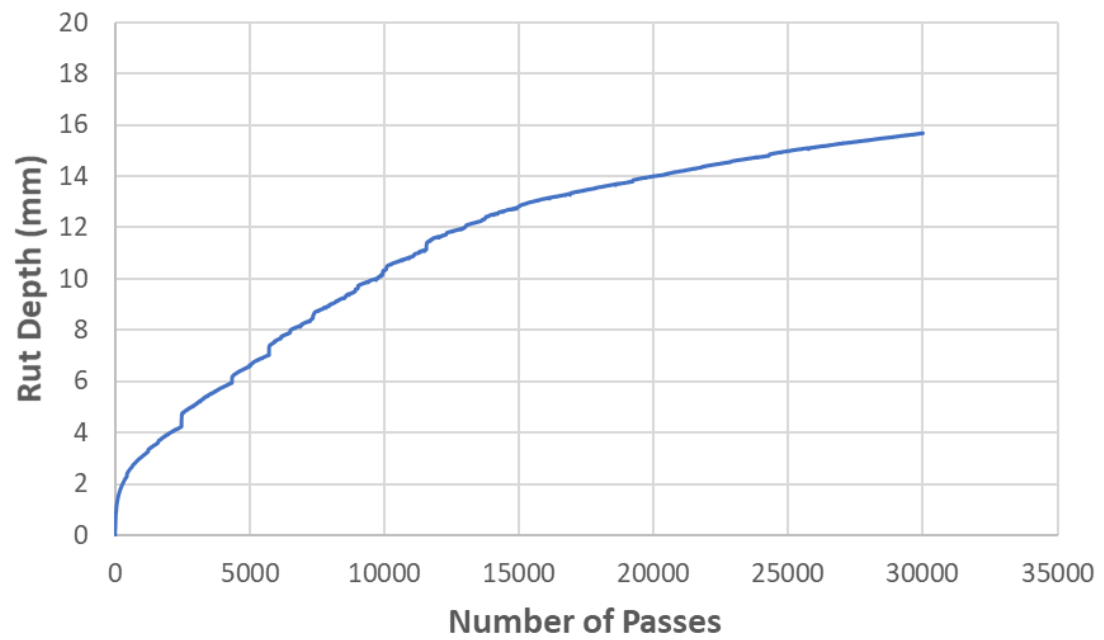
Shallow Modified Centerline Chip



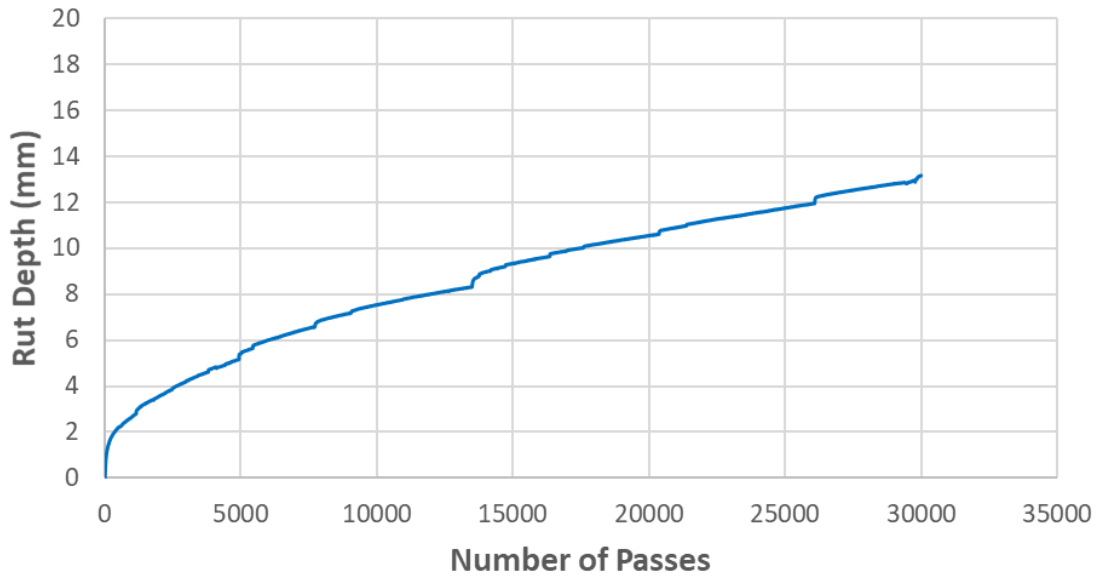
Deep Modified Centerline



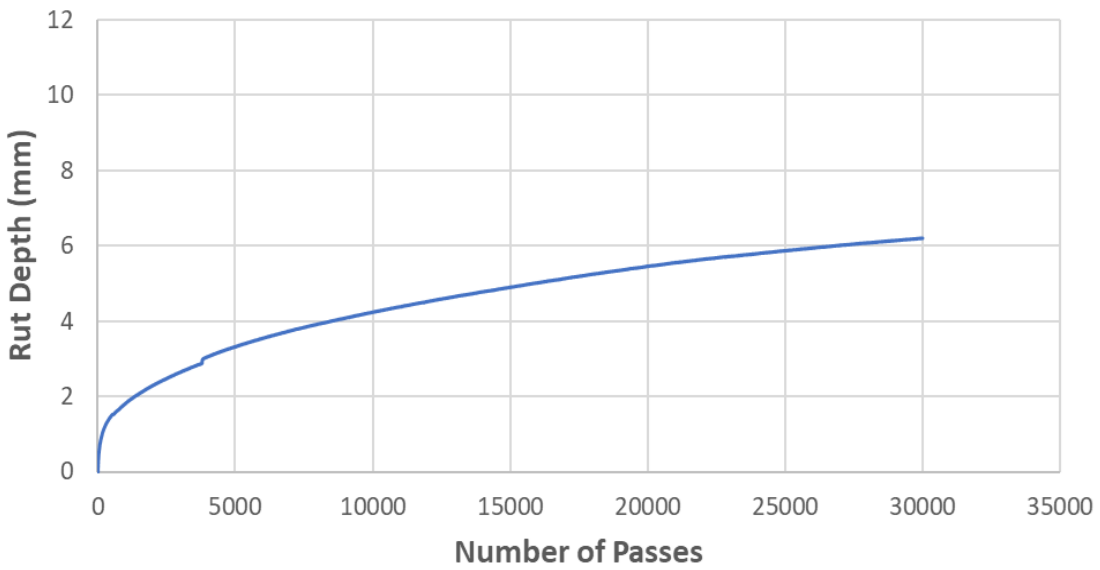
Deep Modified Centerline Chip



Shallow Sinusoidal Mid-Lane Chip



Shallow Sinusoidal Centerline



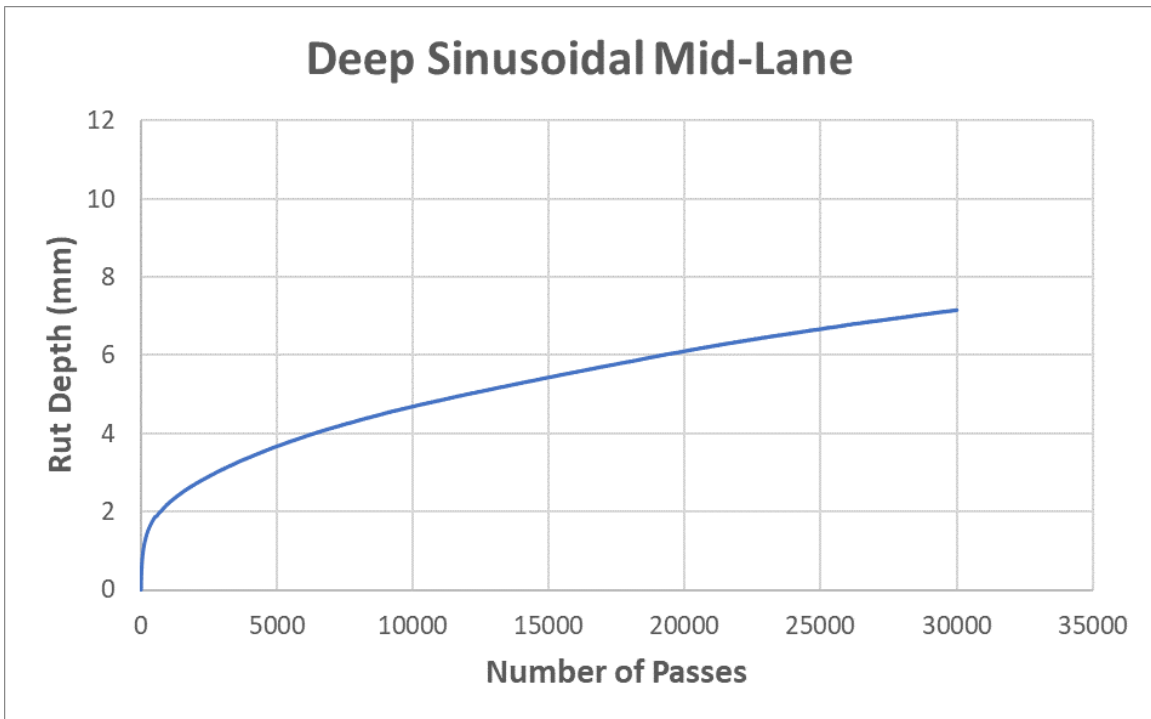
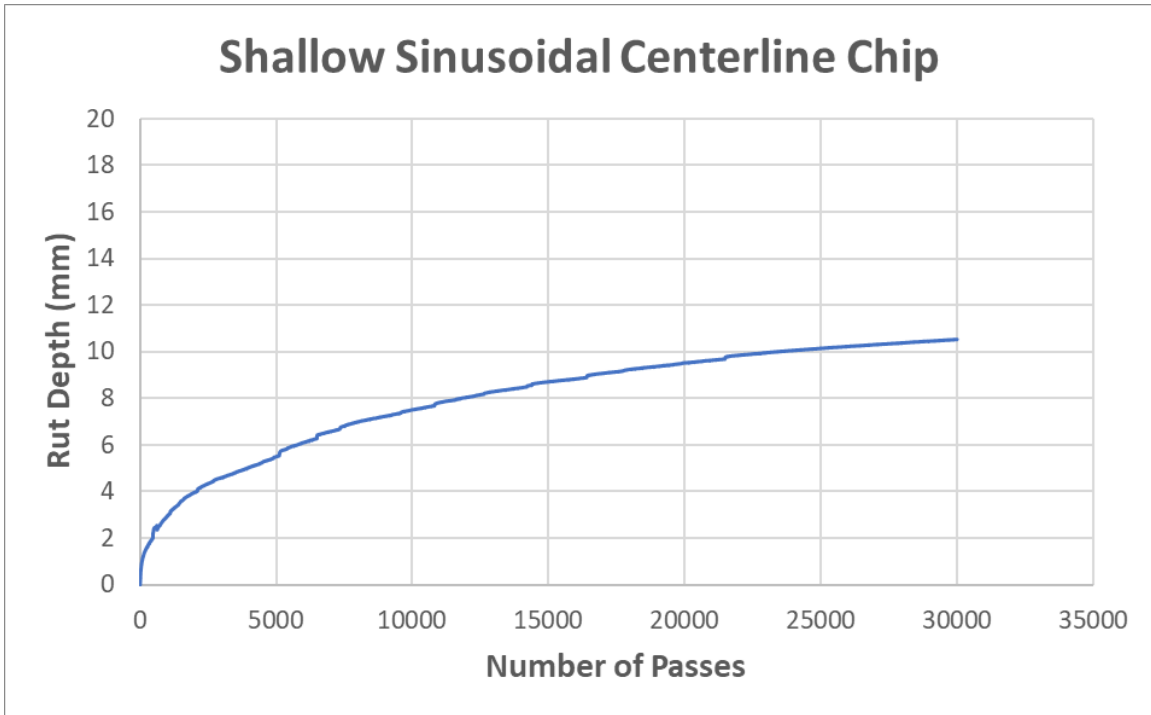


Figure A.1: Hamburg Wheel Tracking (HWTT) composite rutting curves

HWTT comparison photos showing the difference between strategies are shown in Figure A.2:



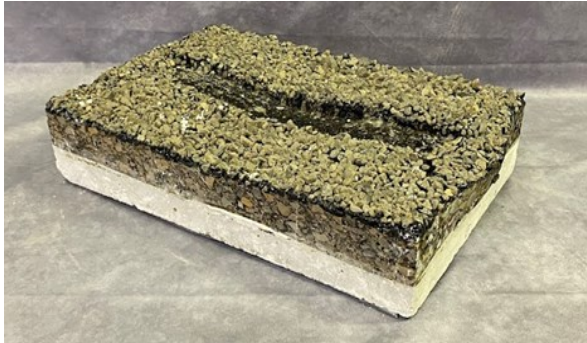
(a) Control, No Treatment



(b) Control, Chip Seal



(c) Rectangular Modified, No Treatment



(d) Rectangular Modified, Chip Seal



(e) Sinusoidal, No Treatment



(f) Sinusoidal, Chip Seal

Figure A.2: Tested HWTT samples demonstrating different treatment strategies